A vertical sorting model for rivers with non-uniform sediment and dunes

Samenstelling promotiecommissie:

prof. dr. ir. H. J. Grootenboer	Universiteit Twente, voorzitter/secretaris
prof. dr. ir. H. J. de Vriend	Technische Universiteit Delft, promotor
prof. dr. G. Parker	University of Minnesota, promotor
dr. ir. J. S. Ribberink	Universiteit Twente, assistent promotor
prof. dr. ir. C. B. Vreugdenhil	Universiteit Twente
prof. dr. S. J. M. H. Hulscher	Universiteit Twente
prof. dr. H. W. den Hartog	Rijksuniversiteit Groningen
dr. ir. C. J. Sloff	WL | Delft Hydraulics

Front cover: Skykomish River, Washington, USA, August 1995. Image courtesy Erik Mosselman

Printed by Universal Press, Veenendaal, the Netherlands

ISBN 90-9016663-7

A VERTICAL SORTING MODEL FOR RIVERS WITH NON-UNIFORM SEDIMENT AND DUNES

PROEFSCHRIFT

ter verkrijging van

de graad van doctor aan de Universiteit Twente,

op gezag van de rector magnificus,

prof. dr. F. A. van Vught,

volgens besluit van het College voor Promoties

in het openbaar te verdedigen

op donderdag 6 maart 2003 om 15:00 uur

door

Astrid Blom

geboren op 4 augustus 1973

te Rijnsburg

Dit proefschrift is goedgekeurd door de promotoren:

prof. dr. ir. H. J. de Vriend
prof. dr. G. Parker

en door de assistent promotor:

dr. ir. J. S. Ribberink

Summary

Vertical sorting fluxes and the resulting organisation of grain size fractions over bed elevations, i.e. the vertical sorting profile, influence bedform dimensions and the bed surface composition. As a result, they will affect the bed roughness, the rate and composition of the sediment transport, the large-scale river morphology, and water levels during floods. An important problem of present morphological model systems for rivers with non-uniform sediment is their neglect of vertical sorting fluxes other than through net aggradation or degradation. The objective of the present study is to develop a method in order to better account for vertical sorting processes in the river bed.

Net aggradation or degradation of the river bed results from divergences in the sediment transport rate, which is expressed by the mass balance equation. In rivers with non-uniform sediment, a divergence in the transport rate of a specific size fraction will result in changes in the composition of the bed surface and net aggradation or degradation of the river bed. A further complication in the mass balance is the vertical sorting. A plane bed is usually covered with a coarse bed layer (mobile pavement or armour layer), whereas in bedform-dominated conditions the coarse size fractions are mainly found in the lower parts of the bedforms.

In a morphological model system for non-uniform sediment, the above interaction is described in terms of sediment continuity models. *Hirano* (1971) was the first to develop such a model. Yet, the Hirano active layer model and most of its variants suffer from a number of shortcomings. Most bed layer models do not account for vertical sorting other than through net aggradation or degradation, whereas flume experiments have shown that vertical sorting also occurs through grain size-selective deposition down a bedform lee face and the variability in trough elevations. Hirano's assumption that the bed elevations interacting with the flow constitute a distinct surface layer seems too limited to adequately account for these sorting processes. A final problem of these models with discrete bed layers is that in certain situations the set of equations becomes elliptic in parts of the space-time domain. This means that solving the equations would require future time-boundaries, which is physically unrealistic.

In the present study, two sets of flume experiments have been conducted, in order to obtain a better insight into vertical sorting processes and to obtain data on vertical sorting in bedforms under well-controlled laboratory conditions. Vertical sorting profiles were measured using newly-developed core sampling boxes. The experiments have shown that the sorting within migrating bedforms is dominated by (1) grain size-selective deposition down the avalanche lee face (resulting in a downward coarsening trend within the bedforms), (2) partial transport, and (3) the winnowing of fines from the trough surface and subsurface. The experiments point towards a close relation between the variability in trough elevations and the (time scale of) vertical sorting. This can be understood when considering that, through migration, a dune redistributes all bed material above its trough elevation.

The author has developed a new continuum vertical sorting model for conditions dominated by bedforms and bed load transport. It is based on (1) the Parker-Paola-Leclair framework for sediment continuity, (2) the *Einstein* step length formulation, (3) a newly-developed lee sorting function, and (4) a newly-developed method to account for the variability in bedform trough elevations. *Parker et al.* (2000) developed a new type of framework for sediment continuity that no longer distinguishes discrete bed layers, thus enabling us to relate entrainment and deposition fluxes in the bed to the likelihood of a bed elevation being exposed to the flow. Parameters in the framework such as the grain size-specific and entrainment and deposition fluxes vary continuously over bed elevations. The present study comprehends the derivation of formulations for these fluxes for bedform-dominated conditions.

For equilibrium conditions, the continuum sorting model is reduced to an equilibrium sorting model, which comprises two methods to solve for the equilibrium sorting profile. For non-equilibrium conditions, the continuum sorting model is reduced to a sorting evolution model. It solves for the time evolution of both the vertical sorting profile and the bed load transport composition from the following parameters: the initial sorting profile, the total bed load transport rate, and the probability density function (PDF) of relative trough elevations. Both reduced models describe sorting through grain size-selective deposition down the bedform lee face and the variability in trough elevations. In addition, methods are proposed to account for vertical sediment fluxes through both a change in time of the PDF of relative trough elevations and net aggradation or degradation. However, testing the continuum sorting model for situations with net aggradation or degradation was beyond the scope of the thesis.

In a morphological model system, the equilibrium sorting model may be applied instantaneously in case the time scale of large-scale morphological changes is much

larger than the time scales of vertical sorting, vertical dune dimensions, and dune migration. This constraint seems to be satisfied in situations with large-scale aggradation or degradation, such as long-term bed degradation after a river bend cut-off or long-term aggradation or degradation due to river training works. For situations with local small-scale aggradation or degradation, e.g., in river bends, it is likely that the time evolution of sorting needs to be accounted for when computing changes in morphology. In that case, the sorting evolution model must be applied.

The equilibrium sorting model was calibrated and verified against flume experiments. Two constants in the lee sorting function were used as calibration constants. The sorting evolution model was verified by comparing the computed time evolution of both the vertical sorting profile and the bed load transport composition to measured data from flume experiments. No parameters were calibrated upon. The computations by both models agree reasonably well with the measured data.

Note that the continuum sorting model computes the bed load transport composition by itself. This suggests that there is a strong interaction among (1) the vertical sorting profile, (2) the PDF of relative trough elevations, and (3) the bed load transport composition. It is believed that this strong interaction does not allow for one of the components to be modelled independently from one another. The results indicate that also the bed roughness is intimately connected to the vertical sorting profile and the PDF of trough elevations.

The new continuum sorting model is deterministic in the computation of the vertical sorting profile, but probabilistic in terms of the bed surface. This probabilistic element arises from the fluctuations of the bed surface due to the presence of bedforms. The continuum sorting model is the first to incorporate sediment sorting fluxes through grain size-selective deposition down the bedform lee face, the variability in trough elevations, a change in time of the PDF of relative trough elevations, and net aggradation or degradation. Because of its improved description of the vertical sorting profile, the continuum sorting model yields better predictions of the bed surface composition than the discrete bed layer models presently available. Since the bed surface composition plays a crucial role in the sediment transport, it is believed that the model will also lead to improved predictions of sediment transport rates and thus morphological changes, although testing the model as part of a morphological model system was beyond the scope of the present study. In order to use the new continuum sorting model in predictive applications, the model needs to be extended to plane-bed conditions and a sub-model for the PDF of relative trough elevations needs to be developed.

Samenvatting

Verticale sedimentfluxen in de rivierbodem en het resulterende verticale sorteringsprofiel beïnvloeden duinafmetingen en de samenstelling van het bodemoppervlak. Ze zijn daarom van invloed op de bodemruwheid, de samenstelling en de totale hoeveelheid van het sedimenttransport, de grootschalige riviermorfologie en waterstanden tijdens hoogwaters. Echter, in bestaande morfologische modelsystemen voor rivieren met niet-uniform sediment treden verticale sedimentfluxen alleen op als er sprake is van netto erosie of sedimentatie. Het doel van dit onderzoek is daarom een model te ontwikkelen dat de verticale sorteringsfluxen in de rivierbodem beter beschrijft.

Netto erosie of sedimentatie treedt op als gevolg van divergenties in het sedimenttransport, wat wordt weergegeven met de sedimentbalansvergelijking. In rivieren met niet-uniform sediment veroorzaken divergenties in het sedimenttransport van een bepaalde korrelfractie een verandering in de samenstelling van het bodemoppervlak en netto erosie of sedimentatie. Een factor die de sedimentbalans voor niet-uniform sediment nog complexer maakt is de verticale sortering. Een vlakke bodem is vaak bedekt door een grove toplaag (een afpleisteringslaag), terwijl in situaties met rivierduinen het grove sediment zich juist vooral bevindt in het onderste gedeelte van de duinen.

In een morfologisch modelsysteem voor niet-uniform sediment wordt deze interactie beschreven door een zogenaamd sedimentbalansmodel. *Hirano* (1971) was de eerste die een dergelijk model heeft ontwikkeld. Het actieve-laagmodel van Hirano en de meeste van zijn varianten gaan echter gebukt onder een aantal tekortkomingen. Deze modellen beperken zich tot het beschrijven van verticale sedimentfluxen die optreden door netto erosie of sedimentatie, terwijl gootexperimenten hebben laten zien dat verticale sortering ook optreedt door selectieve depositie van sediment over de lijzijde van duinen en door de variatie in duintrogniveaus. Hirano's aanname dat de bodemniveaus die in aanraking komen met de stroming een duidelijk te onderscheiden toplaag vormen lijkt te beperkt voor een adequate beschrijving van de verticale sorteringsprocessen. Een laatste probleem van deze sedimentbalansmodellen met discrete bodemlagen is dat onder bepaalde omstandigheden de vergelijkingen

elliptisch worden in delen van het plaats-tijd domein. Dit betekent dat oplossing van het stelsel vergelijkingen toekomstige tijd-randvoorwaarden vraagt, wat fysisch gezien onrealistisch is.

In dit onderzoek zijn twee series gootexperimenten uitgevoerd om een beter inzicht te krijgen in verticale sorteringsprocessen en om data te verkrijgen voor de calibratie en verificatie van een nieuw sorteringsmodel. Verticale sorteringsprofielen werden gemeten met een nieuwe bodembemonsteringsmethode. De experimenten hebben aangetoond dat de verticale sortering in zich voortbewegende duinen wordt gedomineerd door (1) selectieve depositie van sediment over de lijzijde van duinen, (2) selectief sedimenttransport waarbij het grofste sediment niet of nauwelijks in beweging komt en (3) het uitzeven van fijn sediment in de duintroggen. De gootexperimenten wijzen op een nauwe relatie tussen de variatie in duintrogniveaus en (de tijdschaal van) de verticale sortering. Dit is begrijpelijk, aangezien een zich voortbewegende duin al het sediment boven zijn trogniveau herverdeelt.

De auteur heeft een nieuw continu verticaal sorteringsmodel ontwikkeld gericht op condities met duinen en bodemtransport. Het is gebaseerd op (1) het sedimentbalansraamwerk van *Parker et al.* (2000), (2) de staplengte-theorie van *Einstein* (1950), (3) een nieuwe lijzijdesorteerfunctie en (4) een methode die de variatie in duintrogniveaus in rekening brengt. *Parker et al.* (2000) hebben een nieuw raamwerk voor sedimentbalansmodellen ontwikkeld dat niet langer is gebaseerd op bodemlagen. Daarmee wordt het mogelijk om opname- en depositiefluxen in de bodem te relateren aan de mate waarin een bepaald bodemniveau wordt blootgesteld aan de stroming. Grootheden in het raamwerk, zoals de selectieve opname- en depositiefluxen, variëren continu over de bodemniveaus, maar ze worden horizontaal gemiddeld over een groot aantal duinen. De huidige studie omvat de afleiding van formuleringen voor deze selectieve opname- en depositiefluxen.

Voor evenwichtscondities is het continue sorteringsmodel gereduceerd tot een evenwichtssorteringsmodel, dat twee methoden kent om het evenwichtssorteringsprofiel op te lossen. Voor niet-evenwichtscondities is het continue sorteringsmodel gereduceerd tot een sortingsevolutiemodel. Dit model berekent de tijdsontwikkeling van het verticale sorteringsprofiel en van de samenstelling van het bodemtransport, aan de hand van het gegeven initiële sorteringsprofiel, de totale hoeveelheid bodemtransport en de kansdichtheidsverdeling van relatieve duintrogniveaus. Beide gereduceerde modellen beschrijven verticale sorteringsfluxen die optreden door selectieve depositie van sediment over de lijzijde van duinen en door de variatie in duintrogniveaus. Daarnaast zijn methoden afgeleid om verticale sedimentfluxen in rekening te brengen die optreden door een verandering in de kansdichtheidsverde-

ling van relatieve duintrogniveaus of door netto erosie of sedimentatie. Het testen van het continue sorteringsmodel voor situaties met netto erosie of sedimentatie viel buiten het kader van dit onderzoek.

In een morfologisch modelsysteem mag het evenwichtssorteringsmodel instantaan worden toegepast als de morfologische tijdschaal veel groter is dan de tijdschalen van de verticale sortering, duinafmetingen en duinvoortplanting. Aan deze beperking lijkt te worden voldaan in situaties met grootschalige erosie of sedimentatie, zoals de lange-termijn erosie die optreedt na de afsnijding van een rivierbocht of de lange-termijn erosie of sedimentatie als gevolg van maatregelen voor rivierkanalisatie. Voor situaties met locale kleinschalige erosie of sedimentatie, zoals in een rivierbocht, wordt verwacht dat bij het berekenen van morfologische veranderingen de tijdsontwikkeling van de sortering in rekening gebracht moet worden. In een dergelijke situatie moet het sortingsevolutiemodel worden toegepast.

Het evenwichtssorteringsmodel is gecalibreerd en geverifieerd aan de hand van gootexperimenten. Twee constantes in de lijzijdesorteringsfunctie zijn gebruikt als calibratieconstantes. Het sortingsevolutiemodel is geverifieerd aan de hand van een vergelijking tussen de berekende tijdsontwikkeling van het verticale sorteringsprofiel en de samenstelling van het bodemtransport en gemeten waarden uit gootexperimenten. Er zijn hierbij geen parameters als calibratieconstantes gebruikt. Voor beide modellen komen de berekende en gemeten waarden redelijk goed overeen.

Het continue sorteringsmodel berekent de samenstelling van het bodemtransport zelf. Dit suggereert dat er een sterke interactie is tussen (1) het verticale sorteringsprofiel, (2) de kansdichtheidsverdeling van relatieve trogniveaus en (3) de samenstelling van het bodemtransport. Deze nauwe interactie laat niet toe dat een van deze componenten onafhankelijk van de andere wordt gemodelleerd. De resultaten geven aan dat ook de bodemruwheid nauw is gerelateerd aan het verticale sorteringsprofiel en de kansdichtheidsverdeling van relatieve duintrogniveaus.

Het nieuwe continue sorteringsmodel is deterministisch wat betreft het berekende verticale sorteringsprofiel, maar probabilistisch wat betreft de beschrijving van het bodemoppervlak. Dit probabilistische element komt voort uit de fluctuaties van het bodemoppervlak door de aanwezigheid van bodemvormen. Het continue sorteringsmodel is het eerste model dat sedimentsorteringsfluxen beschijft die optreden door selectieve depositie van sediment over de lijzijde van duinen, de variatie in duintrogniveaus, een verandering in de kansdichtheidsverdeling van relatieve duintrogniveaus en netto erosie of sedimentatie. Vanwege de verbeterde beschrijving van de verticale sortering zal het continue sorteringsmodel leiden tot betere voorspel-

lingen van de samenstelling van het bodemoppervlak dan de bestaande bodemlagenmodellen. Omdat deze samenstelling van het bodemoppervlak een cruciale rol speelt in het sedimenttransport, wordt verwacht dat het model ook zal leiden tot verbeterde voorspellingen van het sedimenttransport en dus ook van morfologische veranderingen, alhoewel het model binnen deze studie niet is getest als onderdeel van een morfologisch modelsysteem.

Om het nieuwe continue sorteringsmodel in voorspellende toepassingen te kunnen gebruiken moet het model worden uitgebreid voor situaties met een vlakke bodem en moet een submodel voor de kansdichtheidsverdeling van relatieve duintrogniveaus worden ontwikkeld.

Contents

Chapter 1
Introduction

River managers may have various objectives to intervene in a river system: flood prevention, flood safety, water supply, irrigation, power supply, recreation, navigation, nature rehabilitation, fish and wildlife, bed sanitation, gravel mining, pollution control, and so on. Examples of such river interventions are river canalisation (dikes, groins), a deepening or widening of the main channel, a lowering of the floodplain, a river bend cut-off, or the creation of an additional distributary. These river interventions often have a large influence upon the river behaviour, which manifests itself in hydraulic, sedimentary, and morphological changes in the river system. Requirements of a river system may be conflicting, which makes it important to analyse and predict the effects of planned interventions. For instance, flood prevention may require a widening and deepening of the river in order to reduce water levels during floods, which, under average river discharges, may lead to water depths too small for navigation.

1.1 Context

Morphological model systems are important tools in the analysis and prediction of the effects of river interventions or, for example, the river's hydraulic and morphological response to a flood event. A morphological model system is defined as a system that couples modules for calculating the flow, the sediment transport, and morphological changes[1]. Examples are the one-dimensional SOBEK model system and the two- and three-dimensional Delft3D model system of WL | Delft Hydraulics and the MIKE model series of the Danish Hydraulics Institute.

In modelling a river's morphological behaviour, the bed material may be characterised by one specific grain size (uniform sediment), in case sediment sorting processes do not play a role in the morphological behaviour. In a sediment mixture, fine grains are generally picked-up and transported more easily than coarse ones, which may induce vertical, lateral, and longitudinal sorting of the bed material (e.g.,

[1]The expressions 'morphological changes', 'net aggradation or degradation', or 'changes in the spatially-averaged (or mean) bed level' all have the same meaning.

Powell, 1998). In this case, we talk about non-uniform sediment. Examples of the above types of sorting are river bed armouring, downward coarsening of bedform material, the formation of coarse layers below migrating bedforms, lateral sorting in river bends and on bars, and downstream fining. Through affecting the small-scale morphology (i.e. the bed surface composition, bedform dimensions, and bed roughness), sediment sorting also influences the sediment transport (rate and composition), the large-scale river morphology, and water levels during floods. Rivers with non-uniform sediment may therefore show a hydraulic-morphological behaviour that largely differs from rivers with uniform sediment (e.g., *Mosselman et al.*, 1999).

Net aggradation or degradation of the river bed results from divergences in the transport rate, which is expressed by the sediment continuity equation or mass balance equation. In cases where the bed material consists of multiple size fractions, divergences in the transport rate of size fractions will result in a change in the composition of the bed surface and/or aggradation or degradation of the river bed. A further complication in the mass balance is the organisation of grain size fractions over bed elevations, i.e. the vertical sorting. A plane bed is often covered with a coarse bed layer (mobile pavement or armour layer), whereas under bedform conditions the coarse size fractions are mainly found in the lower parts of the bedforms (*Bagnold*, 1941; *Allen*, 1965).

Under bedform-dominated conditions, various sediment sorting mechanisms play a role. The above-mentioned downward coarsening trend of bedform material, which is illustrated in Figure 1.1, results from the avalanching of grains down the bedform lee face (*Bagnold*, 1941; *Allen*, 1965). When conditions are well above the shear stresses for incipient motion of all size fractions in the mixture, the coarse sediment in the lower parts of the bedforms takes part in the sediment transport processes, like in the experiments by *Ribberink* (1987). When conditions of partial transport[2] prevail and a significant amount of coarse material is not or barely transported by the flow, the coarse sediment gathers below the migrating bedforms, forming an essentially immobile coarse layer (see Figure 1.1). This was the case in, for instance, the experiments by *Wilcock and Southard* (1989). Besides the avalanching process at the bedform lee face and partial transport, also the winnowing of fines from the trough surface and subsurface contributes to the formation of a coarse bed layer underneath migrating bedforms (*Willis*, 1988; *Wilcock and Southard*, 1989; *Klaassen*, 1990a).

In a morphological model system for non-uniform sediment, this interaction among

[2]Partial transport is defined as the situation in which a significant amount of coarse material is not or barely transported by the flow. Selective transport is defined as the situation in which the proportion of coarse grains in the transported sediment is smaller than their proportion in the bed.

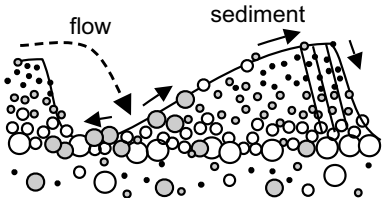

Figure 1.1: Downward coarsening of bedform material and a gathering of coarse material underneath migrating bedforms, revised from *Zanke* (1976).

grain size-selective sediment transport, net aggradation or degradation, and the vertical sorting profile is described in terms of sediment continuity models. *Hirano* (1971) was the first to develop such a model. In his active layer model, the bed is divided into a homogeneous top layer, i.e. the active layer, and an inactive substrate. Only sediment in the active layer interacts with the flow and participates in the transport process. Sediment fluxes between the active layer and the substrate only occur through net aggradation or degradation. In the last few decades, a number of variants to the Hirano active layer model have been proposed in order to overcome several shortcomings and obtain a better description of vertical sediment sorting mechanisms within the active bed.

However, the Hirano active layer model and its variants do not adequately describe the vertical sorting processes in the bed. They do not account for the downward coarsening within bedforms, the formation of coarse bed layers, and the influence of coarse bed layers upon sediment entrainment. Moreover, in most sediment continuity models, vertical sediment fluxes occur through net aggradation or degradation only, whereas previous research has shown that vertical sediment fluxes also occur through grain size-selective deposition down a bedform lee face and the variability in trough elevations (*Crickmore and Lean*, 1962a,b; *Ribberink*, 1987; *Wilcock and Southard*, 1989). Because of this inadequate description of vertical sorting fluxes, it is uncertain whether the bed layer models accurately describe (the time evolution of) the average bed surface composition. Since the latter is one of the main components determining the bed roughness and the grain size-selective sediment transport, it is also uncertain whether morphological model systems based on a bed layer model accurately describe morphological changes and water levels during floods.

In his two-layer model, *Ribberink* (1987) does account for vertical sorting due to the variability in trough elevations by introducing an additional layer below the active layer, i.e. the exchange layer. This exchange layer represents the bed eleva-

tions reached by only the deepest troughs in a series of bedforms and shows a much longer time scale of adaptation of its composition than the active layer. However, the definition of the thickness of such bed layers remains rather arbitrary. It is not straightforward to distinguish, on a physical basis, between the range of bed elevations interacting with the flow regularly (the active layer), the range interacting with the flow only occasionally (the exchange layer), and the range not interacting with the flow, at all (the substrate). In morphological models, the bed layers' thicknesses are therefore often used as calibration parameters. A final problem of the bed layer models is that in certain situations their set of equations may become elliptic in parts of the space-time domain (*Ribberink*, 1987). Apparently, in those circumstances, the bed layer models are not able to describe the sorting processes acting within the river bed.

Examples of rivers characterised by non-uniform sediment are the Rhine distributaries (e.g., *Kleinhans*, 2002; *Frings and Kleinhans*, 2002; *Julien et al.*, 2002) and the Grensmaas River (e.g., *Duizendstra*, 2001). For river management purposes, there is a clear need for improved tools for predicting the morphological behaviour of such rivers. An important problem in predicting this morphological behaviour are the above-mentioned shortcomings of existing sediment continuity models. In the last few decades, relatively much attention has been paid to improving sediment transport models for non-uniform sediment, whereas only little attention has been paid to shortcomings pertaining to sediment continuity models.

Recent progress was made by *Parker et al.* (2000), who developed a new type of framework for sediment continuity without discrete bed layers. The Parker-Paola-Leclair framework is based on the probability density function of bed surface elevations, which indicates the likelihood of a certain bed elevation being exposed to the flow. The framework describes (the time evolution of) the vertical sorting fluxes and the vertical sorting profile continuously over depth. It is here called a 'framework', because formulations for the vertical sorting fluxes within the active bed remained to be derived.

In the present study, it is decided to further elaborate on the Parker-Paola-Leclair framework, since it offers the possibility of describing the vertical sorting fluxes continuously over depth and relating the sorting fluxes at a certain bed elevation to the likelihood of this elevation being exposed to the flow. It is believed that letting go of the concept of discrete bed layers is required to overcome the above problems inherent to existing bed layer models.

1.2 Objectives, limitations, and research questions

The objective of the present study is to modify existing sediment continuity models for rivers with non-uniform sediment, so as to account for vertical sorting fluxes acting in the river bed.

The resulting model is aimed at conditions with bedforms (dunes) and bed load transport, and it is meant to be applied on a scale averaged over a large number of bedforms. The study is limited to investigating vertical sorting processes for cases without net aggradation or degradation. The author will attempt to oversee the implications of this study for morphological model systems, but testing the new continuum sorting model as part of a morphological model system is beyond the scope of this thesis.

We will focus on the following research questions:

1. Which mechanisms affect the vertical sorting profile under conditions with bedforms and partial transport? Which of these mechanisms need to be incorporated in a new sediment continuity model?
2. What types of sediment continuity models for non-uniform sediment can we distinguish? What type enables describing the sorting mechanisms in a realistic way?
3. How can we incorporate the sorting mechanisms in the model?
4. How well does the new continuum sorting model reproduce the vertical sorting profiles measured in the experiments considered for calibrating and verifying the model?
5. How can the new model be incorporated in a predictive morphological model system?
6. How do the present results reflect upon existing bed layer models (e.g., the Hirano active layer model)?

How and in which chapters these questions are addressed will be explained in the next section.

1.3 Research methodology and outline thesis

In order to answer (part of) *research question 1*, first literature on sediment sorting processes is reviewed (Chapter 2). Chapter 3 presents an overview of existing sediment continuity models for non-uniform sediment, thus addressing *research question 2*.

For developing an improved sediment continuity model, there is a need for data from experiments with non-uniform sediment under well-controlled laboratory conditions in which this interaction is studied in detail. So far, only *Ribberink* (1987) and *Klaassen* (1992) have provided such data sets. In the present study, two new series of flume experiments were conducted, under conditions with bedforms, bed load transport, and coarse bed layers. The objectives of the experiments were

- to increase our understanding of mechanisms affecting the vertical sorting profile (*research question 1*, Chapter 4), and
- to provide detailed and comprehensive data for the calibration and verification of the improved sediment continuity model (*research question 4*, Chapters 7 and 8).

The first set of experiments was conducted using a sediment mixture from the river Rhine. To facilitate the analysis of the vertical sorting processes, a second set of experiments was conducted using a mixture of three well-sorted size fractions, i.e. a tri-modal sediment mixture. In all experiments uniform flow was maintained, so that net aggradation or degradation did not occur. For measuring vertical sorting profiles, a new type of core sampling box was developed.

Based on new insights from the literature surveys and the two sets of experiments, a new continuum sorting model is proposed (*research question 3*, Chapter 5). The model is founded on the Parker-Paola-Leclair framework for sediment continuity, the Einstein step length formulation, a newly-developed lee sorting function, and a newly-developed method to account for the variability in trough elevations.

For equilibrium conditions, when all parameters fluctuate around mean values, and under certain assumptions, the model is reduced to an equilibrium sorting model (Chapter 6). The equilibrium sorting model is calibrated by comparing computed equilibrium sorting profiles with data from two of the above experiments with the tri-modal mixture, and verified against two experiments by *Ribberink* (1987) and experiments on sorting down a delta lee face by *Kleinhans* (2002) (*research question 4*, Chapter 7). For non-equilibrium conditions, the full continuum sorting model is reduced to a sorting evolution model. This model is verified by comparing the computed time evolution of the vertical sorting profile with data from two experiments with the tri-modal mixture (*research question 4*, Chapter 8).

Research question 5 (Incorporation in a morphological model system) and *research question 6* (Reflection upon existing bed layer models) will be addressed in Chapter 9. The answers to all research questions are summarised one by one in the final chapter (Chapter 10).

Chapter 2

Literature survey - Vertical sorting in bedforms

The objective of the present study is to modify existing sediment continuity models for non-uniform sediment, so as to take into account vertical sorting processes in bedforms. For that purpose, we first study previous research on

- vertical sorting mechanisms in bedforms (Chapter 2)
- existing sediment continuity models for non-uniform sediment (Chapter 3)

This chapter presents an overview of mechanisms that are important to the vertical redistribution of sediment in bedforms. The founder of our thoughts on the migration of bedforms is *Bagnold* (1941). Studying the transport of sand over desert dunes, he describes how sediment entrained from the stoss face of a bedform is transported over its crest and deposited at its lee face (Section 2.1). Section 2.2 briefly addresses the structure of the flow over a bedform.

Allen (1965, 1984) and *Zanke* (1976) conducted pioneering work on the migration of bedforms composed of non-uniform sediment (Section 2.3). They studied the grain size-selective sorting down the avalanche lee face of a bedform, in which the fine particles prefer being deposited onto the upper part of the lee face and the coarse ones onto the lower part (see Figure 2.1). How the vertical sorting in a series of irregular bedforms changes with changing flow conditions was studied by *Ribberink* (1987) and *Klaassen* (1990b, 1992).

Figure 2.1 also shows another feature of sediment sorting: the formation of a essentially immobile coarse bed layer underneath migrating bedforms (Section 2.4), which has also been observed for sub-aerial bedforms by *Bagnold* (1941). A coarse bed layer forms when the sediment mixture is widely graded and a significant amount of coarse material is barely or not transported by the flow.

One of the important factors affecting the vertical sorting profile is the variability in trough elevations and bed surface elevations (Section 2.5). A point at a lower ele-

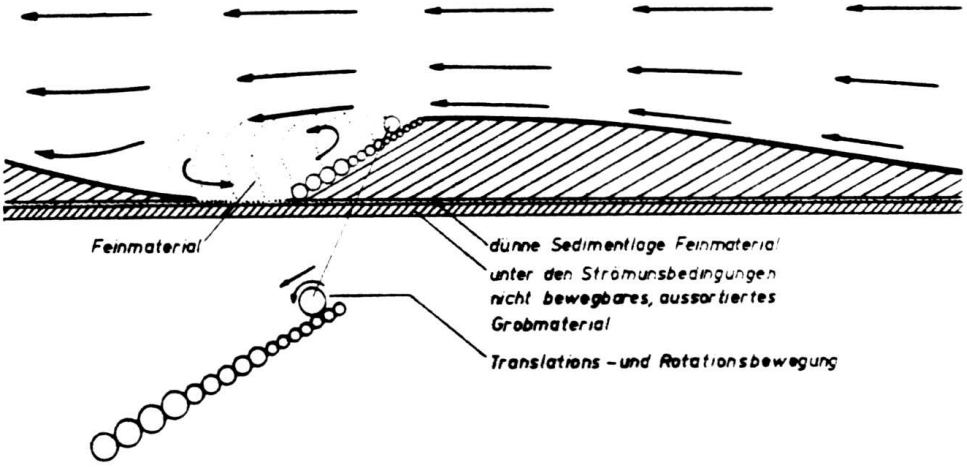

Figure 2.1: Vertical sorting under bedform conditions (*Zanke*, 1976, Fig.40, p.77).

vation of the active bed[1] is less frequently exposed to the flow because it spends a larger fraction of time buried by sediment than a point higher up.

It has been observed that fine particles may be winnowed or washed out from the bed surface and subsurface[2] in the trough zones of bedforms (Section 2.6), which may affect the vertical sorting profile. Unfortunately, this mechanism of winnowing has never been directly measured.

2.1 Bedform migration

Considering flow over aeolian or sub-aerial bedforms, *Bagnold* (1941) observed that for small slopes there is no air flow separation over a bedform (Figure 2.2a). When bedforms grow and become too steep, flow separation occurs and the bedform becomes asymmetrical (Figures 2.2b and c). Since sediment particles from flows separating over the bedform crest are deposited primarily onto the upper part of the lee face, the lee face deposit, i.e. the wedge, has a tendency to become steeper and steeper. This continues until the maximum angle of repose is reached. Then, the

[1]The *active bed* is defined as the range or spectrum of bed elevations that are exposed to the flow, i.e. the bed *surface* elevations.

[2]The *bed surface* is defined as the sediment directly exposed to the flow, whereas the *subsurface* is defined as the sediment just below the bed surface, not directly exposed to the flow.

wedge suddenly avalanches down the lee face and becomes distributed over the lee face, deposited at an angle somewhat smaller than at the initiation of the avalanche. The intermittent and successive avalanches down the lee face make the lee face migrate downstream and, in the case of non-uniform sediment, invoke specific grain sorting mechanisms. Such a lee face migrating through intermittent avalanches is called a slip face. Section 2.3 will discuss how a mixture of different grain sizes is deposited down a bedform lee face.

This behaviour was confirmed by *Allen* (1965) for subaqueous bedforms in a small recirculating flume (3 m long, 0.3 m wide) with two sand mixtures ($d_{50,1} = 0.5$ mm, $d_{90,1} = 0.7$ mm, $d_{50,2} = 0.6$ mm, $d_{90,2} = 1.2$ mm). Allen indeed observed that the amount of particles settling from the flow onto the lee face decreases rapidly from the crest to the toe, building up a wedge at the upper lee face. This continues until the wedge becomes unstable, initiating an avalanche down the lee face and resulting in the intermittent avalanche process as described by *Bagnold* (1941).

Allen (1965, 1970) found that the frequency of the avalanches is inversely proportional to the flow velocity over the bedform crest, which represents the sediment transport rate over the crest. Above a certain (critical) flow velocity, the removal of grains from the upper lee face by intermittent avalanching cannot keep up with the settling: the avalanching becomes continuous and grains slide down the lee face without waiting for a wedge to become unstable. In conditions with continuous avalanching, the stable slope of the lee face is smaller than for intermittent avalanches (with equal mixtures).

Bagnold (1941) derived a relation for the spatial variation of the total bed load transport rate over a bedform (also see *Fredsøe*, 1982). These relations can be found by applying the simple-wave equation to bedform migration. In this approach bedforms are assumed to be closed units without any bed load transport between one bedform and the next, so that the transport rate in the troughs equals zero. The bedforms may have an arbitrary shape, but this shape remains invariant. Local aggradation and degradation along a bedform is described by the sediment continuity equation:

$$c_b \frac{\partial \eta}{\partial t} = -\frac{\partial q}{\partial x} \tag{2.1}$$

where c_b denotes the sediment concentration in the bed ($c_b = 1 - \lambda_p$, where λ_p denotes the porosity), η the local elevation of the bedform surface, x the horizontal co-ordinate, t the time co-ordinate, and q the local volume of bed load transport over the bedform per unit width and time. Assuming no deformation of the bedform, a

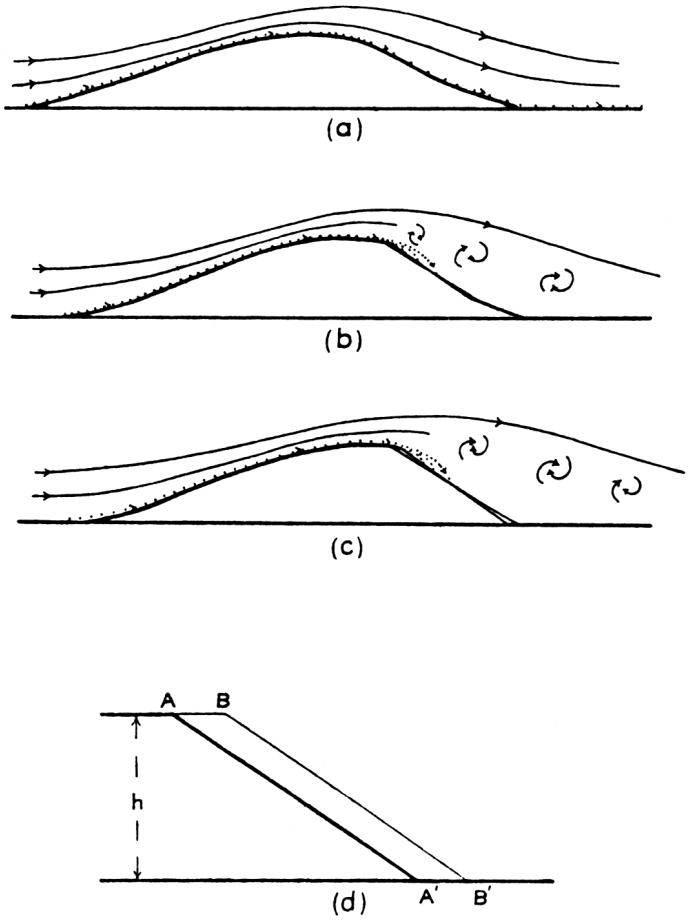

Figure 2.2: Formation of a slip face (*Bagnold*, 1941, Fig.71, p.202).

simple-wave equation is used to describe its migration:

$$\frac{\partial \eta}{\partial t} + c\,\frac{\partial \eta}{\partial x} = 0 \tag{2.2}$$

where c denotes the migration speed of the bedform. Combination of (2.1) and (2.2) yields

$$\frac{\partial q}{\partial x} - cc_b\frac{\partial \eta}{\partial x} = 0 \tag{2.3}$$

Integration of (2.3) over x leads to $q = cc_b\eta + q_0$, where q_0 is an integration constant. In the troughs the bed load transport rate is assumed to be equal to zero, so that the local bed load transport rate becomes a linear function of the vertical distance to the trough level η_b:

$$q = cc_b\,(\eta - \eta_b) \tag{2.4}$$

At the bedform crest, the vertical distance to the trough level equals the bedform height ($\eta - \eta_b = \Delta$ where Δ denotes the bedform height) and the local bed load transport rate equals q_{top}, so that (2.4) yields

$$c = \frac{q_{top}}{c_b\Delta} \tag{2.5}$$

which is equivalent to Eq. (3) in *Bagnold* (1941) and Eq. (3) in *Fredsøe* (1982). The transport rate averaged over the bedform equals

$$q_a = \frac{1}{\lambda}\int_0^{\lambda} q\,dx = cc_b\beta\Delta \tag{2.6}$$

where q_a denotes the bedform-averaged volume of bed load transport rate per unit width and time, and β the bedform shape factor, which is defined such that the mean bed level, η_a, is located at $\beta\Delta$ above the trough elevation, η_b:

$$\beta = \frac{\eta_a - \eta_b}{\Delta} \tag{2.7}$$

so that for triangular bedforms $\beta = \frac{1}{2}$.

The size-selective deposition over the lee face of a bedform and the effects of the variability in trough elevations are not incorporated in the above description, as the migration of an individual bedform dominated by bed load transport is determined

by the total[3] bed load transport rate. Nevertheless, the resulting formulation for the variation of the total bed load transport rate over a bedform has appeared a useful one and has been used in many studies (e.g., *Fredsøe*, 1982; *McLean et al.*, 1999). The above equations will be applied in the present study several times.

2.2 Flow over bedforms

Important early studies on the flow pattern over dunes are those by *Bagnold* (1941) and *Allen* (1965, 1984). They assess the complex flow structure over dunes (Figure 2.3): the geometrically induced flow acceleration over the stoss face, the growth of the boundary layer over the stoss face, the separation of the flow over the bedform crest, the resulting wake overlying the lee face and the trough zone, the associated return flow moving up the lee face, and the reattachment of the flow impinging on the stoss face of the next bedform. *Allen* (1965) experimentally found that the ratio of the horizontal distance between the bedform crest and the reattachment point, i.e. the point where the flow impinges onto the bed, to the bedform height was about 4.5-5.5, increasing with increasing bedform height and with increasing flow velocity over the bedform crest.

The above-mentioned features of flow over bedforms were also studied by, e.g., *Smith* (1970), *Bradshaw and Wong* (1972), *Fredsøe* (1982), *Nelson et al.* (1993, 1995) and *McLean et al.* (1994, 1996, 1999). *McLean et al.* (1994) found that flow features most important to the geometry of bedforms and the sediment transport over bedforms are the turbulence characteristics and the reattachment of the flow. The turbulence characteristics near the reattachment point induce a much higher sediment transport rate than expected from local mean shear stress. Also *Allen* (1965) mentions the high rate of turbulence in the reattachment zone, being the zone of maximum entrainment and active erosion. Figures 2.3 and 2.4 show the structure of a separating flow over a dune-like feature and a backward-facing step, respectively, both of which are very similar to the flow structure downstream of the crest of a natural dune.

Based on a set of detailed flume experiments, *McLean et al.* (1994) argue that, in non-uniform flow fields such as those over bedforms, it is inadequate to base predictions of sediment transport on the local mean shear stress, because the measured local sediment transport rates appeared rather related to the local statistics of the turbulent flow. Near the point of reattachment, measured transport rates were significantly greater than ones computed using sediment transport models derived for uniform flow and based on the local mean shear stress. The turbulent flow may in-

[3] summed over all size fractions

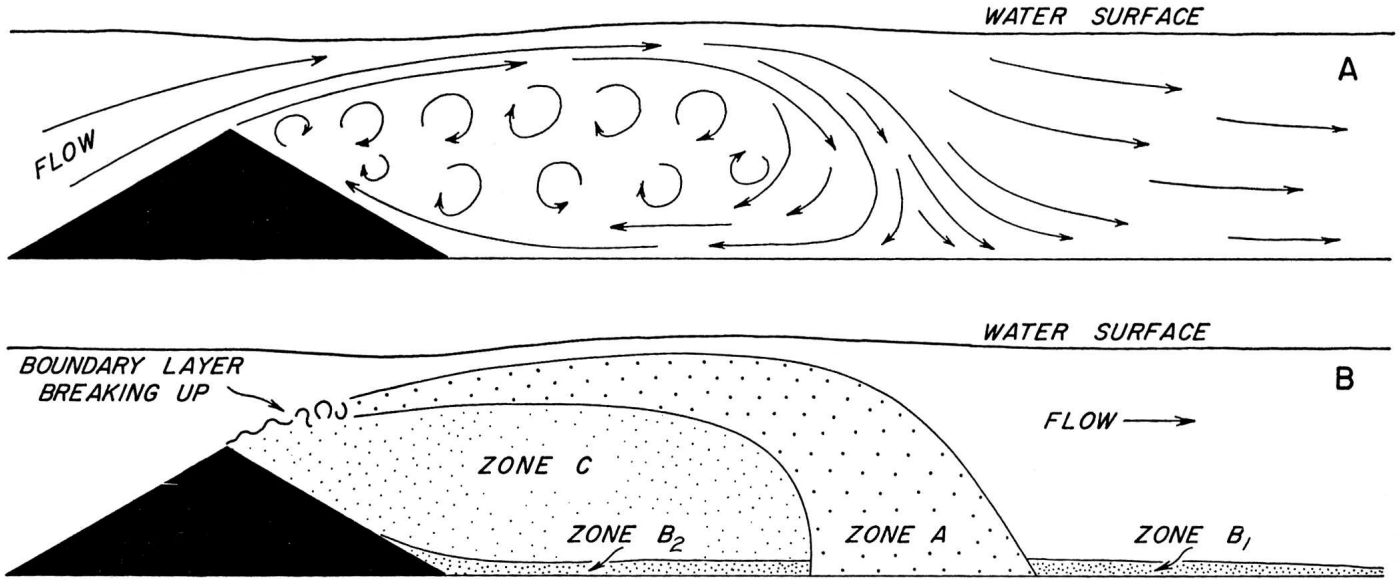

FIG. 4.—Generalized flow pattern round sand wave (see fig. 3, *A*, *C*). *A*, flow lines; *B*, small-scale turbulence structure zones

Figure 2.3: Flow structure downstream of a dune-like feature (*Allen*, 1965, Fig.4, p.99).

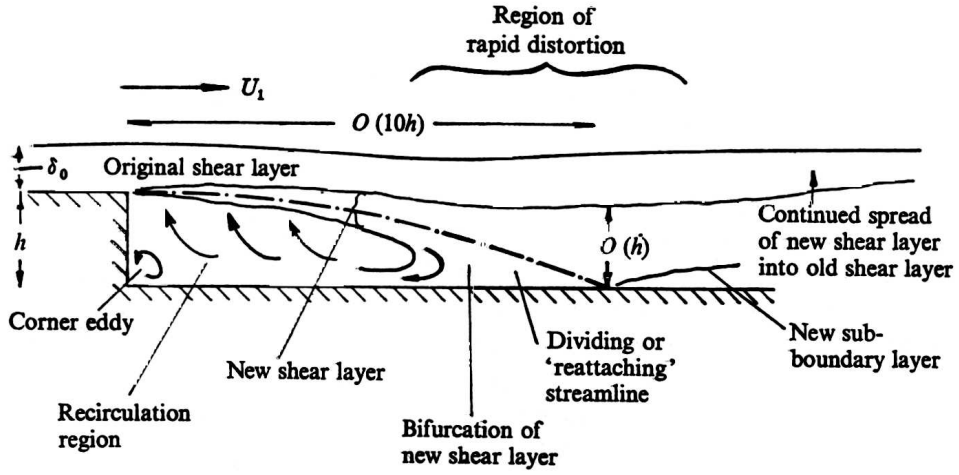

Figure 2.4: Flow structure downstream of a backward-facing step (*Bradshaw and Wong*, 1972, Fig.2, p.116).

duce sediment movement, while the mean velocity is well below critical conditions for incipient motion (*McLean et al.*, 1996). It was found that the spatial variation of the turbulence statistics over a bedform is considerable, as a result of the complex interaction between the overlying wake and the internal boundary layer.

In order to overcome this problem, *McLean et al.* (1999) propose a different method for predicting the sediment transport rate over bedforms for conditions dominated by bed load transport. They use a two-dimensional flow model for predicting the flow velocity at the bedform crest, where the effects of the overlying wake and turbulence field are minimal and conditions are close to being uniform. The near-bed velocity at the crest yields the local shear stress, which, using some type of bed load transport model, yields the local bed load transport rate. The variation of the bed load transport rate over the bedform can then be calculated from (2.4) and (2.5):

$$q = q_{top}\frac{\eta - \eta_b}{\Delta} \tag{2.8}$$

Bed load transport rates computed using this method were in good agreement with measured transport rates.

The flow pattern *through* a bedform has a significant influence upon the transport of contaminants or pollutants in rivers, since the transport of solutes is partially de-

termined by their intrusion into the river bed. Among others, *Bencala* (1984), *Elliott and Brooks* (1997a,b), and *Packman et al.* (2000) study to what extent and how solutes enter the bed, where and how long they are stored, and how and where they are released back into the water column. For ripple and dune conditions, *Elliott and Brooks* (1997a,b) consider solutes that do not react with or sorb to the sediment. They introduce the terms *pumping* and *turnover*, where pumping is defined as the flow through the bed induced by dynamic pressure variations over bedforms, and turnover as the release of water in the pores of the entrained sediment at the stoss face and the trapping of water in the pores of the deposited sediment at the lee face. The acceleration of the flow over bedforms and the flow separation at the bedform crest give rise to spatial pressure variations, which induce flow into the bed at the bedform stoss face and flow out of the bed at the downstream lee face and trough. *Elliott and Brooks* (1997a) propose a theoretical model describing the exchange of solutes through pumping and turnover for dunes and ripples. In a companion paper (*Elliott and Brooks*, 1997b), they present experimental results and compare those with results of the theoretical model.

Clearly, the mechanisms that induce an exchange of solutes between the flow and the bed surface or in the bed are very different from those that induce an exchange of sediment in the bed. Yet, the flow patterns within bedforms may have some effect on the sediment transport processes. The inflow of water into the stoss face may stabilise the sediment there, and the outflow out of the lee face destabilises that part of the bedform.

2.3 Grain size-selective deposition down the lee face

When a mixture of different grain sizes is transported over the bedform crest, *Bagnold* (1941) and *Allen* (1965) observed that coarser particles settle from the flow onto the lee face close to the crest or even slide over onto the lee face, whereas the very fines are taken along by the flow as suspended load and settle onto the lower parts of the lee face and the trough area. The path of a particle depends on the ratio between the flow velocity over the crest and the settling velocity of the grains (*Allen*, 1965). With increasing flow velocity, the sorting of the material settling from the flow onto the lee face (from coarse near the crest to fine near the toe) becomes less apparent. As described in Section 2.1, a wedge builds up at the upper part of the lee face, which continues until it becomes unstable. Suddenly, the mass of sediment avalanches down the lee face, resulting in a reverse sorting pattern (from fine near the crest to coarse near the toe), forming the foreset of the bedform. *Zanke* (1976) argued that a coarse grain rolls further down the lee face than a fine one (Figures 1.1 and 2.1), because (1) a coarse grain has a higher velocity when rolling down the lee face than a fine

one, due to its larger radius and thus larger weight per unit surface area, (2) a coarse grain experiences less friction in rolling down the lee face than a fine one, since a large grain rolls easier over small ones than a small grain over large ones, and (3) a coarse grain experiences less support to find a resting place than a fine one.

However, when a mass of grains, i.e. an avalanche, moves down the lee face, another mechanism dominates the size-selective deposition down the lee face. *Bagnold* (1941) and *Allen* (1965) observed that the finer particles in an avalanche filter down to the interface over which the avalanche is moving and the coarser particles are worked up to the surface of the avalanche. Due to shearing forces between the avalanche and the interface and within the avalanching mass, the finer particles move more slowly and become lodged more easily, whereas the coarser particles overtake the finer ones and move more easily to the toe of the lee face (*Bagnold*, 1941). *Kleinhans* (2002) argues that kinematic sorting and percolation are the dominant mechanisms in causing the coarse particles to move upward and the fines downward within the avalanche. Kinematic sorting and percolation occur through motion of sediment: the colliding grains make the pore space increase, so that fine grains move down and coarse ones up, irrespective of their weight.

For intermittent avalanches, the difference in mean grain size between the crest and the toe appeared to become less pronounced with increasing flow velocity (*Allen*, 1965). For intermittent avalanches, the sorting over the lee face was found to be stronger than for higher flow rates with continuous avalanches.

Kleinhans (2002) argues that in avalanches, besides the mechanisms mentioned above, an additional mechanism plays a role. An avalanche moving down the lee face produces a significant drag effect upon the previous avalanche deposit, out of which primarily the coarsest particles protrude. The avalanche preferably drags these protruding coarse grains down with it, thus increasing the vertical sorting trend within the bedform. This was confirmed experimentally, by studying the grain size-selective deposition down a delta lee face (*Kleinhans*, 2002), which will be discussed later in this section.

As mentioned above, very fine grains may be transported over the crest along with the flow as suspended load (*Allen*, 1965; *Jopling*, 1967; *Zanke*, 1976). From the wake overlying the lee and trough, these fine particles settle from suspension onto the toe of the lee face and onto the trough surface, forming a thin rippled layer, i.e. the toeset, over which the bedforms migrate (Figure 2.1). *Allen* (1965) observed that the fine particles deposited onto the trough surface may move along with the return flow toward the upstream lee face.

For a review of research in this field, reference is made to *Kleinhans* (2002). After previous researchers, he distinguishes the mechanisms of grain fall and grain flow, where grain fall refers to the settling of a grain from suspension onto the lee face or trough surface, whereas grain flow refers to a mass of grains or avalanche moving down the lee face. The mechanism of grain fall onto the lee face may result in the wedge at the upper lee face reaching its maximum angle of repose and, as such, it will initiate a grain flow down the lee face. Grain fall can also refer to a particle, after settling from suspension, moving down the lee face without interacting with other downward moving grains.

The pattern of grain size-selective sorting within bedforms and how this pattern is affected by changes in flow conditions were studied by *Willis* (1988), *Ribberink* (1987) and *Klaassen* (1990b, 1992). *Marion and Fraccarollo* (1997) measured the vertical sorting (formation of an armour layer) in conditions with alternate bars and antidunes, using a nondestructive sampling technique by freezing large bed elements in order not to disturb the bed. *Ribberink* (1983, 1987) conducted a set of experiments in a recirculating flume under uniform flow conditions with a mixture of two well-sorted sand fractions ($d_{50,1} = 0.78$ mm, $d_{50,2} = 1.29$ mm). The discharge was varied between the experiments. Figure 2.5 shows the sorting profiles of a number of samples taken in experiment E3. The pattern of downward coarsening is clearly recognised, and the thin coarse top layer is attributed to (1) size-selective entrainment on the stoss face forming a thin mobile armour layer and (2) the deposition of grains that were transported over the stoss face until the flow was turned off for the bed sampling session. Note that for elevations between 1.5 cm and 5 cm below the mean bed level, the bed composition becomes finer again. The less these bed levels have been disturbed by the flow, the more the composition becomes closer to the composition of the undisturbed bed material. A description of the experiments by *Klaassen* (1990b, 1992) will be given in the next sections.

Kleinhans (2002) recently conducted a set of experiments in which he studied the size-selective deposition over a delta lee face. A delta face is defined as a slope (at about the angle of repose) over which sediment is deposited when the water depth suddenly and largely increases, due to, for example, a river flowing into a deep lake or ocean. The results confirmed his hypothesis of a grain flow dragging coarse particles protruding from a previous grain flow deposit further down the lee face. *Kleinhans* showed that the downward coarsening trend becomes (1) less with increasing migration speed, (2) greater with increasing standard deviation of the mixtures, (3) slightly greater with increasing bedform height, and (4) slightly less with increasing discharge. The mechanism of size-selective deposition over the lee face of a delta is similar to size-selective deposition over the lee face of a river dune, but there are

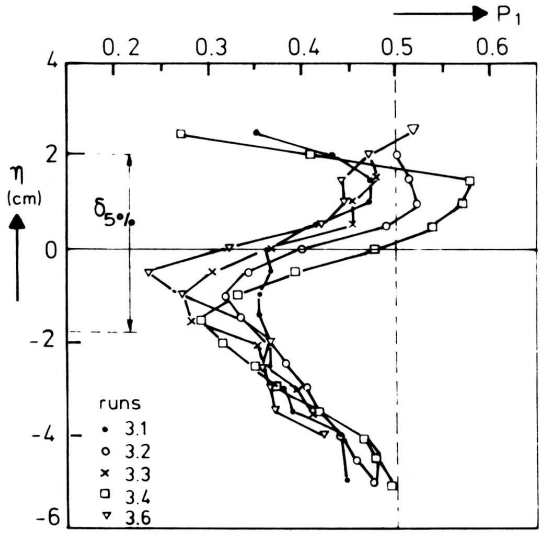

Figure 2.5: Variation over depth (relative to the mean bed level) of the volume fraction content of the fine size fraction within bedforms composed of two well-sorted sand fractions (*Ribberink*, 1987, Fig.3.14, p.45). The dashed line indicates the volume fraction content of the fine size fraction in the transported sediment. The range $\delta_{5\%}$ indicates the spectrum of bed surface levels for which 5% of the active bed levels is located above this range, and 5% below this range.

some differences (*Kleinhans*, 2002). For a dune, the effects of the wake overlying the lee and the trough (i.e. the return flow and turbulence effects) are stronger than for a delta. In addition, the flow over a delta crest is nearly uniform, whereas the flow over a dune crest is non-uniform due to flow acceleration over the stoss face. Because of these differences, *Kleinhans* expects the mechanisms of grain fall and toeset deposition by suspended fines for dunes to be less apparent than for a delta face.

Kleinhans (2002) also reviewed research on the sorting down a lee face of sediment mixtures composed of well-sorted sediment fractions that differ both in angularity (thus in angle of repose) and in grain size by, among others, *Makse et al.* (1997), *Makse* (1997), and *Koeppe et al.* (1997). As an instability between size and shape segregation, a stratified pattern develops that is very different from the commonly observed downward coarsening trend within bedforms. In the present study, this mechanism is left out of consideration.

2.4 Coarse bed layer below migrating bedforms

Studying sub-aerial dunes, *Bagnold* (1941) observed that a coarse bed layer may form underneath the migrating dunes. This was confirmed for sub-aqueous dunes by *Zanke* (1976) (Figure 2.1). The layer consists of particles that under the prevailing flow conditions are barely or not entrained by the flow. Such a coarse bed layer may develop in case of partial transport conditions, when a significant amount of coarse material does not or barely participate in the sediment transport processes. Coarse bed layers underneath migrating bedforms were also observed by *Willis* (1988), *Wilcock and Southard* (1989), *Klaassen* (1990b, 1992), and *Kleinhans* (2002).

Wilcock and Southard (1989) conducted experiments in a 23 m long recirculating flume, under uniform flow conditions. The bed developed into a coarse bed layer underneath migrating bedforms of finer material. Unfortunately, these authors did not measure the vertical sorting profile. Yet, their remarks increase our understanding of the behaviour of the coarse bed layer and its influence on the transport process. The coarse layer was called *'a partial static armor, wherein some individual grains become essentially immobile even though other grains in the same fraction remain in transport.'* They mention that *'size dependent vertical sorting can serve to concentrate these coarser grains on the bed surface over which the bedforms move'* and observed that at higher flows the coarse layer was eliminated by scour in the lee of the bedforms.

Wilcock and Southard (1989) emphasise the strong interaction among size-selective transport, the bedforms, and the vertical sorting. They underline the large influence of these three interacting factors on the equilibrium situation for the vertical sorting and the bed load transport. *Wilcock and Southard*: *'In our runs the processes leading to a coarse surface layer, which include the development of a partial static armor, vertical bed sorting, and bedform mining of coarse grains, produce a stronger coarse surface layer as* τ *increases, at least to the point where the coarse surface layer is entirely broken up by the intense flow in the lee of the bedforms.'* The time evolution of the composition of the transported sediment showed a decrease in the mobility of the coarse fractions as the system adjusted towards equilibrium. This was explained by the formation of a coarse bed layer, wherein some proportion of the coarse fractions find stable resting places and become essentially immobile. *Kleinhans* (2002) recently conducted a flume experiment under unsteady flow conditions and varying bedform heights. He was able to couple the elevations of resulting coarse bed layers to the elevations of the deepest troughs in each stage of the experiment.

Also *Klaassen* (1992) clearly observed the downward coarsening trend in migrating bedforms in experiments in a recirculating flume. In samples taken at bedform crests

only, the lower elevations of the active bed showed a clear coarsening compared to their initial composition. Yet, from the description it is not clear if this coarse sediment was essentially immobile, or took fully part in the transport process. The latter was the case in the experiments by *Ribberink* (1987). The downward coarsening trend in the bedforms was clearly identified and the lower elevations of the bedforms were coarse relative to their initial composition (Figure 2.5). Yet, this 'coarse layer' was not immobile but fully active, since flow conditions were well above the critical conditions for incipient motion of the two well-sorted sand fractions.

2.5 Statistics of trough elevations and bed surface elevations

The migration of bedforms over the river bed often results in stacked cross-sets, which is due to the large variation in bedform trough elevations (*Jopling*, 1967). Figure 2.6 shows a stacked cross-set measured by Leclair, who conducted a large set of experiments to study the migration of bedforms composed of non-uniform sediment (*Leclair*, 2000, 2002; *Leclair and Bridge*, 2001). Figure 2.6 illustrates the trough elevations of successive bedforms. The lowest lines indicate the bedforms with the deepest troughs, whereas the higher ones are formed by relatively small bedforms migrating through the flume shortly before the experiment was stopped. Since a migrating bedform induces the sediment above its trough elevation to be redistributed or reworked, the stochastic nature of these trough elevations obviously significantly influences both the vertical exchange of sediment particles in the active bed and its time scale. Besides a vertical scale, Figure 2.6 also shows a horizontal one, which tells something about the longevity of the deepest troughs. It suggests that their depths rapidly change, i.e. a deep trough remains deep only over a short distance. This seems to be confirmed by the study by *Jopling* (1967, Fig.1, p.288).

Studying the time evolution of the vertical sorting profile of tracer particles offers an excellent opportunity for studying sediment exchange processes in the bed without encountering the difficulties of grain size-selective entrainment and deposition. Important early work on the influence of the probability density function (PDF) of bed surface elevations on the vertical exchange of sediment in the active bed was done by *Crickmore and Lean* (1962a). They conducted a set of flume experiments with ripples, in which they studied the longitudinal and vertical dispersion of radio-active tracer particles in well-sorted fine sand (geometric mean grain size 0.18 mm, ranging from 0.1 to 0.3 mm). At the start of each experiment, at a tracer injection strip some distance from the upstream end of the reach, tracer particles were uniformly mixed with regular sediment over all bed elevations active under the prevailing flow conditions. At the upstream edge of the strip, only regular sand can be deposited, and more and more tracer particles are entrained and removed. Figure 2.7 shows the probability

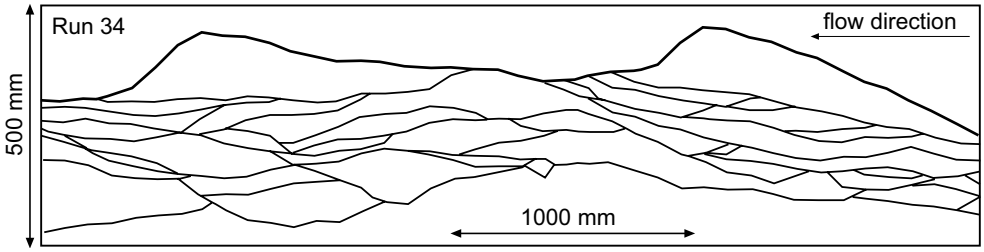

Figure 2.6: Observed stacked cross-sets in a flume experiment with non-uniform sediment (*Leclair*, 2002, Fig.8, run 34).

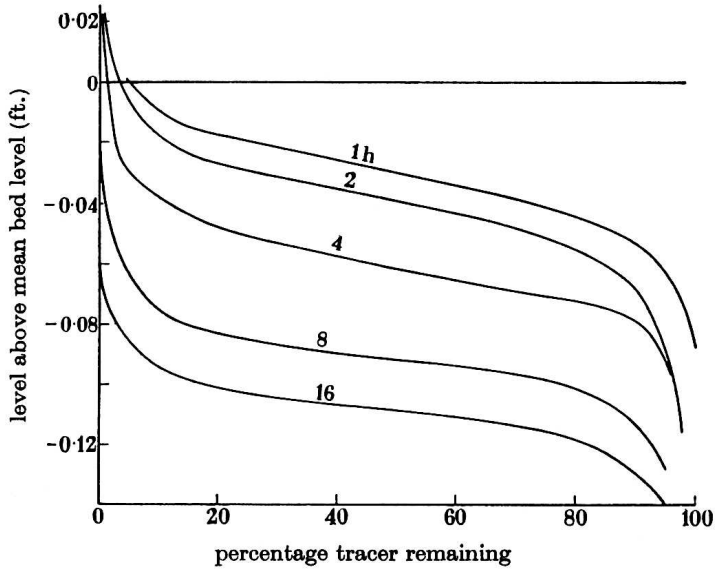

Figure 2.7: Measured probability distribution of remaining tracer particles in a flume experiment with ripples and 0.18 mm sand at the upstream edge of the tracer injection strip at various times (*Crickmore and Lean*, 1962a, Fig.10, p.418).

distribution of remaining tracer particles at the upstream edge of the tracer injection strip at various times. It illustrates that tracer particles are entrained from the upper bed elevations first. Gradually, also the lower bed elevations release their tracer particles when ripples with deeper trough elevations pass the strip. *Crickmore and Lean* (1962a) argue that, under these conditions of limited supply of tracer particles, the tracer particles will eventually be found primarily at the lower elevations of the active bed, since the occasionally deep trough elevations act as a sink for the particles.

Hubbell and Sayre (1964) conducted a similar set of experiments, both in a flume and in the field (also see *Galvin Jr* (1965) and *Hubbell and Sayre* (1965)). At the start of each experiment, a certain amount of tracer particles was released at the upstream end of the reach. Figure 2.8 shows the vertical distribution of tracer activity at various locations and times. The further below the bed surface, the smaller was the tracer concentration. This was attributed to the variation over depth of the probability density of bed surface elevations (*Crickmore and Lean*, 1962a; *Galvin Jr*, 1965). Namely, the tracer particles can only be deposited at these deep elevations in case the elevations are exposed to the flow, that is, in case the troughs of the ripples reach these elevations.

In the experiments by *Crickmore and Lean* (1962a), the PDF of bed surface elevations was approximately Gaussian. *Galvin Jr* (1965) argues that this non-uniform vertical distribution of bed surface elevations results in a non-uniform vertical distribution of tracer particles in the active bed, when assuming (1) particles to be transported only when they are exposed at the bed surface and (2) all exposed particles to have an equal probability of entrainment. Based on this rationale and the experimental results by *Crickmore and Lean* (1962a) and *Hubbell and Sayre* (1964), *Galvin Jr* (1965) believes that the proportion of tracer particles must decrease with decreasing bed elevation. He argues that a uniform distribution of tracer particles only occurs when each bed surface elevation is exposed to the same extent, like in a series of regular triangular bedforms.

However, the author can only agree with *Galvin Jr* (1965) when considering periods that are short compared to the time scale of vertical sediment exchange. For much longer periods and on condition that particles do not show any preference for certain elevations, the distribution of tracers is believed to gradually become uniform over the active bed. This behaviour is confirmed by *Hassan and Church* (1994).

Hassan and Church (1994) conducted a set of field experiments in which they measured the time evolution of the vertical sorting of non-uniform tracer particles in four gravel bed rivers. At the field sites, the ratio of the median grain size of the sur-

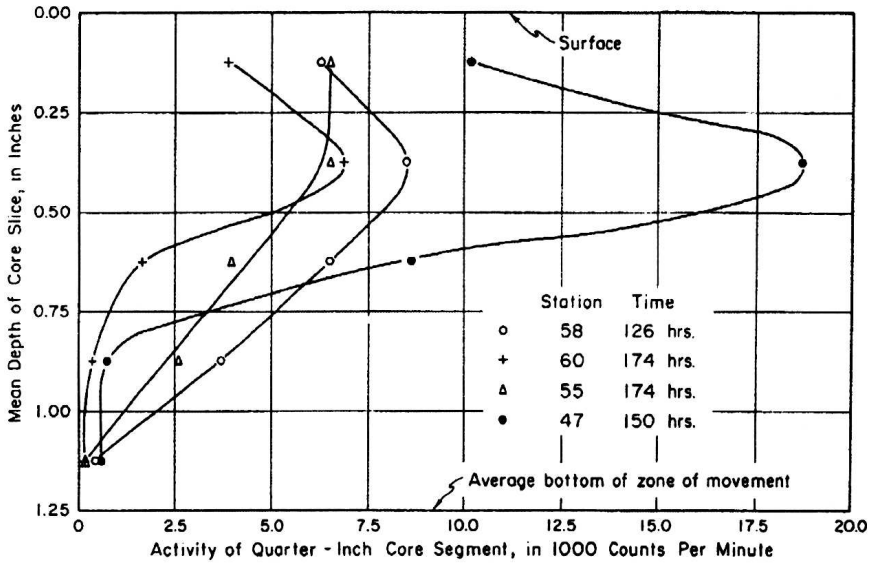

Figure 2.8: Measured vertical distribution of tracer activity in a flume experiment with ripples and 0.19 mm sand at various locations and times (*Galvin Jr*, 1965, Fig.15, p.175, which is based on Fig.8 in *Hubbell and Sayre* (1964)).

face layer to the one of the subsurface varied between 1.6 to 3, indicating the presence of an armour layer. At the beginning of each experiment, the tracer particles were located on the bed surface. After each flow event they were excavated and then reburied at the position at which they were found. There appeared to be no straightforward relation between burial depth and grain size. After a single flood event, the distribution of tracer particles appeared negatively exponential with depth. Yet, after a complete season, the vertical distribution was found to be more or less uniform. *Hassan and Church* (1994) developed two sorting models, describing the vertical sorting of tracer particles after a single flood and the vertical sorting after a series of floods, respectively (see Section 3.1).

For a mixture of two well-sorted sand fractions, *Ribberink* (1983, 1987) studied the influence of the variability in trough elevations on the vertical exchange of sediment in the active bed. Experiments were conducted in a recirculating flume under uniform flow conditions. *Ribberink* found that, since the deepest trough elevations are exposed to the flow only occasionally, the time scale of adaptation of their compo-

sition is relatively large. There was no immobile coarse bed layer below migrating bedforms, since conditions were well above the critical Shields stress for both size fractions. Figure 2.9 shows the transition phase between experiments E8 and E9. In both experiments and their transition phase, bedforms were present. The proportion of the coarse size fraction in the transported sediment was about 57% in E8 and 100% in E9. In the transition phase, instead of recirculating the transported material, sediment was fed to the system. In the first 30 flow hours, the amount of the coarse size fraction in the fed material was slowly increased from 55% to 100%. The markers indicate the bed elevations characterised by the volume fraction content of the fine size fraction being smaller than 2% above which the bed is almost completely coarse, at three times (after 50, 55, and 128 flow hours). The shaded areas indicate the bed material characterised by the volume fraction content of the fine size fraction being smaller than 2%, at the times of the bed sampling sessions. The figure shows how the coarsening slowly proceeds in the flow direction and that the coarse size fraction is gradually settling to lower and lower bed elevations, even though the bed is slowly aggrading. This slow exchange mechanism arises from occasionally deep troughs and the accompanying low bed elevations being only occasionally reached by the flow. These elevations therefore adapt very slowly towards the equilibrium sorting profile.

Wilcock and Southard (1989) emphasise the influence of the presence of a coarse surface layer on the variability in trough elevations: *'In the range of τ where both bedforms and a coarse surface layer exist, the coarse surface layer may serve to regulate the size and variability of the bedforms by limiting the depth of scour in the bedform troughs.'* The presence of a coarse layer below migrating bedforms will strongly decrease the variability in trough elevations, and it therefore reduces the vertical exchange of sediment from and to elevations below this coarse bed layer.

A better understanding of the complex interaction between the stochastic nature of trough elevations or bed surface elevations and the vertical sorting profile is an important requisite in further advances in morphological modelling of rivers with non-uniform sediment. As a first step, *Leclair and Blom* (2003) qualitatively analyse this interaction, based on flume experiments with bedforms, various sediment mixtures, and with or without the presence of an essentially immobile coarse bed layer below migrating bedforms. They underline that the interaction among the Shields parameter, the vertical sorting profile, and the PDF of bed surface elevations is strong and complex and that these three components cannot be considered independently of one another.

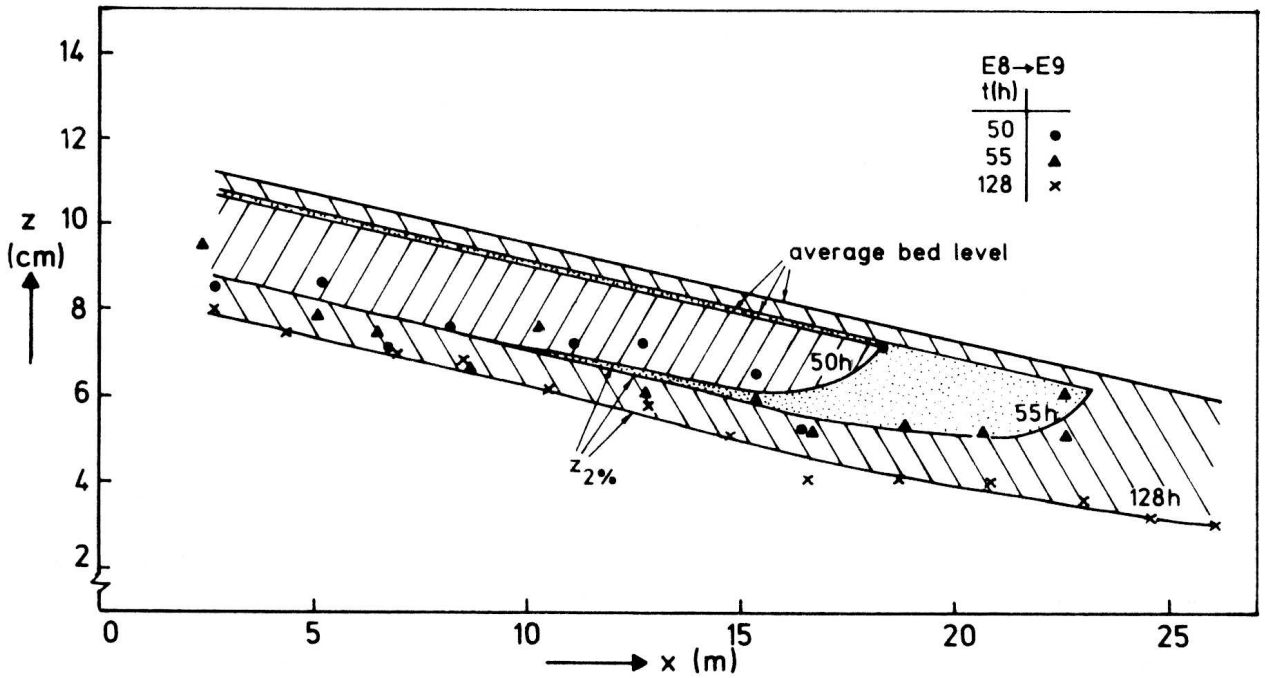

Figure 2.9: A transition experiment with two well-sorted sand fractions (*Ribberink*, 1987, Fig.6.11, p.114). The amount of the coarse size fraction in the sediment fed to the flume is increased from 55% to 100% in the first 30 flow hours. Bedforms migrate over a slowly aggrading bed. The markers indicate the bed elevations characterised by the volume fraction content of the fine size fraction being smaller than 2% above which the bed is almost completely coarse, at three times (after 50, 55, and 128 flow hours). The shaded areas indicate the bed material characterised by the volume fraction content of the fine size fraction being smaller than 2%, at the times of the bed sampling sessions.

2.6 Winnowing of fines from the troughs

Another mechanism that may affect the vertical sorting in bedforms is the winnowing or washing out of fines from between and below a coarse bed layer located at the trough elevations. This mechanism will be indicated as winnowing from the trough surface and subsurface. It was observed by *Willis* (1988), *Wilcock and Southard* (1989), and *Klaassen* (1986, 1990a) in experiments dominated by bedforms. When conditions of partial transport induce the formation of an essentially immobile coarse bed layer below migrating bedforms (Section 2.4), the entrainment of sediment from below the coarse layer will be severely hindered. Yet, though essentially immobile, this coarse bed layer is not impermeable and often not completely continuous. The winnowing of fines from the trough surface and subsurface can result in a net vertical flux of sediment.

Wilcock and Southard (1989) remark that: *'A coarse surface layer and bedforms coexist over a finite range of τ. When both are present, the coarse surface layer'* (underneath the migrating bedforms - A.B.) *'does not constitute the entire bed surface that is visible at any time, but is exposed only in the bedform troughs. The coarse surface layer is the surface on which, or through which, size-dependent exchange of grains occurs. As such, the coarse surface layer plays a role in determining the grain size distribution of the transported sediment and therefore of the bedforms.'*

Based on flume experiments (*Klaassen*, 1986), *Klaassen* (1990a, p.8) describes the entrainment of fine bed material from underneath a coarse layer (see Figure 2.10): *'During investigation M2061 it was observed that the instability of the armour layer was caused by small bedforms that developed on top of the armour layer. The material from which these bedforms were made of originated from underneath the armour layer and was sucked through this layer from underneath slightly unstable individual particles.'* Fines were winnowed from the trough surface and subsurface, resulting in a lowering of the coarse bed layer (Figure 2.10). *Klaassen* (1990a) describes how the coarse bed layer breaks up : *'The occurrence of bedforms initiated the breaking up of the armour layer. This was caused by the turbulence generated in the wake of the bedforms. The increased turbulence caused the momentary maximum shear stresses to increase and this caused increased instability of the armour layer downstream of the bedforms.'* Also *Willis* (1988) observed the processes of winnowing and a sinking coarse bed layer: *'With the passage of subsequent dune troughs, the gravel particles sank further until finally the gravel constituted a new layer at or even slightly below the deepest trough penetration of the dunes.'*

In flume experiments under plane-bed conditions and without upstream sediment input, also *Diplas and Parker* (1992) found that, when particles from the armour layer

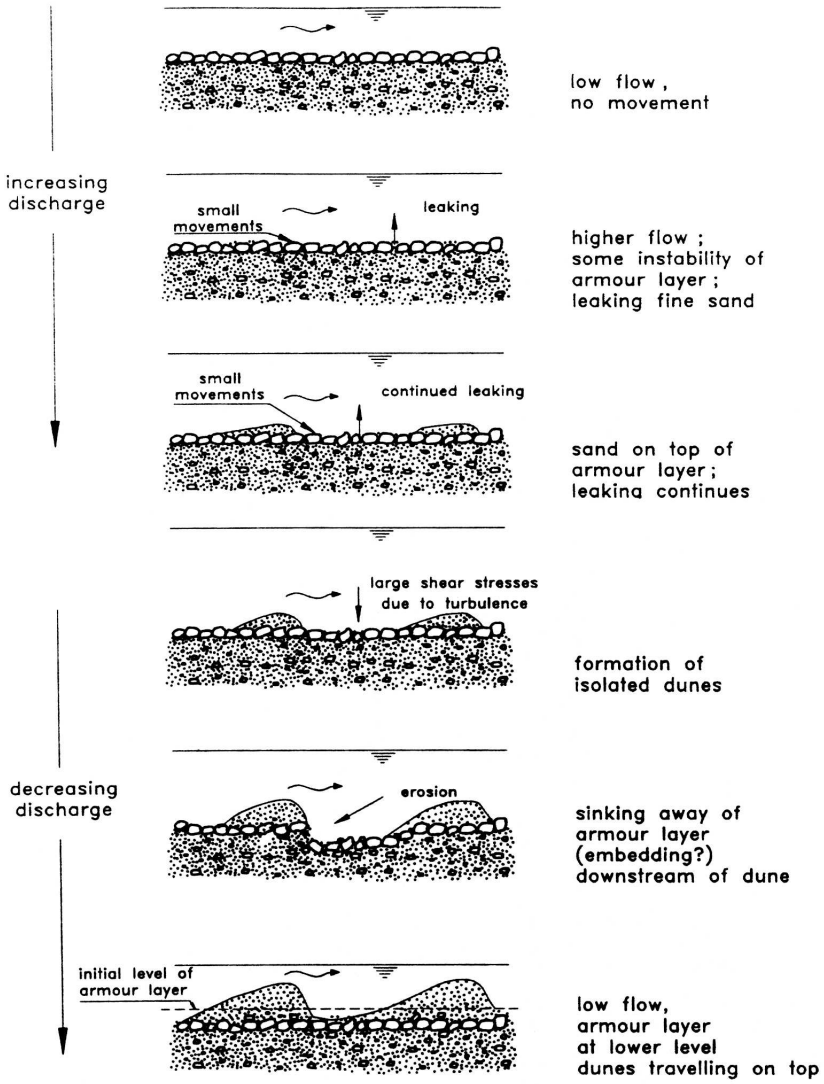

Figure 2.10: Behaviour of a coarse layer during a flood event (*Klaassen*, 1990a, Fig. 1.1, p.4).

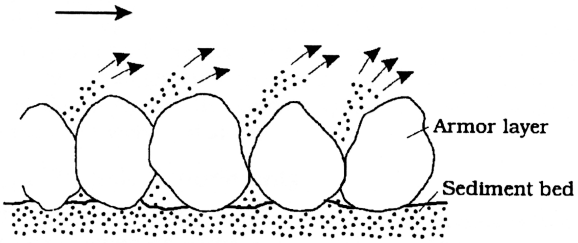

Figure 2.11: Washing out of fines from below an armour layer (*Sumer et al.*, 2001, Fig.1).

were slightly mobilised, fines were entrained from the subsurface (below the coarse armour layer). *Allan and Frostick* (1999) describe how bed surface particles can be disturbed by the intermittent effects of turbulent forces upon the bed surface. The probability to entrain the finer particles from surface pores is significantly higher than coarser particles, since finer particles have a smaller critical entrainment velocity and they are ejected to positions higher in the flow.

For scour protection around cylinders or pipelines, a widely used method is rock dumping on a sand bed. Usually, filters are used to prevent the base material below the rock or armour layer from being washed out. *Sumer et al.* (2001) study the entrainment of fine sediment from between armour stones in a plane-bed situation (Figure 2.11). They list relevant research in this field and studied the mechanism of entrainment in experiments. They found that a vortex forms in a hole between two stones in the armour layer and that this vortex is the key element in the entrainment of fines. The fines are swept into the vortex and are eventually put into the main body of the flow. Both the critical condition of entrainment and the time evolution of the lowering of the coarse layer appeared to be governed by the Shields parameter and the ratio of the grain size of the stones to the one of the fines. *Sumer et al.* propose a model for the critical condition of the entrainment of the base material and define a time scale for the lowering of the stone layer.

The author believes that the mechanism of entrainment induced by a vortex between stones as described by *Sumer et al.* (2001) is different from the mechanism that induces the winnowing of fines from the trough surface and subsurface downstream of a bedform crest. In the experiments by *Sumer et al.*, the ratio of the grain size of the stones to the one of the fines varied between 125-500 (fines 0.2 mm, stones 2.5-10 cm). For the mixtures of *Wilcock and Southard* (1989) and *Klaassen* (1990a), the ratio of some representative grain size of the sediment in the coarse bed layer to the grain size of

the fines was more than one order of magnitude smaller. As such, it seems that the vortex is not the dominant mechanism in the winnowing of fines from the trough surface and subsurface. As indicated by *McLean et al.* (1994), the author believes that the statistics of turbulent flow cause the high activity and high entrainment rates in the trough zones of the bedforms.

2.7 Discussion

2.7.1 Sorting through variability in trough elevations

Besides vertical sorting through grain size-selective deposition down a bedform lee face, the PDF of trough elevations (or bed surface elevations) plays an important role in the vertical redistribution of sediment and its time scale (*Crickmore and Lean*, 1962a,b; *Galvin Jr*, 1965; *Ribberink*, 1987). The likelihood of a certain bed elevation being exposed to the flow significantly affects the rate of entrainment from and deposition onto this elevation. That the statistics of the trough elevations indeed strongly influence (the time scale of) vertical sorting can also be understood by considering that a migrating bedform induces only the sediment above its trough elevation to be redistributed or reworked. The sediment below a bedform's trough elevation is not affected and is only reworked by less frequently occurring deeper troughs.

With respect to the statistics of trough elevations and bed surface elevations, the author believes that two factors are important in the vertical redistribution of sediment and its time scale:

- the amount of exposure to the flow of a certain bed elevation. For instance, a deeper elevation of the active bed is less exposed to the flow. Thus, the occasions in which sediment is entrained or deposited onto this level will be less, so that the time scale of adaptation of its composition is longer.
- the proportion of the bed covered with sediment at a certain bed elevation. For instance, at a deeper elevation in the active bed, more sediment is present. Thus, averaged over a large number of bedforms, more sediment needs to be exchanged to reach the same amount of change in composition. This increases the time scale of adaptation of the composition at a deeper elevation even more.

In order words, the deeper you go into the active bed, the more work needs to be done (in terms of amount of sediment exchange) and the smaller fraction of time is available for that work. Thus, both factors cause the time scale of adaptation of its composition to go up. Both factors need to be accounted for when modelling the vertical redistribution of bed material in sediment continuity models.

A still unexplored field of research is the interaction between the probability distribution of bed surface elevations, the vertical sorting profile, and the Shields parameter. This interaction is strong and very complex, which is corroborated by the fact that an essentially immobile coarse bed layer below migrating bedforms strongly decreases the variability in trough elevations. The coarse bed layer therefore reduces the vertical exchange of sediment in the active bed: sediment entrainment from and deposition onto elevations below the coarse bed layer is severely hindered. The strong interaction implies that we cannot consider the components independently from one another.

2.7.2 Winnowing and infiltration of fines

In Section 2.6, it was discussed that fines may be winnowed from the trough surface and subsurface due to the turbulent fluctuations in the reattachment zone. This leads to an increased porosity of the surface layer and the subsurface in the troughs. The author now hypothesises that, when considering a fixed location in a series of migrating bedforms, the porosity at the elevations of the troughs and just below fluctuates. The porosity increases when a trough zone approaches, while it decreases again when the next bedform migrates over this fixed location, inducing fines to infiltrate into the coarse bed layer. Yet, there is only indirect evidence for the occurrence of the winnowing of fines from and the infiltration of fines into the surface and subsurface of bedform troughs, since they have never been directly measured.

Under plane-bed conditions, the infiltration of fines into a framework of coarse sediment was studied by *Frostick et al.* (1984), *Diplas and Parker* (1992), and *Allan and Frostick* (1999). In a set of field experiments, *Frostick et al.* (1984) studied the infiltration of fines (1) into the bed surface and (2) further down to the subsurface. The first process was found to be related to the ratio of grain size and shape to pore size and the local turbulence intensity, whereas the second was controlled by only the ratio of grain size to pore size. Similar to *Frostick et al.* (1984), *Diplas and Parker* (1992) found that the depth of infiltration depends on the difference in grain size of the infiltrating fines and the coarse framework material, and on the Shields stress. When more fines are added, the fines saturate the subpavement, start appearing in the surface layer, and interact with the flow. Whether infiltration of fines also plays a role in bedform conditions has never been studied, so far. In flume experiments with two well-sorted size fractions (fine 0.66 mm and coarse 8.7 mm) under plane-bed conditions, *Allan and Frostick* (1999) found that, just before the moment of entrainment of the coarse particles, the coarse framework lifts and dilates, allowing the fines to move down into subsurface pores. It is not known whether framework dilation also occurs for more natural sediment mixtures.

2.7.3 Grain size-selective entrainment over the stoss face

Another feature that may affect the vertical sorting profile is grain size-selective entrainment and deposition over the stoss face. Little is known on this subject, since it is hard to measure the variation in entrainment and deposition rates over areas exposed to an accelerating flow. In case of non-uniform sediment, the entrainment and deposition is grain size-selective, which would complicate measurements even more. Moreover, during bedform migration the stoss face of a bedform is being eroded, which complicates measurements meant to be done at a specific stoss surface elevation.

Willis (1988) conducted a set of flume experiments in which he varied the proportion of gravel in a layer installed on top of a substrate composed of only sand. He found that with increasing flow more and more sand particles are washed out from around the gravel particles until either the gravel particles become buried at the base of the migrating bedforms, or the gravel particles become mobile, as well. The author believes that this mechanism also applies to relatively coarse particles that are located somewhere on the stoss face and cannot (or no longer, e.g., in case of a decreasing flow rate after a flood event) be transported by the flow. If fines are entrained from around and below the coarse particle, the coarse particle gradually settles as the bedform migrates, until it reaches the trough elevation. Note that in such a situation the coarse grain reaches the trough elevation without being transported over the bedform crest. This mechanism may also act upon coarse particles after being entrained in the trough zone due to the highly turbulent flow and then being transported up the stoss face for a short distance.

In two recently conducted sets of experiments, attention is paid to the relative importance of the sorting mechanisms discussed in the present chapter to the vertical redistribution of sediment within bedforms (see Chapter 4).

Chapter 3

Literature survey - Sediment continuity models

After describing previous research on sorting mechanisms that play a role in bedform conditions, the present chapter goes into existing sediment continuity models. A *sediment continuity model* is defined as a model that describes the complex interaction among the grain size-selective sediment transport, net aggradation or degradation, and the vertical sorting profile. Such a model is an essential part of morphological model systems for non-uniform sediment. For uniform sediment, the sediment continuity equation is the elementary mass balance, stating that divergences in the sediment transport rate result in net aggradation or degradation.

If the river bed is composed of a range in grain sizes and if vertical, lateral, or longitudinal sorting plays a role, we need to use a sediment transport model that is suitable for non-uniform sediment. The model needs to take into account (1) the proportion of each size fraction at the bed surface, (2) the fine size fractions in the mixture being more easily entrained and transported than the coarser ones, and (3) hiding-exposure effects. Hiding-exposure means the sheltering of fines in the lee of the coarse grains and the greater exposure of coarse grains than in uniform sediment of this grain size, due to their greater protrusion into the flow. Besides the need for a different type of sediment transport model, the model for sediment continuity becomes more complicated than the elementary mass balance. Besides divergences in the total sediment transport rate, also divergences in the transport rate of size fractions play a role. Furthermore, we need to take into account that the bed composition may vary over bed elevations (i.e. the vertical sorting profile). *Hirano* was the first to develop such a sediment continuity model (*Hirano*, 1970, 1971, 1972).

This chapter presents an overview of existing sediment continuity models for non-uniform sediment. Four types are distinguished:

- burial depth models
- bed layer models
- grain-scale models
- depth-continuous models

Burial depth models describe the time evolution of the movement of (tracer) particles (in uniform or non-uniform sediment) and their burial into the bed. Note that these models do not describe the interaction among the sediment transport rate, net aggradation or degradation, and the vertical sorting profile. Therefore, they cannot be called sediment continuity models, and cannot be used as such in a morphological model system. Nevertheless, they are discussed here, since they give useful insight into possibilities for modelling the redistribution of sediment in the active bed.

Bed layer models are sediment continuity models in which the bed is divided into a certain number of discrete bed layers. Each layer is assumed to be homogeneous and vertical sediment fluxes are assumed to occur only between the bed layers and between the top layer and the flow.

Grain-scale models are defined as sediment continuity models that consider sediment entrainment and deposition at the scale of grains, whereas the other types consider sediment exchange processes at a scale averaged over a large number of bedforms.

Depth-continuous models do not distinguish discrete bed layers. A probability density function of bed surface elevations is used to describe the active bed, i.e. the part of the bed that is exposed to the flow and thus subject to entrainment and deposition. Consequently, the bed composition and the (grain size-selective) vertical sediment fluxes are described at each elevation of the bed.

3.1 Burial depth models

For an overview of research in which the mechanisms of particle burial were studied, reference is made to Section 2.5. The present section presents an overview of existing models for the burial of (tracer) particles.

Pioneering work was done by *Crickmore and Lean* (1962a,b), who developed a two-layer and a three-layer model to describe the evolution of the vertical and longitudinal distributions of tracer particles in uniform sediment. The model was based on observations in a set of tracer experiments (see Section 2.5). Their rationale for introducing multiple bed layers was that sediment in the lower part of the active bed is entrained less frequently than in the upper part, since these lower bed elevations are exposed to the flow less frequently than the upper ones: *'A particle close to the limiting depth of movement in the ripples will have to wait for a long time before a ripple occurs in its vicinity which is deep enough to uncover it.'* (*Crickmore and Lean*, 1962b, p.33). The layers below the top layer represent the bed elevations reached by rela-

tively deep bedform troughs. Motion of particles is modelled using the Lagrangian method (*Einstein*, 1950) and occurs by a series of constant or arbitrarily distributed step lengths and exponentially distributed rest periods. In the model, motion of particles in the upper layer results in an exchange of particles between the layers. The proportions of tracer particles entrained from the upper and lower layers in their two-layer model, c_a and c_b, respectively, were simply set by the authors. The tracer particles entrained from the two layers are then mixed and return to the two layers in the ratio c_a to c_b.

Based on a set of tracer experiments (upstream release of uniform tracers in case of a rippled bed, flume and field experiments, see Section 2.5), *Hubbell and Sayre* (1964, 1965) developed a model that describes the horizontal displacement of tracer particles. Motion of particles occurs by a series of exponentially distributed step lengths and exponentially distributed rest periods. The model cannot be called a burial depth model, however, since the tracer particles are assumed to be uniformly distributed over depth at any time. Also *De Vries* (1966) proposes a model for the horizontal displacement of tracer particles without taking into account their vertical distribution.

Similar to the work by *Crickmore and Lean* (1962a,b), also *Schick et al.* (1987a,b) propose a conceptual model of two layers, a surface and a subsurface layer, in order to describe the evolution of burial of coarse tracer particles into the bed. *Schick et al.* (1987a) define the rate of burial b_r (e.g., 50%) as the amount of particles located at the bed surface (i.e. in the surface layer) that become buried (i.e. into the subsurface layer) after one flood event. The rate of exposure e_r (e.g., 20%) is defined as the amount of tracers reexposed by the second flood event after being buried by the previous flood event. The authors recommend relating the rate of burial to the flood event magnitude, the flood event frequency, the range of bed elevations exposed to the flow during a flood event, and the initial concentration of coarse particles in the active bed. Yet, they remark that the mechanisms of sediment exchange, as such, were not understood.

Hassan and Church (1994) developed a model describing the burial of tracer particles after a single flood event, in which they assume the distribution of the proportion of particles after displacement to be negatively exponential with depth (also see Section 2.5). After *Galvin Jr* (1965), they argue that after a single flood event the vertical distribution of tracer particles must be related to the probability of a bed elevation being exposed to the flow. Deep bed elevations are exposed only during high flows and for relatively short time periods, whereas the probability of particle exchange between bed elevations close to the surface is much higher. The agreement of the model results with field data for single flood events is promising.

Besides a model for single flood events, *Hassan and Church* (1994) also developed a model describing the burial depth of tracer particles after a series of discrete flood events. The mean bed level is assumed to be steady (i.e. no large-scale aggradation or degradation). After the first flood event, the distribution of tracers is assumed to be negatively exponential with depth, equal to the burial depth model for a single flood event. In the subsequent flood events (of equal magnitude), the proportion of particles at a certain bed elevation that move to a different elevation has a similar negatively exponential distribution, since they assume that the vertical exchange of particles depends on the elevation's likelihood of being exposed to the flow. The particles that move from this elevation are distributed over all active elevations according to the same distribution. After multiple flood events, the computed distribution of tracer particles over the active bed elevations is very different from the distribution after a single flood event. The larger the number of flood events, the more uniform the distribution of tracer particles becomes. This agrees well with *Hassan and Church*'s burial depth data of Carnation Creek over the periods 1990-1991 and 1991-1992 (Section 2.5). The model does not incorporate grain size-selective entrainment or deposition.

As mentioned before, burial depth models describe the time evolution of the burial depth of tracer particles or specific size fractions, but they do not describe the interaction among (1) (the tracer concentration in) the sediment transport, (2) the vertical distribution of tracer particles, and (3) net aggradation or degradation. As such, they cannot be applied as sediment continuity models in morphological model systems.

3.2 Bed layer models

3.2.1 The Hirano active layer model

Pioneering work was done by *Hirano* (1970, 1971, 1972), who was the first to develop a sediment continuity model for non-uniform sediment. He divided the bed into a homogeneous top layer, i.e. the active layer, and a non-moving homogeneous substrate (Figure 3.1). The active layer is defined as the part of the bed that is involved in the sediment transport process or, in other words, the part of the bed that interacts with the flow and that determines the rate and composition of the transported sediment. Considering plane-bed conditions, *Hirano* assumed the thickness of the active layer to be equal to the maximum grain size in the mixture. This subject matter will be addressed in more detail in Section 3.2.4.

In case of net aggradation, a sediment flux occurs from the active layer to the substrate through a rise in the interface between the active layer and the substrate. In

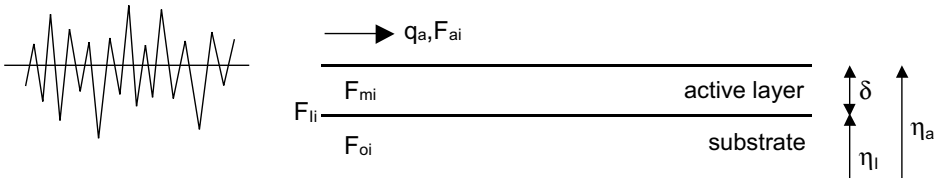

Figure 3.1: The active layer model of *Hirano* (1971), after his Figure 2, p.194.

case of net degradation, the bed surface and the interface between the active layer to the substrate will lower, which induces a sediment flux from the substrate to the active layer. Sediment from the substrate cannot be entrained by the flow directly, only after being entrained into the active layer.

In the active layer model in Figure 3.1, continuity of sediment is guaranteed if

$$\begin{aligned} c_b \Big[& F_{mi}(x, t+\Delta t)\, \delta(x, t+\Delta t) - F_{mi}(x,t)\, \delta(x,t) + \\ & F_{Ii}(x,t) \Big(\eta_I(x, t+\Delta t) - \eta_I(x,t) \Big) \Big] \Delta x = \\ & - \Big[F_{ai}(x+\Delta x, t)\, q_a(x+\Delta x, t) - F_{ai}(x,t)\, q_a(x,t) \Big] \Delta t \end{aligned} \tag{3.1}$$

where, for simplicity, the width is assumed to be uniform and the sediment concentration in the bed ($c_b = 1 - \lambda_p$) is assumed to be steady and uniform. δ denotes the thickness of the active layer, η_I the elevation of the interface between the active layer and the substrate, F_{mi} the volume fraction content of size fraction i in the active layer, F_{Ii} the volume fraction content of size fraction i at the interface between the active layer and the substrate, F_{ai} the volume fraction content of size fraction i in the transported material, and q_a the volume of sediment transport per unit width and time. All parameters are averaged over some horizontal distance, e.g., a large number of bedforms.

Eq. (3.1) can be written as

$$c_b \frac{\partial F_{mi}\, \delta}{\partial t} + c_b\, F_{Ii}\, \frac{\partial \eta_I}{\partial t} = - \frac{\partial F_{ai}\, q_a}{\partial x} \tag{3.2}$$

where

$$F_{Ii} = \begin{cases} F_{mi} & \text{aggradation} \\ F_{oi} & \text{degradation} \end{cases} \tag{3.3}$$

where F_{oi} denotes the volume fraction content of size fraction i in the substrate. *Hirano* (1972) compared results of his active layer model with results from flume experiments for the case of a partial flow constriction, and found reasonable agreement.

3.2.2 Additions to the Hirano active layer model

Since a sediment continuity model for non-uniform sediment is indispensable when modelling grain size-selective processes (e.g., armour layer, downstream fining, and sorting in river bends), the Hirano active layer model has been applied, analysed, and/or adapted by many researchers. Some early users were *Thomas and Prasuhn* (1977), *Bennett and Nordin* (1977), *Deigaard and Fredsøe* (1978), *Karim and Holly* (1986), *Park and Jain* (1987), *Ribberink* (1987), *Armanini and Di Silvio* (1988), and *Rahuel et al.* (1989). A number of additions have been proposed:

- introduction of a term in the sediment continuity equation describing the time evolution of the storage of sediment in a thin bed load layer on top of the active layer (*Armanini and Di Silvio*, 1988; *Parker*, 1991a; *Di Silvio*, 1992a,b), see below;
- introduction of a formulation for suspended load transport (*Armanini and Di Silvio*, 1988; *Holly Jr and Rahuel*, 1990; *Di Silvio*, 1992a,b);
- introduction of a formulation for particle abrasion to study the role of both size-selective sediment transport and abrasion in downstream fining in rivers (*Parker*, 1991a,b);
- introduction of a formulation accounting for the spatial and/or temporal lag of the actual bed load transport to the equilibrium bed load transport capacity (*Rahuel et al.*, 1989; *Holly Jr and Rahuel*, 1990; *Li*, 1995; *Pender and Li*, 1996), see below;
- modifications to the composition of the depositional flux to the substrate (*Parker*, 1991a,b; *Hoey and Ferguson*, 1994; *Toro-Escobar et al.*, 1996), see below;
- introduction of an additional layer below the active layer in order to take into account occasional vertical exchange of size fractions induced by occasionally deep bedform troughs (*Ribberink*, 1987; *Di Silvio*, 1992a,b), see Section 3.2.3;
- subdivision of the non-moving substrate into different layers for bookkeeping purposes (*Duizendstra and Flokstra*, 1998a,b; *Sloff et al.*, 2001).

Armanini and Di Silvio (1988) and *Parker* (1991a) introduced a term in the sediment continuity equation describing the time evolution of the storage of sediment in a

thin bed load layer on top of the active layer. However, when applying the adapted sediment continuity equation, they neglected the term, arguing that the amount of sediment stored in the bed load layer is small compared to the amount stored in the bed. Then, the thickness of the bed load layer remains relevant only to the modelling of suspended load transport, since the top of the bed load layer then represents the interface between the part of the stream where transport occurs through primarily suspended load and the lower part of the stream where transport occurs through primarily rolling, gliding, and saltation of the particles (bed load transport). Section 3.2.4 will address the different methods for defining the thickness of the bed load layer.

For non-equilibrium conditions, *Bell and Sutherland* (1983) and *Philips and Sutherland* (1989) argue that the bed load transport capacity is not instantaneously satisfied, which is due to the time required for the bedform geometry and bed roughness to adapt to the new hydraulic conditions. This results in an asymptotic approach of the actual bed load transport rate to the equilibrium bed load transport capacity. To take into account the spatial lag in the bed load transport to its equilibrium capacity, they developed a so-called loading law, which was introduced into the active layer model by *Rahuel et al.* (1989) and *Holly Jr and Rahuel* (1990). *Li* (1995) includes a formulation taking into account the spatial and temporal lag between the bed load transport rate and the bed load transport capacity (*Philips and Sutherland*, 1990), as well as a description for suspended load transport as proposed by *Holly Jr and Rahuel* (1990) (also see *Pender and Li*, 1996). *Li*'s model was tested to the hypothetical trench filling case of *Armanini and Di Silvio* (1988) and the bed armouring experiment by *Tait et al.* (1992).

The bed layer models by *Parker* (1991a,b), *Hoey and Ferguson* (1994), and *Toro-Escobar et al.* (1996) were developed especially for studying the mechanism of downstream fining, i.e. the gradual or more sudden decrease in grain size of the river bed material in downstream direction of the river. Besides the introduction of the bed load layer, the schematisation by *Parker* (1991a,b) differs from the active layer model in another aspect. Studying depositional processes in case of downstream fining, *Parker* suggests two alternatives for the composition of the flux through the interface, F_{Ii}, for cases with net aggradation: (1) the bed load material is worked down to the substrate ($F_{Ii} = F_{ai}$), e.g., due to a migrating avalanche lee face, or (2) material from the active layer is worked down to the substrate ($F_{Ii} = F_{mi}$), following *Hirano*. Studying the role of size-selective transport and abrasion in downstream fining in the Red Deer River in Alberta, Canada, *Parker* (1991b) shows that the first alternative ($F_{Ii} = F_{ai}$) prevents downstream fining during continuous aggradation. Therefore, *Hoey and Ferguson* (1994) generalise *Parker*'s formulation for F_{Ii} by using a weighing

coefficient:

$$F_{Ii} = \begin{cases} (1-\chi)F_{mi} + \chi F_{ai} & \text{aggradation} \\ F_{oi} & \text{degradation} \end{cases} \tag{3.4}$$

in modelling downstream fining in the Allt Dubhaig, Scotland. Based on flume experiments in which downstream fining was studied (*Seal et al.*, 1997), *Toro-Escobar et al.* (1996) found that $\chi = 0.7$, which indicates that the material transferred to the substrate is biased towards the composition of the bed load, but still coarser than the bed load. *Cui et al.* (1996) apply this result to two other experiments and found good results without any fitting of the model to the data. Nevertheless, *Toro-Escobar et al.* (1996) warn that their result, $\chi = 0.7$, should not be assumed to be generally valid, since it was only verified under conditions for which it was derived. They argued that probably also (1) the ratio of d_i/d_m, where d_i denotes the grain size of size fraction i and d_m the geometric mean grain size of the bed surface, and (2) the bed shear stress based on the d_m play a role in the transfer of sediment to the substrate (also see *Di Silvio and Marion*, 1997).

Mathematically analysing the set of equations of the Hirano active layer model, *Ribberink* (1987) found that the two characteristic celerities of the set of equations may become complex in case both degradation occurs and the substrate is finer than the active layer. The set of equations then becomes elliptic and cannot be solved without boundary conditions at all boundaries of the space-time domain. Yet, knowledge of future time-boundary conditions is physically unrealistic. The problem seems to be related to the oversimplified description of the bed as a homogeneous active layer and a substrate with their instantaneous mixing mechanisms. *Ribberink* (1987) hypothesises that in reality, while sediment from the fine substrate is picked up, coarse sediment settles to the substrate. The active layer model does not account for this type of sediment exchange between the active layer and the bed material underneath. The problem was reduced by introducing a sediment exchange mechanism related to occasionally deep bedform troughs, using an additional layer below the active layer. This will be explained in the next section. *Sieben* (1997) proposes three methods to avoid ellipticity of the set of equations of the Hirano active layer model: (1) limit the active layer thickness to a critical value, or (2) adjust the active layer thickness to changing flow conditions, or (3) use a sediment transport model in which the bed load transport does not instantaneously adapt to changing flow conditions.

For book-keeping purposes, *Duizendstra and Flokstra* (1998a,b) and *Sloff et al.* (2001) divide the non-moving substrate into multiple layers. In this way, the model system registers and remembers the composition of previously deposited sediment, which is

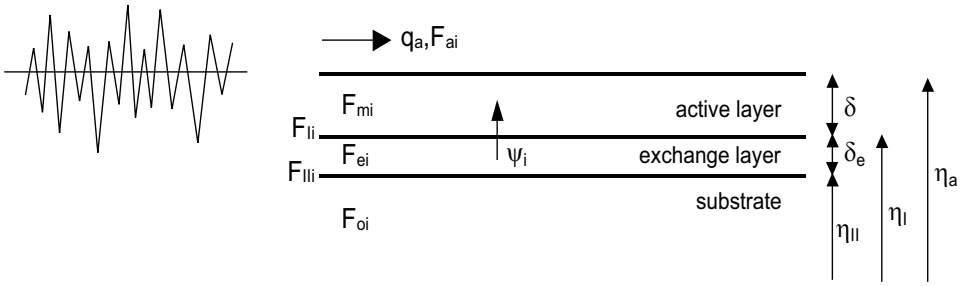

Figure 3.2: The two-layer model of *Ribberink* (1987).

obviously important in situations when degradation follows aggradation. The bookkeeping procedure proved to make the model system more robust.

3.2.3 Sorting other than through net aggradation or degradation

It is important to note that vertical sediment fluxes in the above sediment continuity models are all related to situations with net aggradation or degradation. From the observations discussed in Chapter 2, we know that the migration of regular bedforms[1] in itself will cause sediment to become redistributed over the active bed. The grain size-selective deposition down a bedform lee face results in a downward coarsening trend within bedforms, even in situations without net aggradation or degradation. Another mechanism that affects the vertical sorting is the variability in bedform trough elevations over a series of irregular bedforms (also see Section 2.5).

In flume experiments with bedforms and two well-sorted sand fractions, *Ribberink* (1987) observed that relatively deep troughs in a series of irregular bedforms lead to a vertical exchange of sediment between the upper active layer and deeper bed layers that are less exposed to the flow. This exchange mechanism induces the size fractions to become redistributed over bed elevations even in situations without net aggradation or degradation. Similar to the work by *Crickmore and Lean* (1962a,b), *Ribberink* (1987) introduces an additional layer into the active layer model, i.e. the exchange layer, in order to account for the effects of the variability of trough elevations (Fig. 3.2). Sediment continuity for the active layer and the exchange layer then

[1]Vertical sorting through bedform migration is here defined as vertical sorting through both grain size-selective deposition down a bedform lee face and the variability in trough elevations.

yields

$$\frac{\partial F_{mi}\delta}{\partial t} + F_{Ii}\frac{\partial \eta_I}{\partial t} = \psi_i - \frac{\partial F_{ai} q_a}{\partial x} \tag{3.5}$$

$$\frac{\partial F_{ei}\delta_e}{\partial t} + F_{IIi}\frac{\partial \eta_{II}}{\partial t} - F_{Ii}\frac{\partial \eta_I}{\partial t} = -\psi_i \tag{3.6}$$

where

$$F_{Ii} = \begin{cases} F_{mi} & \text{aggradation} \\ F_{ei} & \text{degradation} \end{cases}$$

$$F_{IIi} = \begin{cases} F_{ei} & \text{aggradation} \\ F_{oi} & \text{degradation} \end{cases}$$

where δ_e denotes the thickness of the exchange layer, F_{ei} the volume fraction content of size fraction i in the exchange layer, F_{Ii} the volume fraction content of size fraction i at the interface between the active layer and the exchange layer, and F_{IIi} the volume fraction content of size fraction i at the interface between the exchange layer and the substrate.

For the derivation of the vertical exchange term ψ_i, reference is made to *Ribberink* (1987). It consists of two components: one representing the total amount of sediment deposited in occasionally deep troughs, D_t, and a component representing the total amount of sediment entrained from these deep bedform troughs, E_t. In other words, D_t denotes the total deposition rate from the active layer into the exchange layer ($D_t = \sum_i^N D_{ti}$, where N denotes the total number of size fractions) and E_t denotes the total entrainment rate from the exchange layer into the active layer ($E_t = \sum_i^N E_{ti}$). It is assumed that the total entrainment rate equals the total deposition rate ($E_t = D_t$), independent of whether there is net aggradation or degradation. The sediment exchange is considered a process taking place on a time scale much smaller than morphological changes and is therefore assumed to be independent of net aggradation or degradation. The exchange term does have a net effect, however, since the sediment that is picked-up generally has a different composition than the deposited sediment:

$$\psi_i = E_{ti} - D_{ti} = \gamma_t \frac{q_a}{\lambda_a}\left(F_{ei} - F_{miD}\right) \tag{3.7}$$

where λ_a denotes the average bedform length, γ_t a proportionality factor depending on the subdivision between the active layer and the exchange layer ($\gamma_t \approx 0.06$), and F_{miD} the volume fraction content of size fraction i in the sediment deposited from the active layer into the exchange layer. This sediment deposited from the active layer into the exchange layer is assumed to be somewhat coarser than the average

composition of the active layer, because of the downward coarsening trend within the bedforms. For a mixture of two well-sorted sand fractions, *Ribberink* found that the volume fraction content of the *finest* fraction deposited from the active layer into the exchange layer is about 70% of that in the active layer:

$$F_{m1D} \approx 0.7 F_{m1} \tag{3.8}$$

Since there were only two size fractions, the volume fraction content of the coarse size fraction deposited from the active layer into the exchange layer logically equals

$$F_{m2D} = 1 - F_{m1D} \tag{3.9}$$

Note that (3.8) and (3.9) only apply to *bi-modal mixtures*. *Ribberink* did not develop formulations for the grain size-specific deposition flux from the active layer to the exchange layer, F_{miD}, for mixtures of more than two size fractions.

Mathematical analysis of the two-layer model indicated that the elliptic character of the set of equations (see Section 3.2.2) is not eliminated completely (*Ribberink*, 1987). Yet, the probability of becoming elliptic is significantly smaller than for the active layer model, since the two-layer model generally tends towards a situation in which the mean grain size in the active layer is smaller than in the exchange layer.

Ribberink (1987) experimentally verified the Hirano active layer model and the Ribberink two-layer model by comparing the computed time evolution of both the vertical sorting profile and the bed load transport composition to measured ones. The Hirano active layer model appeared incapable of describing the slow adaptation of the composition of the substrate and the bed load transport composition. Moreover, its set of equations often became unstable, which *Ribberink* attributed to its tendency of becoming elliptic.

Also *Armanini* (1995) recognised that vertical sediment fluxes need not be related to the occurrence of net degradation and aggradation. *Armanini*'s depth-continuous model for sediment continuity will be described in Section 3.4.

3.2.4 Active layer thickness

The active layer in *Hirano*'s sediment continuity model is considered as the part of the bed that interacts with the flow and that may supply sediment to the transport process. As such, the active layer determines the rate and composition of the transported sediment. In Section 2.5, it was argued that this part of the bed is better de-

scribed in stochastic, rather than in deterministic terms[2]. Nevertheless, in the bed layer models described in the previous sections a deterministic description is used. Section 3.4 will address sediment continuity models in which the active bed is considered in stochastic terms.

Obviously, the thickness of the active layer is related to the roughness of the bed surface and the part of the bed that is exposed to the flow. In plane-bed conditions, the active layer thickness is typically chosen equal to some coarse grain size in the mixture (e.g., $\delta = d_{90}$). In conditions with bedforms, the active layer thickness is typically related to the average bedform height, e.g., $\delta = 0.5\,\Delta$ (*Ribberink*, 1987; *Armanini and Di Silvio*, 1988; *Parker*, 1991a). For an overview of definitions of the active layer thickness, reference is made to *Kelsey* (1996). *Rahuel et al.* (1989) and *Holly Jr and Rahuel* (1990) distinguish between situations of net degradation and aggradation when defining the appropriate active layer thickness. For degradational areas and conditions with bedforms, they follow a bedform height model which is often coupled to the water depth:

$$\delta = c_h\, h \tag{3.10}$$

where c_h is a constant ($0.10 \leq c_h \leq 0.20$) and h denotes the average water depth. When the degradational area is characterised by an armour layer, they follow *Borah et al.* (1982a)'s definition of the active layer thickness:

$$\delta = \frac{1}{c_b} \frac{d_n}{\sum_{i=n}^{N} F_{mi}} \tag{3.11}$$

where d_n indicates the smallest grain size not transported by the flow. For aggradational areas, *Rahuel et al.* (1989) and *Holly Jr and Rahuel* (1990) define the active layer thickness as the thickness of the current deposit, limited to the maximum thickness as defined for degradational cases.

The thickness of the *bed load layer* is often made a function of the water depth (e.g., *Armanini and Di Silvio*, 1988; *Pender and Li*, 1996). *Garcia and Parker* (1991) discuss several possibilities for defining the thickness of the bed load layer: e.g., as a function of water depth, of grain size, or of bedform height, or equal to the height of particle saltations. As mentioned above, the thickness of the bed load layer is relevant only to the description of suspended load transport.

[2] *Sieben* (1997) pointed out that the active layer, defined for the determination of a representative grain size for the bed surface, cannot be interpreted purely physically. He suggested that, therefore, the active layer is better called a *reference layer*.

In the two-layer model by *Ribberink* (1987), the bed layer below the active layer, i.e. the *exchange layer*, represents the bed elevations that are reached by occasionally deep bedform troughs. For his flume experiments, *Ribberink* defined the exchange layer thickness, δ_e, to be the following function of the active layer thickness, δ : $\delta_e = 1.22\,\delta$.

3.3 Grain-scale models

Borah et al. (1982a,b) developed a grain-scale model for sediment continuity, describing the behaviour of sediment mixtures at a scale smaller than the previously described models. Nevertheless, their model is briefly addressed here, since it may lead to a better understanding of the entrainment processes that play a role in modelling sediment mixtures. *Borah et al.*'s model describes how the entrainment of grains from the bed surface exposes the underlying grains to the flow, making the latter available for entrainment. First, the finest grains are entrained from the bed surface, then somewhat coarser grains with their underlying finer grains, subsequently grains again somewhat coarser with their underlying finer grains, and so on. *Borah et al.* (1982b) apply the model to two flume experiments and two field experiments. The model can only be applied when some size fractions remain immobile. The grain-scale model by *Tsujimoto and Motohashi* (1990) resembles *Borah et al.*'s model at the point of particle entrainment. In case of net degradation, in both models newly exposed elevations are assumed to have the same composition as the substrate.

3.4 Depth-continuous models

Armanini (1995) was the first to leave the concept of discrete bed layers. He realised that the discrete active layer is an oversimplification of reality and that this zone of finite thickness where instantaneous and complete mixing occurs does not exist. Besides, *Armanini* recognised that additional vertical sediment fluxes occur that were not incorporated in existing bed layer models. *Armanini*'s depth-continuous model describes the vertical exchange of sediment and the composition of the bed material at each bed elevation. The process of vertical sediment exchange is modelled as a diffusion process. According to *Armanini*, the vertical diffusion coefficient is related to the bedform migration speed, represented by the shear velocity, and the bedform height. For simplicity, in calibrating the model, *Armanini* assumes the vertical diffusion coefficient to be a linear function of the shear velocity, the mean grain size d_m, and a calibration constant. The diffusion coefficient is assumed to decrease exponentially with increasing distance from the bed surface, since lower bed elevations are less exposed to the flow than higher ones and therefore less mixing occurs. In the model, fine or coarse size fractions do not show any preference for being deposited at

certain bed elevations. Therefore, the equilibrium situation of the *Armanini* model, reached after an infinitely long time, is a vertically uniform distribution of grain sizes.

Van Ledden and Wang (2001) apply the *Armanini* diffusion-type model in modelling the morphodynamic behaviour of a sand-mud estuary. They modify the diffusion coefficient, in that they introduce a factor in the mixing coefficient to take into account the effects of biological mixing, occurring only in a discrete bed layer just below the bed surface.

Parker et al. (2000) developed a new type of framework for sediment continuity and sorting dynamics. Like *Armanini* (1995), they recognised that the active layer model and its variants represent only an approximation of a more general formulation that contains no discrete bed layers. In this Parker-Paola-Leclair framework, the bed composition varies continuously over depth below the water-sediment interface, and the same goes for the entrainment and deposition fluxes from and to the bed. The probability density function of bed surface elevations is the basis of the framework.

3.5 Summary

In the last few decades, much progress has been made in the morphological modelling of rivers with non-uniform sediment. The Hirano active layer model was a key element in this development.

A number of additions have been proposed to the Hirano active layer model, e.g., a formulation for suspended load transport, formulations for sediment abrasion, a different composition of sediment deposited to the substrate, an exchange layer taking into account occasional vertical exchange of sediment due to deep bedform troughs, and the division of the substrate into sublayers. Several of these additions point towards a more general description of sediment continuity which allows for a greater variation over bed elevations of the bed composition and the vertical sorting fluxes. An important shortcoming of the Hirano active layer model and its variants is the neglect of vertical sediment fluxes other than through net aggradation or degradation. Experimental research has shown that sediment exchange also occurs through dune migration, i.e. through the grain size-selective deposition down a bedform lee face and the variability in bedform trough elevations. Another shortcoming is that in certain situations the set of equations of the active layer model becomes elliptic in the space-time domain. This means that solving the equations would require future time-boundaries, which is physically unrealistic.

A final problem is the definition of the thickness(es) of the bed layer(s) in the bed layer models. On a physical basis, it is not easy to distinguish between (1) the range of bed elevations interacting with the flow frequently (i.e. the active layer), (2) the range interacting with the flow only occasionally (i.e. the exchange layer), and (3) the range not interacting with the flow, at all (i.e. the substrate). As such, in morphological models the bed layers' thicknesses are often used as calibration constants.

In reality, the bed material interacting with the flow is not contained in a distinct surface layer as proposed by *Hirano*, but is rather controlled by the probability density function of bed surface elevations. Relatively deep bed elevations interact with the flow less frequently and are subject to entrainment and deposition less frequently than higher ones. *Parker et al.* (2000) developed a new framework for sediment continuity and sorting dynamics that no longer distinguishes discrete bed layers and that incorporates the probability density function of bed surface elevations and its influence on the grain size-specific and elevation-specific sediment entrainment and deposition rates. This Parker-Paola-Leclair framework constitutes a very useful basis for the further development of models incorporating the dynamics of vertical sorting processes, since it offers the possibility to relate vertical sorting fluxes to the likelihood of a certain bed level being exposed to the flow. Another advantage of the Parker-Paola-Leclair framework is that vertical sorting fluxes need not arise from net aggradation or degradation, but can also be related to grain size-selective deposition down a bedform lee face and the variability in bedform trough elevations.

The Parker-Paola-Leclair framework for sediment continuity is used as a basis for the present study and will be described in detail in Section 5.1. It is called a *framework* for sediment continuity since it still requires formulations for the grain size-selective vertical sorting fluxes over the range of elevations of the bed surface. In the present study, two sets of detailed flume experiments have been conducted, in order to increase our understanding of the processes controlling these vertical sorting fluxes. The results of these experiments will be described in the next chapter. Another objective of the experiments is to provide data for the derivation of formulations for the size-selective vertical sorting fluxes that are typically valid for bedform-dominated conditions (see Chapters 5 through 8).

Chapter 4

Flume experiments - Vertical sorting in bedforms

This chapter is based on the paper by *Blom et al.* (2003), which is entitled *Vertical sorting in bed forms: Flume experiments with a natural and a tri-modal sediment mixture*, Water Resources Research, in press.

Abstract

Two sets of flume experiments were conducted to examine grain size-selective transport and vertical sorting in conditions with migrating bedforms and bed load transport. In the two sets of experiments we used a sediment mixture from the river Rhine and a tri-modal mixture, respectively. The vertical sorting profiles showed a downward coarsening trend in the bedforms, and in some experiments an essentially immobile coarse bed layer formed underneath the migrating bedforms. Three mechanisms contribute to the formation of such a coarse bed layer: (1) the avalanching process at the lee face, (2) conditions of partial transport in which a relatively large amount of coarse material does not participate in the transport process, and (3) the winnowing of fines from the trough surface and subsurface. The experiments show that vertical sorting fluxes not only occur through net aggradation or degradation, but also through grain size-selective deposition down a bedform lee face and the variability in trough elevations. This is contradictory to the way vertical sorting processes are modelled in most existing sediment continuity models for non-uniform sediment. The present study is therefore also a plea for modifying existing sediment continuity models to account for vertical sorting processes other than through net aggradation or degradation.

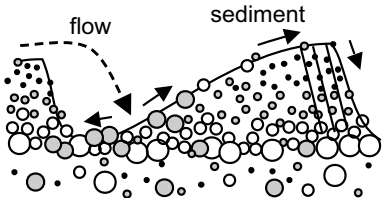

Figure 4.1: Downward coarsening of dune material and a gathering of coarse material underneath migrating dunes, revised from *Zanke* (1976).

4.1 Background

Net aggradation or degradation of the river bed results from divergences in the sediment transport rate, which is expressed by the sediment continuity equation or mass balance equation. In cases where the bed material consists of multiple size fractions, divergences in the transport of size fractions will result in a change in the composition of the bed surface and/or net aggradation or degradation of the river bed. A further complication in the mass balance is the variation of the bed composition over depth. Vertical sediment fluxes in the bed result in a certain organisation of particles over depth (i.e. the vertical sorting), which influences the rate and composition of the sediment transport and the bedforms. This affects the bed roughness, the river morphology, and water levels during floods.

For a plane bed, the vertical sorting is typically characterised by a coarse top layer (mobile pavement or armour layer), whereas, in dune conditions, the bed material shows a downward coarsening trend (*Bagnold*, 1941; *Allen*, 1965, and many others), which is illustrated in Figure 4.1. This downward coarsening arises from the size-selective sorting processes at the bedform lee face. Single coarse grains roll further down the lee face than finer grains, since (1) their velocity rolling down the lee face is larger than for finer grains, (2) they experience less friction than finer grains, and (3) they experience less support to find a resting place (*Zanke*, 1976). When a mass of grains (i.e. an avalanche) moves down the lee face, another mechanism plays a dominant role in the lee face sorting process. *Bagnold* (1941) and *Allen* (1965) observed that the fines filter down to the interface over which the avalanche is moving and the coarse grains are worked up to the surface of the avalanche. As such, the finer grains move more slowly and become lodged more easily, whereas the coarser grains overtake the finer ones and move more easily to the toe of the lee face. For an overview of research in this field and recent flume experiments on sediment sorting down a delta face, reference is made to *Kleinhans* (2002).

When flow conditions are well above the threshold for incipient motion for all grain sizes in the mixture, the coarse grains in the lower parts of the bedforms participate in the transport process. This was the case in the experiments by *Ribberink* (1987), who used a mixture of two well-sorted sand fractions ($d_{50,1} = 0.78$ mm, $d_{50,2} = 1.29$ mm). When a mixture is more widely graded and a relatively large amount of the coarse grains do not or barely participate in the transport process, an essentially immobile coarse layer may form below the migrating bedforms (*Zanke*, 1976; *Willis*, 1988; *Wilcock and Southard*, 1989; *Klaassen*, 1990a; *Blom et al.*, 2000; *Kleinhans*, 2002). This is illustrated in Figure 4.1. *Wilcock and Southard* (1989) called the coarse layer *'a partial static armor, wherein some individual grains become essentially immobile even though other grains in the same fraction remain in transport'* and remark that *'size dependent vertical sorting can serve to concentrate these coarser grains on the bed surface over which the bedforms move'*. At higher flows, they observed that the coarse layer was eliminated by scour in the lee of the dunes. This was confirmed by *Klaassen* (1990a): *'The occurrence of bedforms initiated the breaking up of the armour layer. This was caused by the turbulence generated in the wake of the bedforms.'*

Another mechanism that contributes to the formation of a coarse bed layer is the winnowing or washing out of fines from the trough surface and subsurface (*Willis*, 1988; *Wilcock and Southard*, 1989; *Klaassen*, 1990a), although it has never been directly measured. *Wilcock and Southard* (1989) remark that: *'A coarse surface layer and bedforms coexist over a finite range of τ. When both are present, the coarse surface layer does not constitute the entire bed surface that is visible at any time, but is exposed only in the bedform troughs. The coarse surface layer is the surface on which, or through which, size-dependent exchange of grains occurs. As such, the coarse surface layer plays a role in determining the grain size distribution of the transported sediment and therefore of the bedforms.'* Based on observations in the flume experiments by *Klaassen* (1986), also *Klaassen* (1990a) mentions the process of winnowing: *'The material from which these bedforms were made of originated from underneath the armour layer and was sucked through this layer from underneath slightly unstable individual particles.'* (*Klaassen*, 1990a, p.8). *Klaassen* found that the coarse layer lowered through the process of winnowing. This was confirmed by *Willis* (1988): *'With the passage of subsequent dune troughs, the gravel particles sank further until finally the gravel constituted a new layer at or even slightly below the deepest trough penetration of the dunes.'*

In numerical models for rivers with non-uniform sediment, the interaction among grain size-selective sediment transport, net aggradation or degradation, and the vertical sorting profile is described in terms of sediment continuity models, e.g., the active layer model by *Hirano* (1971). However, the Hirano active layer model and its variants do not adequately describe the vertical sorting processes in the bed and

their influence on the sediment transport processes. For instance, they do not account for the downward coarsening within bedforms, the formation of coarse bed layers, and the influence of coarse layers upon sediment entrainment. Moreover, in most sediment continuity models, vertical sediment fluxes occur through net aggradation or degradation only, whereas previous research has shown that this is not required for sediment exchange fluxes to occur (*Ribberink*, 1987; *Wilcock and Southard*, 1989; *Klaassen*, 1992). The two-layer model by *Ribberink* (1987) was the first exception, by taking into account vertical sediment exchange processes due to the variability in bedform trough elevations. A recent and important step forward was made by *Parker et al.* (2000), who developed a new type of framework for sediment continuity without discrete bed layers. The framework is based on the probability density of bed surface elevations and describes (the time evolution of) the vertical sorting profile and the vertical sediment fluxes continuously over depth. The present paper does not go into the translation of the present results into improvements to existing sediment continuity models, yet it helps to better understand their shortcomings and it is a plea for improving them.

As far as known to the authors, up to now, the experiments by *Ribberink* (1987) and *Klaassen* (1992) are the only sets of flume experiments with bedforms and non-uniform sediment in which the interaction among size-selective transport, net aggradation or degradation, the probability density of bed surface elevations, and the vertical sorting profile was studied in detail. The motive of the present study was the need for more data on vertical sorting processes in bedforms under well-controlled laboratory conditions to further develop the above sediment continuity models. This paper presents two new sets of flume experiments that were aimed at conditions with bedforms, partial transport with coarse bed layers, and bed load transport. Partial transport is here defined as the situation in which the transported material is finer than the bed material, since the coarse grains are either transported in a smaller proportion than their presence in the bed or not at all (*Wilcock and McArdell*, 1993). In the first set of experiments (1997/1998), we used a sediment mixture from the river Waal, which is a branch of the river Rhine. In this part of the Rhine it has been observed that coarse bed layers form during flood events at the base of the large dunes (*Kleinhans*, 2002). To facilitate the analysis of the vertical sorting processes, we used an artificial mixture of three well-sorted grain sizes (a tri-modal mixture) in the second set of experiments (1999/2000). During each experiment, the sediment was recirculated and uniform flow conditions were maintained. In this way, the mean bed level remained constant, so that we could focus on the interaction between only size-selective transport, the probability density of bed surface elevations, and the vertical sorting profile. The present experiments differ from those by *Ribberink* (1987) in their more widely graded sediment mixtures. The results of some of the experiments by

Klaassen (1992) ($d_{50} = 0.6$ mm, $\sigma_g = 2.3$) indicate that the coarse material in the lower part of the bedforms had formed a more or less immobile coarse layer.

The focus of the present paper is on the experiments with the tri-modal mixture, since measurements were performed more frequently and in greater detail. Besides, in the experiments with the Rhine mixture, the objective of having conditions with only bed load transport was not fully met, as the fines were transported as suspended load. Yet, the experiments with the Rhine mixture are included in the paper, as they clearly show that the processes observed for the artificial tri-modal mixture also occur for a natural mixture.

4.2 Experimental set-up

4.2.1 The Sand Flume facility

The two sets of experiments were conducted in the Sand Flume facility at WL | Delft Hydraulics in the Netherlands (*Blom and Kleinhans*, 1999; *Blom*, 2000). The length, width, and height of the flume's measurement section are 50 m, 1.5 m, and 1.0 m, respectively. The discharge is controlled by water pumps and a weir at the upstream end of the flume. The downstream water level is controlled by a tailgate at the downstream end of the flume. The sediment is recirculated. Just upstream of the tailgate, the transported sediment is caught in a sediment trap. From there, it is pumped to a hydro-cyclone at the upstream end of the flume. There, the sediment settles to the bottom of the hydro-cyclone. Its remaining volume is filled with water. When the submerged weight of the sediment in the hydro-cyclone reaches a specific value (which occurs when the total weight of the hydro-cyclone reaches a specified value), the sediment is released back into the flume. By recording the moments of these sediment deposits, the total load transport (bed load and suspended load) can be calculated. To determine the grain-size distribution of the total load transport, samples from the sediment deposits were taken regularly. In the second set of experiments (with the tri-modal mixture), the width of the flume was reduced from 1.5 m to 1.0 m. This was done to reduce the bedform adaptation length (i.e. the length from the upstream sediment inlet over which the bedforms increase in height), since previous experiments showed that the bedform adaptation length decreases with decreasing width (*Ribberink*, 1987).

4.2.2 Experimental programme

In the first set of experiments, we used a sediment mixture dredged from the river Waal, a branch of the river Rhine, near Pannerdensche Kop in the Netherlands ($d_{10} =$

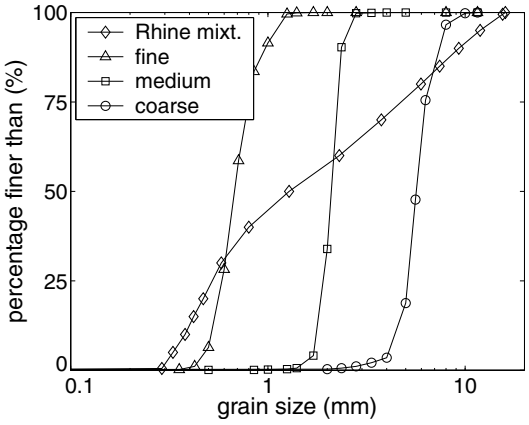

Figure 4.2: Grain size distributions in the experiments with the Rhine mixture and the trimodal mixture.

0.38 mm, $d_{50} = 1.3$ mm, and $d_{90} = 9.3$ mm, Figure 4.2). Sediment particles coarser than 16 mm (the d_{95} of the original mixture) were removed from the original mixture, because these were too coarse to be transported through the sediment recirculation system. The sediment mixture used in the second set of experiments consisted of three well-sorted size fractions: fine $d_{50} = 0.68$ mm, medium $d_{50} = 2.1$ mm, and coarse $d_{50} = 5.7$ mm (Figure 4.2).

In each experiment, the transported sediment was recirculated and uniform flow was maintained, so that the mean bed level remained constant (i.e. no net aggradation or degradation). To this end, the slope of the water level was kept equal to the originally installed bed slope. During an experiment the bedforms developed towards new equilibrium dimensions, which induced changes in bed roughness. Thus, to maintain uniform flow the boundary conditions needed to be adjusted slightly. Each experiment was run until the flow and transport reached an equilibrium stage in which the bed roughness, sediment transport rate and composition, and bedform pattern and dimensions varied around mean values.

In each of the experiments with the Rhine mixture, the average flow velocity was held constant. To maintain both uniform flow and a constant flow velocity, both the downstream water level and the discharge were adjusted slightly. Equilibrium was reached in four experiments with bedforms: T5, T7, T9, and T10 (Figure 4.3a). Experiments T5 and T10 started with a new fully mixed sediment bed. Experiments

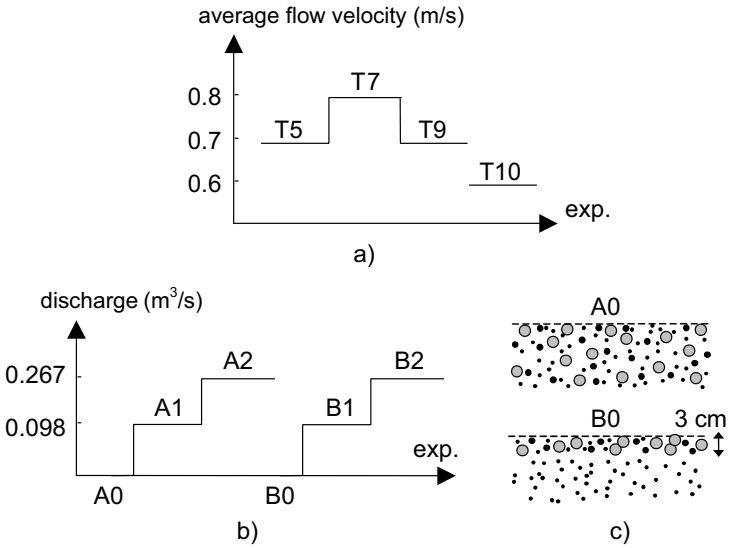

Figure 4.3: a) Average flow velocities in experiments with Rhine mixture, b) discharges in the experiments with the tri-modal mixture, and c) initial sorting profiles A0 and B0.

T7 and T9 started from the final stages of the preceding experiments, i.e. T5 and T7, respectively. In experiment T9, the flow velocity was reduced to the same level as in T5, so that T5, T7, and T9 can be considered as a flood hydrograph.

Four experiments were conducted with the tri-modal mixture: A1, A2, B1, and B2 (Figure 4.3b). To control uniform flow, now for practical reasons the discharge was kept constant and only the downstream water level was adjusted. In experiments A1 and B1, the discharge was set at 0.098 m^3/s, and in A2 and B2 at 0.267 m^3/s. Series A and B differed in their initial sorting profiles (Figure 4.3c). The initial bed of A1 (stage A0) was a flat sloping bed composed of a mixture of equal proportions of the three size fractions. The initial bed of B1 (stage B0) consisted of a mixed layer of 3 cm on top of a substratum composed of only the finest size fraction. The top layer was composed of the same initial mixture as in A0. Experiments A2 and B2 started from the final stages of A1 and B1, respectively. The initial stage B0 was set up in this way in order to study the process of (sudden) entrainment of sediment from a fine substratum and the gradual redistribution of size fractions over depth.

4.2.3 Measurements

This section briefly describes the measuring instruments and the measurements, which are discussed in greater detail by *Blom and Kleinhans* (1999) and *Blom* (2000) for the experiments with the Rhine mixture and the tri-modal mixture, respectively.

Longitudinal water and bed level profiles were measured using the standard automatic measuring carriage. It consists of one conductivity sensor for measuring the longitudinal profile of the water level and three conductivity sensors for measuring bed level profiles at three locations over the width of the flume. This type of sensor was developed by WL | Delft Hydraulics and measures local electrical resistance or conductivity, which is strongly affected by the presence of water or sand. During a measurement, its vertical position is automatically adjusted by striving after a constant conductivity. In this way, it remains at a fixed position above the interface air-water or water-sediment. The carriage moves in downstream direction with a velocity of about 0.15 m/s, recording water and bed levels every 0.01 m in longitudinal direction. In experiments A1, A2, and B1, longitudinal profiles were measured every 15 minutes, in B2 every 10 minutes, and in the Rhine mixture experiments about every hour. Stochastic errors in these measurements are negligible considering that the bed and water level profiles were averaged over the flume width and length and often also over the equilibrium period.

The *rate and composition of the total load transport* were measured as described earlier. In the experiments with the Rhine mixture, the rate and composition of the bed load and suspended load transport were also measured separately (*Blom and Kleinhans*, 1999; *Kleinhans and Van Rijn*, 2002). In the present study, only the measurements of the total load transport are discussed.

Vertical sorting profiles were measured using a new type of core sampling box developed at the University of Twente in 1997. The vertical and two horizontal dimensions of the sampling box were 30 cm, 10 cm, and 15 cm, respectively. To take a core sample, the flume was drained and the sampling box was driven into the bed from a platform. After closing the sampling box by pushing a rectangular plate obliquely into it, the box was removed from the bed (Figure 4.4). The holes in the bed were filled with sediment layers having a similar composition as removed from the bed. The core sample was cut into thin layers using a thin plate (Figure 4.4). The thickness of the layers was varied between 3 and 10 mm (potential error 1 mm, but not cumulative over layers), depending on the expected variation in the sorting profile over depth. In the experiments with the Rhine mixture, 11 core samples were taken both at the start and at the final equilibrium stage of each experiment. To study the

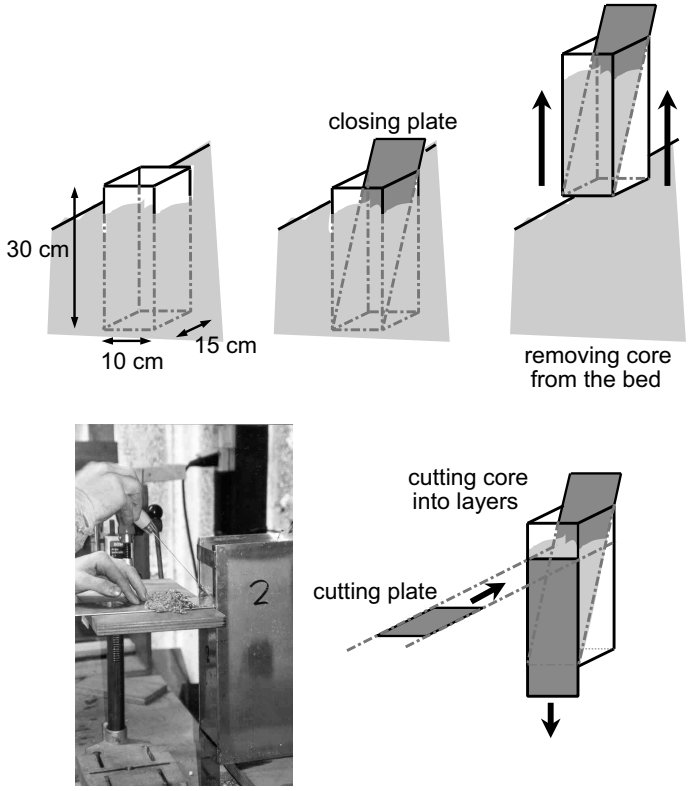

Figure 4.4: Taking core samples from the bed using a new type of core sampling box (upper plots), and cutting the core sample into thin layers (lower plots).

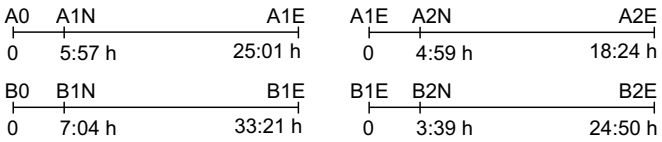

Figure 4.5: Times (in flow hours) of the core sampling sessions in the experiments with the tri-modal mixture.

time evolution of the sorting profile, in the experiments with the tri-modal mixture, samples were also taken once before equilibrium was reached (the non-equilibrium N-stage), in addition to the initial stage and the equilibrium E-stage (Figure 4.5). In each sampling session, 15 core samples were taken. Samples were taken along the flume axis, at the sides, at the bedform crests, in the troughs, as well as at the stoss sides. A remark needs to be made on the dispersive effects of the newly-developed coring method. It may cause relatively coarse grains located near the walls of the sampling box to be pushed down with it. In the present paper no corrections were made for it. As a consequence, in the presented figures the coarse grains may be found at elevations somewhat deeper than their real location. The maximum error in the measured volume fraction content of a certain size fraction at a certain elevation was found to be as large as 0.2, which occurred for the very sharp and unnatural transition in the vertical sorting profile of stage B0. For more natural sorting profiles, the potential error is estimated to be much smaller, about 0.05, especially when the sorting profile is averaged over a number of core samples.

In the experiments with the Rhine mixture, *grain size distributions* were determined as follows. Samples of the transported sediment and subsamples of the cores were analysed using a wet sieving method, in which the material was divided into four size fractions: < 2 mm, $2 - 4$ mm, $4 - 8$ mm and > 8 mm. The smallest size fraction (< 2 mm) was analysed further using a large settling tube, which was calibrated to a standard sieving instrument for a wide range of samples (*Blom*, 1998). During the experiments with the tri-modal mixture, grain size distributions were determined by wet sieving only, using sieves with sieve diameters of 1.4 mm and 3.35 mm. The wet sieving method leads to a potential error in the measured weight percentage of a certain size fraction of about 3%.

4.3 Results

4.3.1 Experimental parameters

Since for each experiment the initial sorting profile and flow conditions were uniform over the flume length and width, at each point in time all properties of flow, sediment transport, and the vertical sorting profile were uniform over the flume (with the exception of fluctuations due to the bedforms). Table 4.1 shows the parameters of each experiment, averaged over the flume width, the flume length (reduced by the bedform adaptation length), and over the period in which the bedform dimensions, the bed roughness, and the sediment transport rate and composition varied around mean values. From now on, this period is called the *equilibrium period*. The symbols denote the flow discharge (Q_w), the water depth (h), the average

exp.	Q_w	h	u	Fr	i_E	C	R	τ
	m^3/s	m	m/s	-	10^{-3}	$m^{\frac{1}{2}}/s$	m	N/m^2
T5*	0.254	0.245	0.69	0.45	1.5	37	0.224	3.4
T7	0.419	0.354	0.79	0.42	1.5	36	0.316	4.8
T9	0.272	0.260	0.70	0.44	1.8	34	0.240	4.1
T10*	0.170	0.193	0.59	0.43	1.2	41	0.176	2.0
A1†	0.098	0.154	0.64	0.52	2.0	38	0.140	2.8
A2	0.267	0.320	0.83	0.47	1.8	38	0.271	4.6
B1‡	0.098	0.155	0.63	0.51	1.9	39	0.140	2.6
B2	0.267	0.389	0.69	0.35	2.2	25	0.351	7.4

Table 4.1: Experimental parameters (averaged over equilibrium period), where * indicates new fully mixed bed, † new bed (A0), and ‡ new bed (B0).

flow velocity (u), the Froude number (Fr), the energy slope (i_E), the Chézy roughness coefficient (C), the hydraulic radius (R), and the bed shear stress (τ). The Chézy roughness coefficient, the hydraulic radius, and the bed shear stress were corrected for side wall roughness, using the method of *Vanoni and Brooks* (1957).

4.3.2 Bedforms

Figure 4.6 shows the bedform pattern in the equilibrium stage of experiment T7: coarse particles gather at the trough elevations and the lee faces show a downward coarsening trend. For the experiments with the tri-modal mixture, the equilibrium bedform patterns are shown in Figure 4.7. Barchan-shaped bedforms were present in the equilibrium stage of experiment A1 (phase A1E). The naturally white-coloured coarsest size fraction was primarily found in a coarse layer underneath the migrating bedforms. The increase in the discharge in A2 led to more two-dimensional bedforms and an increase in bedform height and length. Starting from stage B0, experiment B1 showed a pattern of bedforms that was very similar to A1. The fine substratum appeared not to be exposed to the flow significantly, because it did not noticeably affect the pattern of bedforms. After increasing the discharge in B2, the coarse layer broke up and large bedforms developed with ripples on their stoss sides. Ripples were also observed on the stoss sides of the higher bedforms in the Rhine mixture experiments.

Table 4.2 shows the bedform parameters averaged over the flume width, the flume length (reduced by the bedform adaptation length), and the equilibrium period. In A1 and B1 the bedforms did not migrate over the complete width of the flume (see Figure 4.7). For these experiments, the parameters were averaged over the adjusted

Figure 4.6: Bedform pattern in equilibrium stage of experiment T7.

width W_o, which denotes the width of the flume over which the bedforms migrated. The other symbols denote the bedform length (λ), the average crest elevation relative to the mean bed level (η_t), the average trough elevation relative to the mean bed level (η_b), the average bedform height ($\Delta = \eta_t - \eta_b$), the average bedform shape factor ($\beta = -\eta_b/\Delta$) defined such that the mean bed level η_a is located at $\beta\Delta$ above the average trough elevation η_b (for triangular dunes $\beta = \frac{1}{2}$), the average bedform migration speed (c), and standard deviations of the parameters (σ_x). The ripples on the stoss sides of the bedforms in B2 were not included in calculating the average bedform height and bedform length, since in B2 the avalanche mechanism at the lee faces of the large-scale bedforms is held responsible for the observed trends in the vertical sorting. The bedforms in experiments T5, T10, A1, and B1 may be defined as barchan-type bedforms. Note their large ratio of water depth to bedform height in Table 4.2. The bedforms in the other experiments can be defined as dunes.

Figure 4.8 shows the time evolution of bedform height (upper plots) and trough elevation (lower plots) for experiments A1 and B2 in the flume axis. These two experiments were chosen as they illustrate some important effects of the presence of a coarse layer. First, in A1 the equilibrium bedform height and trough elevation were reached slowly, whereas in B2 they were reached very quickly. In A1, a layer of essentially immobile coarse material quickly formed underneath the small migrating

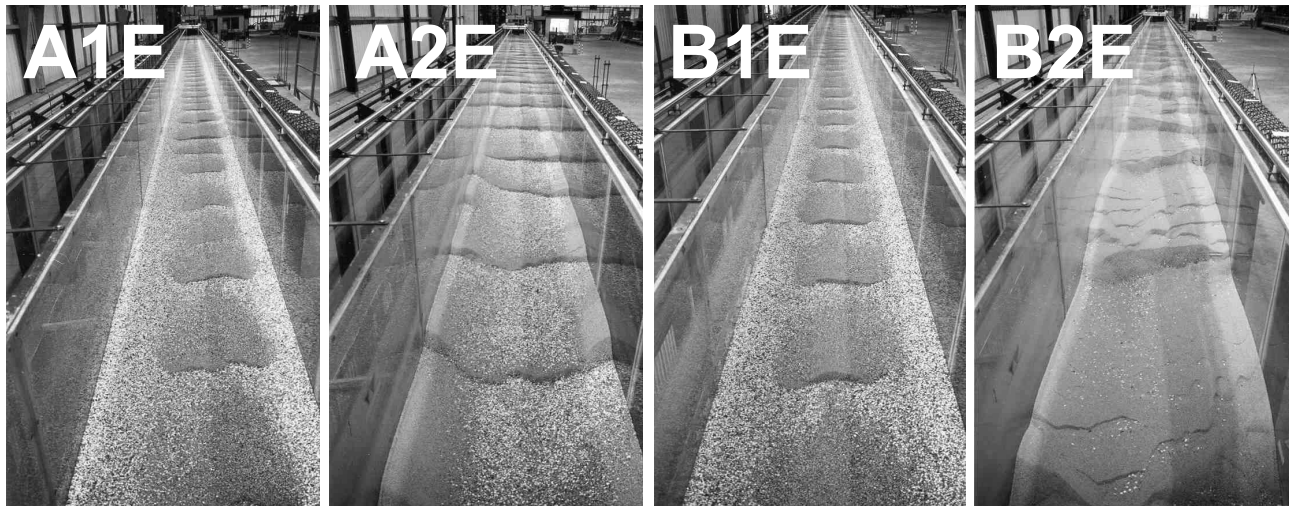

Figure 4.7: Bedform patterns in equilibrium stages of experiments with tri-modal mixture (coarsest fraction is white-coloured).

exp.	W	W_o	λ	η_t	η_b	Δ	β	c	h/Δ	σ_λ	σ_{η_t}	σ_{η_b}	σ_c
	m	m	m	cm	cm	cm	-	m/h	-	m	cm	cm	m/h
T5	1.5	-	1.13	2.1	-1.7	3.8	0.45	-	6.4	0.34	1.0	0.7	-
T7	1.5	-	1.53	3.4	-3.2	6.6	0.49	-	5.4	0.42	1.3	1.2	-
T9	1.5	-	1.34	2.8	-2.9	5.7	0.51	-	4.5	0.39	1.1	1.1	-
T10	1.5	-	0.79	1.0	-0.7	1.7	0.41	-	11.3	0.42	0.6	0.3	-
A1	1.0	0.68	0.90	0.8	-0.8	1.7	0.50	10.3	9.3	0.28	0.6	0.4	0.6
A2	1.0	-	1.38	2.0	-2.9	4.9	0.59	8.8	6.5	0.39	1.2	0.9	1.2
B1	1.0	0.65	0.99	0.9	-0.9	1.8	0.49	10.9	8.5	0.25	0.6	0.4	0.8
B2	1.0	-	1.79	5.0	-7.3	12.2	0.59	3.7	3.2	0.61	2.6	2.6	0.6

Table 4.2: Bedform parameters, averaged over equilibrium period and (adjusted) flume width.

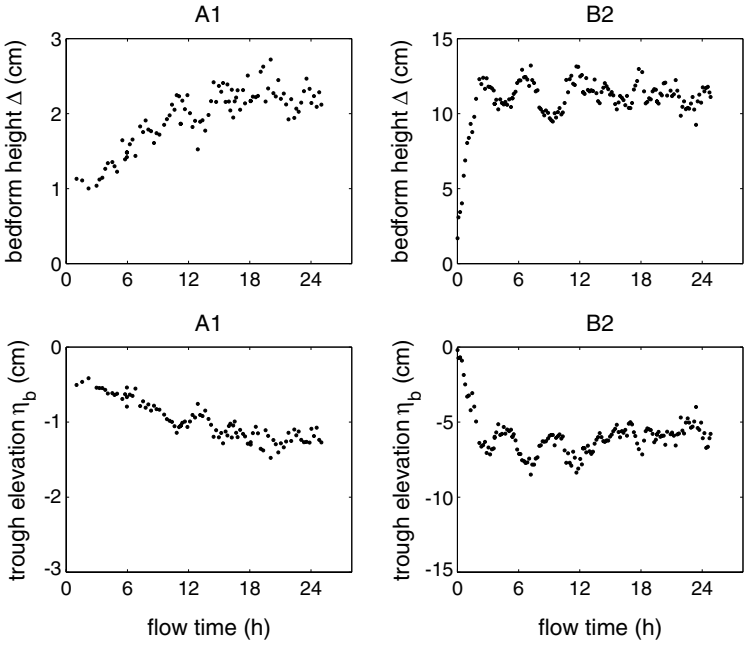

Figure 4.8: Time evolution of bedform height (upper plots) and trough elevation (lower plots) in the flume axis for experiments A1 and B2. Note that the vertical scale for B2 is 5 times larger than for A1.

bedforms. The bedform height gradually increased, due to the slow winnowing of fines from the trough surface and subsurface. Experiment B2 started from the final stage of B1 (B1E), in which small bedforms migrated over a coarse bed layer. In B2, this coarse layer quickly broke up and the dune height adjusted to the new flow conditions very quickly. The next section will show that in B2E the transport rate was four times higher than in A1E, which alone cannot explain the smaller adaptation time scales of B2, since the adaptation time scales in B2 were more than four times smaller than in A1. A second difference between experiments A1 and B2 is seen in the time evolution of the trough elevation (Figure 4.8, lower plots). After the coarse layer broke up in B2, the troughs reached deep bed elevations and the avalanching process at the dune lee redistributed the medium and coarse size fractions over depth, slightly raising the trough elevation again (note the overshoot of the trough elevation in Figure 4.8d).

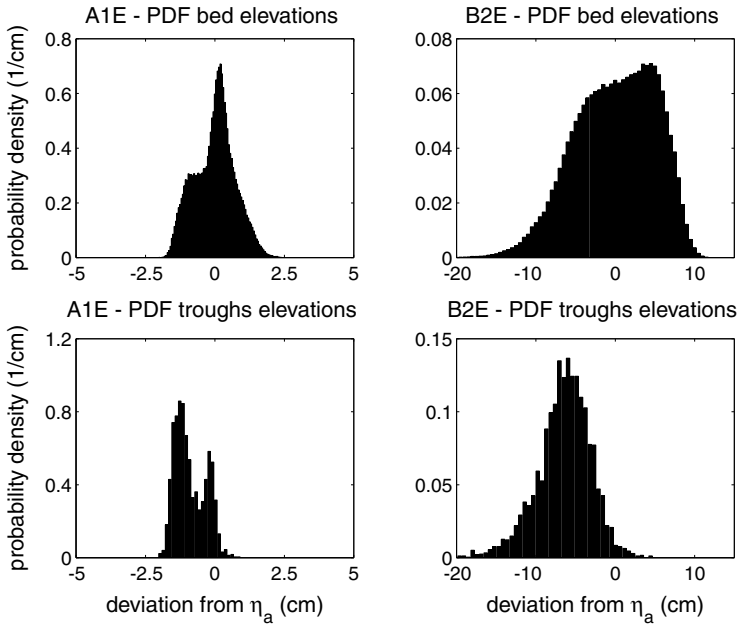

Figure 4.9: Probability density functions (PDFs) of bed surface elevations (upper plots) and of trough elevations (lower plots), for the equilibrium periods of experiments A1 and B2.

The upper plots in Figure 4.9 show the probability density functions (PDFs) of bed surface elevations for stages A1E and B2E. This probability density function represents the probability density that the elevation of the bed surface equals bed elevation z, indicating the likelihood of bed elevation z being exposed to the flow. Whereas B2E shows a long tail of deep bed surface elevations that are exposed to the flow only occasionally, A1E shows a much more abrupt transition at the lower boundary. This is due to the small variability in trough elevations in A1 (Figure 4.9, lower plots), which is attributed to the presence of a distinct coarse layer underneath the migrating bedforms. Also *Wilcock and Southard* (1989) found that the presence of a coarse bed layer underneath migrating bedforms considerably reduces the variability in trough elevations. Hitherto, the interaction between the vertical sorting profile and the probability density function of bed surface elevations has received little attention and is not well understood. A first and qualitative step was made by *Leclair and Blom* (2001, 2003).

exp.	Q_{tot}	q_{tot}	$F_{tot,1}$	$F_{tot,2}$	$F_{tot,3}$	$\sigma_{F_{tot,1}}$	$\sigma_{F_{tot,2}}$	$\sigma_{F_{tot,3}}$
	$10^{-5}\mathrm{m}^3/\mathrm{s}$	$10^{-5}\mathrm{m}^2/\mathrm{s}$	-	-	-	-	-	-
T5	4.73	3.15						
T7	8.19	5.46						
T9	5.66	3.77						
T10	1.72	1.15						
A1	1.13	1.67	0.32	0.51	0.17	0.14	0.09	0.07
A2	4.33	4.33	0.38	0.38	0.24	0.11	0.09	0.10
B1	1.17	1.79	0.34	0.54	0.12	0.11	0.09	0.04
B2	4.45	4.45	0.90	0.05	0.05	0.09	0.05	0.05

Table 4.3: Parameters of total load transport, averaged over equilibrium period.

4.3.3 Sediment transport

Table 4.3 shows the total load transport rates averaged over the equilibrium period, in which Q_{tot} denotes the volume of total load transport per unit time and q_{tot} the volume of total load transport per unit (adjusted) width and time. For the experiments with the tri-modal mixture, Table 4.3 also shows the volume fraction contents of the fine, medium, and coarse size fractions in the total load transport ($F_{tot,1}$, $F_{tot,2}$, and $F_{tot,3}$, respectively) averaged over the equilibrium periods, together with their standard deviations. The measured total load transport rates showed a natural fluctuation between roughly 0 and $2Q_{tot}$, which was due to the natural variation in the transport rate over the bedforms.

Figure 4.10 shows the composition of the total load in the experiments with the Rhine mixture. In each experiment the transported material was much finer than the original bed material, indicating partial transport. Differences in transport composition between the experiments were small. The number of samples of the transported material was limited though, so that no definite conclusions are drawn.

In the experiments with the tri-modal mixture, equilibrium in the rate of the total load transport was reached in 2 to 5 flow hours. In all experiments but B2, equilibrium in its composition was reached after only 2 flow hours (Figure 4.11). The breaking-up of the coarse layer explains the initially large amount of the medium and coarse size fractions in the total load. After this, material from the fine substratum became available to the transport process. Surprisingly, in A1 and B1 the volume fraction content of the medium size fraction in the total load was larger than the finest size fraction. This was attributed to an extreme form of hiding of the finest size fraction in the pores of the coarse bed layer. This seems to be caused by the rather unnatural grain size distribution of the well-sorted tri-modal mixture, having

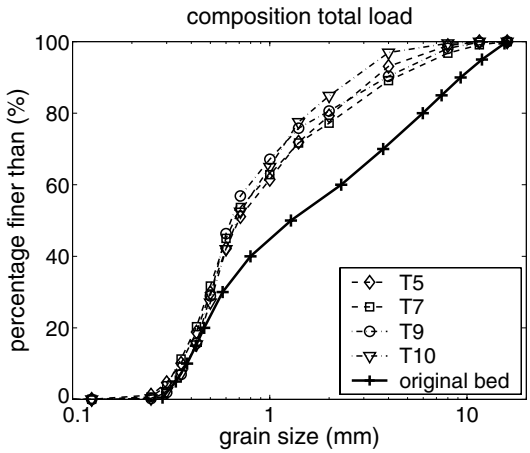

Figure 4.10: Composition of total load transport in experiments with the Rhine mixture (averaged over equilibrium period).

two distinct ranges of 'missing' grain sizes.

For the experiments with the tri-modal mixture, the measured transport rates are compared with the transport rates resulting from the method of dune tracking. This could not be done for the experiments with the Rhine mixture, since bedform migration speeds could not be determined with sufficient accuracy. The dune tracking method is based on the simple-wave approach, in which bedforms are assumed to migrate (1) without a change in dune shape, (2) with a constant migration speed, (3) with all grains participating in the avalanching process at the lee face, and (4) without sediment fluxes between subsequent dunes (*Bagnold*, 1941). The transport rate then equals:

$$q_a = cc_b\beta\Delta \tag{4.1}$$

where q_a denotes the volume of *bed load* transport per unit width and time, and c_b denotes the sediment concentration in the bed ($c_b = 1 - \lambda_p$, where λ_p denotes the porosity). Figure 4.12 shows a comparison between the measured transport rates and the transport rates based on this simple-wave approach. The values agree very well, which indicates that the amount of suspended load transport was indeed negligible and that the amount of particles by-passing the lee face and thus not participating in the avalanching process (*Mohrig and Smith*, 1996) was negligible, as well. In the experiments with the Rhine mixture, measurements of suspended load concentrations

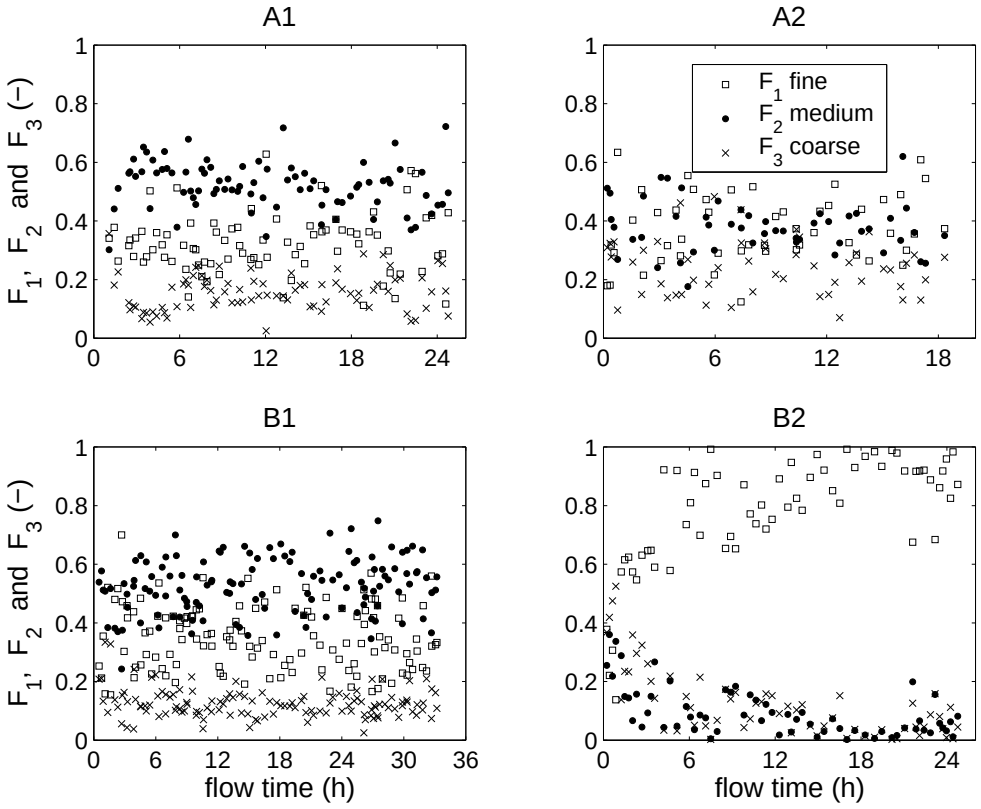

Figure 4.11: Time evolution of the composition of the total load in the experiments with the tri-modal mixture. Legend in upper right-hand plot.

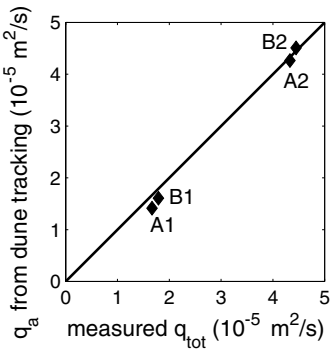

Figure 4.12: Measured total load transport, q_{tot}, compared with bed load transport rates based on the simple-wave approach, q_a, for the experiments with the tri-modal mixture. Parameters are averaged over equilibrium period.

indicated that the amount of suspended load transport varied between 10 and 20% of the total load, depending on the flow conditions (Kleinhans, personal communication, 2000).

4.3.4 Vertical sorting profiles

Figure 4.13 shows the results of six core samples taken at the final stages of experiments T5, T7, and T9, which together resemble a flood hydrograph (Figure 4.3). For each of these experiments, Figure 4.13 shows both one sample taken at or near a bedform crest (left-hand plots) and one sample taken in a trough (right-hand plots). The plots show the variation of d_{10}, d_{30}, d_{50}, d_{70}, and d_{90} of the bed material over depth, as well as the d_{10} to d_{90} of the original mixture.

When comparing the variation in d_{50} over depth with the d_{50} of the original mixture for the crest sample of T5 (upper left-hand plot), we recognise the downward coarsening of the dune material. Between 4 and 8 cm below the local bed level, the bed material was coarser than the original mixture, indicating the presence of a coarse bed layer. In the crest sample of T7 (middle left-hand plot), we again recognise the downward coarsening of the bedform material and the presence of a coarse bed layer, which is now located further below the local bed level than in T5, coinciding with the larger bedforms in T7. The sample in T9 was taken at the stoss side (lower left-hand plot) and shows the downward coarsening of the dune material and the presence of a now very thick coarse layer.

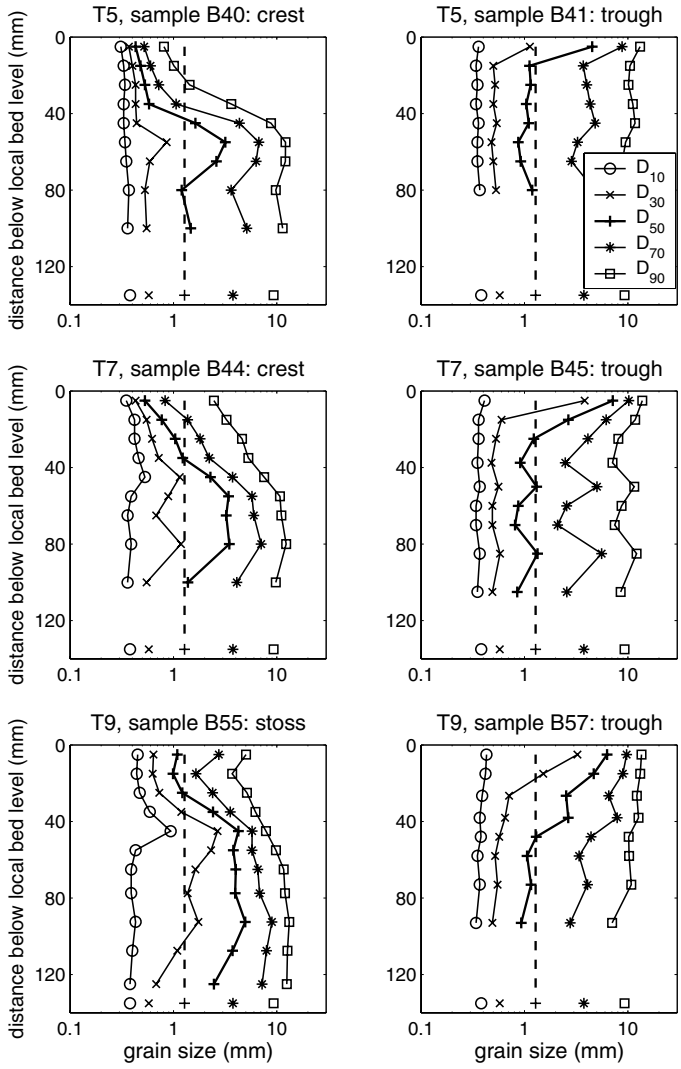

Figure 4.13: Core samples taken at crests and in troughs in experiments T5, T7, and T9 (Rhine mixture): variation of d_{10}, d_{30}, d_{50}, d_{70}, and d_{90} over depth (see legend in upper right-hand plot) compared with d_{10}, d_{30}, d_{50}, d_{70}, and d_{90} of the original mixture (see markers at bottom of each plot). The d_{50} of the original mixture is also indicated by the vertical dashed line.

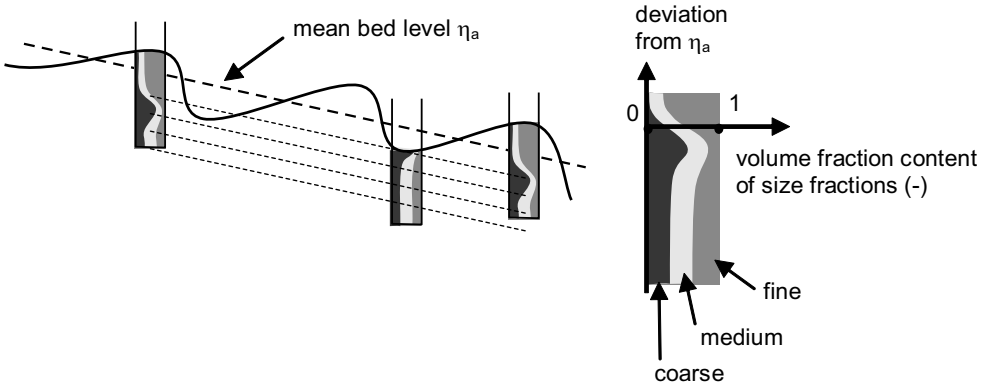

Figure 4.14: Method of averaging core samples in experiments with the tri-modal mixture.

Comparing the crest and trough samples of each experiment, the trough surface appears to be coarser than the coarse layer underneath the dunes. This is attributed to the winnowing of fines from the trough surface and subsurface, although the mechanism was not directly measured. The winnowing led to a higher porosity of the trough surface and a coarsening of it. As soon as a bedform migrated over this area, the pores were filled with finer material and the coarse layer became 'less coarse'.

Figure 4.14 shows the method to determine the average vertical sorting profile, i.e. the variation of the volume fraction contents of size fractions over depth. This was only done for the experiments with the tri-modal mixture. The vertical sorting profiles were averaged along lines parallel to the mean bed level profile. This was done for all stages, i.e. the initial stage, the non-equilibrium N-stage, and the equilibrium E-stage. For each stage, also the probability distribution of bed surface elevations was determined, so that the vertical sorting in the bed can be related to the likelihood of a certain bed elevation being exposed to the flow.

Figure 4.15 shows the time evolution of the vertical sorting profile for experiment A2, for core samples taken only at or near bedform crests. It shows the sorting profiles of (a) the initial stage of A2 (phase A1E), (b) the non-equilibrium stage, after 5 flow hours (phase A2N), and (c) the equilibrium stage, after 18.5 flow hours (phase A2E) (also see Figure 4.5). Figure 4.7a showed that in phase A1E small bedforms migrated over a coarse bed layer. In Figure 4.15a, we recognise the downward coarsening within the bedforms. However, a coarse layer underneath the bedforms cannot be identified. This will be clarified in one of the next paragraphs.

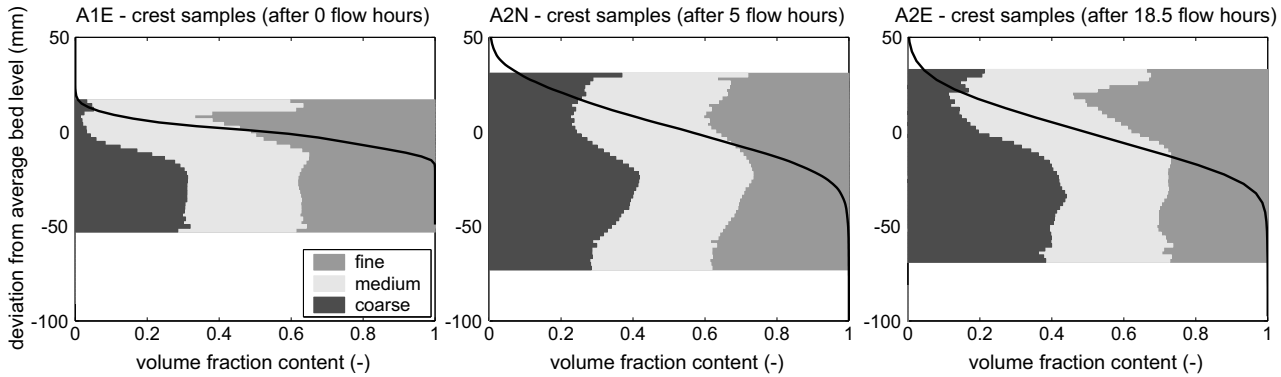

Figure 4.15: Experiment A2 - time evolution of the vertical sorting profile averaged over samples taken at or near bedform crests in a) the initial stage, after 0 flow hours (phase A1E), b) the non-equilibrium stage, after 5 flow hours (phase A2N), and c) the equilibrium stage, after 18.5 flow hours (phase A2E). The solid line represents the probability distribution of bed surface elevations in the corresponding phase of the experiment.

At the top of the sorting profiles in Figure 4.15, we distinguish a top layer of 1 to 1.5 cm that is coarser than the bedform material just below. This seems to have two reasons. First, for taking the core samples, the flow needs to be turned off, and the sediment that is being transported over the stoss face settles on top of it. This sediment is coarser than the bedform material. Secondly, processes of partial entrainment act on the stoss face. Fine grains are entrained and transported more easily than the coarser ones, which may result in a slight coarsening of the surface. The top layer seems to have a thickness larger than a few grain sizes, yet, this is due to the averaging over a large number of samples. The core samples were taken at different elevations relative to the mean bed level, and at each elevation the dune surface is covered by this coarse top layer. The presence of such a coarse top layer on the stoss face was also observed by *Ribberink* (1987).

In the equilibrium stage of A2 (phase A2E), the dune height had increased and more coarse material was present in the active part of the bed (Figure 4.15c). A coarse layer was located at about 30 mm below the mean bed level. For the non-equilibrium stage of A2 (phase A2N), the amount of coarse material in the upper part of the bed was larger than in A2E and a coarse layer was found at about 25 mm below the mean bed level (Figure 4.15b). This indicates that, after 5 flow hours, the coarse material was still being reworked to deeper bed elevations.

Let us now come back to the reason for the 'absence' of the coarse layer in Figure 4.15a. Figure 4.16 presents the average vertical sorting profiles for phase A1E averaged over core samples taken (a) at or near bedform crests, and (b) in troughs. The trough surface at 20 mm below the mean bed level was significantly coarser than the bed material underneath the small bedforms at that same elevation. Turbulent forces in the trough area caused finer particles to be winnowed from the trough surface and subsurface. When a bedform migrates over this area, the pores in the coarse layer become filled again with fines. As shown in Figure 4.16a, this process even caused the coarse layer to be 'absent' in the vertical sorting profile averaged over only crest samples.

Figure 4.17 presents the average vertical sorting profiles in (a) phase B0, (b) the equilibrium stage of B1 (phase B1E), and (c) the equilibrium stage of B2 (phase B2E). The original interface between the two layers is indicated by the dashed line at 30 mm below the mean bed level. However, Figure 4.17a shows that, in the initial stage B0, the medium and coarse size fractions were also found below this interface. This was due to the coring method: driving the sampling box into the bed caused coarser particles that were located very close to the walls of the box to be pushed down with it. This dispersive effect was not corrected for. As a consequence, in the figures

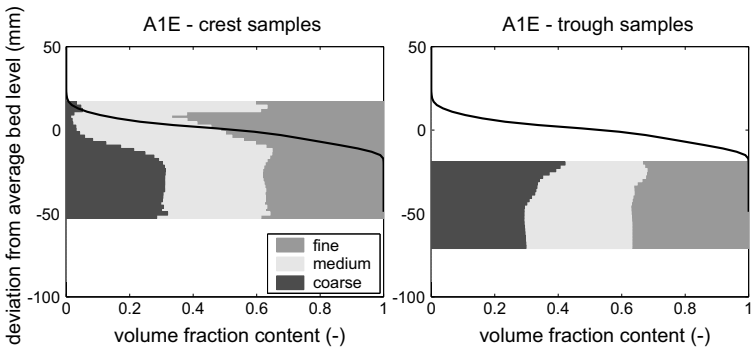

Figure 4.16: Equilibrium stage of experiment A1 (phase A1E) - vertical sorting profiles averaged over a) samples taken at or near bedform crests, and b) samples taken in troughs. The solid line represents the probability distribution of bed surface elevations in the corresponding phase of the experiment.

presented here, the coarse particles may be found at elevations somewhat deeper than their real location. An alternative may be to use the non-destructive sampling method developed by *Marion and Fraccarollo* (1997), in which large elements of the bed are frozen, removed, analysed, and brought back into the flume.

We may conclude that the fine substratum did not have much influence on B1 (Figure 4.17b), since experiment B1 was very similar to A1 (with respect to bed load transport rate and composition, bedform height, bed roughness, and bed surface composition). In B2 the coarse layer quickly broke up and the medium and coarse size fractions were gradually redistributed over a large depth. In B2 it was observed that in the avalanching process the medium and coarse size fractions were often overtopped by other (finer) grains before they reached the trough elevations.

4.4 Discussion

In all experiments, the proportion of coarse fractions in the bed load transport was smaller than in the substratum, indicating that partial transport conditions were present. The study was aimed at conditions with bed load transport only, which were met very well in the experiments with the tri-modal mixture (Figure 4.12). However, in the experiments with the Rhine mixture, the amount of suspended load varied between 10 and 20% of the total load transport. In the present study we do not consider the impacts of suspended load on the vertical exchange of sediment in the bed.

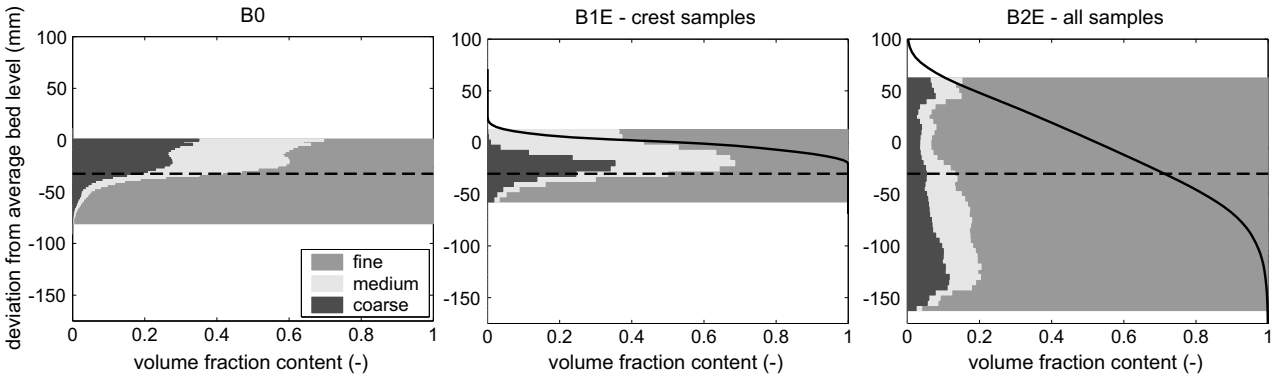

Figure 4.17: Vertical sorting profiles in a) initial stage (phase B0), averaged over all samples (flat bed), b) equilibrium stage of experiment B1 (phase B1E), averaged over only crest samples, and c) equilibrium stage of experiment B2 (phase B2E), averaged over all samples. The solid line represents the probability distribution of bed surface elevations in the corresponding phase of the experiment. The dashed line represents the original interface (in B0) between the top layer and the fine substratum.

Figure 4.18a shows an interpretation of experiments T5, T7, and T9. In experiment T5, which started with a fully mixed bed, small barchan-type bedforms developed that migrated over a coarse bed layer. In experiment T7, the flow velocity was increased, which resulted in higher dunes and a lowering of the coarse layer. This was probably caused by a combination of (1) the (partial) breaking-up of the coarse layer at the start of T7, after which large bedforms developed and the coarse particles were deposited at the lower elevations through the avalanche process at the lee face, and (2) the winnowing of fines from the trough surface and subsurface. In experiment T9, the flow velocity was decreased to the same level as in T5. Particles that were transported in experiment T7, but could no longer be transported in T9, settled on top of the coarse layer that remained as a relic at its deep elevation. The dune height decreased but remained higher than in T5, since more fines had been brought above the level of the protecting coarse layer during T7. In a similar set of experiments, *Klaassen* (1992) did not find significant changes in the vertical sorting between two experiments with similar flow conditions before and after a flood discharge. This, however, may be due to *Klaassen* taking bed samples only at dune crests where the coarse layer may not be identified very well due to the filling up of its pores underneath the migrating dunes.

Figure 4.18b shows an interpretation of the equilibrium stages of the experiments with the tri-modal mixture. In experiment A1, a layer of coarse material quickly formed underneath the migrating bedforms. The bedform height increased gradually through the slow process of winnowing and the lowering of the coarse layer. The presence of the coarse layer limited the variability in trough elevations. After increasing the flow in A2, the dune height increased and the coarse layer was found at a deeper elevation, which was due to the combination of the avalanching process at the dune lee and the winnowing of fines, similar to T7. Experiment B1 was very similar to A1, so that we may conclude that the fine substratum did not have much influence on the final stage of B1.

An especially interesting case is experiment B2, in which the adaptation time scale of the vertical sorting was of the same order as the time scale of the bed load transport composition. Due to the quick breaking-up of the initially present coarse layer, underlying fine material became available and large dunes developed with deep and irregular trough elevations. The avalanching process at the dune lee slowly redistributed the coarse particles over depth, slightly raising the trough elevation again.

A mechanism that may have a significant effect on the vertical sorting in dunes, is the winnowing or washing out of fines from the trough surface and subsurface (*Wilcock and Southard*, 1989; *Klaassen*, 1990a). The mechanism of winnowing has never been

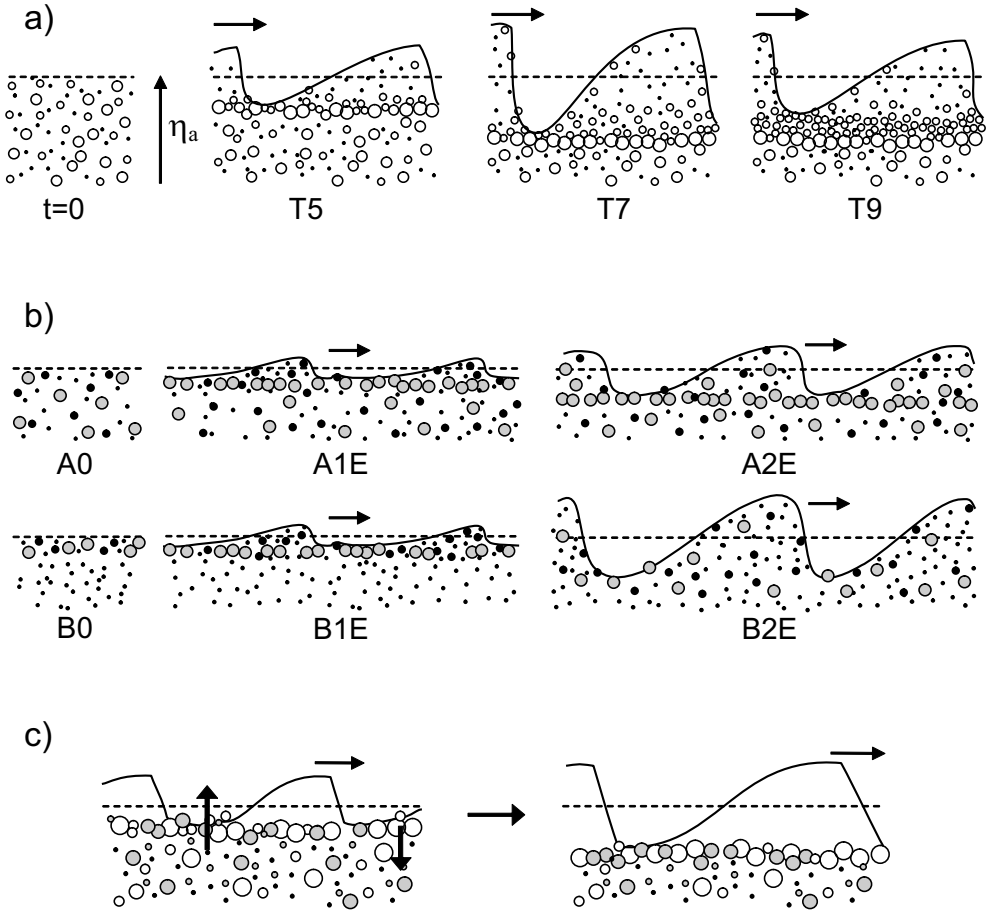

Figure 4.18: Interpretation of: a) equilibrium stages of experiments T5, T7, and T9, b) equilibrium stages of experiments with the tri-modal mixture, and c) winnowing of fines from the trough surface and subsurface resulting in a lowering of the coarse layer. For simplicity, the variability in trough elevations is not drawn. For a better schematisation of the sorting trend within the bedforms, see Figure 4.1.

directly measured and modelled, yet it is attributed to the character of the statistics of the highly turbulent flow in the trough areas. *McLean et al.* (1994) studied the flow structure over dunes and emphasised the important effects of the statistics of the turbulent flow in the trough areas upon sediment entrainment. Winnowing occurs in case (1) partial transport conditions prevail and a relatively large amount of coarse material does not participate in the transport process, (2) the framework of coarse particles is permeable enough to let finer particles pass, and (3) the statistics of the highly turbulent flow in the trough areas allows fine material to be washed out.

The winnowing of fines causes the porosity of the trough surface and subsurface to increase and the coarse layer to coarsen. Gradually, more bed material becomes available to the transport process and the coarse layer may eventually lower (Figure 4.18c). As soon as a dune migrates over the trough area, the pores get filled again with finer material. This may even cause the coarse layer underneath migrating bedforms not to be recognised. The winnowing and lowering of the coarse layer is expected to continue until (1) the sediment transport rate equals the sediment transport capacity, or (2) enough coarse material is gathered to form a stable armour layer through which no sediment can be exchanged (in situations with a large amount of coarse bed material), or (3) the water depth becomes so large that the turbulence intensity in the troughs becomes too small to entrain bed material.

For flows with bed shear stresses that are well above the threshold for incipient motion of all size fractions, it is expected that the coarse bed layer will break-up and participate in the transport process (also see *Wilcock and Southard* (1989) and *Klaassen* (1990a)). The breaking-up of the coarse layer is initiated by the highly turbulent flow in the trough areas. Yet, it is expected that the trend of downward coarsening within the dunes remains but becomes less pronounced, since the mechanism of grain size-selective deposition over the lee face seems only slightly dependent on the bed shear stress. This situation of having only mobile size fractions and thus *mobile* coarse sediment in the lower parts of the bedforms was studied by *Ribberink* (1987).

Experiment A1 showed a very slow adaptation of the average trough elevation, whereas B2 shows an initially very quick and large adaptation and then a second adaptation period in which the adaptation is much slower and smaller (see Figure 4.8). Although vertical sorting profiles were measured at only three points in time during an experiment, the authors believe that the adaptation time scale of the vertical sorting is strongly related to the adaptation time scale of the trough elevation and to the variability in trough elevations, since, through migration, a dune redistributes all bed material above its trough elevation. It is important to note that the adaptation time scale of the vertical sorting depends on the bed elevation. First,

a deeper elevation of the active bed is less exposed to the flow, so that entrainment of particles from and deposition to this elevation occur less frequently. Secondly, at a deeper elevation of the active bed more sediment is present. Thus a higher rate of sediment exchange is required to reach the same amount of change in composition. Both factors cause the time scale of reaching the equilibrium sorting profile to be larger for deeper bed elevations, and need to be taken into account when modelling the vertical redistribution of sediment in the bed.

The results of the present study show that vertical sediment fluxes are not restricted to conditions with net aggradation or degradation and that these fluxes also occur through grain size-selective deposition down a bedform lee face and the variability in trough elevations. Nonetheless, in most sediment continuity models for non-uniform sediment, vertical sediment fluxes only occur in situations with net aggradation or degradation. At present, the results presented here are being used for deriving formulations for the vertical exchange fluxes in the Parker-Paola-Leclair framework for sediment continuity. A first step towards the modelling of the vertical sorting processes of non-uniform sediment was the modelling of the vertical fluxes of tracer particles in uniform sediment in dune conditions (*Blom et al.*, 2001).

4.5 Conclusions

Two new data sets were developed describing size-selective transport and vertical sorting in conditions with bedforms and bed load transport. These data sets will be useful in modelling vertical sorting processes within the river bed and the formation of coarse bed layers.

Vertical sediment fluxes within the bed are not restricted to situations with net aggradation or degradation but also occur through grain size-selective deposition down a bedform lee face and the variability in trough elevations. The results presented here indicate that the description of vertical sorting processes in existing sediment continuity models for non-uniform sediment, e.g., the Hirano active layer model, requires modification to account for vertical sorting processes other than through net aggradation or degradation.

Three mechanisms contribute to the formation of an essentially immobile coarse layer underneath migrating dunes: (1) the avalanching process at the lee face, (2) partial transport in which a relatively large amount of coarse material does not participate in the transport process, and (3) the winnowing of fines from the trough surface and subsurface.

After a flood event, a coarse bed layer may be found at the trough elevations associated with the highest dunes (compare sorting profiles in experiments T5, T7, and T9, Figure 4.18a). During lower flow rates with smaller dunes, this layer of coarse material may become a relic, i.e. it no longer takes part in the transport process.

The winnowing of fines from the trough surface and subsurface was also recognised by *Wilcock and Southard* (1989) and *Klaassen* (1990a), but it has never been directly measured. It is attributed to the character of the statistics of the highly turbulent flow in the reattachment zone. The winnowing of fines may cause (1) the trough surface and subsurface to have an increased porosity and to coarsen, (2) more bed material to become available to the transport process, and (3) the coarse layer to subside until a new dynamic equilibrium between entrainment and deposition in the troughs is reached. When a dune migrates over the trough area, the pores become filled again with finer particles. By taking core samples at dune crests only, one may overlook the presence of a coarse layer underneath the dunes.

The results of the present study point towards a close relation between (the adaptation time scale of and the variability in) trough elevations and (the adaptation time scale of) the vertical sorting. This can easily be understood when considering that, through migration, a dune redistributes all bed material above its trough elevation. Within a series of dunes, the variability in trough elevations can be large, also in conditions without net aggradation or degradation. The variability in trough elevations is strongly limited when a distinct coarse layer is present underneath migrating dunes.

It is important to note that it cannot be concluded from the vertical sorting profile itself whether the lower (coarser) part of a bedform is mobile or essentially immobile. This can only be assessed when studying the sorting profile in combination with the probability distribution of bed surface elevations. In addition, it would be helpful to take box core samples at the bedform crests, as well as at the troughs.

Acknowledgements

The *experiments with the Rhine mixture* were funded by the European Union as a Training and Mobility of Researchers (TMR) project and by the combination RIZA-WL-UT (the Institute for Inland Water Management and Waste Water Treatment of the Ministry of Transport, Public Works, and Water Management in the Netherlands, WL | Delft Hydraulics, and the University of Twente). In 1997, these three institutes started a joint project to finance the Ph.D. research of the first author. The experiments with the Rhine mixture were set-up and conducted by Astrid Blom and Jan Ribberink (University of Twente), Maarten Kleinhans and Janrik van den

Berg (University of Utrecht), Klaus Basso and Andreas Dittrich (University of Karlsruhe), and Luigi Fraccarollo and Aronne Armanini (University of Trento). The authors especially thank Maarten Kleinhans for his participation. The *experiments with the tri-modal mixture* were funded by the combination RIZA-WL-UT and conducted by Astrid Blom, Peter van der Scheer, and Jan Ribberink. The authors thank Joop Ouderling, Freek de Groot, and Erik Mosselman of WL | Delft Hydraulics for their assistance during the experiments. Suzanne Leclair and the reviewers are thanked for their valuable comments on the paper.

Chapter 5

The new continuum sorting model

Models describing the interaction among grain size-selective sediment transport, net aggradation or degradation, and the vertical sorting profile constitute a critical component of morphological model systems for rivers with non-uniform sediment. This interaction is described in terms of sediment continuity models. The first sediment continuity model was the active layer model developed by *Hirano* (1971). Chapter 3 has presented a detailed overview of existing sediment continuity models. Yet, the existing sediment continuity models suffer from a number of shortcomings. They fail to describe vertical sorting fluxes through bedform migration (i.e. grain size-selective deposition down a bedform lee face and the variability in trough elevations), the formation of coarse bed layers, and their influence on sediment entrainment. Moreover, in most sediment continuity models vertical sediment fluxes occur through net aggradation or degradation only, whereas experiments have shown that vertical sorting fluxes are not restricted to conditions with aggradation or degradation (Section 2.5 and Chapter 4).

In order to overcome these shortcomings, the author has developed a new depth-continuous model, i.e. the continuum sorting model. The present chapter describes its derivation. The continuum sorting model is based on the framework for sediment continuity introduced by *Parker et al.* (2000) (Section 5.1). No discrete bed layers are distinguished, whence parameters show a continuous variation over all bed elevations. It has been decided to further elaborate the Parker-Paola-Leclair framework, as it offers the possibility of describing the vertical sorting fluxes continuously over bed elevations and relating the sorting fluxes at a certain bed elevation to its likelihood of being exposed to the flow. The Parker-Paola-Leclair framework for sediment continuity is called a *framework*, because formulations for the grain size-specific and elevation-specific entrainment and deposition fluxes remain to be derived. The objective of the present chapter is to derive formulations for these fluxes for bedform-dominated conditions.

After describing the Parker-Paola-Leclair framework (Section 5.1), we focus on vertical sorting fluxes occurring through the migration of a *single bedform* (Section 5.2). The bedform is divided into two sides, i.e. the stoss and the lee side, in order to sepa-

rately describe their entrainment and deposition fluxes. On the stoss face, we distinguish simultaneous entrainment and deposition fluxes, whereas on the lee face entrainment is neglected. At the stoss face, we apply the step length formulation introduced by *Einstein* (1950). The Einstein step length is defined as the average distance covered by a particle from the moment it is picked up until saltation ceases. The step length formulation yields the relation between grain size-specific deposition and entrainment fluxes over the bedform stoss face (Section 5.2.1). Subsequently, we derive formulations for the average total deposition rate over the lee face (Section 5.2.2) and for the composition of the lee deposit (Section 5.2.3). In Section 5.2.4, all equations are converted into bed elevation-specific ones, so as to make them suitable for being incorporated in the new continuum sorting model. We propose a newly-developed lee sorting function that describes the grain size-specific deposition down the avalanche lee face of a bedform (Section 5.2.5).

Section 5.3 considers the coupling between the single bedform migration approach described in Section 5.2 and the Parker-Paola-Leclair framework described in Section 5.1. Formulations for the elevation-specific entrainment and deposition densities over a series of bedforms are derived from the single bedform migration approach, making the model suitable to a series of *regular* bedforms. We then take into account the irregularities of bedforms by incorporating the statistics of the trough elevations (Section 5.3.2). In Section 5.4, we discuss the possibilities and difficulties of applying an entrainment model for non-uniform sediment. In Section 5.5, we consider the various time scales that play a role when modelling morphological changes of the river bed. The new continuum sorting model is shortly evaluated in Section 5.6.

5.1 The Parker-Paola-Leclair framework for sediment continuity

The Parker-Paola-Leclair framework for sediment continuity is explained in detail in the present section, since it serves as a basis for the new continuum sorting model. *Parker et al.* (2000) consider a certain elevation z where the concentration $\bar{C}_i(x, z, t)$ of size fraction i is given by:

$$\bar{C}_i = c_b \bar{P}_s \bar{F}_i \tag{5.1}$$

where the bar indicates that the specific parameter is averaged over some horizontal distance, e.g., a large number of bedforms, thus emphasising that the parameter varies horizontally only over the scale of successive series of bedforms. x denotes the horizontal co-ordinate on the scale of series of bedforms, z the vertical co-ordinate, t the time co-ordinate, $\bar{F}_i(x, z, t)$ the volume fraction content of size fraction i at elevation z (Figure 5.1), $\bar{P}_s(x, z, t)$ the probability distribution of bed surface elevations

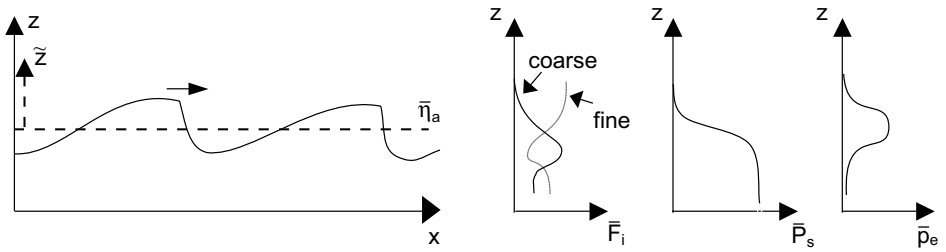

Figure 5.1: A series of bedforms, for which $\bar{F}_i$ expresses the volume fraction content of size fraction i at elevation z, $\bar{P}_s$ the probability that the bed surface elevation is higher than z, $\bar{p}_e$ the probability density that the bed surface elevation is equal to z, and $\bar{\eta}_a$ the mean bed level.

indicating the probability that the bed elevation is higher than z, and c_b the concentration of sediment in the bed ($c_b = 1 - \lambda_b$, where λ_b denotes the porosity). For parameter clarification, reference is made to the Nomenclature.

By studying the vertical exchange of tracer particles in uniform sediment (also see Sections 2.5 and 3.1), *Crickmore and Lean* (1962a,b) were the first to study the relation between the probability density function (PDF) of bed surface elevations and the vertical exchange of sediment in the active bed, i.e. the range of elevations exposed to the flow. The PDF of bed surface elevations, $\bar{p}_e(x, z, t)$, expresses the probability density that the bed surface elevation equals z, or the likelihood of elevation z being exposed to the flow (see Figure 5.1). Integration of the PDF of bed surface elevations, $\bar{p}_e$, over bed elevations $-\infty$ to z yields the probability of exceeding a certain bed elevation, $\bar{P}_s$:

$$\bar{P}_s = 1 - \int_{-\infty}^{z} \bar{p}_e \, dz \tag{5.2}$$

where $\bar{P}_s$ not only indicates the probability that the bed surface elevation is higher than z but also equals the proportion of the bed at elevation z that is covered with sediment (*Crickmore and Lean*, 1962a). This is illustrated in Figure 5.2.

In the present study the porosity is assumed to be steady and uniform over all bed elevations. Note that this is contradictory to what is stated in Section 4.3.4 on the difference in composition at the average trough elevation between samples taken at bedform crests and in troughs (Figure 4.16). The turbulent fluctuations in the trough areas cause the fines to be winnowed from the coarse bed layer located below migrating bedforms. This mechanism results in an increase of the porosity of the coarse

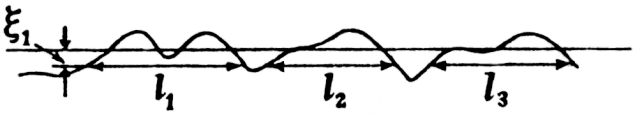

Figure 5.2: The probability distribution of bed surface elevations, $\bar{P}_s$, also expresses the proportion of the bed at elevation z that is covered with sediment: $\bar{P}_s = 1/L \sum l_r$ where L denotes the length of the river reach (*Crickmore and Lean*, 1962a, Figure 6b, p.407).

layer in the trough areas. Nonetheless, for simplicity and also because we did not specifically measure the variation of porosity over bed elevations and time, we assume it to be steady and uniform.

Sediment conservation of size fraction i at elevation z is given by (*Parker et al.*, 2000):

$$\frac{\partial \bar{C}_i}{\partial t} = \bar{D}_{ei} - \bar{E}_{ei} \tag{5.3}$$

where $\bar{D}_{ei}(x, z, t)$ denotes the deposition density of size fraction i defined such that $\bar{D}_{ei}\, dxdz$ is the volume of sediment of size fraction i that is deposited per unit width and time in a bed element with sides dx and dz at elevation z. Similarly, $\bar{E}_{ei}(x, z, t)$ is the entrainment density of size fraction i defined such that $\bar{E}_{ei}\, dxdz$ is the volume of size fraction i entrained per unit width and time from this bed element. With (5.1), (5.3) yields

$$c_b \frac{\partial}{\partial t} \bar{P}_s \bar{F}_i = c_b \bar{P}_s \frac{\partial \bar{F}_i}{\partial t} + c_b \bar{F}_i \frac{\partial \bar{P}_s}{\partial t} = \bar{D}_{ei} - \bar{E}_{ei} \tag{5.4}$$

Since all parameters are averaged over a significant horizontal distance, e.g., a large number of bedforms, it is important to realise that particles deposited at elevation z are assumed to be immediately mixed with all material present at this elevation within the series of bedforms. This may cause the model's time scale of vertical sorting to be somewhat smaller than in reality.

We now perform a co-ordinate transformation:

$$\tilde{x} = x \qquad \tilde{t} = t \qquad \tilde{z} = z - \bar{\eta}_a \tag{5.5}$$

where $\tilde{z}$ is the deviation from the mean bed level, $\bar{\eta}_a(x, t)$ (Figure 5.1). A general parameter α that is a function of (x, z, t) now becomes a function of $(\tilde{x}, \tilde{z}, \tilde{t})$. Applying

the chain rule yields

$$\frac{\partial \alpha}{\partial t} = \frac{\partial \tilde{\alpha}}{\partial t} - \frac{\partial \tilde{\alpha}}{\partial \tilde{z}} \frac{\partial \bar{\eta}_a}{\partial t} \tag{5.6}$$

$$\frac{\partial \alpha}{\partial x} = \frac{\partial \tilde{\alpha}}{\partial x} - \frac{\partial \tilde{\alpha}}{\partial \tilde{z}} \frac{\partial \bar{\eta}_a}{\partial x} \tag{5.7}$$

$$\frac{\partial \alpha}{\partial z} = \frac{\partial \tilde{\alpha}}{\partial \tilde{z}} \tag{5.8}$$

In accordance with (5.6), the time derivative $\partial \bar{P}_s / \partial t$ in (5.4) is written as

$$\frac{\partial \bar{P}_s}{\partial t} = \frac{\partial \tilde{P}_s}{\partial t} - \frac{\partial \tilde{P}_s}{\partial \tilde{z}} \frac{\partial \bar{\eta}_a}{\partial t} = \frac{\partial \tilde{P}_s}{\partial t} + \bar{p}_e \frac{\partial \bar{\eta}_a}{\partial t} \tag{5.9}$$

since

$$\bar{p}_e = -\frac{\partial \bar{P}_s}{\partial z} = -\frac{\partial \tilde{P}_s}{\partial \tilde{z}} \tag{5.10}$$

where $\tilde{P}_s(\tilde{x}, \tilde{z}, \tilde{t})$ denotes the probability distribution of bed surface elevations *relative to the mean bed level*, $\bar{\eta}_a$. With (5.9), (5.4) becomes

$$c_b \bar{P}_s \frac{\partial \bar{F}_i}{\partial t} + c_b \bar{F}_i \frac{\partial \tilde{P}_s}{\partial t} + c_b \bar{F}_i \bar{p}_e \frac{\partial \bar{\eta}_a}{\partial t} = \bar{D}_{ei} - \bar{E}_{ei} \tag{5.11}$$

Adding up (5.11) over all grain sizes yields

$$c_b \frac{\partial \tilde{P}_s}{\partial t} + c_b \bar{p}_e \frac{\partial \bar{\eta}_a}{\partial t} = \bar{D}_e - \bar{E}_e \tag{5.12}$$

where

$$\bar{D}_e = \textstyle\sum_i^N \bar{D}_{ei} \qquad \bar{E}_e = \textstyle\sum_i^N \bar{E}_{ei} \tag{5.13}$$

where N denotes the total number of size fractions, $\bar{D}_e(x, z, t)$ the deposition density defined such that $\bar{D}_e \, dxdz$ is the volume of *all* size fractions deposited in a bed element with sides dx and dz at elevation z per unit width and time, and $\bar{E}_e(x, z, t)$ the entrainment density defined such that $\bar{E}_e \, dxdz$ is the volume of all size fractions entrained from this bed element per unit width and time. Integration of (5.12) over all bed elevations yields

$$c_b \int_{-\infty}^{\infty} \frac{\partial \tilde{P}_s}{\partial t} \, dz + c_b \frac{\partial \bar{\eta}_a}{\partial t} = \bar{D} - \bar{E} \tag{5.14}$$

where $\bar{D}(x,t)$ denotes the volume of all grain sizes deposited per unit area and time, and $\bar{E}(x,t)$ the volume of all grain sizes entrained per unit area and time:

$$\bar{D} = \int_{-\infty}^{\infty} \bar{D}_e \, dz \qquad \bar{E} = \int_{-\infty}^{\infty} \bar{E}_e \, dz \tag{5.15}$$

Appendix A shows that the integral in (5.14) equals zero, so that (5.14) reduces to

$$c_b \frac{\partial \bar{\eta}_a}{\partial t} = \bar{D} - \bar{E} \tag{5.16}$$

in which we recognise the sediment continuity or mass balance equation:

$$c_b \frac{\partial \bar{\eta}_a}{\partial t} = \bar{D} - \bar{E} = -\frac{\partial \bar{q}_a}{\partial x} \tag{5.17}$$

where $\bar{q}_a(x,t)$ denotes the bed load transport rate averaged over a series of bedforms.

Eqs. (5.11), (5.12), and (5.16) comprise the fundamental set of equations of the Parker-Paola-Leclair framework for sediment continuity:

$$\begin{aligned} c_b \bar{P}_s \frac{\partial \bar{F}_i}{\partial t} + c_b \bar{F}_i \frac{\partial \tilde{P}_s}{\partial t} + c_b \bar{F}_i \bar{p}_e \frac{\partial \bar{\eta}_a}{\partial t} &= \bar{D}_{ei} - \bar{E}_{ei} \\ c_b \frac{\partial \tilde{P}_s}{\partial t} + \quad c_b \bar{p}_e \frac{\partial \bar{\eta}_a}{\partial t} &= \bar{D}_e - \bar{E}_e \\ c_b \frac{\partial \bar{\eta}_a}{\partial t} &= \bar{D} - \bar{E} \end{aligned}$$

The Parker-Paola-Leclair framework for sediment continuity constitutes a useful basis for the further development of models incorporating the dynamics of the sorting processes in the river bed, since it offers the possibility of relating the vertical sorting fluxes in the active bed to the likelihood of a certain bed surface elevation being exposed to the flow. Another advantage of the Parker-Paola-Leclair framework is that vertical sorting fluxes need not arise from net aggradation or degradation only, but can also be related to the grain size-selective deposition down a bedform lee face and the variability in bedform trough elevations. Now, to complete this set of equations, we need to derive formulations for the entrainment and deposition densities, $\bar{D}_{ei}$ and $\bar{E}_{ei}$.

Since we focus on bedform-dominated conditions, we will derive formulations for the entrainment and deposition densities $\bar{D}_{ei}$ and $\bar{E}_{ei}$ as required by the Parker-Paola-Leclair framework for a series of migrating bedforms. This is done is a few steps:

1. analysis of the migration of a single bedform, in which we successively
    - derive a relation between the grain size-specific deposition and entrainment fluxes over the bedform stoss face, based on the Einstein step length formulation (Section 5.2.1),
    - derive a formulation for the average total[1] deposition rate over the lee face (Section 5.2.2),
    - derive a formulation for the composition of the lee deposit (Section 5.2.3),
    - convert the equations into bed elevation-specific ones (Section 5.2.4), and
    - develop a lee sorting function describing the grain size-specific deposition down the lee face of a single bedform (Section 5.2.5).
2. coupling of the single bedform migration approach to the Parker-Paola-Leclair framework (Section 5.3.1).
3. introduction of the irregularity of bedforms by incorporating the statistics of trough elevations (Section 5.3.2).

These steps will result in a new continuum sorting model for rivers characterised by non-uniform sediment and bedforms.

5.2 Migration of a single bedform

5.2.1 The Einstein step length formulation

We now divide each bedform into a stoss and a lee side in order to derive formulations for the vertical sorting fluxes at either side of the bedform (Figure 5.3). It is assumed that on the stoss side deposition and entrainment occur simultaneously, and on the lee side only deposition. At the stoss face we apply the step length formulation first introduced by *Einstein* (1950) in order to relate the grain size-specific deposition rate over the bedform stoss face to the grain size-specific entrainment rate.

Einstein (1950) defined the step length Λ as the average distance covered by a particle from the moment it is picked up until saltation ceases and a period of rest on the bed, i.e. the rest period, begins. Note that one step length may consist of several particle saltation steps (Figure 5.4), which is illustrated by *Sekine and Kikkawa* (1992): *'A given particle alternates between periods of rest on the bed, interspersed with periods of successive saltation.'* Cessation of the particle's successive saltation steps can be due to the shear

[1] *total* meaning summed over all size fractions

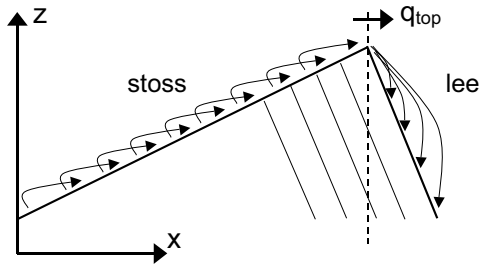

Figure 5.3: Division of bedform in stoss and lee sides with accompanying entrainment and deposition fluxes.

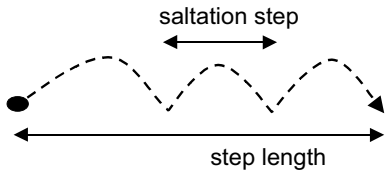

Figure 5.4: Saltation steps and step length.

stress being low compared to the critical shear stress or this particle being captured in an occasional bed cavity (*Sekine and Kikkawa*, 1992).

Based on insights from the experiments by *Einstein* (1937), *Einstein* (1950) proposes that the average distance travelled by any bed load particle between consecutive points of deposition is a distance of about 100 grain diameters, wherein the factor 100 is independent of flow conditions, transport rate, and grain size. Thus, the average step length, Λ, of a particle with grain size d is proposed to be a linear function of its grain size:

$$\Lambda = \alpha\, d \tag{5.18}$$

where d denotes the grain size and α the dimensionless step length, which will be discussed in more detail later in this section.

Let us first consider the relation among entrainment, deposition, bed load transport, and step length in more detail. For uniform sediment and after *Nakagawa and Tsujimoto* (1980), *Parker et al.* (2000) give the fundamental relations between the deposition

rate D and the entrainment rate E, and between the bed load transport q and the entrainment rate E:

$$D(x) = \int_{-\infty}^{x} E(y)\, f_p(x-y)\, dy \tag{5.19}$$

$$q(x) = \int_{-\infty}^{x} \left[E(y) \int_{x-y}^{\infty} f_p(y')\, dy' \right] dy \tag{5.20}$$

where $f_p(\xi)$ denotes the probability density that a particle, once it is entrained, travels a distance ξ. Eq. (5.19) expresses that a particle is deposited by the flow at point x if it has been entrained a certain distance upstream from x multiplied by the probability density that its step length is equal to this distance. Eq. (5.20) expresses that a particle passes a cross-section at x if it has been entrained a certain distance upstream from x multiplied by the probability density that its step length is equal to or larger than this distance. How (5.19) and (5.20) relate to the common sediment continuity equation in (5.17) will be explained in the next two sections.

For plane-bed conditions and uniform sediment, the PDF of step lengths, f_p, and the probability distribution of step lengths, F_p, are given by *Tsujimoto and Motohashi* (1990):

$$f_p(\xi) = \frac{1}{\Lambda} e^{-\frac{\xi}{\Lambda}} \tag{5.21}$$

$$F_p(\xi) = \int_{\xi}^{\infty} f_p(\xi')\, d\xi' = e^{-\frac{\xi}{\Lambda}} \tag{5.22}$$

where $F_p(\xi)$ denotes the probability that the step length is larger than ξ, and Λ is the average step length as defined in (5.18). The probability distribution of step lengths, F_p, according to *Tsujimoto and Motohashi* (1990) is shown in Figure 5.5a. For simplicity, we now assume the step length to be a deterministic parameter, so that f_p and F_p reduce to the Dirac delta function and the Heaviside function, respectively:

$$f_p(\xi) = \begin{cases} \infty & \text{for } \xi = \Lambda \\ 0 & \text{for } \xi \neq \Lambda \end{cases} \qquad F_p(\xi) = \begin{cases} 1 & \text{for } \xi \leq \Lambda \\ 0 & \text{for } \xi > \Lambda \end{cases} \tag{5.23}$$

as is illustrated in Figure 5.5b. Then, (5.19) and (5.20) become

$$D(x) = E(x-\Lambda) \tag{5.24}$$

$$q(x) = \int_{x-\Lambda}^{x} E(y)\, dy \tag{5.25}$$

Eq. (5.24) expresses that the deposition rate at a certain point on the stoss face equals the entrainment rate one step length upstream of this point. Eq. (5.25) expresses that

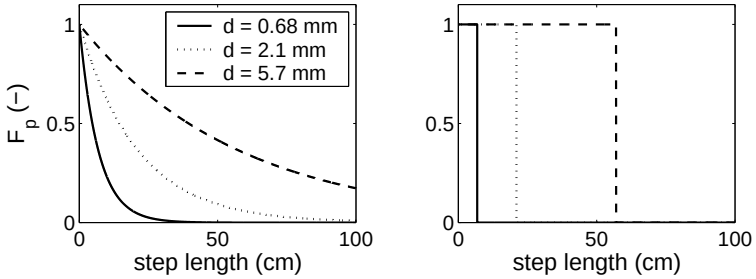

Figure 5.5: a) Probability distribution of step lengths after *Tsujimoto and Motohashi* (1990) for $\alpha = 100$ and three different grain sizes, and b) deterministic step lengths for $\alpha = 100$ and the same grain sizes.

sediment passing the cross-section at x has been picked-up between x and one step length upstream of x. If the entrainment rate E does not vary significantly within the distance of one step length Λ, (5.25) reduces to:

$$q(x) = \Lambda\, E(x - \tfrac{1}{2}\Lambda) \simeq \Lambda\, E(x) \tag{5.26}$$

Let us consider a particle passing a cross-section at co-ordinate x. The exact distance that this particle has covered is unknown, but the particle must have been entrained between x and one step length, Λ, upstream of x. This means that, provided that the step length has a deterministic value and the entrainment rate does not vary significantly within the distance of one step, the sediment transport rate through the cross-section at x must equal the entrainment rate multiplied by the average step length, as expressed by (5.26). This simplified relation between the sediment transport rate and the entrainment rate was first used by *Einstein* (1950).

We now return to non-uniform sediment. Let $E_{si}(x)$ denote the volume of sediment of grain size d_i locally entrained from the stoss face per unit area and time, which is also called the *weighed entrainment rate*:

$$E_{si}(x) = E_{siu}(x) F_i(x) \tag{5.27}$$

where x denotes the horizontal co-ordinate on the scale of a single bedform (Figure 5.3), the subscript s indicates the stoss side, and the subscript i the specific size fraction. The subscript u indicates the case of sediment of only this size fraction. Eq. (5.27) expresses that the entrainment of size fraction i at co-ordinate x equals the entrainment as if it were uniform sediment of grain size d_i multiplied by its proportion at the bed surface at x. This is comparable to calculating the transport rate of size

fraction i in a sediment mixture using $q_i = F_i\, q_{iu}$, where q_{iu}, like E_{siu}, may include hiding-exposure effects.

By assuming deterministic step lengths, it follows for the stoss side that the weighed deposition rate D_{si} of size fraction i at x equals the weighed entrainment rate of this size fraction one step length upstream of x (also see Eq. (5.24)):

$$D_{si}(x) = E_{siu}(x - \Lambda_i)F_i(x - \Lambda_i) \tag{5.28}$$

where

$$E_{siu}(x) = 0 \text{ for } x < 0 \tag{5.29}$$
$$\Lambda_i = \alpha\, d_i \tag{5.30}$$

Eq. (5.28) expresses that the deposition rate of a certain size fraction at a certain point on the stoss face equals the entrainment rate of this size fraction one step length upstream of this point. Similar to (5.25), the local bed load transport rate of size fraction i at the stoss face is given by

$$q_{si}(x) = q_s(x)F_{qsi}(x) = \int_0^{\Lambda_i} E_{siu}(x - y)F_i(x - y)\, dy \tag{5.31}$$
$$q_s(x) = \textstyle\sum_i^N q_{si}(x) \tag{5.32}$$

where $q_{si}(x)$ denotes the transport rate of size fraction i at co-ordinate x at the stoss face, $q_s(x)$ the total transport rate at co-ordinate x at the stoss face, and $F_{qsi}(x)$ the volume fraction content of size fraction i in the transported mixture at co-ordinate x at the stoss face.

As mentioned earlier in this section, *Einstein* (1937) found that the dimensionless step length, α, equals about 100, independent of flow conditions and grain size. *Yalin* (1977) suggested that α is weakly dependent on shear stress, i.e. the step length slowly increases with increasing shear stress, which was confirmed experimentally by *Sekine and Kikkawa* (1992). *Yalin* (1977) found that the dimensionless step length increases with increasing shear stress from 5 to 110, whereas *Fernandez-Luque* found that $\alpha \simeq 288$, independent of the shear stress (*Fernandez-Luque*, 1974; *Fernandez-Luque and Van Beek*, 1976). Field measurements yield results similar to those of flume experiments (*Schmidt and Ergenzinger*, 1992; *McEwan et al.*, 2001). *Sekine and Kikkawa* (1992) propose a step length model that solves for the dimensionless step length from the ratio of the shear velocity to the fall velocity of sediment in water. The model compares reasonably well with data from flume experiments.

For non-uniform sediment, *Tsujimoto* (1990, 1999) showed that the dimensionless step length, α, is smaller than for uniform sediment. In experiments with uniform sediment, α varied between 50 and 150, depending on bed shear stress, whereas for non-uniform sediment $\alpha \simeq 30$. The dimensionless step length appeared slightly dependent on the shear stress and increased from 10 to 50 with increasing shear stress.

For simplicity, we assume the dimensionless step length, α, to be independent of the shear stress, whence it is not affected by the variation of the bed shear stress over the stoss face. In addition, we assume the step length small compared to the stoss length, so that we may neglect the reduction in step length that occurs when a particle falls over the crest of the bedform.

The present section has shown how the Einstein step length formulation enables us to relate the grain size-specific deposition rate to the grain size-specific entrainment rate at the stoss face of a bedform.

5.2.2 Deposition rate at the lee face

In the present section, a formulation for the average total deposition rate over the bedform lee face will be derived by applying the sediment continuity equation in (5.17) to the local bedform surface. This yields

$$c_b \frac{\partial \eta(x)}{\partial t} = D(x) - E(x) = -\frac{\partial q(x)}{\partial x} \tag{5.33}$$

where $\eta(x)$ denotes the local bed surface elevation. Averaging (5.33) over one bedform yields

$$c_b \frac{\partial \eta_a}{\partial t} = -\frac{\lambda_s}{\lambda} E_{snet} + \frac{\lambda_l}{\lambda} D_l = -\frac{\partial q_a}{\partial x} \tag{5.34}$$

wherein entrainment on the lee face is neglected, and where λ denotes the bedform length (see Figure 5.6), λ_s the horizontal length of the stoss face, λ_l the horizontal length of the lee face, D_l the average total deposition rate on the lee face, and E_{snet} the net[2] entrainment rate on the stoss face, which will be discussed in the next paragraph. The bedform-averaged transport rate, q_a, and the bedform-averaged bed level, η_a, are given by

$$q_a = \frac{1}{\lambda} \int_0^{\lambda} q(x)\, dx \qquad \eta_a = \frac{1}{\lambda} \int_0^{\lambda} \eta(x)\, dx \tag{5.35}$$

[2] *net* meaning entrainment minus deposition, integrated over the stoss face

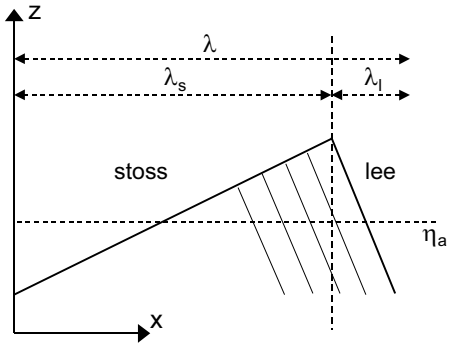

Figure 5.6: Definition of bedform parameters for a triangular bedform.

Note that the average transport rate, q_a, and the mean bed level, η_a, are defined here as averaged over a single bedform. They can still show a spatial variation between bedforms, as suggested by (5.34).

The net entrainment rate on the stoss face, E_{snet}, equals

$$\begin{aligned} E_{snet} &= \frac{1}{\lambda_s}\sum_i^N \int_0^{\lambda_s} \left(E_{si}(x) - D_{si}(x)\right)\, dx \\ &= \frac{1}{\lambda_s}\sum_i^N \left[\int_0^{\lambda_s} E_{siu}(x)F_i(x)\, dx - \int_{-\Lambda_i}^{\lambda_s-\Lambda_i} E_{siu}(x)F_i(x)\, dx\right] \end{aligned} \tag{5.36}$$

which is found by introducing (5.28). Consistent with (5.29), we neglect the contribution from $-\Lambda_i$ to 0 in the second integral, so that (5.36) reduces to

$$E_{snet} = \frac{1}{\lambda_s}\sum_i^N \int_{\lambda_s-\Lambda_i}^{\lambda_s} E_{siu}F_i\, dx \tag{5.37}$$

Comparison of (5.37) with (5.31) and (5.32) shows that the total rate of sediment transport approaching the bedform crest, q_{top}, is related to the net entrainment rate, E_{snet}, in the following logical way:

$$q_{top} = \lambda_s E_{snet} \tag{5.38}$$

in which

$$q_{topi} = \int_0^{\Lambda_i} E_{siu}(\lambda_s - y) F_i(\lambda_s - y)\, dy \tag{5.39}$$

$$q_{top} = \sum_i^N q_{topi} \qquad F_{topi} = \frac{q_{topi}}{q_{top}} \tag{5.40}$$

where $q_{top}(x,t)$ denotes the total bed load transport rate at the bedform crest, $q_{topi}(x,t)$ denotes the bed load transport rate of size fraction i at the bedform crest, and $F_{topi}(x,t)$ the volume fraction content of size fraction i in the sediment transported over the bedform crest. Using (5.38), (5.34) can be written as

$$\lambda_l D_l = q_{top} - \lambda \frac{\partial q_a}{\partial x} \tag{5.41}$$

which tells us that the average lee face deposition rate is determined by (1) the net entrainment rate on the stoss face (which equals the amount of sediment transported over the crest divided over the length of the stoss face), and (2) the divergence in the total bed load transport rate.

Thus, Eq. (5.41) provides another component of the formulations for the vertical sorting fluxes required for the new continuum sorting model: the formulation for the average total deposition rate over the lee face.

5.2.3 Composition of the lee face deposit

Now that the Einstein step length formulation has allowed us to relate the grain size-specific deposition rate over the bedform stoss face to the grain size-specific entrainment rate and a formulation for the average total deposition rate over the bedform lee face has been derived, we need to find a formulation for the composition of the total lee face deposit.

For this purpose, we apply the sediment continuity equation (5.17) to the local bedform surface again, but now we consider only a single size fraction:

$$D_i(x) - E_i(x) = -\frac{\partial q_i(x)}{\partial x} \tag{5.42}$$

where D_i, E_i, and q_i are related to D, E, and q according to

$$D(x) = \sum_i^N D_i(x) \qquad E(x) = \sum_i^N E_i(x) \qquad q(x) = \sum_i^N q_i(x) \tag{5.43}$$

Averaging (5.42) over one bedform yields

$$\frac{1}{\lambda}\int_0^{\lambda_s}\left(D_{si}(x)-E_{si}(x)\right)\,dx+\frac{\lambda_l}{\lambda}D_l F_{leei}=-\frac{\partial q_{ai}}{\partial x} \tag{5.44}$$

which, using (5.36) and (5.38), can be reformulated to

$$F_{leei}=\frac{1}{\lambda_l D_l}\left(q_{topi}-\lambda\frac{\partial q_{ai}}{\partial x}\right) \tag{5.45}$$

where F_{leei} denotes the volume fraction content of size fraction i in the deposit at the bedform lee face, q_{ai} the bedform-averaged bed load transport rate of size fraction i ($q_{ai}=F_{ai}\,q_a$), and F_{ai} the bedform-averaged volume fraction content of size fraction i in the bed load transport. Eq. (5.45) tells us that the composition of the lee face deposit, F_{leei}, is determined by (1) the composition of sediment transported over the bedform crest, and (2) the divergence in the bed load transport of size fractions. Together with the formulation for the average total deposition rate over the bedform lee face in (5.41), Eq. (5.45) shows that, when net aggradation or degradation does not occur ($\partial q_{ai}/\partial x=0$), the composition of the lee face deposit, F_{leei}, is equal to the composition of the sediment transported over the crest, F_{topi}.

In order to solve for the average total deposition rate over the bedform lee face, D_l, in (5.41) and the composition of the lee face deposit, F_{leei}, in (5.45), we need a formulation for the bedform-averaged bed load transport rate of size fraction i, q_{ai}. For that purpose, we first consider the transport rate over the lee face and apply (5.33) to the bedform lee face. We assume the lee face of each bedform to have a *uniform slope* and, as mentioned before, we assume sediment entrainment at the lee face to be negligible. By applying the simple-wave theory to bedform migration (*Bagnold*, 1941), we know that then D_l is uniform over the lee face:

$$D_l(x)=D_l=-\frac{\partial q_l}{\partial x} \tag{5.46}$$

As a boundary condition, we assume the transport rate equal to zero at the trough ($q_l=0$ at $x=\lambda$), which results in

$$q_l(x)=(\lambda-x)\,D_l \tag{5.47}$$

which expresses that the transport rate over the lee face drops linearly from $D_l\lambda_l$ at the top to 0 at the trough. The average transport rate of size fraction i over the lee face, q_{lai}, is now approximated by

$$q_{lai}=\tfrac{1}{2}D_l\lambda_l F_{leei} \tag{5.48}$$

in which, for simplicity, the effect of lee face sorting is neglected. In reality, there will be a slight bias towards the coarser particles since, on average, they will be transported further down the lee face than the finer ones. The bedform-averaged bed load transport rate of size fraction i, q_{ai}, is then obtained by using (5.31) for the stoss face and (5.48) for the lee face:

$$q_{ai} = \frac{1}{\lambda} \int_0^{\lambda_s} \int_0^{\Lambda_i} E_{siu}(x-y) F_i(x-y)\, dy\, dx + \frac{\lambda_l}{2\lambda} D_l \lambda_l F_{leei} \tag{5.49}$$

$$q_a = \Sigma_i^N q_{ai} \qquad F_{ai} = \frac{q_{ai}}{q_a} \tag{5.50}$$

Using (5.45), (5.41), and (5.49), we are now able to solve for the composition of the total lee face deposit. As a next step, we need to develop a lee sorting function that describes how the size fractions in the lee deposit are distributed over the bedform lee face. First, however, the present formulations dependent on x will be transformed into formulations dependent on z.

5.2.4 Conversion to bed elevation-specific formulations

In the previous sections, we have derived formulations for (1) the grain size-specific deposition rate over the stoss face as a function of the grain size-specific entrainment rate over the stoss face, $D_{si}(x) = E_{si}(x - \Lambda_i)$, (2) the average total deposition rate over the lee face, D_l, and (3) and the composition of the total lee face deposit, F_{leei}. These formulations all depend on the co-ordinate x on the scale of a single bedform. The Parker-Paola-Leclair framework for sediment continuity describes entrainment and deposition fluxes on the scale of a large number of bedforms, and the formulations for the grain size-specific entrainment and deposition fluxes are bed elevation-specific. We therefore need to transform the formulations derived in the previous few sections into formulations dependent on bed elevation z. To that end, we introduce the dimensionless co-ordinates x_s^*, x_l^*, and z^*:

$$x_s^* = \frac{x}{\lambda_s} \qquad x_l^* = \frac{x - \lambda_s}{\lambda_l} \qquad z^* = \frac{z - \eta_a}{\Delta} \tag{5.51}$$

where x_s^* denotes the dimensionless horizontal co-ordinate for the bedform stoss face ranging from 0 to 1 between trough and crest, x_l^* the dimensionless horizontal co-ordinate for the bedform lee face ranging from 0 to 1 between crest and trough, and z_s^* the dimensionless vertical co-ordinate. Δ denotes the bedform height, which is given by $\Delta = \eta_t - \eta_b$, where η_b and η_t denote the lower and upper limits of the bedform, respectively. The dimensionless local elevation of the bed surface η is now expressed by:

$$\eta^*(x) = \frac{\eta(x) - \eta_a}{\Delta} \tag{5.52}$$

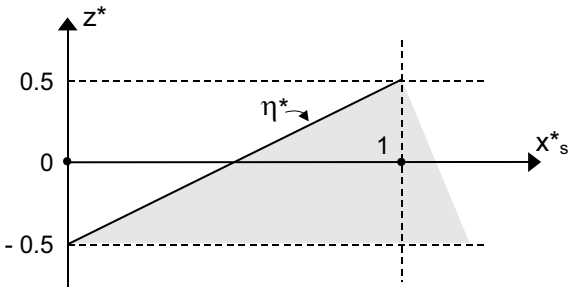

Figure 5.7: The dimensionless elevation η^* over the stoss face of a triangular bedform.

By definition, the dimensionless mean bed level, η_a^*, equals 0. In the case of a triangular bedform, the dimensionless lower limit, η_b^*, equals $-\frac{1}{2}$ and the upper limit, η_t^*, equals $\frac{1}{2}$ (see Figure 5.7).

We now define dimensionless probability density functions of the bed surface elevations for the stoss side, p_{se}^*, and the lee side, p_{le}^*:

$$p_{se}^*(z) = \frac{dx_s^*}{d\eta^*} = \Delta\, p_{se}(z) \tag{5.53}$$

$$p_{le}^*(z) = -\frac{dx_l^*}{d\eta^*} = \Delta\, p_{le}(z) \tag{5.54}$$

where $d\eta^* = d\eta/\Delta$. For the derivation of (5.46), we assumed the lee face of each bedform to have a uniform slope, so that the probability density of each elevation of the lee face reduces to $p_{le}^* = 1$ or $p_{le} = 1/\Delta$. The probability density of elevations other than those of the stoss or lee face equals 0. For a triangular bedform, the probability density functions yield

$$p_e(z) = p_{se}(z) = p_{le}(z) = \frac{J(z)}{\Delta} \tag{5.55}$$

$$p_e^*(z) = p_{se}^*(z) = p_{le}^*(z) = J(z) \tag{5.56}$$

where

$$J(z) = \begin{cases} 1 & \text{if } \eta_b \le z \le \eta_t \\ 0 & \text{if } z < \eta_b \text{ or } z > \eta_t \end{cases} \tag{5.57}$$

The bedform-averaged probability density of bed surface elevations is given by

$$p_e(z) = \frac{\lambda_s}{\lambda} p_{se}(z) + \frac{\lambda_l}{\lambda} p_{le}(z) = \frac{J(z)}{\Delta\,\lambda} \left(\lambda_s p_{se}^*(z) + \lambda_l\right) \tag{5.58}$$

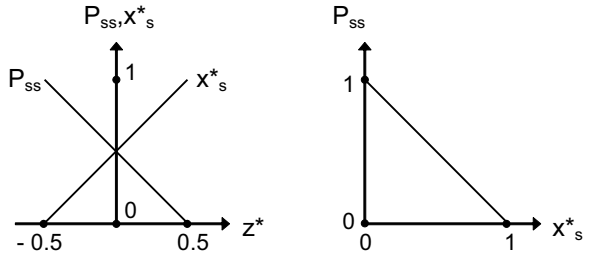

Figure 5.8: Relation between x_s^* and the probability distribution of bed surface elevations P_{ss} for a triangular bedform.

in which the stoss face is not necessarily characterised by a uniform slope. Like $p_e = -\partial P_s/\partial\eta$ in (5.10), the probability density of bed surface elevations for the stoss face equals

$$p_{se}(z) = -\frac{\partial P_{ss}(z)}{\partial \eta} \qquad\qquad p_{se}^*(z^*) = -\frac{\partial P_{ss}(z)}{\partial \eta^*} \tag{5.59}$$

where $P_{ss}(z)$ denotes the probability that the stoss face elevation is higher than z. Now, comparing (5.59b) with (5.53), and studying the example of a triangular bedform in Figure 5.8 yields

$$x_s^* = 1 - P_{ss}(z) \tag{5.60}$$

For the stoss face, we now introduce the function f_{ds} that expresses the dimensionless elevation of the stoss face as a function of the dimensionless horizontal co-ordinate, and its inverse, the function g_{ds}:

$$\eta^* = f_{ds}(x_s^*) \qquad\qquad x_s^* = g_{ds}(\eta^*) \tag{5.61}$$

Comparison of (5.60) and (5.61b) yields

$$g_{ds}(z^*) = 1 - P_{ss}(z) \tag{5.62}$$

In order to transform the equations listed in the previous few sections into equations dependent on bed elevation z, we rewrite the integrals over dx, e.g., in (5.39), into integrals over dz. When considering the stoss face, we replace dx by:

$$dx = \lambda_s \, dx_s^* = \lambda_s p_{se}^* \, dz^* = \lambda_s p_{se} \, dz \tag{5.63}$$

In addition, we translate the step length Λ_i into a dimensionless *vertical step length*, η^*_{stepi}:

$$\eta^*_{stepi} = \eta^* - f_{ds}\left[g_{ds}(\eta^*) - \Lambda^*_i\right] \tag{5.64}$$

where $\eta^*_{stepi} = \eta_{stepi}/\Delta$ and $\Lambda^*_i = \Lambda_i/\lambda_s$. This is illustrated in Figure 5.9. Using (5.63) to manipulate q_{topi} in (5.39), we find

$$q_{topi} = \lambda_s \int_{\eta_t - \eta_{stepi}}^{\eta_t} E_{siu}(\lambda_s g_{ds}(\frac{z-\eta_a}{\Delta}))F_i(\lambda_s g_{ds}(\frac{z-\eta_a}{\Delta}))$$
$$p_{se}(\lambda_s g_{ds}(\frac{z-\eta_a}{\Delta}))\, dz \tag{5.65}$$

For clarity, we no longer present the arguments in the parameters E_{siu}, F_i, and p_{se} as x-coordinates ($x = \lambda_s g_{ds}(\frac{z-\eta_a}{\Delta})$), but we abbreviate these functional relations such that $E_{siu}(z)$, $F_i(z)$, and $p_{se}(z)$ are their equivalents, respectively. Then, q_{topi} in (5.65) and q_{ai} in (5.49) are written as

$$q_{topi} = \lambda_s \int_{\eta_t - \eta_{stepi}}^{\eta_t} E_{siu}(z)F_i(z)p_{se}(z)\, dz \tag{5.66}$$

$$q_{ai} = \frac{\lambda_s^2}{\lambda} \int_{\eta_b}^{\eta_t} \int_0^{\eta_{stepi}} E_{siu}(z-z')F(z-z')p_{se}(z)p_{se}(z')\, dz'\, dz +$$
$$\frac{\lambda_l}{2\lambda} D_l \lambda_l F_{leei} \tag{5.67}$$

Thus, we have converted the formulations previously written as a function of the coordinate x into formulations dependent on bed elevation z, so as to make them suitable for being incorporated into the Parker-Paola-Leclair framework for sediment continuity.

5.2.5 Lee sorting function

In the present section, we will derive a formulation for the grain size-specific deposition down the bedform lee face. To that end, we introduce the quantity $F_{leeloci}(z,t)$ which denotes the volume fraction content of size fraction i in the sediment deposited at elevation z at the bedform lee face. The amount of sediment of size fraction i deposited at elevation z at the lee face then equals $D_l F_{leeloci}(z)$. We define $F_{leeloci}$ as:

$$F_{leeloci}(z) = F_{leei}\, \omega_i(z) \tag{5.68}$$

where ω_i is the *lee sorting function*, which determines to what extent a specific size fraction that is transported over the bedform crest is deposited at a certain elevation

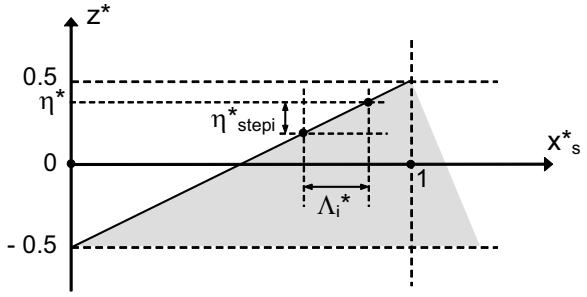

Figure 5.9: The dimensionless distance of one step length in horizontal and vertical directions, for a triangular bedform.

of the lee face. Naturally, the fine size fractions in a sediment mixture prefer being deposited at the upper parts of the lee face, and the coarse size fractions at its lower parts. A first constraint to the lee sorting function is that integration of the composition of the deposited sediment over the lee face, $F_{leeloci}$, must result in the composition of the lee face deposit, F_{leei}:

$$F_{leei} = \frac{1}{\lambda_l} \int_{\lambda_s}^{\lambda} F_{leeloci}\, dx \tag{5.69}$$

Two other constraints are

$$\Sigma_i^N F_{leeloci}(z) = 1 \tag{5.70}$$

$$0 \leq F_{leeloci}(z) \leq 1 \tag{5.71}$$

expressing that, at each bed elevation, the total volume fraction content of all size fractions must equal unity and the volume fraction content of each size fraction must be larger than or equal to zero and smaller than or equal to unity.

In Sections 2.3 and 4.3.4, it was explained that a coarse grain transported over the bedform crest prefers to be deposited at the lower elevations of the bedform lee face. As mentioned in the previous section, each bedform lee face is assumed to have a uniform slope. Based on insights from the flume experiments in Chapter 4, we now assume that the coarse size fraction is distributed over this uniformly sloped lee face with its volume fraction content decreasing linearly with elevation, and propose the following form for the lee sorting function, ω_i:

$$\omega_i(z) = J(z)\,(1 + \delta_i\, \hat{z}^*) \tag{5.72}$$

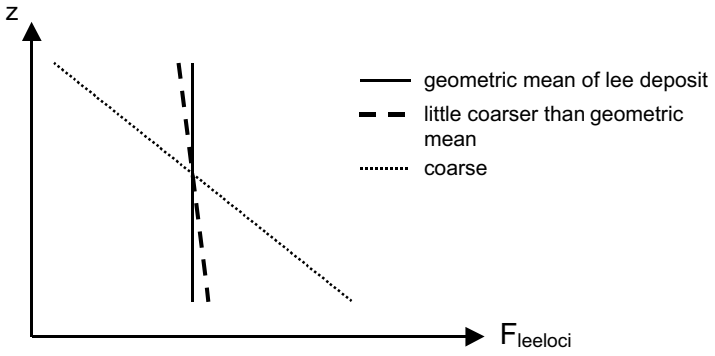

Figure 5.10: Lee sorting of three size fractions in one sediment mixture.

where the lee sorting parameter δ_i is a grain size specific constant, which will be considered in detail below, and where $\hat{z}^*$ is a dimensionless vertical co-ordinate relative to the average elevation of the lee face:

$$\hat{z}^* = z^* - \tfrac{1}{2} - \eta_b^* \tag{5.73}$$

By definition, $\hat{z}^* = -\frac{1}{2}$ at the lower limit of the lee face (where $z^* = \eta_b^*$) and $\hat{z}^* = \frac{1}{2}$ at the upper limit of the lee face (where $z^* = \eta_t^*$). In Appendix B, it is demonstrated that (5.72) together with (5.68) indeed meets the constraint in (5.69).

In order to have the δ_i-sub-model capture the principal effects of lee sorting, the author believes the model should at least incorporate the effects of

1. the difference in grain size between size fraction i and the geometric mean grain size of the lee deposit, expressed by $\phi_{mlee} - \phi_i$
2. the arithmetic standard deviation of the lee deposit, σ_a
3. the dimensionless bed shear stress, τ_b^*

which will be explained in the next three paragraphs.

Ad 1 It is likely that, the larger the difference in grain size between a specific size fraction i and the geometric mean grain size of the lee deposit ($\phi_{mlee} - \phi_i$), the larger the effect is of grain sorting at the lee face and, thus, the larger δ_i should be (see Figure 5.10).

Ad 2 To understand the effect of the gradation of the mixture, specified by σ_a, we consider one specific grain size ϕ_i in two mixtures: a widely graded mixture and a narrowly graded mixture (Figure 5.11). The two mixtures are characterised by identical geometric mean grain sizes of the lee deposit, ϕ_{mlee}. In this example, size fraction i is finer than the geometric mean grain size of the lee deposit. Namely, the larger the grain size on ϕ-scale, the smaller is the grain size d_i. Figure 5.11 illustrates why, for the widely graded mixture, the sorting of size fraction i at the lee face will be less than in the narrowly graded mixture, despite the difference between ϕ_{mlee} and ϕ_i for the two mixtures being identical. This is caused by size fraction i being *relatively* closer to the geometric mean grain size for the widely graded mixture, due to its larger gradation. For the widely graded mixture, the amount of size fractions finer than size fraction i is larger, and these all need to be deposited in the upper part of the lee face.

Ad 3 It is expected that the bed shear stress has little influence on the sorting mechanism at the lee face (which would result in a small value for κ), since the avalanching is considered mainly a gravitational process. There is, however, some experimental evidence that the sorting trend becomes smaller with increasing shear stress (*Allen*, 1965; *Kleinhans*, 2002). In the calibration procedure described in the next chapter, κ will be used as a calibration coefficient.

Based on these considerations, the author proposes the following formulation for the lee sorting parameter δ_i:

$$\delta_i = -\gamma \frac{\phi_{mlee} - \phi_i}{\sigma_a} \left(\tau_b^*\right)^{-\kappa} \tag{5.74}$$

where

$$\phi_{mlee} = \sum_i^N \phi_i F_{leei} \tag{5.75}$$

$$\sigma_a^2 = \sum_i^N \left(\phi_i - \phi_{mlee}\right)^2 F_{leei} \tag{5.76}$$

$$\tau_b^* = \tau_b / \left[(\rho_s - \rho) g d_{mlee}\right] \tag{5.77}$$

$$d_{mlee} = \tfrac{1}{1000}\, 2^{-\phi_{mlee}} \tag{5.78}$$

where d_{mlee} denotes the geometric mean grain size of the lee deposit in meters, ϕ_{mlee} the geometric mean grain size of the lee deposit on ϕ-scale, ϕ_i the grain size of size fraction i on ϕ-scale ($\phi_i = -^2\log 1000\, d_i$ with d_i in meters), τ_b^* the dimensionless bed shear stress averaged over the bedform length, and σ_a the arithmetic standard deviation of the lee deposit. The constant γ represents the relative importance of the relative grain size, i.e. the ratio on the sight-hand side of (5.74), while κ represents

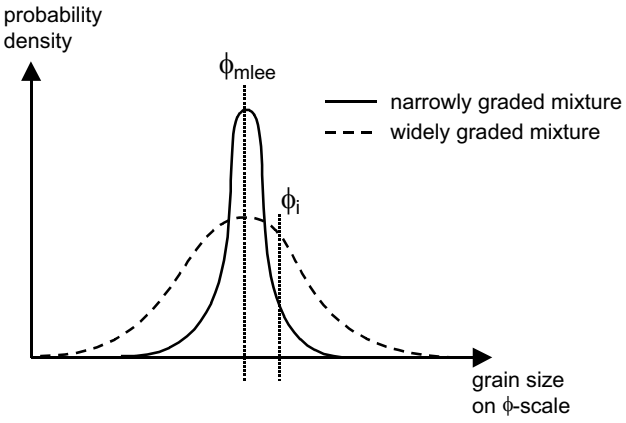

Figure 5.11: Influence of the gradation of a mixture on sorting at the lee face.

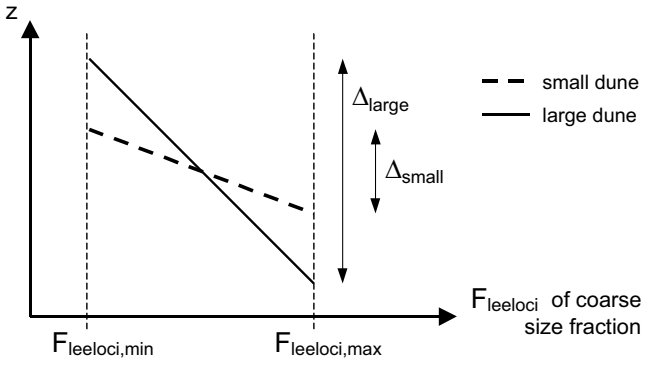

Figure 5.12: Lee sorting of a coarse size fraction for a small bedform (Δ_{small}) and a large bedform (Δ_{large}), when the mixtures transported over their crests are identical.

the relative importance of the dimensionless bed shear stress. The constants γ and κ are assumed to have a general validity, and in Chapter 7 they will be used as calibration coefficients (Section 7.2). The resulting values for γ and κ will be verified upon two independently conducted experiments and upon experimens on vertical sorting down a delta lee face from *Kleinhans* (2002) (Section 7.3).

Finally, we consider two bedforms having different bedform heights and assume that the sediment transported over their crests is identical in composition. The formulation for $F_{leeloci}$ in (5.68) and (5.72) implies that, at the lower (and upper) boundaries of the two bedforms, the volume fraction content of each size fraction in the deposit is identical. This is illustrated in Figure 5.12. It implies that the sorting trend becomes stronger with decreasing bedform height. Studying the sorting process of sediment over a delta face (see Section 2.3), *Kleinhans* (2002) indeed found that the delta height has little influence on the volume fraction content of size fractions deposited at the upper and lower boundaries of the delta front and that the sorting trend becomes stronger with decreasing bedform height.

In summary, we propose a new trend-based lee sorting function, meant for deriving a formulation for the grain size-specific deposition over the bedform lee face. The lee sorting function is considered suitable for sand-gravel mixtures and is deliberately kept simple, since it needs to be suitable to be included in the Parker-Paola-Leclair framework for sediment continuity. It seems to be the simplest form of a lee face sorting model that has any hope of capturing the effects in question.

5.3 Coupling framework and bedform migration approach

In the present section, the bedform migration approach will be coupled to the Parker-Paola-Leclair framework for sediment continuity. We first convert the entrainment and deposition rates as used in the bedform migration approach into entrainment and deposition densities as used in this framework (Section 5.3.1). Subsequently, we incorporate the irregularities of bedforms by taking into account the stochastic nature of the trough elevations (Section 5.3.2).

5.3.1 Regular bedforms

In Section 5.2, we distinguished an entrainment flux at the stoss face, a deposition flux at the stoss face, and a deposition flux at the lee face, so that we rewrite the right-hand terms in the fundamental equation of the Parker-Paola-Leclair framework for

sediment continuity, (5.11):

$$c_b \bar{P}_s(z) \frac{\partial \bar{F}_i(z)}{\partial t} + c_b \bar{F}_i(z) \frac{\partial \tilde{P}_s(z)}{\partial t} + c_b \bar{F}_i(z) \bar{p}_e(z) \frac{\partial \bar{\eta}_a}{\partial t} = \bar{D}_{eis}(z) - \bar{E}_{eis}(z) + \bar{D}_{eil}(z) \tag{5.79}$$

where the entrainment density $\bar{E}_{eis}$ of size fraction i on the stoss face is defined such that $\bar{E}_{eis}\, dxdz$ is the volume of size fraction i entrained from a bed element with sides dx and dz at elevation z at the stoss face, per unit width and time. The parameter is averaged over a large number of bedforms. $\bar{D}_{eis}$ and $\bar{D}_{eil}$ are defined likewise and denote the deposition density on the stoss face and on the lee face, respectively. For clarity, (5.79) only shows the argument in z-direction and leaves out the arguments x and t.

Note that, in the present section, we deal with series of *regular* bedforms, so that the parameters averaged over a series of bedforms are simply identical to the corresponding parameters of the single bedform, e.g.

$$\bar{F}_i(z) = F_i(z) \qquad \bar{E}_{siu}(z) = E_{siu}(z)$$
$$\bar{F}_{leeloci}(z) = F_{leeloci}(z) \qquad \bar{\lambda}_s = \lambda_s$$
$$\bar{p}_{se}(z) = p_{se}(z)$$

Now, let us consider the relation between the entrainment density $\bar{E}_{eis}$ in (5.79) and the entrainment rate $\bar{E}_{siu}$. The entrainment rate $\bar{E}_{siu}$ is defined as the volume of sediment of size fraction i picked up from the bed per unit length, width, and time, if only size fraction i would be present. As explained near (5.27), $\bar{E}_{siu}$ may include hiding-exposure effects. Thus, the volume of sediment of size fraction i picked up from the stoss face from a bed layer with a thickness dz_s per unit width and time equals

$$\bar{E}_{siu}(z) \bar{F}_i(z) dx_s \tag{5.80}$$

where dx_s is the horizontal extent over which the bed layer with thickness dz_s is exposed to the flow at the stoss face. According to (5.63), dx_s can be written as

$$dx_s = \bar{\lambda}_s \bar{p}_{se}(z)\, dz$$

As mentioned above, the entrainment density $\bar{E}_{eis}$ of size fraction i is defined such that $\bar{E}_{eis}\, dxdz$ is the volume of size fraction i entrained from a bed element with sides

dx and dz at elevation z at the stoss face, per unit width and time. Thus, the entrainment density at the stoss face equals

$$\bar{E}_{eis}(z) = \frac{\bar{E}_{siu}(z)\bar{F}_i(z)\bar{\lambda}_s\bar{p}_{se}(z)\,dz}{\bar{\lambda}\,dz} = \frac{\bar{\lambda}_s}{\bar{\lambda}}\bar{p}_{se}(z)\bar{E}_{siu}(z)\bar{F}_i(z) \tag{5.81}$$

Then, in accordance with the Einstein step length formulation, the deposition density at the stoss face is given by

$$\bar{D}_{eis}(z) = \frac{\bar{\lambda}_s}{\bar{\lambda}}\bar{p}_{se}(z)\bar{E}_{siu}(z - \eta_{stepi}(z))\bar{F}_i(z - \eta_{stepi}(z)) \tag{5.82}$$

The deposition density at the lee face is given by

$$\bar{D}_{eil}(z) = \frac{\bar{\lambda}_l}{\bar{\lambda}}\bar{p}_{le}(z)\bar{D}_l\bar{F}_{leeloci}(z) \tag{5.83}$$

where $\bar{F}_{leeloci}$ allows for grain size sorting down the avalanche lee face (see Section 5.2.5). The bed load transport rate of size fraction i averaged over the series of bedforms, $\bar{q}_{ai}$, equals the bed load transport rate of size fraction i averaged over a single bedform, q_{ai}, and is given by (5.67). Likewise, the bed load transport rate of size fraction i transported over the bedform crest and averaged over the series of bedforms, $\bar{q}_{topi}$, equals q_{topi} and is given by (5.66).

Thus, we have coupled the single bedform migration approach to the Parker-Paola-Leclair framework for sediment continuity, but the resulting set of equations is still only valid for a series of regular dunes. In reality, the variation of bedform geometry can be large, which gives rise to vertical sorting fluxes at bed elevations that are only reached by bedforms with very deep troughs. It is therefore important to account for the variability in trough elevations, which will be done in the next section.

5.3.2 Irregular bedforms

In this section, the irregularities of bedforms are taken into account by incorporating the statistics of the trough elevations. We suppose that each individual bedform in a series of irregular bedforms is characterised by the vertcal distance from its trough to the mean bed level. The latter is also indicated in terms of the *relative trough elevation* Δ_b ($\Delta_b = \bar{\eta}_a - \eta_b$). The probability density function (PDF) of relative trough elevations is given by $\tilde{p}_{\eta_b}$. All bedforms in the series are assumed to have the same *characteristic shape*, expressed by the dimensionless probability density functions of bed surface elevations for the stoss and the lee face, $\bar{p}^*_{se}$ and $\bar{p}^*_{le}$, respectively. As mentioned before, each lee face is assumed to have a uniform slope, so that $\bar{p}^*_{le} = J(z)$.

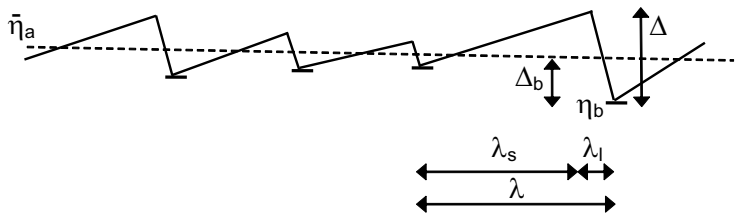

Figure 5.13: Bedform parameters. For clarity, the bedforms are here assumed to have a triangular shape.

All bedform-specific features, e.g., bedform height and bedform length, are simply related to the relative trough elevation by

$$\Delta = 2\,\Delta_b \tag{5.84}$$
$$\lambda = (\lambda_a/\Delta_a)\,\Delta \tag{5.85}$$
$$\lambda_l = \Delta/\tan(\nu) \tag{5.86}$$
$$\lambda_s = \lambda - \lambda_l \tag{5.87}$$

where Δ_a denotes the average bedform height and λ_a the average bedform length. Also see Figure 5.13 for the definition of these parameters. The crests of the triangular bedforms are assumed to have the same absolute distance to the mean bed level as the troughs, and the steepness of the lee faces is assumed to be equal to the angle of repose (ν). The bedform length is assumed to be proportional to the bedform height and the ratio of the average bedform length to the average bedform height. One may say rightfully claim that the parameters Δ, λ, λ_l, and λ_s may be related to the relative trough elevation in a way different from (5.84) through (5.87). The purpose of these formulations is to account for the irregularity of bedforms in a relatively simple way, so that the method can be incorporated in the new continuum sorting model. Eqs. (5.84) through (5.87) are not supposed to be generally valid and when applying these formulations, their applicability should be checked against data.

Let us now address the procedure of averaging some general bedform-specific parameter, μ, over a series of irregular bedforms. Averaging μ over various bedforms requires the parameter to be weighed by the proportion of the total length of the series of bedforms that is related to a specific relative trough elevation. Yet, the PDF of relative trough elevations, $\tilde{p}_{\eta_b}$, only expresses the likelihood that a certain trough elevation occurs, but not what proportion of the total length of the series of bedforms is involved. Therefore, in averaging some general bedform-specific parameter, μ, over

the various bedforms, it should not only be weighed by the probability density that a specific relative trough elevation occurs, but also by the bedform length:

$$\bar{\mu} = \frac{1}{\hat{\lambda}} \int_{\eta_{bmin}}^{\eta_{bmax}} \lambda \, \mu \, \tilde{p}_{\eta_b} \, d\eta_b \tag{5.88}$$

where $\bar{\mu}$ is called the *overall*[3] parameter μ. The weighed bedform length, $\hat{\lambda}$, is meant to normalise (5.88) and is given by

$$\hat{\lambda} = \int \lambda \, \tilde{p}_{\eta_b} \, d\eta_b \tag{5.89}$$

For clarity, we now define an adapted PDF of relative trough elevations, $\tilde{p}_b$, which equals the PDF of relative trough elevations, $\tilde{p}_{\eta_b}$, weighed by the proportion of the total length of the series of bedforms that is related to a specific relative trough elevation:

$$\tilde{p}_b = \frac{\lambda}{\hat{\lambda}} \tilde{p}_{\eta_b} \tag{5.90}$$

so that the overall parameter μ in (5.88) can be rephrased to

$$\bar{\mu} = \int_{\eta_{bmin}}^{\eta_{bmax}} \mu \, \tilde{p}_b \, d\eta_b \tag{5.91}$$

Likewise, using (5.58) and (5.53), we find that the overall PDF of bed surface elevations, $\bar{p}_e$, is now determined by the characteristic bedform shape, $\bar{p}^*_{se}$, and the PDF of relative trough elevations, $\tilde{p}_b$, according to

$$\bar{p}_e(z) = \int_{\eta_{bmin}}^{\eta_{bmax}} p_e(z) \, \tilde{p}_b \, d\eta_b = \int_{\eta_{bmin}}^{\eta_{bmax}} \frac{J(z)}{\lambda \Delta} \left(\lambda_s \bar{p}^*_{se}(z) + \lambda_l \right) \, \tilde{p}_b \, d\eta_b \tag{5.92}$$

Note that the parameters J, Δ, λ, λ_s, and λ_l are all related to the specific relative trough elevation, Δ_b, which is expressed by (5.57) and (5.84) through (5.87). Appendix C explains the determination of the PDF of bed surface elevations, $\bar{p}_e$, for the simple case of two triangular dunes. The overall probability distribution of bed surface elevations, $\bar{P}_s$, is given by (5.2).

The derivation of the entrainment and deposition densities averaged over a series of irregular bedforms ($\bar{E}_{eis}$, $\bar{D}_{eis}$, and $\bar{D}_{eil}$) is similar to those for regular bedforms,

[3] *overall* meaning averaged over a series of irregular bedforms

given by (5.81), (5.82), and (5.83). Yet, we have to average the right-hand terms over all trough elevations:

$$\bar{E}_{eis}(z) = \int_{\eta_{bmin}}^{\eta_{bmax}} \frac{\lambda_s}{\lambda} p_{se}(z) E_{siu}(z)\, \bar{F}_i(z)\, \tilde{p}_b\, d\eta_b \tag{5.93}$$

$$\bar{D}_{eis}(z) = \int_{\eta_{bmin}}^{\eta_{bmax}} \frac{\lambda_s}{\lambda} p_{se}(z) E_{siu}(z - \eta_{stepi}(z))\, \bar{F}_i(z - \eta_{stepi}(z))\, \tilde{p}_b\, d\eta_b \tag{5.94}$$

$$\bar{D}_{eil}(z) = \int_{\eta_{bmin}}^{\eta_{bmax}} \frac{\lambda_l}{\lambda} p_{le}(z) D_l\, F_{leeloci}(z)\, \tilde{p}_b\, d\eta_b \tag{5.95}$$

Herein, we assume that the vertical sorting profiles within individual bedforms, F_i, are identical to the sorting profile globally averaged over the series of bedforms, $\bar{F}_i$. Thus, we do not distinguish sorting profiles within individual bedforms. Note that sediment deposited at elevation z at the lee face of one bedform is assumed to be immediately mixed with all sediment present at this elevation over the entire series. This assumption will be shortly evaluated in Section 9.7.2.

In order to determine the rate and composition of the bed load transport averaged over the series of irregular bedforms, $\bar{q}_a$ and $\bar{F}_{ai}$, we average q_{ai} in (5.67) over all trough elevations:

$$\begin{aligned}\bar{q}_{ai} &= \int_{\eta_{bmin}}^{\eta_{bmax}} q_{ai}\, \tilde{p}_b\, d\eta_b \;= \\ &= \int_{\eta_{bmin}}^{\eta_{bmax}} \left[\frac{\lambda_s^2}{\lambda} \int_{\eta_b}^{\eta_t} \int_0^{\eta_{stepi}} E_{siu}(z - z') F(z - z') p_{se}(z) \right. \\ &\qquad \left. p_{se}(z')\, dz'\, dz \;+ \frac{\lambda_l}{2\lambda} D_l \lambda_l F_{leei} \right] \tilde{p}_b\, d\eta_b \end{aligned} \tag{5.96}$$

$$\bar{q}_a = \Sigma_i^N \bar{q}_{ai} \qquad\qquad \bar{F}_{ai} = \frac{\bar{q}_{ai}}{\bar{q}_a} \tag{5.97}$$

Likewise, the rate and composition of sediment transported over the bedform crest averaged over the series of bedforms, $\bar{q}_{top}$ and $\bar{F}_{topi}$, are found by averaging q_{topi} in (5.66) over all trough elevations:

$$\begin{aligned}\bar{q}_{topi} &= \int_{\eta_{bmin}}^{\eta_{bmax}} q_{topi}\, \tilde{p}_b\, d\eta_b = \\ &= \int_{\eta_{bmin}}^{\eta_{bmax}} \left[\lambda_s \int_{\eta_t - \eta_{stepi}}^{\eta_t} E_{siu}(z) F_i(z) p_{se}(z)\, dz \right] \tilde{p}_b\, d\eta_b \end{aligned} \tag{5.98}$$

$$\bar{q}_{top} = \Sigma_i^N \bar{q}_{topi} \qquad\qquad \bar{F}_{topi} = \frac{\bar{q}_{topi}}{\bar{q}_{top}} \tag{5.99}$$

Thus, we have coupled the single bedform migration approach to the Parker-Paola-Leclair framework for sediment continuity for a series of *irregular* bedforms. The irregularities of bedforms have been taken into account by incorporating the PDF of relative trough elevations, $\tilde{p}_b$. The bedform-specific parameters, e.g., bedform height and bedform length, are related to the relative trough elevation according to simple formulations. To average parameters over the series of irregular dunes, the bedform-specific parameters are averaged over all relative trough elevations, by weighing with the PDF of relative trough elevations. The result of the previous sections is a new continuum sorting model for bedform-dominated conditions, although the model still lacks a sub-model for the grain size-specific entrainment over the stoss face of a bedform.

5.4 A grain size-selective entrainment model

In order to be able to compute the time evolution of the sorting profile, $\bar{F}_i$, and the mean bed level, $\bar{\eta}_a$, we need to make the set of equations complete. A straightforward way to do so would be to acquire sub-models for the grain size-selective entrainment rate over bedforms and for the lower and upper limits of the active bed (η_b and η_t). Would we acquire these models, the method for solving (5.11), (5.12), and (5.16) would be to

1. use the formulations for the grain size-specific and elevation-specific entrainment and deposition densities $\bar{E}_{ei}$ and $\bar{D}_{ei}$ listed above
2. calculate the elevation-specific entrainment and deposition densities $\bar{E}_e$ and $\bar{D}_e$, by adding up $\bar{E}_{ei}$ and $\bar{D}_{ei}$ over all grain sizes
3. calculate the entrainment and deposition rates $\bar{E}$ and $\bar{D}$, by integrating $\bar{E}_e$ and $\bar{D}_e$ over all bed elevations
4. calculate $\partial\bar{\eta}_a/\partial t$ by solving (5.16)
5. calculate $\partial\tilde{P}_s/\partial t$ by solving (5.12)
6. calculate $\partial\bar{F}_i/\partial t$ by solving (5.11) and determine how $\bar{F}_i$ varies in time

In addition, this method would result in a new bed load transport model for non-uniform sediment.

Fernandez-Luque (1974) developed an entrainment model for lower-regime plane-bed conditions and uniform sediment, but as far as known to the author, *Tsujimoto* (1990, 1999) was the only one who developed an entrainment model especially for non-uniform sediment. Unfortunately, this entrainment model has never been verified

for a wide range of conditions, and it is not known whether it gives a good description of entrainment along bedforms, since flow patterns over bedforms are strongly non-uniform and very complex. Besides the entrainment model, another source of uncertainty is the variation of a representative measure for the skin friction, τ_i^*, over the stoss face, which is not easily determined.

Moreover, *McLean et al.* (1994, 1999) experimentally found that the sediment transport rate over a bedform does not directly depend on the variation of the mean bed shear stress over it. They argue that the sediment transport rate should be related to the statistics of the near-bed turbulence, which varies over the bedform in a complex manner as a result of the geometrically induced flow acceleration over the stoss face, the growing boundary layer over the stoss face, and the wake that partly overlays the stoss face. Because lift and drag forces on grains are directly related to instantaneously fluctuating velocities, the structure of the near-bed turbulence is ultimately responsible for sediment entrainment and transport.

It is thus not known whether an entrainment model based on skin friction would give satisfactory results in predicting the size-selective entrainment rate over the stoss face. It was therefore decided to take on another approach, which will be explained in Chapters 6 through 8.

5.5 Time scales

When applying the new continuum sorting model, we can distinguish the following time scales (see Figure 5.14):

- the time scale of dune migration, T_c
- the time scale of vertical dune dimensions, T_p
- the time scale of vertical sorting, $T_f(z)$
- the time scale of large-scale morphological changes, T_m

where the time scale of dune migration, T_c, is defined as the time required for a bedform to cover its average bedform length, $\bar{\lambda}$:

$$T_c = \frac{\bar{\lambda}}{c} \tag{5.100}$$

The time scale of dune dimensions may also be called the time scale of relative trough elevations. Note that the time scale of vertical sorting, T_f, is a function of bed elevation z, since, at the deeper elevations of the active bed, the bed composition adjusts more slowly to changing conditions than at higher bed elevations. This is due to (1)

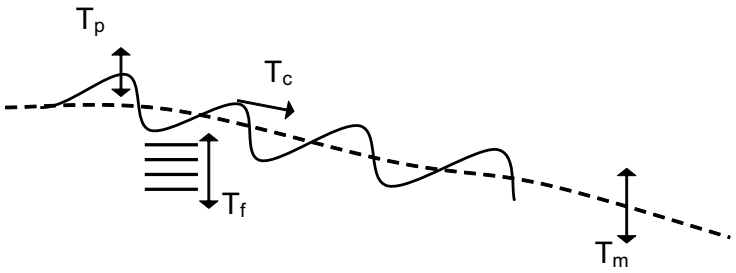

Figure 5.14: Four time scales are involved when applying the new continuum sorting model: (1) the time scale of dune migration, T_c, (2) the time scale of vertical dune dimensions, T_p, (3) the time scale of vertical sorting, $T_f(z)$, and (4) the time scale of large-scale morphological changes, T_m.

the very low elevations of the active bed being reached by the flow only occasionally, and (2) more bed material being present at lower bed elevations than at higher elevations.

Since all parameters in the continuum sorting model are averaged over a series of bedforms, sediment deposited at elevation z is assumed to be mixed immediately with all material present at this elevation. This implies that, for applying the continuum sorting model, it is required that the time scale of dune migration is much smaller than the time scales of dune dimensions, vertical sorting, and morphological changes:

$$T_c \ll \min\{T_p, T_f, T_m\}$$

This is consistent with the description of large-scale morphological changes in many existing morphological model systems. Namely, for using our common sediment transport models, which are derived for *equilibrium* conditions, it is required that the time scale of morphological changes is much larger than the one of dune migration:

$$T_c \ll T_m$$

Likewise, for using models for the *equilibrium* bed roughness, bedform height, and bedform length, it is required that the time scale of dune dimensions is larger than the one of dune migration, and that the time scale of morphological changes is larger than the one of dune dimensions:

$$T_c \ll T_p$$
$$T_p \ll T_m$$

Let us now consider the relation between the sorting time scale, T_f, and the time scale of dune dimensions, T_p. It seems that the latter is either smaller than the sorting time scale or of the same order of magnitude:

1. $T_p \ll T_f$
   In conditions with high bed shear stresses that are well above the critical Shields stresses of all grain sizes in the mixture, deeper bed layers that are reached by the flow only occasionally will slowly change in composition. The PDF of bed surface elevations may have reached equilibrium much faster. This was the case in, for instance, experiment B2 (present study, Chapter 4).

2. $T_p \simeq T_f$
   In conditions with relatively low bed shear stresses and widely graded sediment mixtures that are predominated by partial transport, with the coarsest size fractions not or barely being transported, the time evolution of the PDF of bed surface elevations is directly related to the time evolution of the sorting profile. Coarse bed layers may develop that hinder the entrainment of bed material and thus the growth of bedforms. Fine sediment may be winnowed from below a coarse bed layer, which may result in a very slow adaptation of the bedform height. This was the case in, for instance, experiments A1 and B1 (present study, Chapter 4).

When the time scale of morphological changes, T_m, is of the same order of magnitude as the ones of dune dimensions, T_p and vertical sorting, T_f, we need to take into account the time evolution of both the dune dimensions and the vertical sorting profile when computing changes in morphology. A method for doing so will be explained in Chapter 8.

A special situation occurs when the time scale of morphological changes is much larger than the sorting time scale and the time scale of dune dimensions:

$$T_m \gg \max\{T_p, T_f\} \qquad \min\{T_p, T_f\} \gg T_c \tag{5.101}$$

If, in this case, one is interested in processes at the time scale of morphological changes, T_m, we may assume that the PDF of relative trough elevations, $\tilde{p}_b$, and the vertical sorting profile, $\bar{F}_i$, have reached a state of quasi-equilibrium at every point in time. In these quasi-equilibrium conditions, we may apply equilibrium similarity profiles for $\tilde{p}_b$, E_{siu}, and $\bar{F}_i$ (see Chapter 6). This equilibrium approach will be a useful possibility for applying the new continuum sorting model to field cases.

Section 9.2 will address the requirements for applying the continuum sorting model and will come back to the topic of the various time scales.

5.6 Discussion

In the present chapter we have considered the derivation of a new continuum sorting model for non-uniform sediment. It is based on

1. the Parker-Paola-Leclair framework for sediment continuity,
2. the Einstein step length formulation,
3. a newly-developed lee sorting function, and
4. a newly-developed method to account for the variability in bedform trough elevations.

Each bedform in a series of irregular bedforms is assumed to be characterised by its trough elevation relative to the mean bed level, i.e. the relative trough elevation. All bedform-specific features, e.g., the bedform height and the bedform length, are related to this relative trough elevation according to simple relations. Note that these relations are not assumed to be generally valid and that their applicability should be checked against data before using them.

In its present form, the new continuum sorting model incorporates only bed load transport. Further research is required to include also suspended load transport. Yet, a simple way of incorporating suspended load transport will be explained in Sections 9.3 and 9.4.5. Application of the present model should be limited to bedform-dominated conditions. Further study is required to derive formulations for the grain size-specific and elevation-specific entrainment and deposition fluxes under plane-bed conditions (also see Section 9.5).

The continuum sorting model incorporates sorting through the grain size-selective deposition down an avalanche lee face, the variability in bedform trough elevations, and net aggradation or degradation. In order to incorporate sorting through the avalanche mechanism at the lee face, a new lee sorting function has been developed. This lee face sorting model is a simple trend-based model, and it seems to be the simplest form that has any hope of capturing the effects in question. The final form of the lee sorting function, i.e. the coefficients γ and κ, will be derived by calibration (Chapters 6 and 7). It will depend on the approach taken on in Chapters 6 through 8 whether and how the continuum sorting model will incorporate sorting through grain size-specific entrainment and deposition over the stoss face, the winnowing of fines from the trough surface and subsurface, and the settling of immobile coarse particles. The incorporation of vertical sorting mechanisms will be evaluated in greater detail in Section 9.7.1.

Section 9.7.2 will go into the implications of the following assumptions made in this chapter:

- A series of irregular bedforms is considered as a series of triangular bedforms with varying trough elevations.
- The porosity is assumed to be steady and uniform over all bed elevations.
- The sediment deposited at a specific elevation of the active bed is assumed to be immediately mixed will all sediment in the series of bedforms at that elevation.

Chapter 6

The equilibrium sorting model

In the previous chapter, a new continuum sorting model for non-uniform sediment was proposed. The model is based on (1) the Parker-Paola-Leclair framework for sediment continuity, (2) the Einstein step length formulation, (3) a newly-developed lee sorting function, and (4) a newly-developed method to account for the variability in bedform trough elevations. The model would be complete using sub-models for the size-selective entrainment over bedforms and for the lower and upper limits of the active bed. Unfortunately, such models are not available. Therefore, we will take on another approach.

In the present chapter we consider only *equilibrium conditions*, which is also indicated as the equilibrium approach. Equilibrium is here defined as the situation in which all parameters, e.g., grain size-specific transport rates and the mean bed level, vary around mean values. Under these conditions, the continuum sorting model as described in Chapter 5 can be reduced to an *equilibrium sorting model*.

As a first step towards non-uniform sediment, we consider *uniform sediment* (Section 6.1), for which the equilibrium sorting model provides a solution to the elevation-specific entrainment and deposition densities. Considering *tracer particles in uniform sediment* is a next step forward, but still grain size-selective processes do not play a role. For tracer particles, the equilibrium sorting model solves for the elevation-specific entrainment and deposition densities, which logically equal those for uniform sediment, and for the equilibrium vertical profile of tracer concentration (Section 6.2). Finally, we consider *non-uniform sediment* (Section 6.3), for which the equilibrium sorting model computes the equilibrium sorting profile from either a given bed load transport composition or a given vertical sorting profile at another point in time, together with a given probability density function (PDF) of relative trough elevations.

In Chapter 7, the equilibrium sorting model will be calibrated and verified, and the two constants in the newly-developed lee sorting function will be used as calibration coefficients.

6.1 Uniform sediment

As a first step towards non-uniform sediment, we consider a series of irregular bedforms migrating over a bed composed of uniform sediment. For uniform sediment in equilibrium conditions ($\partial/\partial t = 0$), both (5.11) and (5.12) reduce to the same equation, which is rephrased using (5.93), (5.94), and (5.95):

$$0 = \bar{D}_{esE}(z) - \bar{E}_{esE}(z) + \bar{D}_{elE}(z) = \int_{\eta_{bmin}}^{\eta_{bmax}} \left[\frac{\lambda_s}{\lambda} p_{se}(z) E_{suE}(z - \eta_{step}(z)) - \frac{\lambda_s}{\lambda} p_{se}(z) E_{suE}(z) + \frac{\lambda_l}{\lambda} p_{le}(z) D_{lE} \right] \tilde{p}_{bE}\, d\eta_b \tag{6.1}$$

where the subscript E indicates equilibrium conditions. For parameter clarification, reference is made to the Nomenclature. In order to find the overall[1] elevation-specific deposition and entrainment fluxes over a series of irregular bedforms, $\bar{D}_{esE}$, $\bar{E}_{esE}$, and $\bar{D}_{elE}$, we need to solve for the entrainment rate E_{suE} over individual bedforms.

Eq. (6.1) is further reduced by assuming that not only each individual *lee* face has a uniform slope ($p_{le}(z) = J(z)/\Delta$), but also each *stoss* face ($p_{se}(z) = J(z)/\Delta$). Thus, we have simplified the series of irregular bedforms to a series of triangular bedforms with varying bedform heights and bedform lengths. Now (6.1) yields

$$0 = \int_{\eta_{bmin}}^{\eta_{bmax}} \frac{J(z)}{\lambda \Delta} \left[\lambda_s E_{suE}(z - \eta_{step}(z)) - \lambda_s E_{suE}(z) + q_{topE} \right] \tilde{p}_{bE}\, d\eta_b \tag{6.2}$$

since in equilibrium conditions (5.41) reduces to $D_{lE} = q_{topE}/\lambda_l$. Eq. (6.2) expresses that, in equilibrium conditions, at each bed elevation z there is a dynamic equilibrium between

- the *net*[2] entrainment flux at the stoss face, averaged over all bedforms
- the deposition flux at the lee face, averaged over all bedforms

which is illustrated in Figure 6.1. The constraint given by (6.2) is met if, for each individual bedform in a series of irregular triangular bedforms, the following equation is satisfied:

$$\lambda_s E_{suE}(z - \eta_{step}(z)) - \lambda_s E_{suE}(z) + q_{topE} = 0 \tag{6.3}$$

which expresses that, for each bedform in a series of irregular triangular bedforms, the net entrainment flux at bed elevation z at the stoss face equals the deposition rate at the lee face.

[1] *overall* meaning being averaged over a series of bedforms
[2] *net* meaning the difference between the entrainment flux and the deposition flux

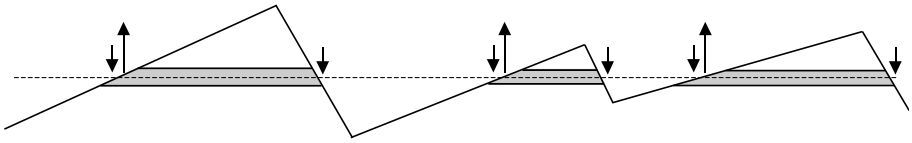

Figure 6.1: Sediment fluxes onto bed elevation z for a series of irregular triangular bedforms.

Now, in order to find a solution to $E_{suE}(z)$ that fulfills (6.3), we first have a look at the formulation for the bed load transport rate over the bedform crest, q_{topE}. For non-uniform sediment, the bed load transport over the bedform crest for an individual bedform is given by (5.66) and (5.40). Similar to the analysis leading to (5.26) in Section 5.2.1, the bed load transport rate over the bedform crest for uniform sediment is given by

$$q_{topE} = \Lambda E_{suE}(z_t - \tfrac{1}{2}\eta_{step}(z_t)) \tag{6.4}$$

where z_t denotes the crest elevation of the specific bedform ($z_t = \eta_t = \bar{\eta}_a + \frac{1}{2}\Delta$). According to (5.64), the arguments in (6.3) and (6.4) are

$$z - \eta_{step}(z) = \Delta f_{ds}\left[g_{ds}(z^*) - \frac{\Lambda}{\lambda_s}\right] + \eta_a \tag{6.5}$$

$$z_t - \tfrac{1}{2}\eta_{step}(z_t) = \Delta f_{ds}\left[1 - \frac{\Lambda}{2\lambda_s}\right] + \eta_a \tag{6.6}$$

where the functions g_{ds} and f_{ds} in (5.61) are

$$f_{ds}(x^*) = x^* - \tfrac{1}{2} \qquad g_{ds}(z^*) = z^* + \tfrac{1}{2} \tag{6.7}$$

since each stoss face is assumed to have a uniform slope.

Analysing (6.3) through (6.6), it is found that a possible solution to the entrainment rate E_{suE} is a linear function of g_{ds}, so that we propose the following relation for the entrainment rate over an individual bedform:

$$E_{suE}(z) = a_E\, g_{ds}(z) + b_E \tag{6.8}$$

where a_E and b_E are constants, independent of z. Note that (6.8), combined with (6.7b), imply that for a triangular bedform the entrainment rate E_{suE} increases linearly with increasing bed surface elevation. This can also be understood by considering the simple-wave analysis in Section 2.1 together with the Einstein step length formulation in Section 5.2.1. Applying the simple-wave analysis to dune migration

has shown that the local bed load transport rate over a bedform is proportional to the vertical distance to the trough elevation, as is expressed by (2.4). Since (5.26) tells us that the local entrainment rate is a linear function of the local bed load transport rate, $q = \Lambda E$, it is understandable that (6.8) reflects that for a triangular dune the entrainment rate increases linearly with increasing bed surface elevation.

Combination of (6.3) through (6.6) and (6.8) yields $b_E = a_E \Lambda/(2\lambda_s)$, so that (6.8) and (6.4) yield, respectively

$$E_{suE}(z) = a_E \left(g_{ds}(z^*) + \frac{\Lambda}{2\lambda_s} \right) \tag{6.9}$$

$$q_{topE} = \Lambda \, a_E \tag{6.10}$$

where a_E is expected to be determined by the total bed load transport rate, q_{aE}. To find out whether a_E indeed depends on q_{aE}, we rephrase the transport rate averaged over an individual bedform in (5.67) and (5.50) for uniform sediment in equilibrium conditions to

$$q_{aE} = \frac{\lambda_s}{\lambda} \Lambda \int_{\eta_b^*}^{\eta_t^*} J(z) \, E_{suE}(z - \tfrac{1}{2}\eta_{step}(z)) \, dz^* + \frac{\lambda_l}{2\lambda} q_{topE} \tag{6.11}$$

where the argument equals

$$z - \tfrac{1}{2}\eta_{step}(z) = \Delta f_{ds} \left[g_{ds}(z^*) - \frac{\Lambda}{2\lambda_s} \right] + \eta_a \tag{6.12}$$

Now, with (6.10), (6.9), and (6.12), and after integration over η_b^* to η_t^*, Eq. (6.11) results in the following relation between a_E and q_{aE}, showing that, for a triangular bedform, the bed load transport rate over the crest is twice as large as the average bed load transport rate:

$$a_E = 2 \, q_{aE}/\Lambda \tag{6.13}$$

$$q_{topE} = 2 \, q_{aE} \tag{6.14}$$

We now assume that the total bed load transport rate is identical for each individual bedform, which implies that

$$q_{aE} = \bar{q}_{aE} \tag{6.15}$$

$$q_{topE} = \bar{q}_{topE} \tag{6.16}$$

$$a_E = \bar{a}_E = 2 \, \bar{q}_{aE}/\Lambda \tag{6.17}$$

The constant $\bar{a}_E$ is thus determined by the equilibrium bed load transport rate, $\bar{q}_{aE}$, whence it is dependent on bed shear stress.

The set of equations is now complete. That is, for a given average bed load transport rate, $\bar{q}_{aE}$, and a given probability density function (PDF) of relative trough elevations, $\tilde{p}_{bE}$, we can determine the equilibrium overall entrainment and deposition densities over a series of irregular bedforms composed of uniform sediment, i.e. $\bar{E}_{esE}$, $\bar{D}_{esE}$, and $\bar{D}_{elE}$. Eqs. (5.93), (5.94), and (5.95) reduce to

$$\bar{E}_{esE}(z) = \int_{\eta_{bmin}}^{\eta_{bmax}} \frac{\lambda_s}{\lambda} \frac{J(z)}{\Delta} E_{suE}(z)\, \tilde{p}_{bE}\, d\eta_b \tag{6.18}$$

$$\bar{D}_{esE}(z) = \int_{\eta_{bmin}}^{\eta_{bmax}} \frac{\lambda_s}{\lambda} \frac{J(z)}{\Delta} E_{suE}(z - \eta_{step}(z))\, \tilde{p}_{bE}\, d\eta_b \tag{6.19}$$

$$\bar{D}_{elE}(z) = 2\,\bar{q}_{aE} \int_{\eta_{bmin}}^{\eta_{bmax}} \frac{J(z)}{\lambda\Delta}\, \tilde{p}_{bE}\, d\eta_b \tag{6.20}$$

where E_{suE} in (6.9) is given by

$$E_{suE}(z) = 2\,\frac{\bar{q}_{aE}}{\Lambda} \left(z^* + \tfrac{1}{2} + \frac{\Lambda}{2\lambda_s} \right) \tag{6.21}$$

The average bed load transport rate, $\bar{q}_{aE}$, and the PDF of relative trough elevations, $\tilde{p}_{bE}$, need to be determined from either predictions or measurements.

Note that the constraint that the average transport rate is identical for each bedform implies that bedforms with different bedform heights Δ migrate with different migration speeds c, which can be concluded from (2.6):

$$c = \frac{\bar{q}_{aE}}{c_b \beta \Delta} \tag{6.22}$$

where β denotes the bedform shape factor ($\beta = \frac{1}{2}$ for triangular bedforms). Eq. 6.22 implies that a large bedform in a series of bedforms migrates at a smaller speed than a smaller bedform, and that, even in equilibrium conditions, smaller bedforms may migrate over larger bedforms. This has been confirmed by flume experiments (*Leclair*, 2000).

6.2 Tracers in uniform sediment

After deriving the equilibrium entrainment and deposition densities over a series of irregular bedforms composed of uniform sediment, we will make another step towards the equilibrium vertical sorting profile for non-uniform sediment. The present

section explains the derivation of the equilibrium vertical profile of tracer concentration. Compared to non-uniform sediment, the case of tracer particles in uniform sediment is still a straightforward one, since grain size-selective processes, such as the grain size-selective sorting down a bedform lee face, do not play a role.

An important assumption is that no distinction in sorting is made between bedforms in a series of bedforms, so that each individual bedform is characterised by the same absolute vertical profile of tracer concentration (except for bed elevations not covered by the bedform):

$$f_E(z) = \bar{f}_E(z) \tag{6.23}$$

where the volume fraction content f for tracer particles and $1-f$ for non-tracer particles are equivalent to the elevation-specific volume fraction content of size fraction i, F_i, in non-uniform sediment. Similar to the analysis for uniform sediment, we assume the average bed load transport rate identical for each individual bedform ($q_{aE} = \bar{q}_{aE}$). Eq. (6.14) shows that this implies that the bed load transport rate over the bedform crest is identical over each individual bedform, as well ($q_{topE} = \bar{q}_{topE}$).

In equilibrium conditions, Eqs. (5.11) and (5.12) reduce to

$$0 = \bar{D}_{eisE}(z) - \bar{E}_{eisE}(z) + \bar{D}_{eilE}(z) \tag{6.24}$$

$$0 = \Sigma_i^2 \left[\bar{D}_{eisE}(z) - \bar{E}_{eisE}(z) + \bar{D}_{eilE}(z)\right] \tag{6.25}$$

Here, the subscript i denotes one of the two sediment fractions, tracer particles and non-tracer particles. These equations express that, at each bed surface elevation z, there is a dynamic equilibrium in both *composition*[3] and *total*[4] *amount* between:

- the net entrainment flux at the stoss face, averaged over all bedforms
- the deposition flux at the lee face, averaged over all bedforms

We can see that, in case (6.24) is met, (6.25) is satisfied, as well. Again, we assume each bedform to have a triangular shape, so that $p_e(z) = p_{le}(z) = p_{se}(z) = J(z)/\Delta$. Furthermore, the elevation-specific entrainment rate for bedforms composed of uniform sediment, $E_{suE}(z)$ in (6.9), must be valid for both the tracer and the non-tracer particles, since the tracer and non-tracer particles constitute a mixture of uniform sediment. Now, combination of (6.24), (5.93), (5.94), and (5.95) yields

$$0 = \int_{\eta_{bmin}}^{\eta_{bmax}} \frac{J(z)}{\lambda\Delta} \Big[\lambda_s E_{suE}(z - \eta_{step}(z))\bar{f}_E(z - \eta_{step}(z)) - \lambda_s E_{suE}(z)\bar{f}_E(z) + \bar{q}_{topE} f_{leelocE}(z)\Big] \tilde{p}_{bE}\, d\eta_b \tag{6.26}$$

[3] *composition* here meaning the volume fraction content of tracer particles

[4] *total* here meaning summed over the two sediment fractions: tracer and non-tracer particles

For uniform sediment, there is no selective deposition at the lee face, so that, for a specific bedform, the volume fraction content of tracers in the sediment deposited at elevation z at the lee face equals the volume fraction content of tracer particles in the lee deposit, f_{leeE}:

$$f_{leelocE}(z) = f_{leelocE} = f_{leeE} \tag{6.27}$$

Thus, $f_{leelocE}$ is independent of bed elevation, that is, for elevations within the limits of the active bed. For tracers in equilibrium conditions, (5.45) yields $f_{leeE} = f_{topE}$, which tells us that the volume fraction content of tracer particles in the sediment transported over the bedform crest equals the volume fraction content of tracer particles in the lee deposit.

Since we consider equilibrium conditions, changes in time of the elevation-specific bed composition do not occur. This implies that the volume fraction content of tracers in the net entrainment flux at elevation z, as well as the overall volume fraction content of tracers in the sediment deposited at elevation z at the lee face, $\bar{f}_{leelocE}$, must equal the volume fraction content of tracers in the bed at elevation z, $\bar{f}_E(z)$:

$$\bar{f}_E(z) = \bar{f}_E = \bar{f}_{leelocE} \tag{6.28}$$

Since there are no preferential deposition processes for tracers or non-tracers, the equilibrium volume fraction content of tracers particles, $\bar{f}_E$, will be uniform over depth. Now, the volume fraction content of tracer particles in the sediment transported over the bedform crest must equal the equilibrium volume fraction content of tracers in the bed, $\bar{f}_E$:

$$f_{topE} = \bar{f}_{topE} = \bar{f}_E \tag{6.29}$$

since grain size-selective entrainment over the stoss face does not occur.

One method to solve for the equilibrium volume fraction content of tracers in the bed, $\bar{f}_E$, is to derive it from the given equilibrium volume fraction content of tracers in the bed load transport, $\bar{f}_{aE}$. The bed load transport rate and composition averaged over an individual bedform are given by (5.67) and (5.50). Similar to the analysis for uniform sediment in equilibrium conditions, for tracer particles in uniform sediment, we can rephrase (5.67) to

$$\bar{q}_{aE} f_{aE} = \frac{\lambda_s}{\lambda} \Lambda \int_{\eta_b^*}^{\eta_t^*} J(z)\, E_{suE}(z - \tfrac{1}{2}\eta_{step}(z))\, \bar{f}_E\, dz^* + \frac{\lambda_l}{2\lambda} \bar{q}_{topE} \bar{f}_{topE} \tag{6.30}$$

By substituting (6.10), (6.9), and (6.12) into (6.30), and integrating over η_b^* to η_t^*, Eqs. (6.30) and (5.50) reduce to

$$\bar{q}_{aE} f_{aE} = \tfrac{1}{2} a_E \Lambda \bar{f}_E \qquad\qquad \bar{q}_{aE} = \tfrac{1}{2} a_E \Lambda \tag{6.31}$$

which yields

$$f_{aE} = \bar{f}_{aE} = \bar{f}_E \tag{6.32}$$

which expresses that the equilibrium volume fraction content of tracers in the bed $\bar{f}_E$, being uniform over all elevations of the active bed, equals the equilibrium volume fraction content of tracer particles in the bed load transport, $\bar{f}_{aE}$.

Instead of deriving the equilibrium volume fraction content of tracers in the bed, $\bar{f}_E$, from the bed load transport composition, we can solve it from a given profile of tracer concentration in the active bed at another point in time, $\bar{f}_{ini}$. When there are no divergences in the rate and composition of the sediment transport, the total volume of tracer particles in the active bed is steady. This total volume of tracer particles in the active bed can be expressed by the volume fraction content of tracer particles averaged over the active bed, $\bar{\bar{f}}$. The equilibrium volume fraction content of tracers in the bed, $\bar{f}_E$, must be identical to $\bar{\bar{f}}$, since either of them are uniform over all elevations of the active bed:

$$\bar{f}_E = \bar{\bar{f}} = \frac{\int_{\eta_{mn}}^{\eta_{mx}} \bar{C}_{ini}(z)\, dz}{\int_{\eta_{mn}}^{\eta_{mx}} \sum_i^N \bar{C}_{ini}(z)\, dz} = \frac{\int_{\eta_{mn}}^{\eta_{mx}} \bar{P}_{sini}(z) \bar{f}_{ini}(z)\, dz}{\int_{\eta_{mn}}^{\eta_{mx}} \bar{P}_{sini}(z)\, dz} \tag{6.33}$$

where $\bar{C}_{ini}(z)$ denotes the overall concentration of tracer particles at bed elevation z at the point in time for which the profile of tracer concentration is known ($\bar{C}_{ini} = c_b \bar{P}_{sini} \bar{f}_{ini}$), and $\bar{f}_{ini}(z)$ the overall volume fraction content of tracer particles at bed elevation z at the specific point in time, which is also called the *initial* situation. The porosity and thus the sediment concentration in the bed, c_b, are assumed to be uniform over depth. $\bar{P}_{sini}(z)$ denotes the probability distribution of bed surface elevations, which is determined from the given PDF of relative trough elevations at the specific point in time, $\tilde{p}_{bini}$, using (5.92) and (5.2). In all integrals in (6.33), η_{mn} and η_{mx} denote the lower and upper levels of the active bed of either the initial or the equilibrium stage, that is, the stage in which the active bed covers the widest range of bed elevations. *Note that this initial sorting profile method may be used only if, from the moment that the bed composition is known until the moment equilibrium conditions are reached, divergences in the grain size-selective transport have been negligible.*

Thus, for tracer particles in uniform sediment, there are two methods to solve for the equilibrium volume fraction content of tracers in the bed, $\bar{f}_E$. Note that this quantity is uniform over all elevations of the active bed. One method to solve for $\bar{f}_E$ is based on a given bed load transport composition, $\bar{f}_{aE}$, whereas the second method is based on a given profile of the volume fraction content of tracer particles at another point in time, $\bar{f}_{ini}(z)$, together with its PDF of relative trough elevations, $\tilde{p}_{bini}$.

6.3 Non-uniform sediment

6.3.1 Dynamic equilibrium

We now return to the most interesting case: the equilibrium vertical sorting profile of non-uniform sediment. The analyses for uniform sediment and tracer particles in the two previous sections have served as stepping stones for the present analysis of non-uniform sediment. The main difference between the analysis for tracer particles and the present analysis for non-uniform sediment is that the latter is characterised by grain size-selective processes, such as the grain size-selective deposition down a bedform lee face.

Similar to the analyses for uniform sediment and tracer particles, we assume that the average bed load transport rate over each individual bedform is identical, so that $q_{aE} = \bar{q}_{aE}$. Furthermore, we make no distinction in sorting between different bedforms within one series of bedforms, so that

$$F_{iE}(z) = \bar{F}_{iE}(z) \tag{6.34}$$

In equilibrium conditions, Eqs. (5.11) and (5.12) reduce to

$$0 = \bar{D}_{eisE}(z) - \bar{E}_{eisE}(z) + \bar{D}_{eilE}(z) \tag{6.35}$$

$$0 = \sum_i^N \left[\bar{D}_{eisE}(z) - \bar{E}_{eisE}(z) + \bar{D}_{eilE}(z)\right] \tag{6.36}$$

These equations express that, at each bed surface elevation, there is a dynamic equilibrium in both *composition* and *total*[5] *amount* of:

- the net entrainment flux at the stoss face, averaged over all bedforms
- the deposition flux at the lee face at the same elevation, averaged over all bedforms

We can see that if (6.35) is fulfilled, (6.36) is automatically satisfied, as well. Using (5.93), (5.94), and (5.95) and again assuming each stoss side to have a uniform slope, (6.35) yields

$$0 = \int_{\eta_{bmin}}^{\eta_{bmax}} \frac{J(z)}{\lambda\Delta} \Big[\lambda_s E_{siuE}(z - \eta_{stepi}(z))\bar{F}_{iE}(z - \eta_{stepi}(z)) - \lambda_s E_{siuE}(z)\bar{F}_{iE}(z) + q_{topE}F_{leelociE}(z)\Big]\ \tilde{p}_{bE}\, d\eta_b \tag{6.37}$$

Since we consider equilibrium conditions, other vertical sediment fluxes do not occur, i.e. the net effect of winnowing and infiltration of fines is negligible, as well as

[5] *total* meaning summed over all size fractions

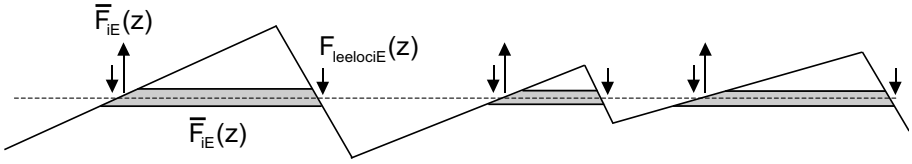

Figure 6.2: Composition of sediment fluxes onto elevation z.

the settlement of particles too coarse to be transported. This means that the *overall* composition of sediment deposited at the lee face at elevation z must equal the *overall* bed composition at that same elevation:

$$\bar{F}_{leelociE}(z) = \bar{F}_{iE}(z) \tag{6.38}$$

Now, the equilibrium state also requires that the volume fraction content of size fraction i in the net entrainment flux at bed elevation z at the stoss face equals the equilibrium bed composition at that same elevation, $\bar{F}_{iE}(z)$, which is illustrated in Figure 6.2. Note that the composition of sediment deposited over the lee face of an individual bedform, $F_{leeloci}(z)$, may differ from the bed composition at that same elevation, $\bar{F}_{iE}(z)$ (see Figure 6.2). Yet, averaged over all bedforms, the composition of sediment deposited at elevation z at the lee face, $\bar{F}_{leeloci}(z)$, must equal $\bar{F}_{iE}(z)$.

In order to find a solution to the equilibrium sorting profile for non-uniform sediment, $\bar{F}_{iE}(z)$, we need to solve (6.37). We can see that (6.37) is satisfied when the following equation is met for each individual bedform in the series of bedforms:

$$\begin{aligned}&\lambda_s E_{siuE}(z - \eta_{stepi}(z))\bar{F}_{iE}(z - \eta_{stepi}(z)) - \lambda_s E_{siuE}(z)\bar{F}_{iE}(z) + \\ &\quad q_{topE}F_{leelociE}(z) = 0\end{aligned} \tag{6.39}$$

Like the bed load transport over the bedform crest for uniform sediment in (6.4), the grain size-selective bed load transport rate over the crest, q_{topi}, in (5.66) reduces to

$$q_{topiE} = \Lambda_i E_{siuE}(z_t - \tfrac{1}{2}\eta_{stepi}(z_t))\, \bar{F}_{iE}(z_t - \tfrac{1}{2}\eta_{stepi}(z_t)) \tag{6.40}$$

$$q_{topE} = \textstyle\sum_i^N q_{topiE} \tag{6.41}$$

We now substitute Θ_{iE} for the weighed entrainment rate $E_{siuE}\bar{F}_{iE}$, so that (6.39) can be rephrased to

$$\lambda_s\, \Theta_{iE}(z - \eta_{stepi}(z)) - \lambda_s\, \Theta_{iE}(z) + \Lambda_i\, \omega_{iE}(z)\, \Theta_{iE}(z_t - \tfrac{1}{2}\eta_{stepi}(z_t)) = 0 \tag{6.42}$$

where the arguments can be written as

$$z - \eta_{stepi}(z) = \Delta f_{ds} \left[g_{ds}(z^*) - \frac{\Lambda_i}{\lambda_s} \right] + \eta_a \tag{6.43}$$

$$z_t - \tfrac{1}{2}\eta_{stepi}(z_t) = \Delta f_{ds} \left[1 - \frac{\Lambda_i}{2\lambda_s} \right] + \eta_a \tag{6.44}$$

and where, for equilibrium conditions, the lee sorting function in (5.72) is written as

$$\omega_{iE}(z) = J(z)\,(1 + \delta_{iE}\,\hat{z}^*) \tag{6.45}$$

Analysing (6.42) with its arguments, we find that a possible solution to the weighed entrainment rate, Θ_{iE}, is a quadratic function of g_{ds}:

$$\Theta_{iE}(z) = E_{siuE}(z)\bar{F}_{iE}(z) = a_{iE}\, g_{ds}^2(z^*) + b_{iE}\, g_{ds}(z^*) + c_{iE} \tag{6.46}$$

Now, combination of (6.42) through (6.46) yields

$$b_{iE} = a_{iE} \left(\frac{2}{\delta_{iE}} + \frac{\Lambda_i}{\lambda_s} - 1 \right) \tag{6.47}$$

$$c_{iE} = \frac{a_{iE}\Lambda_i}{2\lambda_s} \left(\frac{2}{\delta_{iE}} + \frac{\Lambda_i}{2\lambda_s} - 1 \right) \tag{6.48}$$

The local bed load transport rate of size fraction i over the stoss face of an individual bedform, $q_{siE}(z)$, and the total bed load transport rate, $q_{sE}(z)$, are now given by

$$q_{siE}(z) = \Lambda_i\, \Theta_{iE}(z - \tfrac{1}{2}\eta_{stepi}(z)) = \Lambda_i a_{iE} \left[g_{ds}^2(z^*) + g_{ds}(z^*)\,(2/\delta_{iE} - 1) \right] \tag{6.49}$$

$$q_{sE}(z) = \textstyle\sum_i^N q_{siE}(z) \tag{6.50}$$

where $g_{ds} = z^* + \frac{1}{2}$. This tells us that the bed load transport rate of size fraction i over the stoss face, q_{siE}, increases from 0 at the trough to q_{topiE} at the bedform crest, where q_{topiE} is given by

$$q_{topiE} = 2\frac{a_{iE}\Lambda_i}{\delta_{iE}} \tag{6.51}$$

Note that the bed load transport rate of size fraction i over the stoss face, q_{siE}, is not a linear function of the bed surface elevation. However, since the set of equations automatically guarantees that

$$\textstyle\sum_i^N \Lambda_i a_{iE} = 0 \tag{6.52}$$

the *total* bed load transport rate over the stoss face, q_{sE}, does increase linearly with increasing bed surface elevation, viz. from 0 in the trough to $q_{topE} = \sum_i^N q_{topiE}$ at the bedform crest:

$$q_{sE}(z) = 2\, g_{ds}(z^*) \sum_i^N \frac{a_{iE}\Lambda_i}{\delta_{iE}} \tag{6.53}$$

This was also found by applying the simple-wave equation to bedform migration, as is expressed by (2.4). The total bed load transport rate over the bedform crest is thus twice the bedform-averaged total bed load transport rate: $q_{topE} = 2\, q_{aE}$.

In order to find out how the constant a_{iE} is related to the bed load transport rate, we rephrase the bed load transport rate of size fraction i in (5.67) to

$$q_{aiE} = \frac{\lambda_s}{\lambda}\Lambda_i \int_{\eta_b^*}^{\eta_t^*} \Theta_{iE}(z - \tfrac{1}{2}\eta_{stepi}(z))\, dz^* + \frac{\lambda_l}{2\lambda} q_{topiE} \tag{6.54}$$

where the argument equals

$$z - \tfrac{1}{2}\eta_{stepi}(z) = \Delta f_{ds} \left[g_{ds}(z^*) - \frac{\Lambda_i}{2\lambda_s} \right] + \eta_a \tag{6.55}$$

Using (6.51), (6.46), (6.47), (6.48), and (5.85), we can elaborate (6.54) to

$$q_{aiE} = a_{iE}\Lambda_i \left[\frac{1}{\delta_{iE}} - \frac{1}{6} + \frac{\Delta_a}{6\lambda_a \tan(\nu)} \right] \tag{6.56}$$

Since we assumed the total bed load transport to be identical for each dune ($q_{aE} = \bar{q}_{aE}$), we find the following relation for a_{iE}:

$$a_{iE} = \frac{\bar{q}_{aiE}}{\Lambda_i} \left[\frac{1}{\delta_{iE}} - \frac{1}{6} + \frac{\Delta_a}{6\lambda_a \tan(\nu)} \right]^{-1} \tag{6.57}$$

which shows that a_{iE} is independent of the specific trough elevation, whence $\bar{a}_{iE} = a_{iE}$. Eq. (6.51) shows that in that case also the bed load transport rate of size fraction i over the bedform crest is independent of the specific trough elevation ($q_{topiE} = \bar{q}_{topiE}$), as well as the volume fraction content of size fraction i in the sediment transported over the bedform crest and in the lee deposit ($F_{topiE} = \bar{F}_{topiE} = \bar{F}_{leeiE}$).

These formulations serve as a basis for the derivation of the equilibrium vertical sorting profile, $\bar{F}_{iE}(z)$, which will be addressed in the next two sections.

6.3.2 Sorting based on transport composition

Similar to the analysis of the equilibrium vertical profile of tracer concentration, one method for solving for the equilibrium sorting profile, $\bar{F}_{iE}$, is to derive it from the measured or computed bed load transport composition, $\bar{F}_{aiE}$. The second method, which is based on a vertical sorting profile known at another point in time, $\bar{\bar{F}}_{ini}$, will be discussed in the next section.

According to (6.38), the equilibrium sorting profile, $\bar{F}_{iE}$, equals the equilibrium volume fraction content of size fraction i deposited at elevation z at the lee face, $\bar{F}_{leelociE}$. The latter quantity can also be written as the amount of size fraction i deposited at that elevation of the lee face divided by the total amount of sediment deposited at that elevation of the lee face:

$$\bar{F}_{iE}(z) = \bar{F}_{leelociE}(z) = \frac{1}{\sum_i^N \bar{D}_{eilE}(z)} \bar{D}_{eilE}(z) \tag{6.58}$$

where the overall grain size-specific and elevation-specific deposition density, $\bar{D}_{eilE}$, is given by (5.95) and the equilibrium volume fraction content of size fraction i deposited at elevation z at the lee face, $F_{leelociE}$, by (5.68):

$$\bar{D}_{eilE}(z) = \bar{q}_{topE} \int_{\eta_{bmin}}^{\eta_{bmax}} \frac{J(z)}{\lambda\Delta} F_{leelociE}(z)\, \tilde{p}_{bE}\, d\eta_b \tag{6.59}$$

$$F_{leelociE}(z) = \bar{F}_{leeiE}\, \omega_{iE}(z) = \bar{F}_{topiE}\, \omega_{iE}(z) \tag{6.60}$$

so that (6.58) can be rephrased to

$$\bar{F}_{iE}(z) = \frac{\bar{F}_{topiE}}{\int_{\eta_{bmin}}^{\eta_{bmax}} \frac{J(z)}{\lambda\Delta}\, \tilde{p}_{bE}\, d\eta_b} \int_{\eta_{bmin}}^{\eta_{bmax}} \frac{J(z)}{\lambda\Delta} \omega_{iE}(z)\, \tilde{p}_{bE}\, d\eta_b \tag{6.61}$$

where $\bar{F}_{topiE}$ can be derived from (6.51):

$$\bar{F}_{topiE} = \frac{\bar{q}_{topiE}}{\bar{q}_{topE}} = \frac{\bar{F}_{aiE} \left(1 - \frac{\delta_{iE}}{6} + \frac{\delta_{iE}\Delta_a}{6\lambda_a \tan(\nu)}\right)^{-1}}{\sum_i^N \left[\bar{F}_{aiE} \left(1 - \frac{\delta_{iE}}{6} + \frac{\delta_{iE}\Delta_a}{6\lambda_a \tan(\nu)}\right)^{-1}\right]} \tag{6.62}$$

Eq. (6.61) solves for the equilibrium sorting profile, $\bar{F}_{iE}$, from the volume fraction content of size fractions in the bed load transport, $\bar{F}_{aiE}$, the PDF of relative trough elevations, $\tilde{p}_{bE}$, and the lee sorting function, ω_{iE}. The formulation for the lee sorting function, ω_{iE}, in (6.61) is given below. Note that the equilibrium sorting profile is

affected neither by the total bed load transport rate, $\bar{q}_{aE}$, nor by the dimensionless step length, α.

The lee sorting function, ω_{iE}, in (6.61) is given by (5.72) and (5.74), which for equilibrium conditions and triangular dunes become

$$\omega_{iE}(z) = J(z)\,(1 + \delta_{iE}\,\hat{z}^*) \tag{6.63}$$

$$\delta_{iE} = -\gamma\,\frac{\bar{\phi}_{mleeE} - \phi_i}{\bar{\sigma}_{aE}}\,(\bar{\tau}^*_{bE})^{-\kappa} \tag{6.64}$$

where

$$\hat{z}^* = z^* = \frac{z - \bar{\eta}_a}{\Delta}$$

$$\bar{\tau}^*_{bE} = \frac{\bar{\tau}_{bE}}{(\rho_s - \rho)\,g\,\bar{d}_{mleeE}}$$

$$\bar{d}_{mleeE} = \tfrac{1}{1000}2^{-\bar{\phi}_{mleeE}}$$

where the equilibrium bed shear stress, $\bar{\tau}_{bE}$, is known from either measurements or predictions and where γ and κ are constants that will be used as calibration coefficients in the next chapter. The geometric mean grain size of the lee deposit, $\bar{\phi}_{mleeE}$, and the arithmetic standard deviation, $\bar{\sigma}_{aE}$, are given by

$$\bar{\phi}_{mleeE} = \textstyle\sum_i^N \phi_i \bar{F}_{leeiE} \tag{6.65}$$

$$\bar{\sigma}^2_{aE} = \textstyle\sum_i^N (\phi_i - \bar{\phi}_{mleeE})^2\,\bar{F}_{leeiE} \tag{6.66}$$

In equilibrium conditions, the composition of the lee deposit, $\bar{F}_{leeiE}$, equals the composition of the sediment transported over the bedform crest, $\bar{F}_{topiE}$. Since the geometric mean grain size of the lee deposit, $\bar{\phi}_{mleeE}$, and the arithmetic standard deviation, $\bar{\sigma}_{aE}$, depend on the composition of the lee deposit, $\bar{F}_{leeiE}$, the equilibrium sorting profile, $\bar{F}_{iE}$, in (6.61) needs to be solved iteratively.

At each bed elevation, the volume fraction content summed over all size fractions must equal unity and the volume fraction content of each size fraction must be larger than or equal to zero and smaller than or equal to unity, which is expressed by the two constraints in (5.70) and (5.71). Substituting the above-mentioned formulations for the lee sorting function and the geometric mean grain size of the lee deposit, $\bar{\phi}_{mleeE}$, into (5.70), we find that the constraint in (5.70) is satisfied automatically. The

second constraint can be written as

$$-2 \leq \delta_{iE} \leq 2 \tag{6.67}$$

$$-2\left(\frac{1}{\bar{F}_{leeiE}}-1\right) \leq \delta_{iE} \leq 2\left(\frac{1}{\bar{F}_{leeiE}}-1\right) \tag{6.68}$$

These constraints need to be taken into account when solving for the equilibrium sorting profile.

6.3.3 Sorting based on initial sorting profile

Instead of deriving the equilibrium sorting profile, $\bar{F}_{iE}$, from the measured or computed volume fraction content of size fractions in the bed load transport, $\bar{F}_{aiE}$, we can solve $\bar{F}_{iE}$ from a given vertical sorting profile at another point in time, $\bar{\bar{F}}_{inii}$, and its accompanying PDF of relative trough elevations, $\tilde{p}_{bini}$. This other point in time is also called the *initial phase*. For both methods, the actual PDF of relative trough elevations, $\tilde{p}_{bE}$, needs to be known, from either measurements or predictions.

Note that this so-called *initial sorting profile method* may be used only if, from the moment that the bed composition is specified until equilibrium conditions are reached, divergences in the grain size-selective transport have been negligible. Consequently, the total volume of each size fraction in the active bed remains steady, as well as the volume fraction content of size fraction i averaged over the active bed, $\bar{\bar{F}}_i$:

$$\bar{\bar{F}}_i = \frac{\int_{\eta_{mn}}^{\eta_{mx}} \bar{C}_i(z)\,dz}{\int_{\eta_{mn}}^{\eta_{mx}} \sum_i^N \bar{C}_i(z)\,dz} = \frac{\int_{\eta_{mn}}^{\eta_{mx}} \bar{P}_s(z)\bar{F}_i(z)\,dz}{\int_{\eta_{mn}}^{\eta_{mx}} \bar{P}_s(z)\,dz} \tag{6.69}$$

Thus, when flow conditions are uniform from the moment the bed composition is specified (subscript *ini*) until the moment equilibrium is reached (subscript E), the volume fraction content of size fraction i averaged over the active bed, $\bar{\bar{F}}_i$, must be identical at both times, so that $\bar{\bar{F}}_{iE} = \bar{\bar{F}}_{inii}$:

$$\frac{\int_{\eta_{mn}}^{\eta_{mx}} \bar{P}_s(z)\bar{F}_{iE}(z)\,dz}{\int_{\eta_{mn}}^{\eta_{mx}} \bar{P}_s(z)\,dz} = \frac{\int_{\eta_{mn}}^{\eta_{mx}} \bar{P}_{sini}(z)\bar{F}_{inii}(z)\,dz}{\int_{\eta_{mn}}^{\eta_{mx}} \bar{P}_{sini}(z)\,dz} \tag{6.70}$$

In (6.70), η_{mn} and η_{mx} denote the lower and upper levels of the active bed of either the initial or the equilibrium stage, that is, the stage in which the active bed covers the widest range of bed elevations.

Note that for solving the equilibrium sorting profile, $\bar{F}_{iE}$, from (6.70), we need to use an iterative method imposing different combinations for the proportions of all size

fractions in the bed load transport, $\bar{F}_{aiE}$. Subsequently, for each proposed bed load transport composition, $\bar{F}_{aiE}$, we need to calculate its accompanying equilibrium sorting profile, $\bar{F}_{iE}$, using (6.61). Finally, we check whether the accompanying volume fraction content of size fraction i averaged over the active bed, $\bar{\bar{F}}_{iE}$, equals the initial volume fraction content of size fraction i averaged over the active bed, $\bar{\bar{F}}_{inii}$. Naturally, the constraints given by (6.67) and (6.68) must be satisfied for this solution method, as well.

Comparison of the two methods for solving the equilibrium sorting profile, $\bar{F}_{iE}$, shows that the solution method based on a given bed load transport composition results in a set of equations that can be solved straightforwardly, whereas the solution method based on a given vertical sorting profile is somewhat more elaborate.

6.3.4 Parameter study

In this section, we analyse the sensitivity of the equilibrium sorting profile, $\bar{F}_{iE}$, to the constants γ and κ in the lee sorting function. The relation between these parameters is expressed by (6.61) through (6.64). For predicting the equilibrium sorting profile, we apply the method based on the bed load transport composition as described in Section 6.3.2. Note that application of the method based on a given initial sorting profile would result in the same trends.

In this parameter study we consider one of the experiments described in Chapter 4, experiment A2, and impose its measured equilibrium PDF of relative trough elevations, $\tilde{p}_{bE}$. The crests of the triangular bedforms are assumed to have the same absolute distance to the mean bed level as the troughs, which is expressed by (5.84), and the angle of repose of the lee faces is assumed to be equal to 30°. The grain sizes on ϕ-scale of the three well-sorted size fractions (fine, medium, and coarse) were $\phi_{fine} = 0.56$, $\phi_{medium} = -1.07$, and $\phi_{coarse} = -2.51$, respectively. Actually, the grain size on ϕ-scale has a unit, but it is simply left out since it a nonsensical one, i.e. ^{2} log mm. The measured average volume fraction contents of the three size fractions in the bed load transport, $\bar{F}_{aiE}$, were 0.38, 0.38, and 0.24. The average bed shear stress was $\bar{\tau}_b = 4.6\ \mathrm{Nm}^{-2}$.

To study the effect of the parameters γ and κ on the computed equilibrium sorting profile, first we vary γ over the values $[-1, -0.5, 0.5, 1]$, while κ is set such that the bed shear stress has no effect on the avalanche mechanism at the lee face, at all ($\kappa = 0$). Figure 6.3 shows the computed equilibrium sorting profiles for the series of irregular bedforms. For negative values of γ, the coarse material prefers being deposited at the higher elevations of the active bed. This is contradictory to experimen-

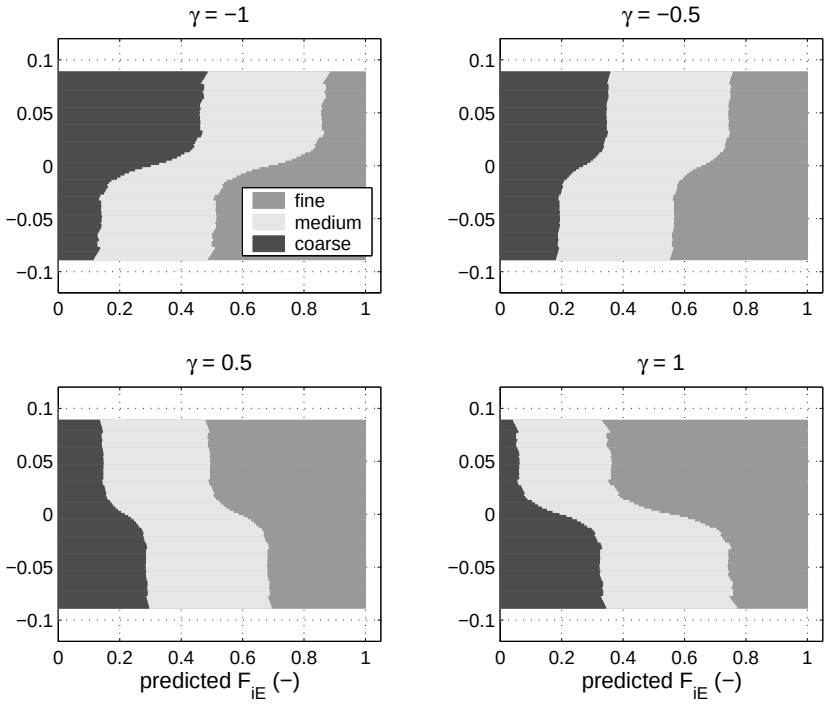

Figure 6.3: Influence of the constant γ in the lee sorting function on the computed equilibrium sorting profile, $\bar{F}_{iE}$, while $\kappa = 0$.

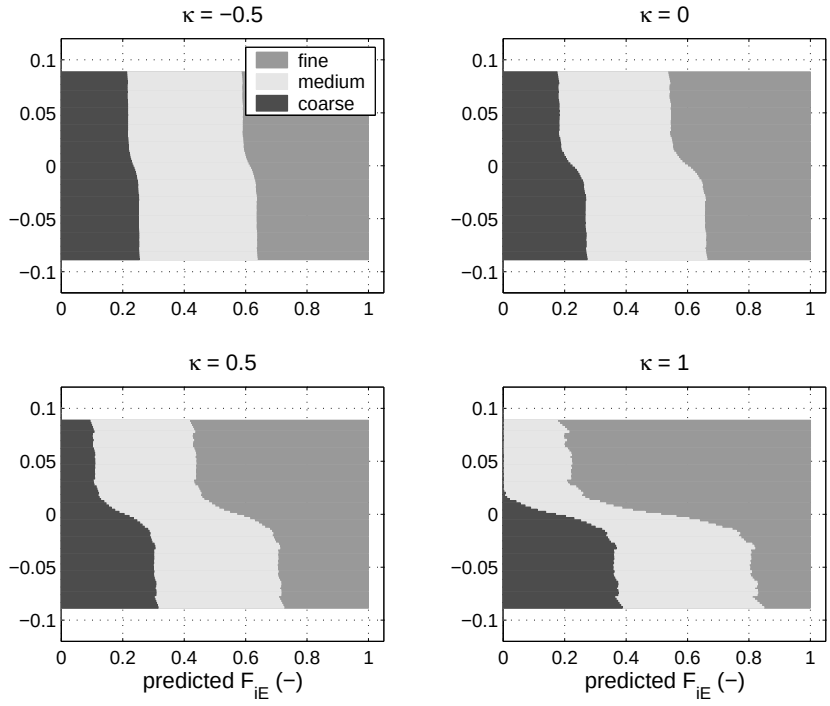

Figure 6.4: Influence of the constant κ in the lee sorting function on the computed equilibrium sorting profile, $\bar{F}_{iE}$, while $\gamma = 0.3$.

tal studies on the avalanche mechanism at the lee face, so that we may conclude that γ must have a positive value. Furthermore, it shows that the larger γ, the stronger is the sorting trend in the active bed. To study the effect of κ, we vary κ over the values $[-0.5, 0, 0.5, 1]$, while $\gamma = 0.3$. Figure 6.4 shows the results for the series of irregular bedforms. It clearly shows that the smaller the value for κ, the smaller is the sorting in the active bed.

In Chapter 7, we will determine the γ and κ from calibrating the equilibrium sorting model to measured data.

6.4 Summary and discussion

In this chapter, we have reduced the continuum sorting model derived in Chapter 5 to the case of equilibrium conditions, which leads to an equilibrium sorting model that solves for the equilibrium vertical sorting profile of non-uniform sediment. As stepping stones, we have first analysed the set of equations for the cases of uniform sediment and tracer particles in uniform sediment. For tracer particles, the equilibrium sorting model solves for the equilibrium volume fraction content of tracer particles in the active bed. It appears to be uniform over all elevations of the active bed, which confirms the author's statement on this subject matter in Section 2.5.

For non-uniform sediment, the equilibrium sorting trend is primarily determined by the newly-developed lee sorting function. For computing the equilibrium sorting profile, the equilibrium PDF of relative trough elevations needs to be known, from either model predictions or measurements. One method for solving the equilibrium sorting profile is based on a given bed load transport composition, either measured or computed, whereas the second method requires information on the vertical sorting profile at another point in time with its accompanying PDF of relative trough elevations. The second method is somewhat more elaborate than the first and may be used only if, from the moment that the bed composition is specified until the moment equilibrium conditions are reached, divergences in the grain size-selective transport have been negligible. The equilibrium sorting profile appears to be affected neither by the average bed load transport rate, nor by the dimensionless step length.

By using either one of the two solution methods, we avoid introducing the uncertainties accompanying the use of an -as yet not well verified- model for the grain size-specific entrainment rate over the bedform surface. Section 5.4 has addressed the problems of using such a model, one of which is the lack of a sub-model for the variation of skin friction over bedforms. This chapter has provided two methods for computing the equilibrium sorting profile. One method is based on a given bed

load transport composition. However, when solving the equilibrium sorting profile from a given bed load transport composition and applying existing sediment transport models for predicting the transport composition, we have to be aware that the accompanying uncertainties can be large, as well (*Van der Scheer et al.*, 2002).

As addressed in the discussion on time scales in Section 5.5, the equilibrium approach presented in this chapter may be instantaneously applied in morphological models if the time scale of large-scale morphological changes, T_m, is much larger than the ones of vertical sorting, T_f, and vertical dune dimensions, T_p. The latter two time scales, by themselves, should be larger than the time scale of dune migration, T_c. This subject matter will be discussed in more detail in Section 9.2. The second method for solving the equilibrium sorting profile is based on a given vertical sorting profile at a previous time. It would interesting to asses whether it is allowed to apply this solution method to a slowly rising flood event. This will be addressed in Section 9.9.

In the next chapter, we will consider the calibration and verification of the equilibrium sorting model. Herein, the constants γ and κ in the newly-developed lee sorting function will be used as calibration coefficients.

Chapter 7

Calibration and verification of the equilibrium sorting model

Chapter 6 has described the derivation of the equilibrium sorting model, in which the size-selective deposition down the avalanche lee face of bedforms is the main mechanism determining the equilibrium sorting profile. This mechanism is described using a newly-developed lee sorting function. We derived two methods for solving the equilibrium sorting profile, which both require the equilibrium probability density function (PDF) of relative trough elevations, $\tilde{p}_{bE}$, to be known. The first method is based on a given bed load transport composition, $\bar{F}_{aiE}$, whereas the second is based on a given vertical sorting profile at some other point in time, $\bar{\bar{F}}_{inii}$, together with its accompanying PDF of relative trough elevations, $\tilde{p}_{bini}$. The equilibrium sorting profile, $\bar{F}_{iE}$, appeared to be affected neither by the total bed load transport rate, $\bar{q}_{aE}$, nor by the dimensionless step length, α. The present chapter deals with the calibration and verification of the equilibrium sorting model. We apply the solution method based on a given bed load transport composition to compute the equilibrium sorting profile.

For the calibration of the equilibrium sorting model, we consider the equilibrium phases of experiments B2 and A2 (present study, Chapter 4), and for the verification the equilibrium phases of experiments E3 and E7 by *Ribberink* (1987). Measured values for the bed load transport composition, $\bar{F}_{aiE}$, the average bed shear stress, $\bar{\tau}_{bE}$, the PDF of relative trough elevations, $\tilde{p}_{bE}$, and the ratio of the average bedform height to the average bedform length are used as input to the model. The two constants in the lee sorting parameter, γ and κ, are used as calibration coefficients. To find the optimum values for γ and κ, we compare the computed equilibrium sorting profiles for various combinations of γ and κ with the measured ones for experiments B2 and A2, and strive after the smallest difference between the computed and measured sorting profiles. In the verification, we apply these optimum values for γ and κ to compute the equilibrium sorting profile for experiments E3 and E7, and again compare the measured and computed sorting profiles. In addition, the performance of the lee sorting function is tested against a number of experiments on sorting down a delta lee face conducted by *Kleinhans* (2002).

7.1 Experimental data

We consider the equilibrium phases of experiments B2 and A2 (present study, Chapter 4) for calibrating the equilibrium sorting model, and those of experiments E3 and E7 by *Ribberink* (1987) for verifying it. The experiments by *Ribberink* (1987) were conducted under circumstances very similar to the ones in the present study. Uniform flow conditions were maintained ($\partial/\partial x = 0$) and the sediment was recirculated in order to avoid aggradation or degradation over the full length of the flume ($\partial \bar{\eta}_a/\partial t = 0$). In all experiments, the bed was covered by bedforms. *Ribberink* used a sediment mixture of two sand fractions (d_1 =0.78 mm, d_2 =1.29 mm), having negligible overlap. The length, width, and height of the flume's measurement section were 29 m, 0.3 m, and 0.5 m, respectively. Bed samples were taken using sampling pipes pressed into the bed near the bedform crests. Through the sampling pipes, sand layers with a thickness of 0.5 cm were removed by syphoning. The small samples were dried and sieved and the bed was restored by returning the sediment samples in reverse order in order to keep the disturbance of the bed as small as possible.

In the equilibrium phase of the experiments B2 and A2, about 15 box core samples were taken over the complete measurement section in order to measure the vertical sorting profile (Section 4.2.3). In the equilibrium phase of experiment E3, about 50 samples were taken along the flume axis and 10 samples at the side of the flume, and in experiment E7 20 samples along the flume axis and 20 at the side. The measured sorting profiles will be shown in the next sections, together with computed ones.

The bedforms are assumed to have a triangular shape with varying trough elevations. All other bedform features are assumed to be related to the relative trough elevation, Δ_b, according to (5.84) through (5.87):

$$\Delta = 2\,\Delta_b$$
$$\lambda = (\lambda_a/\Delta_a)\,\Delta$$
$$\lambda_l = \Delta/\tan(\nu)$$
$$\lambda_s = \lambda - \lambda_l$$

which indicates that a crest is assumed to have the same absolute distance to the mean bed level as its trough, and that the bedform length is assumed to be proportional to the bedform height and the ratio of the average bedform length to the average bedform height. The angle of repose of the lee faces is assumed to be equal to 30°. The upper plots of Figure 7.1 show the relation between measured bedform lengths and bedform heights for individual bedforms, together with (5.85). The relation between the measured bedform lengths and bedform heights shows large scatter, but

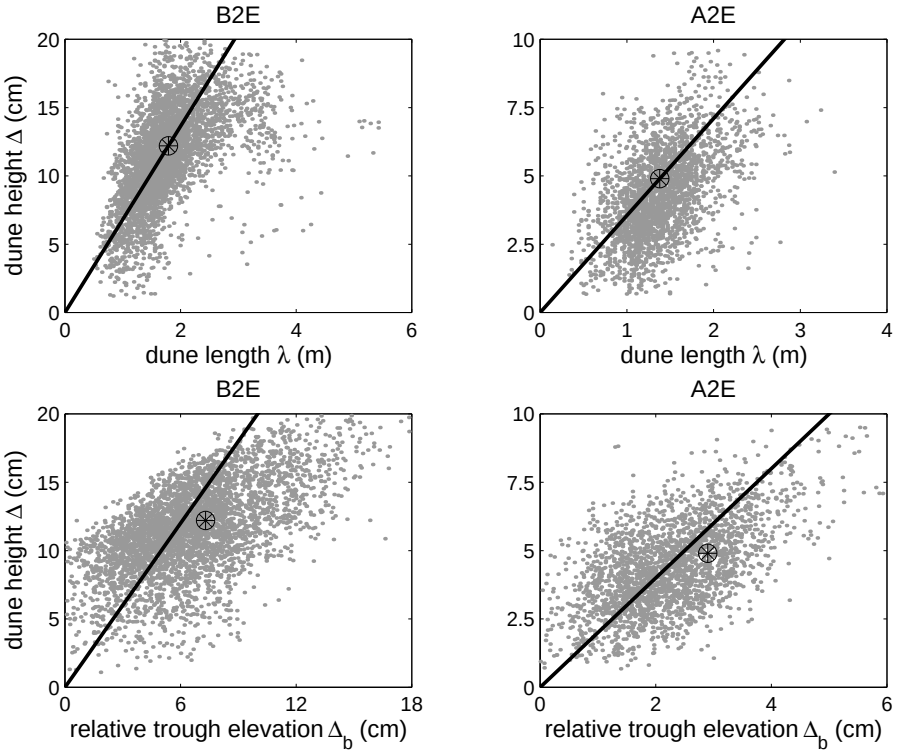

Figure 7.1: *Upper plots*: relations (1) between measured bedform lengths and bedform heights for individual bedforms (small dots), (2) between the average the bedform length, λ_a, and the average bedform height, Δ_a (large dot), and (3) between the bedform length and bedform height according to (5.85), which is applied in the calibration and verification procedures (line). *Lower plots*: relations (1) between measured relative trough elevations and bedform heights for individual bedforms (small dots), (2) between the average relative trough elevation, Δ_{ba}, and the average bedform height, Δ_a (large dot), and (3) between the relative trough elevation and bedform height according to (5.84), which is applied in the calibration and verification procedures (line).

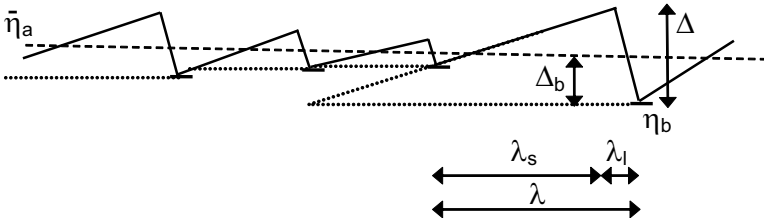

Figure 7.2: Influence of adjacent bedforms upon the bedform length.

(5.85) covers the possible trend reasonably well. The large scatter in Figure 7.1 seems partly due to the bedform length (i.e. the distance between two consecutive troughs) also being determined by the adjacent bedforms (see Figure 7.2).

The lower plots in Figure 7.1 show the relation between measured relative trough elevations, Δ_b, and bedform heights, Δ, for individual bedforms. Eq. (5.84) is applied in the calibration and verification procedures as a fit to the measured data. In spite of the large scatter, (5.84) represents the trend in the relation between the measured data for experiment A2E reasonably well, but for the higher dunes in experiment B2E (5.84) deviates from the measured trend. Figure 7.1 (lower plots) illustrates that the following relation would yield better results than (5.84):

$$\Delta = \frac{\Delta_a}{\Delta_{ba}} \Delta_b \tag{7.1}$$

where Δ_{ba} denotes the average relative trough elevation ($\Delta_{ba} = \bar{\eta}_a - \eta_{ba}$, where η_{ba} is the average trough elevation). However, it is chosen to apply (5.84) instead of (7.1), since in using the latter the mean bed level would not remain the same. It has not been checked whether the assumption of the slopes of the lee faces being equal to 30° represents the measured data.

Table 7.1 lists the experimental data serving as input to the equilibrium model: the grain sizes on ϕ-scale of the different size fractions, ϕ_i, the volume fraction content of size fractions in the bed load transport, $\bar{F}_{aiE}$, the average bed shear stress, $\bar{\tau}_{bE}$, the average bedform height, Δ_a, and the average bedform length, λ_a.

For the calibration procedure, a model for the PDF of relative trough elevations, $\tilde{p}_{bE}$, is not required, since in experiments A2 and B2 the PDF of relative trough elevations is determined from measurements. For experiments E3 and E7, the PDF of relative trough elevations was not measured. For these experiments, it is derived from the

test	ϕ_1	ϕ_2	ϕ_3	$\bar{F}_{a1E}$	$\bar{F}_{a2E}$	$\bar{F}_{a3E}$	$\bar{\tau}_{bE}$	Δ_a	λ_a
				-	-	-	Nm^{-2}	cm	m
B2E	0.56	-1.07	-2.51	0.90	0.05	0.05	7.4	12.2	1.79
A2E	0.56	-1.07	-2.51	0.38	0.38	0.24	4.6	4.9	1.38
E3	0.36	-0.37	-	0.50	0.50	-	2.0	4.4	0.91
E7	0.36	-0.37	-	0.80	0.20	-	1.4	4.7	1.10

Table 7.1: Experimental data used as input to the equilibrium sorting model.

probability distribution of bed surface elevations, $\bar{P}_s$, under the assumption of triangular dunes according to (5.84) through (5.87). The derivation is explained in Appendix D. For the equilibrium phases of experiments B2, A2, E3, and E7, Figure 7.3 shows

1. the PDF of relative trough elevations, $\tilde{p}_b$, measured for A2 and B2 and derived from $\bar{P}_s$ for E3 and E7
2. the PDF of bed surface elevations $\bar{p}_e$ determined from $\tilde{p}_{bE}$ according to (5.92), and the measured $\bar{p}_e$
3. the probability distribution of bed surface elevations $\bar{P}_s$ determined from $\tilde{p}_b$ according to (5.2), and the measured $\bar{P}_s$

The right-hand plots in Figure 7.3 show that the probability distributions of bed surface elevations, $\bar{P}_s$, determined from the PDF of relative trough elevations, $\tilde{p}_{bE}$, resemble the measured $\bar{P}_s$ well enough, especially when considering the uncertainties accompanying the assumptions made in the derivation of the equilibrium sorting model.

7.2 Calibration

The equilibrium sorting model is calibrated by comparing the measured equilibrium sorting profile, $\bar{F}_{iE}$, with computed ones. Applying the solution method based on a given bed load transport composition, the set of equations for solving the equilibrium sorting profile, $\bar{F}_{iE}$, is given by (6.61) through (6.68). Computations are made for a large number of given combinations of γ and κ. For each combination of γ and κ, we determine the absolute difference between the computed and measured equilibrium sorting profile, $\bar{F}_{iE}$, averaged over four bed elevations (Table 7.2) and over each of the size fractions, i.e. the *average error in* $\bar{F}_{iE}$.

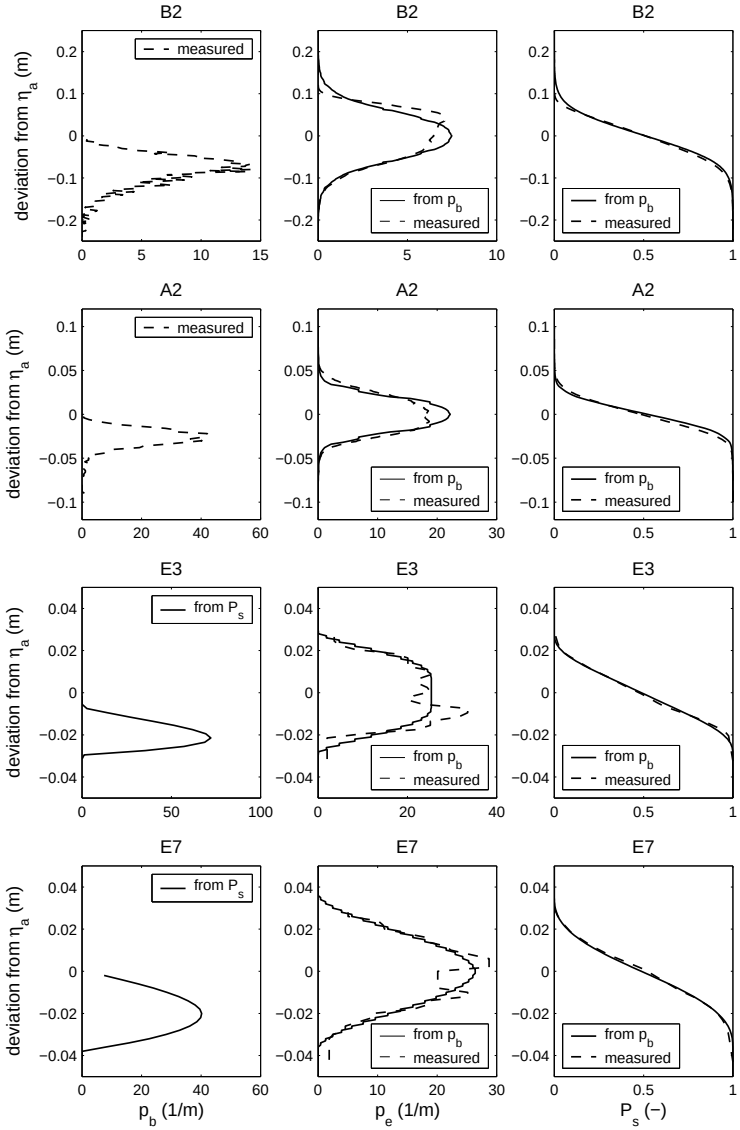

Figure 7.3: Probability density functions of trough elevations, $\tilde{p}_{bE}$, probability density functions of bed surface elevations, $\bar{p}_e$, and the probability distributions of bed surface elevations, $\bar{P}_s$, for the equilibrium phases of experiments B2, A2, E3, and E7.

B2E	A2E	E3	E7
2.5	1.5	1.0	1.0
-2.5	0	0	0
-7.5	-1.5	-1.5	-1.5
-12.5	-3.0	-2.5	-3.0

Table 7.2: Bed elevations (in cm) relative to the mean bed level, $\bar{\eta}_a$, for which the absolute difference between the computed and measured equilibrium sorting profile, $\bar{F}_{iE}$, is determined.

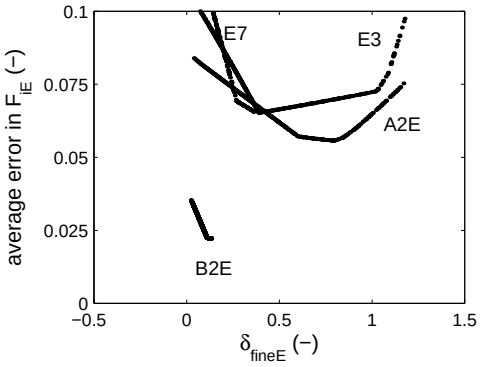

Figure 7.4: Lee sorting parameter for the finest size fraction, $\bar{\delta}_{fineE}$, and accompanying average difference between the measured equilibrium sorting profile, $\bar{F}_{iE}$, and the computed one, for the equilibrium phases of experiments B2, A2, E3, and E7.

Figure 7.4 shows that for each experiment, for one typical value of the lee sorting parameter for the finest size fraction, $\bar{\delta}_{fineE}$, the average error in the equilibrium sorting profile is minimal. The $\bar{\delta}_{iE}$-sub-model in (6.64) tells us that this optimum value for $\bar{\delta}_{fineE}$ can be found for multiple combinations of γ and κ.

For experiment A2, Figure 7.5 shows the given combinations of γ and κ with the accompanying average errors in $\bar{F}_{iE}$. We can distinguish the combinations of γ and κ for which the average error in $\bar{F}_{iE}$ is minimal, which are also plotted in Figure 7.6.

For each of the two experiments used for calibrating the equilibrium sorting model, B2 and A2, we find such a series of combinations for γ and κ that result in an optimum prediction of the equilibrium sorting profile, $\bar{F}_{iE}$ (Figure 7.6). The point of

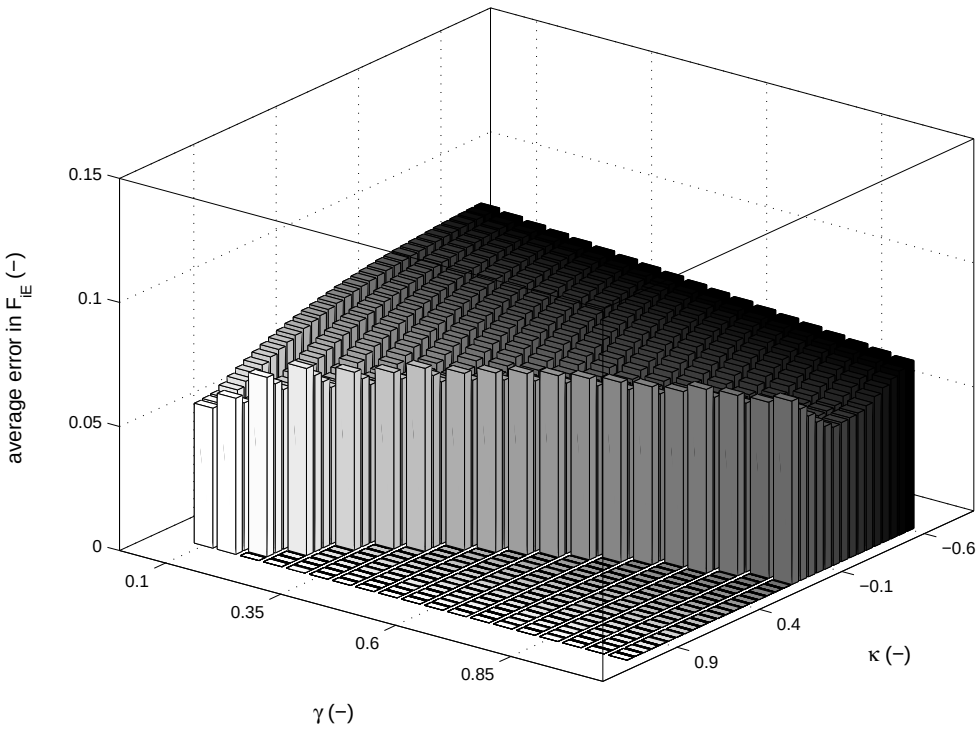

Figure 7.5: Combinations of γ and κ with accompanying average differences between the measured equilibrium sorting profile, $\bar{F}_{iE}$, and the computed ones, for the equilibrium phase of experiment A2.

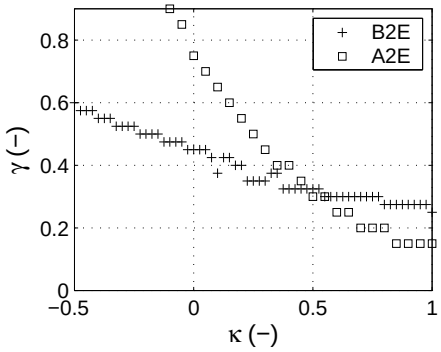

Figure 7.6: Combinations of γ and κ for which the difference between the measured equilibrium sorting profile, $\bar{F}_{iE}$, and the computed ones is minimal, for the equilibrium phases of experiments B2 and A2.

intersection of the two series yields the optimum values for both γ and κ:

$$\gamma = 0.3 \tag{7.2}$$

$$\kappa = 0.5 \tag{7.3}$$

so that the lee sorting parameter δ_{iE} in (6.64) reduces to

$$\bar{\delta}_{iE} = -0.3 \, \frac{\bar{\phi}_{mleeE} - \phi_i}{\bar{\sigma}_a} \, (\bar{\tau}^*_{bE})^{-0.5} \tag{7.4}$$

The grain size-selective deposition down the lee face appears primarily determined by the difference in the geometric mean grain size of the lee deposit and the grain size of size fraction i ($\bar{\phi}_{mleeE} - \phi_i$), and the arithmetic standard deviation of the mixture, $\bar{\sigma}_a$. However, the resulting value for κ implies that the bed shear stress does affect the avalanche process, probably through the flow velocity at the bedform crest and/or the lee vortices downstream of the bedform. The sorting trend of bedform material appears to become smaller with increasing bed shear stress. This was confirmed experimentally by *Allen* (1965) (also see Section 2.3).

For the equilibrium phases of experiments B2 and A2, Figures 7.7 and 7.8 show the measured equilibrium sorting profile and the computed one, using the calibrated lee sorting parameter in (7.4). Remarkable in the measured sorting profiles is the presence of a top layer of 1 to 2 cm that is significantly coarser than the material underneath. This coarse top layer originates from two processes. The first is the formation of a thin mobile armour layer on the stoss face, which increases the amount of

exposure of the coarser grains and hinders the entrainment of fines, so as to counterbalance the higher mobility of the fines. The second process concerns the deposition of sediment that was being transported over the bedform until the flow was turned off. Namely, for taking the core samples, the flow needs to be turned off, and the sediment that was being transported over the bedform settles on top of the bedform surface. At the upper elevations of the stoss face, the transported sediment is coarser than the bedform material itself, which contributes to the presence of the coarse top layer in the measured sorting profile.

The coarse top layer in the measured sorting profiles seems to have a thickness larger than a few grain sizes. However, this is due to the averaging procedure. Either of the measured sorting profiles in Figures 7.7 and 7.8 was determined by averaging over about 15 core samples. These 15 samples were taken at locations with different bed surface elevations relative to the mean bed level. Since their elevation relative to the mean bed level was different from each other, the averaging procedure smears the coarse top layer over a larger range of bed elevations. Since in the sorting model it is assumed that the composition of the net entrainment at a certain elevation of the stoss face equals the bed composition at that elevation, this coarse top layer does not show up in the computed sorting profiles.

Figures 7.7 and 7.8 show another notable difference between the measured and computed sorting profiles. The range of bed elevations covered by the core samples seems small compared to the range covered by the computations. Note however that the upper elevations of the active bed are rarely reached by the bedform crests. Since their probability density of being exposed to the flow, $\bar{p}_e$, is very small, these elevations have negligible influence on, for example, the composition of the sediment transported over the crests. The computed upper elevations of the active bed may not even have been reached by the bedform crests at all, since the assumption of each bedform crest being located at the same vertical distance from the mean bed level as its trough, which is expressed by (5.84), is not necessarily true. In reality, the deepest bedform troughs are usually not accompanied by the highest crests (*Leclair and Blom*, 2003).

The measured sorting profile of experiment B2E suggests that the equilibrium state was not completely reached, primarily in the lower parts of the active bed (Figure 7.7, left plot). The lowest bed elevations covered by the core samples are characterised by a strong reduction in the proportions of the medium and coarse size fractions. Although the measured sorting profile does not cover the complete range of lower elevations of the active bed, the proportions of the medium and coarse size fractions probably decrease to zero just below the lower boundary of the core samples. Would

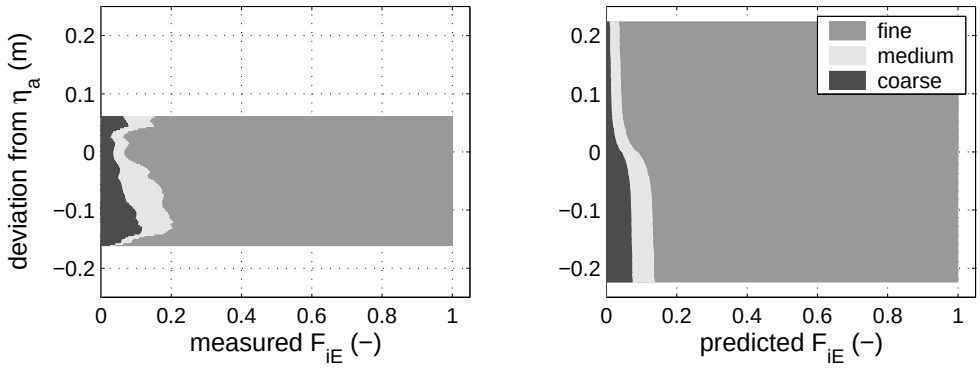

Figure 7.7: Measured and computed equilibrium sorting profiles, $\bar{F}_{iE}$, for the equilibrium phase of experiment B2, using the calibrated lee sorting function.

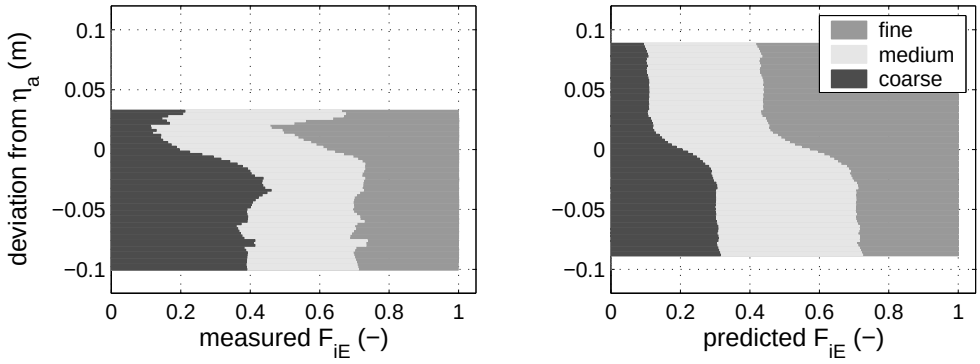

Figure 7.8: Measured and computed equilibrium sorting profile, $\bar{F}_{iE}$, for the equilibrium phase of experiment A2, using the calibrated lee sorting function.

experiment B2 have been continued for a longer time, the composition at the lower elevations of the active bed would be more uniform, as is suggested in the computed sorting profile for B2E.

We can see that the sorting model does not describe the formation of the coarse bed layer in experiment A2 very well (Figure 7.8). This suggests that in A2 the sorting profile with its coarse bed layer was not only determined by the lee face avalanche mechanism, but also by the winnowing of fines from the trough surface and subsurface (Sections 2.6 and 4.3.4, Figure 4.16) and the settlement of immobile coarse particles (Section 2.7.3). The mechanisms of winnowing of fines and the settlement of immobile coarse particles have not been included in the present version of the model.

We may say that the computed sorting profiles agree rather well with the measured ones. Note however that the coefficients γ and κ were calibrated especially for these experiments, so we cannot draw any conclusions on the general validity of the values for γ and κ. Nonetheless, the order of magnitude of the volume fraction contents of size fractions in the active bed is predicted well. Note that the total volume of each fraction in the active bed is not imposed on the computed equilibrium sorting profile, since we chose to apply the solution method based on a given bed load transport composition. Also the sorting trend over depth is predicted reasonably well.

7.3 Verification

This section covers the verification of the equilibrium sorting model. The resulting values for the calibration coefficients γ and κ in the lee sorting function, 0.3 and 0.5 respectively, are used to compute the equilibrium sorting profiles of experiments E3 and E7 by *Ribberink* (1987). Let us compare the computed equilibrium sorting profiles with the measured ones, which are shown in Figures 7.9 and 7.10. Since the mixture used in experiments E3 and E7 was composed of two well-sorted size fractions, it is sufficient to show the sorting profile of one size fraction. In order to show the large variation in vertical sorting over the flume, the figures show (1) the measured sorting profile averaged over samples taken along the flume axis, (2) the measured sorting profile averaged over samples taken at the sides of the flume, and (3) their average.

The agreement between the measured and computed sorting profiles is very similar to experiments B2 and A2. First, as in experiments B2 and A2, the measured sorting profiles show a coarse top layer originating from mobile armouring and the deposition of sediment that was being transported over the bedform until the flow was turned off (see previous section). Secondly, the order of magnitude of the volume

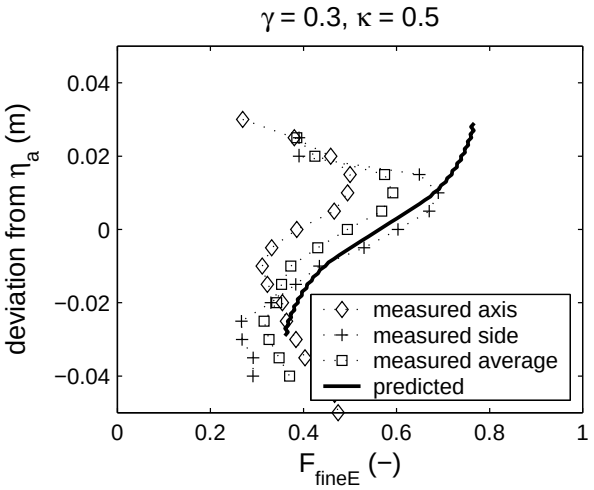

Figure 7.9: Measured and computed equilibrium sorting profile, $\bar{F}_{iE}$, of the fine size fraction in the bimodal mixture, for the equilibrium phase of experiment E3, using the calibrated lee sorting function.

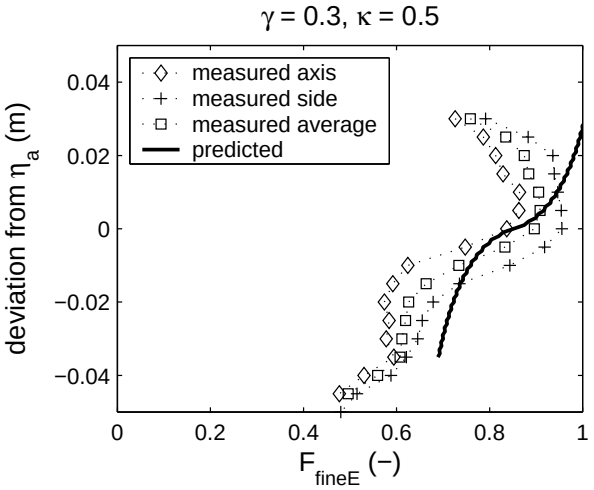

Figure 7.10: Measured and computed equilibrium sorting profile, $\bar{F}_{iE}$, of the fine size fraction in the bimodal mixture, for the equilibrium phase of experiment E7, using the calibrated lee sorting function.

fraction contents of size fractions in the active bed is predicted well. And finally, the computed vertical variation of sorting over the active bed agrees very well with the measured sorting.

In addition, the calibrated lee sorting function is verified against data on the grain size-selective deposition down a delta lee face as measured by *Kleinhans* (2002) (also see Section 2.3). A delta face is defined as a slope (at about the angle of repose) over which sediment is deposited when the water depth suddenly and largely increases, due to, for instance, a river flowing into a deep lake or ocean. Figures 7.11 and 7.12 show the measured and computed sorting profiles for various delta faces. In about half of the cases, the computed sorting profile covers the measured data reasonably well (N9B, N10B, U1, and S2B), but for the other cases the computed sorting is less strong than the measured one (N2A, N5B, M1, and C1).

An explanation for the computed sorting for delta faces being less strong than the measured one may be that the bed shear stress applied for the delta faces is inconsistent to the one for dunes. The bed shear stress in (7.4) represents the bed shear stress averaged over a series of dunes (thus averaged over dune crests, stoss faces, and trough zones), while for the deltas we apply the bed shear stress on the delta crest. This implies that the bed shear stress for the deltas is relatively higher, resulting in a sorting trend that is relatively smaller. A correction factor seems necessary in order to eliminate this inconsistency. In addition, *Kleinhans* (2002) mentions some reasons why the sorting process down a delta face may be different from a dune (see Section 2.3).

7.4 Discussion

In the present chapter, the equilibrium sorting model derived in Chapter 6 has been calibrated and verified. The equilibrium sorting model comprehends two methods for predicting the equilibrium sorting profile: (1) based on a given bed load transport composition, and (2) based on a given vertical sorting profile at another point in time. The first method has been applied in calibrating and verifying the equilibrium sorting model. The equilibrium phases of experiments B2 and A2 have been considered in the calibration, and the ones of experiments E3 and E7 by *Ribberink* (1987) in the verification. The two constants in the lee sorting function, γ and κ, have been used as calibration coefficients.

The resulting value for κ implies that in the newly-developed sorting model the bed shear stress has a small effect upon the avalanche mechanism at the lee face. The avalanching of particles down the lee face seems predominated by gravitational

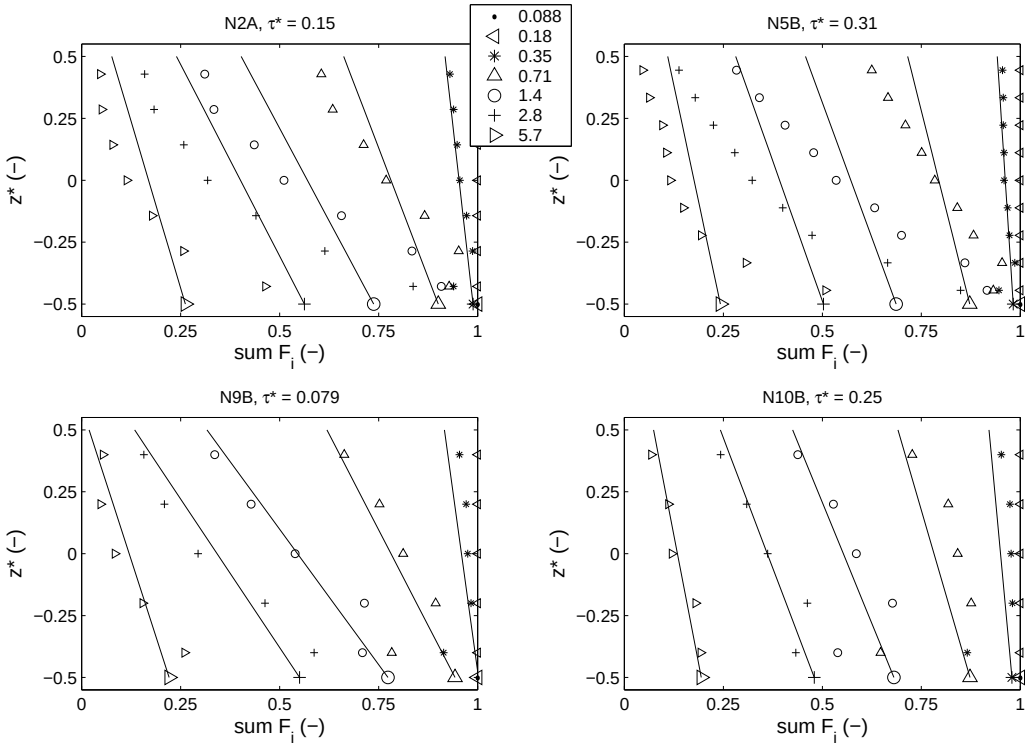

Figure 7.11: Measured vertical sorting profiles over delta lee faces composed of natural mixtures (data from *Kleinhans*, 2002), indicated by the markers, and computed ones using the calibrated lee sorting function, indicated by the lines. The large marker at the lower limit of a line indicates the specific grain size, which is shown in the legend (in mm). Note that the volume fraction content of a specific size fraction over the delta face is indicated by the difference between two lines or two types of markers. For instance, the volume fraction content of the 2.8 mm size fraction is indicated by the difference between the plus-signs and the triangles pointing right.

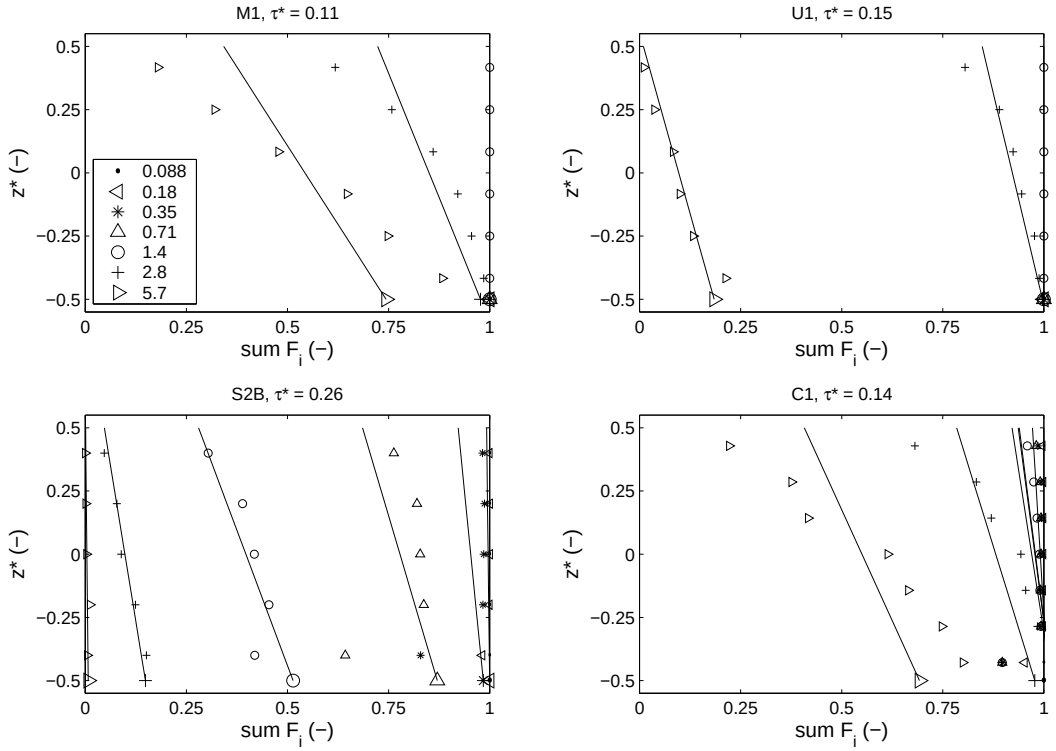

Figure 7.12: Measured vertical sorting profiles over delta lee faces composed of artificial mixtures (data from *Kleinhans*, 2002), indicated by the markers, and computed ones using the calibrated lee sorting function, indicated by the lines. The large marker at the lower limit of a line indicates the specific grain size, which is shown in the legend (in mm). Note that the volume fraction content of a specific size fraction over the delta face is indicated by the difference between two lines or two types of markers. For instance, the volume fraction content of the 2.8 mm size fraction is indicated by the difference between the plus-signs and the triangles pointing right.

forces and frictional forces between particles, but apparently the influence of the flow velocity at the crest and/or the lee vortices downstream of the bedform on the avalanching process may not be neglected.

For the four experiments considered for the calibration and verification, the measured sorting profiles were compared with computed ones. The order of magnitude of the computed volume fraction contents of size fractions in the active bed is good, considering that the total volume of each size fraction in the active bed is not imposed. Also the computed trend in the vertical sorting profile agrees reasonably well with the measured sorting trend. The disagreements between the measured and computed sorting profiles appear to be small, considering

- the simple form of the lee sorting function implemented in the continuum sorting model;
- the assumption of considering the series of irregular bedforms as a series of triangular bedforms with varying trough elevation;
- the dispersive effects of the core sampling method (see Section 4.2.3), and the relatively small amount of bed samples taken, so that the measured equilibrium sorting profile may not be fully representative;
- the experiments not having reached the equilibrium state completely, primarily in the lower parts of the active bed.

Yet, a number of observations can be made on the measured and computed sorting profiles.

All measured sorting profiles show a coarse top layer that originates from (1) the presence of a thin mobile armour layer on the stoss face and (2) the deposition of sediment that was being transported over the bedform until the flow was turned off. Because of the assumption that the composition of the net entrainment at a certain elevation of the stoss face is equal to the bed composition at that elevation, this coarse top layer does not show up in the computed sorting profiles. In reality, the net entrainment flux at some elevation of the stoss face may be somewhat finer than the average bed composition at that elevation. The composition of the net entrainment flux may be close to the composition averaged over *all* bed material present at that elevation in the series of bedforms, with the exception of the coarse top layer. Clearly, the above assumption prevents armouring from happening completely. It needs to be studied whether it is desirable (and possible) to loosen the above assumption. We will come back to this topic in Section 9.7.2.

The uppermost elevations of the active bed do not seem to be adequately described. This shortcoming arises from the simple relation between the bedform height and the relative trough elevation for individual bedforms, which is given by (5.84). Yet, the uppermost elevations do not influence the model results very much (e.g., with respect to the average composition of the bed surface), since these elevations are barely exposed to the flow.

The mechanisms of the winnowing of fines from the trough surface and subsurface and the settling of immobile coarse particles do seem to have a significant influence on the sorting profile. It is suggested to include these mechanisms in a future version of the model.

In addition, the lee sorting function was tested against data from flume experiments on the grain size-selective deposition down a delta lee face which were conducted by *Kleinhans* (2002). For about half of the cases, the computed sorting trend was quite reasonable, but for the other cases the computed sorting was too weak. This may be caused by the fact that the bed shear stress for the delta faces (i.e. on the delta crest) was inconsistent to the one applied in the lee sorting function (i.e. averaged over a series of dunes). For this reason, the bed shear stress for the delta faces may have been 'too high' and the sorting trend thus too weak.

For the experiments with dunes considered in this chapter, the calibrated lee sorting parameter in (7.4) served us well. Yet, the important question is: How generally applicable is this lee sorting parameter? The question is strongly related to the ranges of the parameters that served as input for the calibration and verification of the equilibrium sorting model, i.e. its validity ranges. In the four experiments, the average bed shear stress, $\bar{\tau}_{bE}$, varied between 1.4 and 7.4 Nm^{-2}, and the dimensionless bed shear stress, $\bar{\tau}^*_{bE}$, between 0.10 and 0.59. The grain sizes in the tri-modal mixture were d_1 =0.68 mm, d_2 =2.1 mm, and d_3 =5.7 mm (B2 and A2), and in the bi-modal mixture d_1 =0.78 mm and d_2 =1.29 mm (E3 and E7). Other characteristics of the experiments were the negligible amount of suspended load transport and conditions of partial transport. Note that the mixtures were artificial. How well the lee sorting parameter acts for dunes composed of natural sediment mixtures is yet not clear. Further research is required on the avalanche mechanism at the lee face of dunes in order to increase the validity ranges of the lee sorting parameter.

Clearly, we are not only interested in the sorting profile in its equilibrium state, but also in the evolution of the sorting profile in time. Therefore, a *sorting evolution model* will be derived in the next chapter.

Chapter 8

The sorting evolution model

In this chapter, we reduce the new continuum sorting model as derived in Chapter 5 through assumptions similar to the ones in Chapter 6:

- the composition of the net[1] entrainment at bed elevation z at the stoss face is assumed to be equal to the bed composition at that elevation;
- the vertical sorting profile, F_i, is assumed not to vary between bedforms with different trough elevations (except for elevations not reached by a bedform);
- the total bed load transport rate, q_a, and the bed load transport composition over the bedform crest, F_{top}, are assumed not to vary between bedforms;
- the lee sorting function as calibrated for equilibrium conditions is assumed to be valid for non-equilibrium conditions, as well;
- the probability density function (PDF) of trough elevations, $\tilde{p}_b$, is assumed to be steady relative to the mean bed level.

The present chapter will show that, under these assumptions, we are able to derive a model that solves for the time evolution of both the vertical sorting profile and the bed load transport composition, without applying a model for the grain size-specific and elevation-specific entrainment over bedforms. The difficulties of applying such an entrainment model have been discussed in Section 5.4. The resulting sorting model is called the *sorting evolution model*.

In fact, the latter of the above assumptions may not be made, since in reality the PDF of relative trough elevations does vary in time with changing hydraulic conditions, which may significantly affect the sorting profile. For instance, a temporary increase in the bed shear stress may cause bedform crests to become higher and troughs to become deeper, which results in the deposition and storage of the coarse size fractions in the mixture at the deepest bed elevations exposed to the flow (also see Figure 4.18a). Clearly, we need to incorporate these effects of unsteady trough elevations in the sorting evolution model, a method for which will be explained in

[1] *net* meaning the difference between the entrainment flux and the deposition flux

Section 8.2. In the next chapter, Section 9.1 will underline that the sorting model resulting from this study incorporates three types of vertical sorting fluxes: (1) through bedform migration, i.e. grain size-selective deposition down a bedform lee face and the variability in trough elevations, (2) through a change in time of the PDF of relative trough elevations, and (3) through net aggradation or degradation. For simplicity, it is assumed that these three types of vertical sorting fluxes do not interact with one another. A method for incorporating net aggradation or degradation in the continuum sorting model will be proposed in Sections 9.1 and 9.3.

The sorting evolution model is verified against experiments B2 and A2 (present study, Chapter 4). It is important to note that, except for the yet calibrated lee sorting function, no parameters in the sorting evolution model are calibrated upon. Like for the equilibrium sorting model (Chapter 6), the PDF of relative trough elevations, $\tilde{p}_b$, is required as input to the sorting evolution model and it needs to be determined from either measurements or an external sub-model. In the present study, we use the measured (time evolution of the) PDF of relative trough elevations as input to the sorting calculations.

Section 8.1 explains the derivation of the sorting evolution model. In Section 8.2, we derive a method for incorporating the time evolution of the PDF of relative trough elevations in the model. The sorting evolution model can be characterised as a relaxation-type model, of which the time scale of sorting is dependent on bed elevation (Section 8.3). The model is verified by comparing computed sorting profiles with measured ones, for the non-equilibrium N-phases and the equilibrium E-phases of experiments B2 and A2 (Section 8.4). In Section 8.5, we evaluate the results of the present chapter.

8.1 Derivation

Like in the analyses for uniform sediment, tracers in uniform sediment, and non-uniform sediment in Chapter 6, we assume the average bed load transport rate to be identical for each bedform in the series of bedforms. Besides, we impose the composition of the sediment transported over each crest to be the same, as well as the composition of the lee deposit. Finally, we make no distinction in sorting between bedforms within one series of bedforms:

$$q_a = \bar{q}_a \qquad F_{topi} = \bar{F}_{topi}$$
$$F_{leei} = \bar{F}_{leei} \qquad F_i = \bar{F}_i$$

When describing the time evolution of the sorting profile, we assume the PDF of relative trough elevations to be steady ($\tilde{p}_b(z,t) = \tilde{p}_b(z)$). This implies that the resulting probability distribution of bed surface elevations relative to the mean bed level, $\tilde{P}_s$, is steady, as well. In reality, the PDF of relative trough elevations does vary in time, which affects the sorting profile. How vertical sediment fluxes through a change in time of the PDF of relative trough elevations are incorporated in the sorting evolution model will be explained in Section 8.2.

Thus, in the present section, $\tilde{p}_b$ and $\tilde{P}_s$ are assumed to be steady. Note that the probability distribution of bed surface elevations, $\bar{P}_s$, is still time dependent, since the mean bed level, $\bar{\eta}_a$, is allowed to vary in time. Then, the fundamental equations of the Parker-Paola-Leclair framework for sediment continuity, i.e. Eqs. (5.11), (5.12), and (5.16) reduce to

$$c_b \bar{P}_s \frac{\partial \bar{F}_i}{\partial t} + c_b \bar{F}_i \bar{p}_e \frac{\partial \bar{\eta}_a}{\partial t} = \bar{D}_{ei} - \bar{E}_{ei} \tag{8.1}$$

$$c_b \bar{p}_e \frac{\partial \bar{\eta}_a}{\partial t} = \bar{D}_e - \bar{E}_e \tag{8.2}$$

$$c_b \frac{\partial \bar{\eta}_a}{\partial t} = \bar{D} - \bar{E} \tag{8.3}$$

where

$$\bar{E}_e = \sum_i^N \bar{E}_{ei} \qquad \bar{D}_e = \sum_i^N \bar{D}_{ei}$$
$$\bar{E} = \int_{-\infty}^{\infty} \bar{E}_e \, dz \qquad \bar{D} = \int_{-\infty}^{\infty} \bar{D}_e \, dz$$

The parameters $\bar{F}_i$, $\bar{P}_s$, $\bar{p}_e$, $\bar{D}_{ei}$, $\bar{E}_{ei}$, $\bar{D}_e$, and $\bar{E}_e$ all depend on the vertical co-ordinate z, the horizontal co-ordinate x, and the time co-ordinate t, whereas $\bar{\eta}_a$, $\bar{D}$, and $\bar{E}$ depend only on the horizontal co-ordinate x and the time co-ordinate t. Note that the co-ordinate x varies only over the scale of large numbers of bedforms. For clarity, the co-ordinates have been left out of the equations.

Over the stoss face of a bedform, we distinguish simultaneous entrainment and deposition fluxes, and only deposition fluxes over the lee face:

$$\bar{E}_{ei} = \bar{E}_{eis} \qquad \bar{D}_{ei} = \bar{D}_{eis} + \bar{D}_{eil}$$

where the overall[2] entrainment and deposition densities for the stoss and lee faces

[2] *overall* meaning averaged over a series of irregular bedforms

are given by (5.93), (5.94), and (5.95):

$$\bar{E}_{eis} = \int_{\eta_{bmin}}^{\eta_{bmax}} \frac{\lambda_s}{\lambda} p_{se} E_{siu}(z) \bar{F}_i(z)\, \tilde{p}_b\, d\eta_b$$

$$\bar{D}_{eis} = \int_{\eta_{bmin}}^{\eta_{bmax}} \frac{\lambda_s}{\lambda} p_{se} E_{siu}(z - \eta_{stepi}) \bar{F}_i(z - \eta_{stepi})\, \tilde{p}_b\, d\eta_b$$

$$\bar{D}_{eil} = \int_{\eta_{bmin}}^{\eta_{bmax}} \frac{\lambda_l}{\lambda} p_{le} D_l F_{leeloci}(z)\, \tilde{p}_b\, d\eta_b$$

The overall PDF of bed surface elevations, $\bar{p}_e$, is determined by the PDF of relative trough elevations, $\tilde{p}_b$, and the characteristic bedform shape, $\bar{p}^*_{se}$, which is expressed by (5.92).

With (5.93), (5.94), and (5.95), Eqs. (8.1) and (8.2) yield

$$c_b \bar{P}_s \frac{\partial \bar{F}_i}{\partial t} + c_b \bar{F}_i \bar{p}_e \frac{\partial \bar{\eta}_a}{\partial t} = \int_{\eta_{bmin}}^{\eta_{bmax}} \frac{p_e}{\lambda \Delta} \Big[\lambda_s E_{siu}(z - \eta_{stepi}) \bar{F}_i(z - \eta_{stepi}) - \lambda_s E_{siu}(z) \bar{F}_i(z) + \lambda_l D_l F_{leeloci}(z) \Big]\, \tilde{p}_b\, d\eta_b \tag{8.4}$$

$$c_b \bar{p}_e \frac{\partial \bar{\eta}_a}{\partial t} = \int_{\eta_{bmin}}^{\eta_{bmax}} \frac{p_e}{\lambda \Delta} \sum_i^N \Big[\lambda_s E_{siu}(z - \eta_{stepi}) \bar{F}_i(z - \eta_{stepi}) - \lambda_s E_{siu}(z) \bar{F}_i(z) + \lambda_l D_l F_{leeloci}(z) \Big]\, \tilde{p}_b\, d\eta_b \tag{8.5}$$

Like in the equilibrium sorting model in Chapter 6, we assume the bedforms to have a triangular shape with varying trough elevations, so that for each bedform $p_e = p_{se} = p_{le} = J(z)/\Delta$ and $\bar{p}^*_{se} = J(z)$. In order to find a solution to the time evolution of the vertical sorting profile of non-uniform sediment, $\bar{F}_i$, we need to solve (8.4) and (8.5).

Since the probability distribution of bed surface elevations relative to the mean bed level, $\tilde{P}_s$, is steady, the total amount of sediment at each elevation relative to the mean bed level is steady, as well. This will be satisfied when the total net entrainment flux over a bedform (1) is independent of the local bed composition $\bar{F}_i(z)$, (2) is independent of the bed surface elevation z, and (3) has a composition equal to the local bed composition $\bar{F}_i(z)$. These constraints are satisfied when the following equation is met for each individual bedform:

$$E_{snet} \bar{F}_i(z) = E_{siu}(z) \bar{F}_i(z) - E_{siu}(z - \eta_{stepi}) \bar{F}_i(z - \eta_{stepi}) \tag{8.6}$$

where $E_{snet} = q_{top}/\lambda_s$. The total bed load transport rate over the bedform crest, q_{top},

is twice the average total bed load transport rate, $\bar{q}_a$:

$$q_{top} = \bar{q}_{top} = 2\,\bar{q}_a \tag{8.7}$$

so that also the bed load transport rate over the bedform crest is the same for each individual bedform. This relation was found when we applied the simple-wave equation to bedform migration; substitute (2.5) into (2.6) for bedforms having a triangular shape ($\beta = \frac{1}{2}$).

With (8.5) and (8.6), (8.4) reduces to a relaxation-type sorting evolution model:

$$\frac{\partial \bar{F}_i}{\partial t} = \frac{1}{c_b \bar{P}_s} \int_{\eta_{bmin}}^{\eta_{bmax}} \frac{1}{\lambda} \lambda_l D_l p_e \left[F_{leeloci} - \bar{F}_i\right]\ \tilde{p}_b\, d\eta_b \tag{8.8}$$

Note that λ, λ_l, p_e, D_l, $F_{leeloci}$, and $\tilde{p}_b$ all depend on the specific trough elevation η_b. The parameter $\lambda_l D_l$ represents the total deposition rate on the bedform lee face. Eq. (8.8) shows that equilibrium is reached when the overall composition of the sediment deposited at elevation z at the lee face equals the composition of the bed at that elevation. It also shows that the adaptation towards the equilibrium sorting profile is faster for:

- higher rates of deposition onto the lee face, $\lambda_l D_l$;
- a smaller relative amount of sediment at bed elevation z, expressed by $c_b \bar{P}_s(z)$;
- a larger likelihood of being exposed to the flow, expressed by $p_e(z)$;
- a smaller bedform length λ.

Eq. (8.8) shows that the sorting time scale depends on bed elevation z through the PDF of bed surface elevations, p_e, and the probability distribution of bed surface elevations, $\bar{P}_s$. The time scale of the adaptation of the sorting profile will be considered in further detail in Section 8.3.

The volume fraction content of size fraction i in the sediment deposited at elevation z at the lee face, $F_{leeloci}$, for a series of irregular triangular dunes can be written as (see Section 5.2.5):

$$F_{leeloci} = \bar{F}_{leei}\, \omega_i(z) = \bar{F}_{leei} J(z)\ (1 + \bar{\delta}_i\, z^*) \tag{8.9}$$

In Chapter 7, the coefficients γ and κ in (6.64) were used as calibration coefficients, which resulted in the formulation for the lee sorting parameter in (7.4). Although

the calibration was done for equilibrium conditions (in which all parameters vary around mean values), we assume (7.4) to be generally valid:

$$\bar{\delta}_i = -0.3\,\frac{\bar{\phi}_{mlee} - \phi_i}{\bar{\sigma}_a}\,(\bar{\tau}_b^*)^{-0.5} \tag{8.10}$$

where the geometric mean grain size on ϕ-scale of the lee deposit, $\bar{\phi}_{mlee}$, is given by $\bar{\phi}_{mlee} = \sum_i^N \phi_i \bar{F}_{leei}$ and the arithmetic standard deviation of the lee deposit, $\bar{\sigma}_a$, is given by $\bar{\sigma}_a^2 = \sum_i^N (\phi_i - \bar{\phi}_{mlee})^2 \bar{F}_{leei}$.

The overall volume fraction content of size fraction i in the lee deposit, $\bar{F}_{leei}$, in (5.45) and the total deposition rate over the lee face $\lambda_l D_l$ in (5.41) can be written as

$$\bar{F}_{leei} = \frac{1}{\lambda_l D_l}\left[\bar{q}_{topi} - \lambda\,\frac{\partial \bar{q}_{ai}}{\partial x}\right] \qquad \lambda_l D_l = \bar{q}_{top} - \lambda \frac{\partial \bar{q}_a}{\partial x} \tag{8.11}$$

where $\bar{q}_{topi} = \bar{q}_{top}\bar{F}_{topi}$. Herein, $\bar{F}_{topi}$ is given by

$$\bar{F}_{topi} = \frac{1}{\bar{E}_{snet}} \int_{\eta_{bmin}}^{\eta_{bmax}} E_{snet} \int_{\eta_b}^{\eta_t} \bar{F}_i\, p_e\, dz\;\; \tilde{p}_b\, d\eta_b \tag{8.12}$$

where the overall net entrainment rate, $\bar{E}_{snet}$, is given by

$$\bar{E}_{snet} = \int_{\eta_{bmin}}^{\eta_{bmax}} E_{snet}\, \tilde{p}_b\, d\eta_b \tag{8.13}$$

Eq. (8.12) expresses that the volume fraction content of size fraction i transported over an individual crest is equal to the integral over bed elevations of the vertical sorting profile multiplied by its PDF of bed surface elevations, p_e. This is true since the net entrainment rate over the bedform stoss face, E_{snet}, is uniform over all bed surface elevations, where $E_{snet} = \bar{q}_{top}/\lambda_s$, and the composition of the net entrainment at elevation z is assumed to be equal to the bed composition at that elevation, $\bar{F}_i$. To find the *overall* composition of sediment transported over the bedform crest, $\bar{F}_{topi}$, the composition of the sediment transported over an individual crest is averaged over all trough elevations while weighed by its probability density of occurrence, $\tilde{p}_b$.

Similar to the formulation for the overall composition of sediment transported over the bedform crest, $\bar{F}_{topi}$, the volume fraction content of size fraction i in the bed load transport at bed surface elevation z, $\bar{F}_{qsi}$, is given by

$$\bar{F}_{qsi}(z) = \frac{1}{\hat{E}_{snet}(z)} \int_{\eta_{bmin}}^{\eta_{bmax}} \frac{E_{snet}}{\int_{\eta_b}^{z} p_e\, dz} \int_{\eta_b}^{z} \bar{F}_i\, p_e\, dz\;\; \tilde{p}_b\, d\eta_b \tag{8.14}$$

where the entrainment rate, $\hat{E}_{snet}$, is given by

$$\hat{E}_{snet}(z) = \int_{\eta_{bmin}}^{\eta_{bmax}} J(z)\, E_{snet}\ \tilde{p}_b\, d\eta_b \qquad J(z) = \begin{cases} 1 & \text{if } \eta_b \leq z \leq \eta_t \\ 0 & \text{if } z < \eta_b \text{ or } z > \eta_t \end{cases} \tag{8.15}$$

Now, the bed load transport composition, $\bar{F}_{ai}$, is found by averaging the size-specific and elevation-specific bed load transport rate, $\bar{F}_{qsi}$, over all elevations of the active bed:

$$\bar{F}_{ai} = \int_{\eta_{mn}}^{\eta_{mx}} \bar{F}_{qsi}\, \bar{p}_e\, dz \tag{8.16}$$

where η_{mn} and η_{mx} denote the lower and upper limits of the active bed, respectively.

For a series of *regular* bedforms, $\bar{p}_e = p_e$, $\bar{\lambda} = \lambda$, and $\bar{F}_{leeloci} = F_{leeloci}$. In that case, (8.8) and (8.12) would reduce to

$$\frac{\partial \bar{F}_i}{\partial t} = \frac{\bar{\lambda}_l \bar{D}_l\, \bar{p}_e}{c_b\, \bar{P}_s\, \bar{\lambda}} \left[\bar{F}_{leeloci} - \ \bar{F}_i\right] \tag{8.17}$$

$$\bar{F}_{topi} = \int_{\eta_b}^{\eta_t} \bar{F}_i\, \bar{p}_e\, dz \tag{8.18}$$

In the experiments discussed in Chapter 4, uniform conditions have been imposed ($\partial/\partial x = 0$), so that no net aggradation or degradation occurs ($\partial \bar{\eta}_a/\partial t = 0$). As a consequence, besides the probability distribution of bed surface elevations relative to the mean bed level, $\tilde{P}_s$, also the probability distribution of bed surface elevations, $\bar{P}_s$, and the PDF of bed surface elevations, $\bar{p}_e$, are steady. This means that the continuity equations (8.1), (8.2), and (8.3) reduce to:

$$c_b \bar{P}_s \frac{\partial \bar{F}_i}{\partial t} = \bar{D}_{eis} - \bar{E}_{eis} + \bar{D}_{eil} \tag{8.19}$$

$$0 = \bar{D}_e - \bar{E}_e \tag{8.20}$$

$$0 = \bar{D} - \bar{E} \tag{8.21}$$

With (8.9), (8.8) now reduces to a relatively simple relaxation-type model describing the time evolution of sorting in uniform conditions:

$$\frac{\partial \bar{F}_i}{\partial t} = \frac{\bar{q}_{top}}{c_b\, \bar{P}_s} \int_{\eta_{bmin}}^{\eta_{bmax}} \frac{p_e}{\lambda} \left[\bar{F}_{topi}\, \omega_i - \bar{F}_i\right]\ \tilde{p}_b\, d\eta_b \tag{8.22}$$

since in uniform conditions

$$\lambda_l D_l = \bar{q}_{top} = 2\bar{q}_a \tag{8.23}$$

$$\bar{F}_{leei} = \bar{F}_{topi} \tag{8.24}$$

The overall volume fraction content of size fraction i transported over the bedform crest, $\bar{F}_{topi}$, is given by (8.12) and the bed load transport composition, $\bar{F}_{ai}$, is given by (8.16).

The resulting model computes the time evolution of both the vertical sorting profile and volume fraction contents of size fractions in the bed load transport from the following input parameters:

- the initial sorting profile
- the time evolution of the PDF of relative trough elevations
- the time evolution of the total bed load transport rate (not its composition)
- the time evolution of the ratio of the average bedform length to the average bedform height

Experiments B2 and A2 are considered for verifying the sorting evolution model, which will be addressed in Section 8.4. No net aggradation or degradation occurred during the experiments, so that we can apply (8.22) to compute the evolution of sorting during these experiments.

Thus, the set of equations derived in the present section comprises a sorting evolution model for rivers characterised by non-uniform sediment and bedforms. The input parameters of the sorting evolution model are the average total bed load transport rate, $\bar{q}_a$, (not its composition), the PDF of relative trough elevations, $\tilde{p}_b$, and the ratio of the average bedform length to the average bedform height, λ_a/Δ_a.

Sections 9.1 and 9.3 will explain how we include the effects of net aggradation or degradation upon the vertical sorting profile in the continuum sorting model.

8.2 Unsteady PDF of relative trough elevations

A change in time of the PDF of relative trough elevations, $\tilde{p}_b$, results from entrainment and deposition fluxes from and to bed surface elevations. These fluxes are simply considered to be independent of the entrainment and deposition fluxes through

both bedform migration (i.e. through grain size-selective deposition down a bedform lee face and the variability in trough elevations) and net aggradation or degradation. This will be considered in further detail in Sections 9.1. At times when the PDF of relative trough elevations, $\tilde{p}_b$, changes in time, the mean bed level is assumed to be constant, so that the total[3] entrainment rate equals the total deposition rate. In addition, vertical sediment fluxes through bedform migration are assumed to be negligible. The PDF of bed surface elevations, $\bar{p}_e$, and the probability distribution of bed surface elevations, $\bar{P}_s$, are related to $\tilde{p}_b$ according to (5.92) and (5.2), where $\bar{p}^*_{se} = J(z)$ because of the triangular shape of the dunes:

$$\bar{p}_e = \int_{\eta_{bmin}}^{\eta_{bmax}} \frac{J}{\Delta}\, \tilde{p}_b \, d\eta_b \tag{8.25}$$

$$\bar{P}_s = 1 - \int_{-\infty}^{z} \bar{p}_e \, dz \tag{8.26}$$

Since the PDF of relative trough elevations at the new time step, $\tilde{p}_b(z, t + \Delta t)$, is given, we can determine $\bar{P}_s(z, t + \Delta t)$ using (8.25) and (8.26), which is illustrated in Figure 8.1.

At elevations where $\bar{P}_s(z, t + \Delta t) > \bar{P}_s(z, t)$, sediment has been deposited. At elevations where $\bar{P}_s(z, t + \Delta t) < \bar{P}_s(z, t)$, sediment has been entrained. Since the mean bed level remains constant, the net amount of deposition equals the net amount of deposition, which has also been explained in Section 5.1. It is simply assumed that sediment entrained from bed surface elevation z has the same composition as present at that elevation. We can now determine the average volume fraction content of size fraction i in the total amount of sediment entrained from the bed, $\bar{\bar{F}}_{iP}$:

$$\begin{aligned} \bar{\bar{F}}_{iP}(t) &= \frac{\int_{\eta_{mn}}^{\eta_{mx}} I(z) \left[\bar{C}_i(z,t) - \bar{C}_i(z,t+\Delta t)\right] dz}{\int_{\eta_{mn}}^{\eta_{mx}} \sum_i^N I(z) \left[\bar{C}_i(z,t) - \bar{C}_i(z,t+\Delta t)\right] dz} = \\ &= \frac{\int_{\eta_{mn}}^{\eta_{mx}} I(z) \left[\bar{P}_s(z,t) - \bar{P}_s(z,t+\Delta t)\right] \bar{F}_i(z,t)\, dz}{\int_{\eta_{mn}}^{\eta_{mx}} I(z) \left[\bar{P}_s(z,t) - \bar{P}_s(z,t+\Delta t)\right] dz} \end{aligned} \tag{8.27}$$

where

$$I(z) = \begin{cases} 1 & \text{if } \bar{P}_s(z, t+\Delta t) < \bar{P}_s(z,t) \\ 0 & \text{if } \bar{P}_s(z, t+\Delta t) \geq \bar{P}_s(z,t) \end{cases}$$

and where η_{mn} and η_{mx} denote the lower and upper levels of the active bed at either time t or $t + \Delta t$, that is, when the active bed covers the widest range of bed elevations.

[3] *total* here meaning summed over all bed elevations and all size fractions

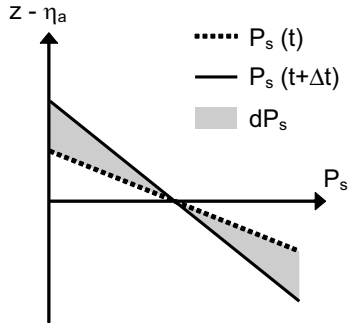

Figure 8.1: The change in time of the probability distribution of bed surface elevations, $\bar{P}_s$, caused by the change in time of the PDF of relative trough elevations, $\tilde{p}_b$.

At the bed elevations where deposition occurs, the composition of the deposited sediment is assumed to be equal to the average composition of the total amount of sediment entrained from the bed, $\bar{\bar{F}}_{iP}(t)$. The bed composition at the new time step then equals:

$$\bar{F}_i(z,t+\Delta t) = \begin{cases} \bar{F}_i(z,t) & \text{if } \bar{P}_s(z,t+\Delta t) \leq \bar{P}_s(z,t) \\ 1/\bar{P}_s(z,t+\Delta t)\left[\bar{P}_s(z,t)\bar{F}_i(z,t) + \right. & \\ \left. \quad (\bar{P}_s(z,t+\Delta t) - \bar{P}_s(z,t))\,\bar{\bar{F}}_{iP}(t)\right] & \text{if } \bar{P}_s(z,t+\Delta t) > \bar{P}_s(z,t) \end{cases}$$

Note that this method for accounting for a change in time of the PDF of relative trough elevations does not incorporate grain size-selective processes. In reality, however, grain size-selective processes will surely play a role. For instance, the winnowing of fines from the trough surface and subsurface may cause the coarse bed layer below migrating bedforms to subside and the range of elevations of the active bed to gradually increase.

8.3 Time scale of vertical sorting

Eq. (8.22) describes the evolution of sorting in situations without net aggradation or degradation. It is a relaxation-type equation, but a formulation for the time scale of the adaptation of sorting is not straightforward. This is due to the fact that most parameters in (8.22) depend on time and the trough elevation, η_b. Yet, in cases where

- net aggradation or degradation is negligible,

- the PDF of relative trough elevations is steady,
- the total bed load transport rate is steady, and
- the composition of the sediment transported over the crest is steady,

the time scale of the adaptation of sorting is of the order of

$$T_f(z) = \frac{\bar{\lambda}}{2\,\bar{q}_a} \frac{c_b \bar{P}_s(z)}{\bar{p}_e(z)} \tag{8.28}$$

which tells us that

- the larger the relative amount of sediment at bed elevation z, the slower is the adaptation of sorting. The relative amount of sediment at bed elevation z is represented by the probability distribution of bed surface elevations averaged over the series of bedforms, $\bar{P}_s(z)$, multiplied by the sediment concentration in the bed, c_b;
- the larger the exposure to the flow of elevation z, the faster is the adaptation of sorting. The exposure to the flow of elevation z is represented by the PDF of bed surface elevations, $\bar{p}_e(z)$;
- the larger the average bedform length, $\bar{\lambda}$, the slower is the adaptation of sorting. Namely, the larger the average bedform length, $\bar{\lambda}$, the smaller is the amount of bedforms over some fixed distance, and the smaller are the entrainment and deposition rates;
- the larger the total bed load transport rate, $\bar{q}_a$, the faster is the adaptation of sorting.

Note that the sorting time scale, T_f, depends on bed elevation z through both the PDF of bed surface elevations, $\bar{p}_e$, and the probability distribution of bed surface elevations, $\bar{P}_s$. The sorting time scale appears to increase with decreasing bed elevation. Deeper elevations are less exposed to the flow, thus the adaptation of sorting is slower. Moreover, at deeper elevations the amount of sediment is larger, which increases the time required for the adaptation of sorting even more. This confirms the author's statements on this topic in Section 2.7.1.

Figure 8.2 shows the time scale of the adaptation of sorting, $T_f(z)$, according to (8.28) for experiments B2 and A2, together with the time scale of dune migration, T_c, which is defined as the time required for a bedform to cover the average bedform length, $\bar{\lambda}$. This is expressed by (5.100):

$$T_c = \frac{\bar{\lambda}}{c}$$

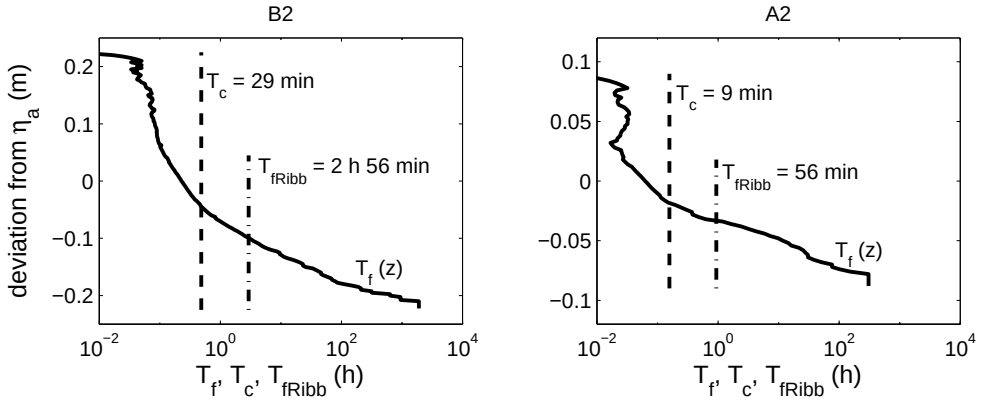

Figure 8.2: The time scale of the adaptation of sorting, $T_f(z)$, according to (8.28), the time scale of dune migration, T_c, according to (5.100), and the time scale of the exchange layer composition according to (8.29), for experiments B2 and A2. Note the log-scale on the x-axis.

In the lower parts of the active bed, the time scale of sorting, $T_f(z)$, appears to be much larger than the time scale of dune migration, whereas in the upper parts the time scale of sorting is smaller than one of dune migration. One of the constraints of the sorting evolution model is, however, that the time scale of migration must be smaller than the time scale of sorting. This constraint arises from the assumption that the sediment deposited at elevation z is immediately mixed with all sediment present at this elevation. This implies that the time evolution of the sorting in the upper parts of the active bed may not be adequately described by the model.

For the Ribberink two-layer model (see Section 3.2.3), *Ribberink* (1987) defined a time scale for the adaptation of the composition of the exchange layer. This exchange layer is located below the active layer and represents the bed elevations exposed only by relatively deep bedform troughs. The time scale of the adaptation of the composition of the exchange layer was defined as

$$T_{f\,Ribb} = \frac{c_b\,\bar{\lambda}}{\gamma_r\,\bar{q}_a}\,\frac{\delta_e}{1+\alpha_r\,\delta_e/\delta} \tag{8.29}$$

in which $\alpha_r = d_m/d_{md}$ where d_m denotes the geometric mean grain size of the active layer. The parameter d_{md} denotes the geometric mean grain size of the sediment deposited from the active layer to the exchange layer through the variability in trough elevations. Since bedforms mostly show a downward coarsening trend, sediment deposited from the active layer to the exchange layer is assumed to be coarser than the

average composition of the active layer, which implies that α_r is larger than 1. The constant γ_r relates the amount of deposition into the deepest troughs (being equal to the entrainment rate from these deepest troughs) to the bed load transport rate. As recommended by *Ribberink*, we assume $\alpha_r = 1.5$, $\gamma_r = 0.06$, $\delta = 0.5\,\Delta_a$, and $\delta_e = 1.22\,\delta$. The time scale of the adaptation of the exchange layer composition for experiments B2 and A2 is plotted in Figure 8.2.

According to the present sorting evolution model, for the lower elevations of the active bed, the time scale of sorting is much larger than the time scale of adaptation of the composition of the exchange layer as proposed by *Ribberink* (1987). This is confirmed by the measured time evolution of the sorting profile in experiments B2 and A2.

8.4 Verification

8.4.1 Short description of the experiments

The verification of the sorting evolution model is based on a comparison between the measured and computed sorting profiles for experiments B2 and A2. The experiments are here described only shortly. For a more detailed description of the experiments, reference is made to Chapter 4.

The experiments were conducted using mixtures composed of three well-sorted grain size fractions. During the experiments, uniform conditions were maintained and the transported sediment was recirculated. The sediment transport consisted solely of bed load transport.

Experiment B2 started from the final stage of experiment B1. The initial bed of B2 consisted of a coarse bed layer on top of a substrate composed of only the fine size fraction. Small barchan-type bedforms were present on top of this coarse top layer. Right after the start of the experiment, the discharge was increased and the coarse layer was entrained. After this, the underlying fine sediment became available to the transport process and the bedform height quickly increased. The proportion of the fine size fraction in the transported material gradually increased, whereas the proportion of the medium and coarse fractions in the transported material slowly decreased, since they were gradually worked down to lower bed elevations. The coarse material in the lower parts of the bedforms did not constitute a distinct coarse bed layer over which the bedforms migrated, but participated in the transport process. The vertical sorting profile seemed to be primarily determined by grain size-selective deposition down the avalanche lee face.

Experiment A2 started from the final stage of experiment A1. The initial bed of A2 consisted of a coarse bed layer on top of a substrate composed of a mixture of equal proportions of the three size fractions. Small barchan-type bedforms were present on top of this coarse top layer. Right after the start of the experiment, the discharge was increased to the same rate as in B2. The bedform height increased and the proportion of the coarse fraction in the transported material quickly increased. The lower elevations of the active bed showed a clear coarsening compared with the upper ones. It seems that the vertical sorting profile was determined by the grain size-selective deposition down the avalanche lee face, as well as the winnowing of fines from the trough surface and subsurface, and partial transport.

8.4.2 Unsteady PDF of relative trough elevations

In Section 8.2, we have seen how, at the moments the PDF of relative trough elevations is assumed to change in time, the sediment is artificially rearranged over bed elevations. Figures 8.3 and 8.4 show the measured time evolution of the PDF of relative trough elevations, $\tilde{p}_{\eta_b}$, for experiments B2 and A2 (see Section 5.3.2). Appendix E shows the measured time evolution of the PDF of bed surface elevations, $\bar{p}_e$. We can see that the greatest changes in the PDF of relative trough elevations occur within 0 to 3 flow hours. After that, only small changes occur. For experiment B2, Appendix F shows the results of the sediment rearrangement procedure at the moments the PDF of relative trough elevations is assumed to change in time.

8.4.3 Time evolution of vertical sorting

In order to describe the time evolution of sorting in a situation without net aggradation or degradation, we apply (8.22) and follow the procedure described in Section 8.2 to account for the time evolution of the PDF of relative trough elevations. The time series of the PDF of relative trough elevations as shown in Figures 8.3 and 8.4 are used as input to the sorting evolution model. Only trough elevations below the mean bed level are accounted for. The PDF of relative trough elevations changes in time at the transitions between the periods shown in Figures 8.3 and 8.4.

Note that the average bedform length, λ_a, the average bedform height, Δ_a, and the total bed load transport rate, $\bar{q}_a$, are assumed to be steady during the experiments. Their values have been set equal to their equilibrium values, which are given in Tables 4.2 and 4.3. The angle of repose of the lee faces is assumed to be equal to 30°.

The figures below show the computed (and measured) time evolution of the vertical sorting profile. They also show the probability distribution of bed surface elevations,

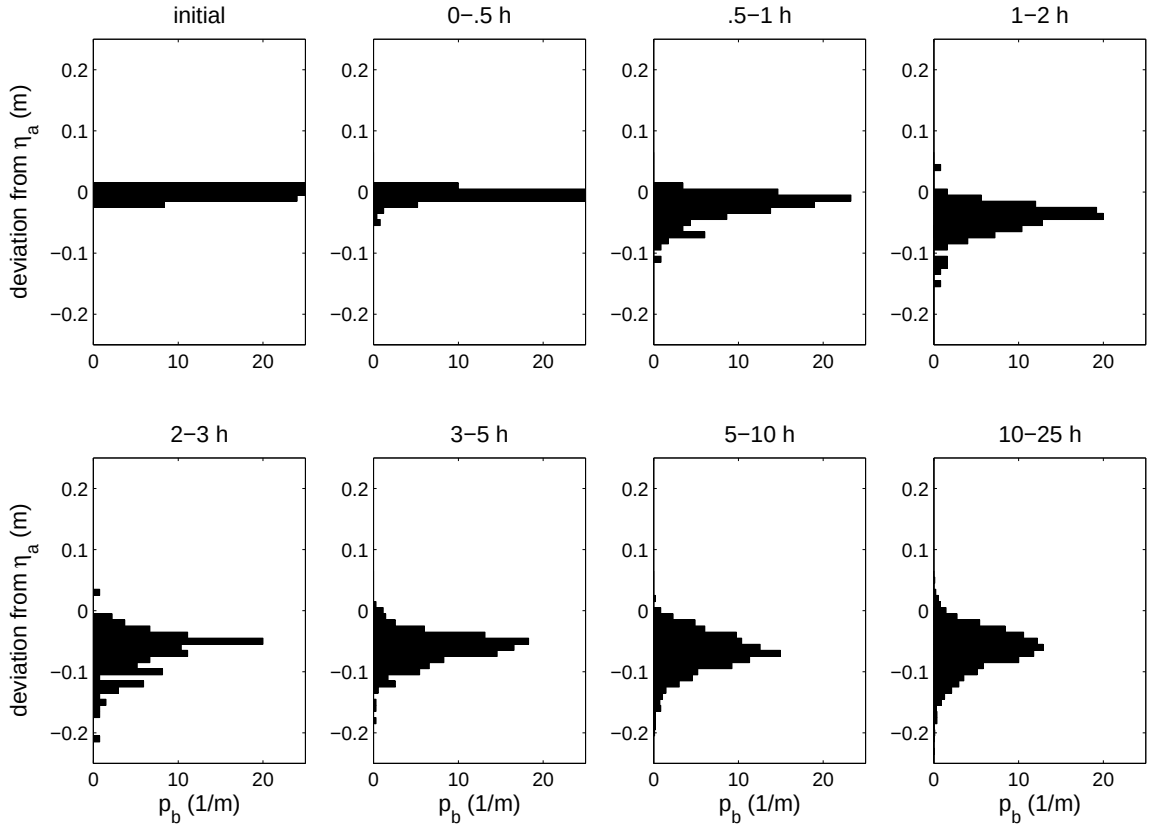

Figure 8.3: Measured time evolution of the PDF of relative trough elevations, $\tilde{p}_{\eta_b}$, for experiment B2.

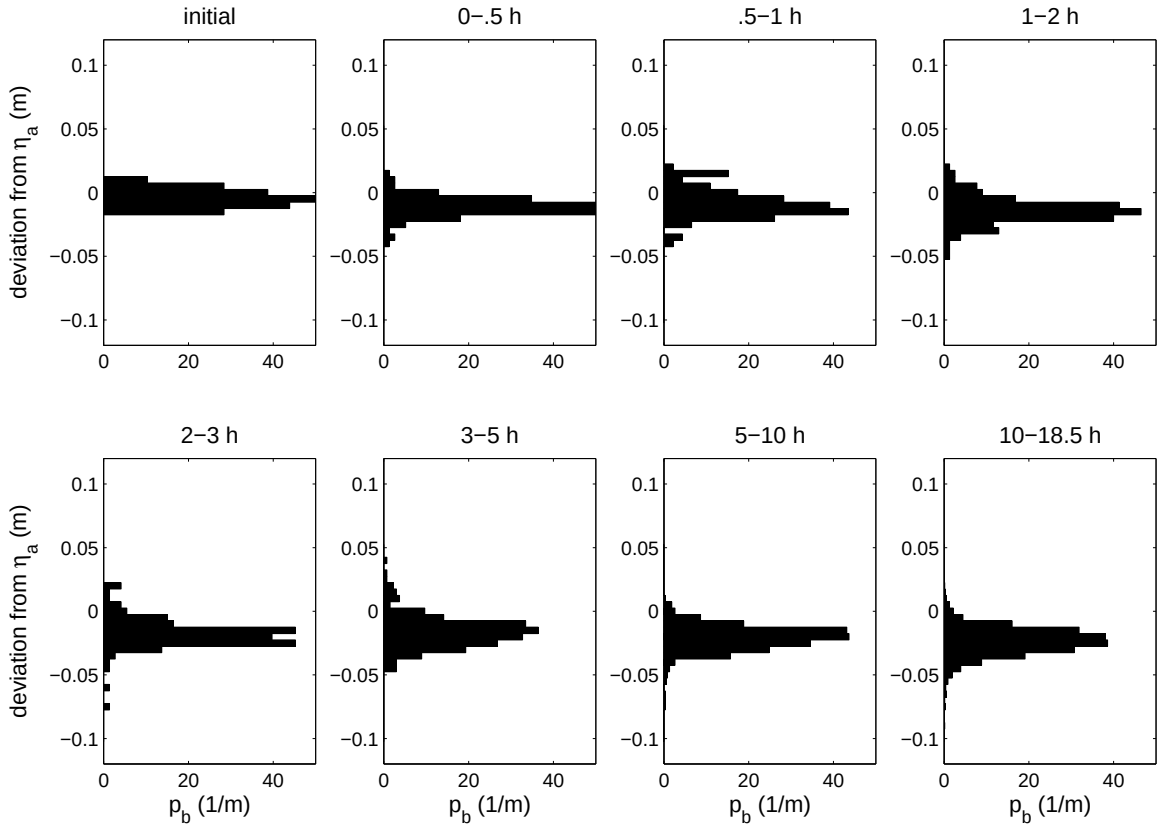

Figure 8.4: Measured time evolution of the PDF of relative trough elevations, $\tilde{p}_{\eta_b}$, for experiment A2.

$\bar{P}_s$, at the specific time, which indicates which bed elevations are exposed to the flow, that is, the bed elevations where $0 < \bar{P}_s < 1$. Eqs. (8.25) and (8.26) show how $\bar{P}_s$ is determined from the given time evolution of the PDF of relative trough elevations. The measured initial sorting profiles of experiments B2 and A2 (stages B1E and A1E, respectively, also see Section 4.2.2) are imposed to the calculations.

Figure 8.5 shows how the computed sorting pattern of experiment B2 gradually develops towards its equilibrium profile and that the range of active bed elevations over which the sorting takes place increases. The coarse particles settle primarily to the lower lee face elevations and the finer particles to the upper lee face elevations. Note that the inflection point of the vertical sorting profile is always located at the mean bed level. This is due to the ways of modelling the grain size-selective deposition down a lee face and the irregularity of bedforms. Individual stoss and lee faces are assumed to be anti-symmetric around the mean bed level: $\eta_t - \bar{\eta}_a = \bar{\eta}_a - \eta_b$ (see Section 5.3.2). Figure 8.5 illustrates that at the lower elevations of the active bed the bed composition adapts more slowly than at the upper ones.

In Figure 8.6, the computed sorting profiles are compared to the measured ones, for the non-equilibrium N-stage (B2N) and the equilibrium E-stage (B2E) (also see Section 4.2.2). The measured sorting profile of phase B2E shows a top layer coarser than the material underneath. This is due to (1) the formation of a thin mobile armour layer over the stoss face and (2) deposition of sediment that was being transported until the flow was turned off. This phenomenon has been addressed in detail in Section 7.2. The computed sorting profiles do not show such a coarse top layer, since in the sorting evolution model it is assumed that the composition of the net entrainment flux on the stoss face has the same composition as the bed material at that elevation.

The computed sorting profile for the non-equilibrium N-stage (B2N) shows reasonable agreement with the data. The sorting trend is somewhat too strong, but the computed volume fraction contents of the size fractions have the right order of magnitude. The computed sorting profile for the equilibrium stage B2E agrees well with the measured one, considering the large variation in the sorting profiles from different core samples.

The range of bed elevations covered by the core samples seems small compared to the range of elevations covered by the computations (Figure 8.6). For more information on this topic, reference is made to Section 7.2. Note that the upper elevations of the active bed are rarely reached by the bedform crests, as the probability density of being exposed to the flow, $\bar{p}_e$, is very small. As such, these elevations have a negligible influence on, for example, the composition of the sediment transported

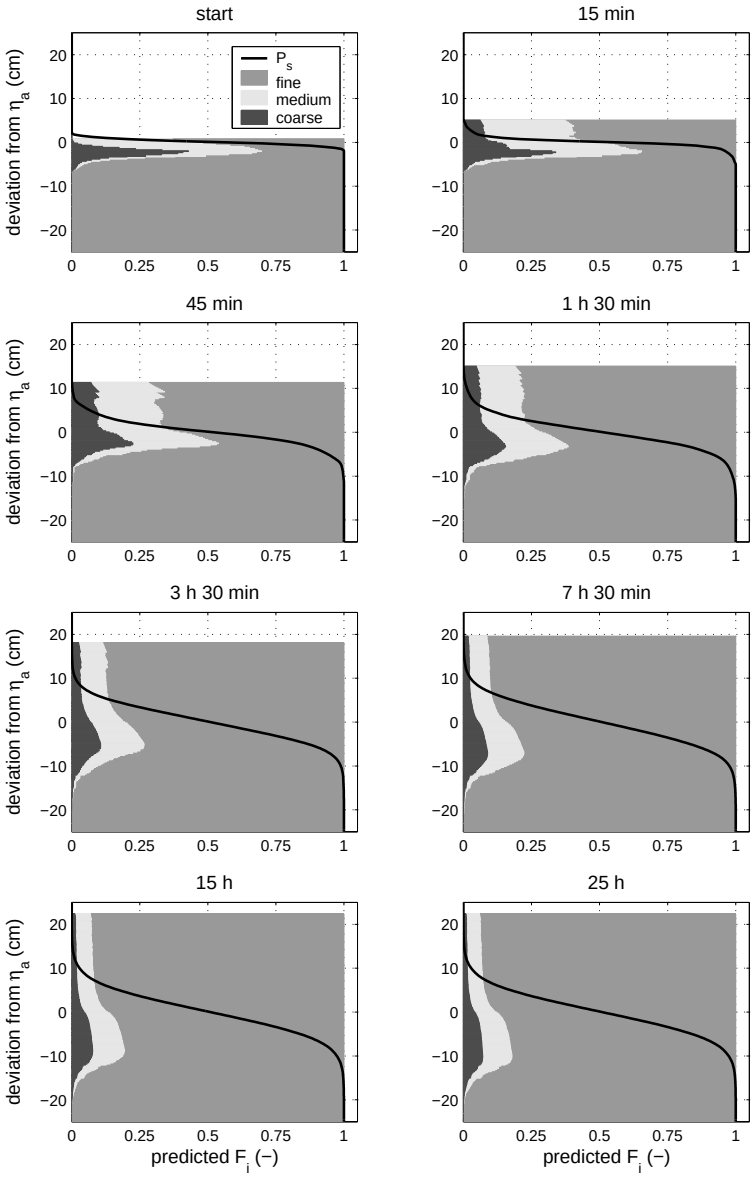

Figure 8.5: The computed time evolution of the sorting profile, $\bar{F}_i$, for experiment B2.

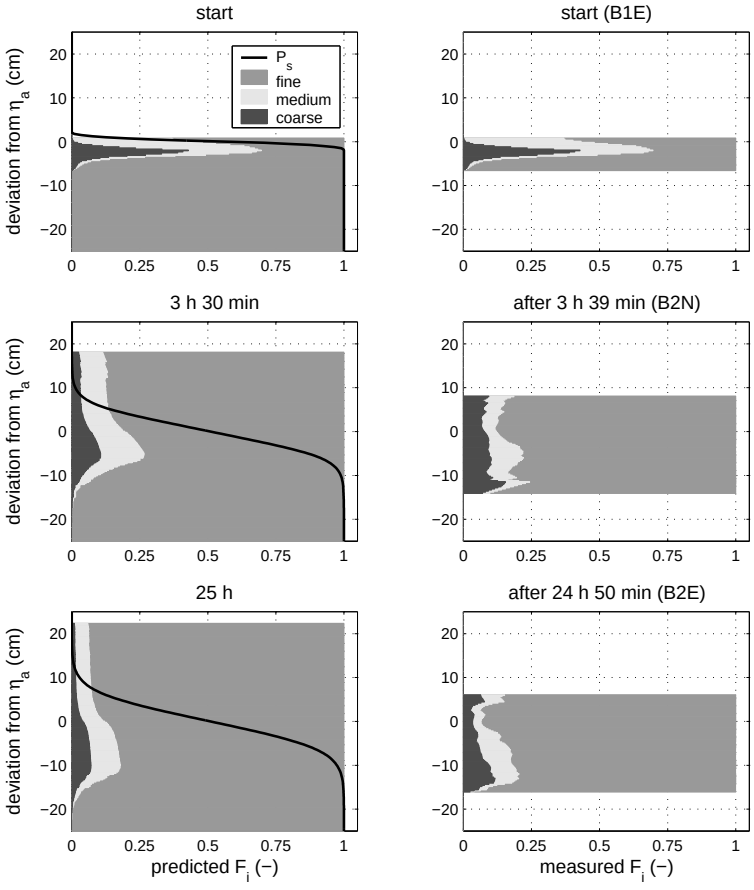

Figure 8.6: Comparison of the measured and computed sorting profiles, $\bar{F}_i$, for the non-equilibrium N-stage and the equilibrium E-stage of experiment B2.

over the crests. More important to the sorting evolution calculations than these upper elevations are the lower elevations of the active bed . Unfortunately, these lower elevations are not entirely covered by the core samples.

Figure 8.7 shows the measured and computed time evolution of the average composition of the bed load transport for experiment B2. Note that the large markers on the right-hand side of the plot represent the measured composition of the bed load transport averaged over the equilibrium period. The agreement between the measured and computed time evolution of the average transport composition is reasonably good, which implies that the physical processes as described in Section 8.4.1 are simulated rather well by the model. The computed values are close to the measured composition of the sediment transport averaged over the equilibrium period. Note that the 'creases' in the computed composition are not due to numerical problems, but to the imposed transitions in the time evolution of the PDF of relative trough elevations (see Figures 8.3 and 8.4).

Since conditions were uniform in the experiments, the amount of sediment integrated over all elevations of the active bed must be constant, $\bar{C}_{tot}$, as well as the volume fraction content of each grain size fraction in the bed, $\bar{\bar{F}}_i$. This is confirmed by Figure 8.8. Herein, $\bar{\bar{F}}_i$ is given by (6.69), where the limits η_{mn} and η_{mx} are the limits of the active bed in the stage in which the active bed covers the widest range of bed elevations:

$$\bar{\bar{F}}_i = \frac{\int_{\eta_{mn}}^{\eta_{mx}} \bar{C}_i(z)\, dz}{\int_{\eta_{mn}}^{\eta_{mx}} \sum_i^N \bar{C}_i(z)\, dz} = \frac{\int_{\eta_{mn}}^{\eta_{mx}} \bar{P}_s(z)\bar{F}_i(z)\, dz}{\int_{\eta_{mn}}^{\eta_{mx}} \bar{P}_s(z)\, dz} \tag{8.30}$$

and $\bar{C}_{tot}$ is given by

$$\bar{C}_{tot} = \int_{\eta_{mn}}^{\eta_{mx}} \bar{C}_i(z)\, dz = \int_{\eta_{mn}}^{\eta_{mx}} c_b \bar{P}_s(z)\bar{F}_i(z)\, dz \tag{8.31}$$

Figure 8.9 shows the computed time evolution of the vertical sorting profile for experiment A2. Again note that the 'creases' in the computed sorting profile are not due to numerical problems, but to the imposed transitions in the time evolution of the PDF of relative trough elevations. The initial sorting profile of experiment A2 was the final stage of experiment A1 (stage A1E), in which small bedforms migrated over a coarse bed layer. During the experiment, the downward coarsening trend remains, but covers an increasing range of bed elevations. By comparing the computed sorting profiles with the measured ones (Figure 8.10), we can see that the formation of the coarse layer is not adequately described by the model. Yet, the order of magnitude of the sorting profiles and the sorting trend is predicted reasonably well.

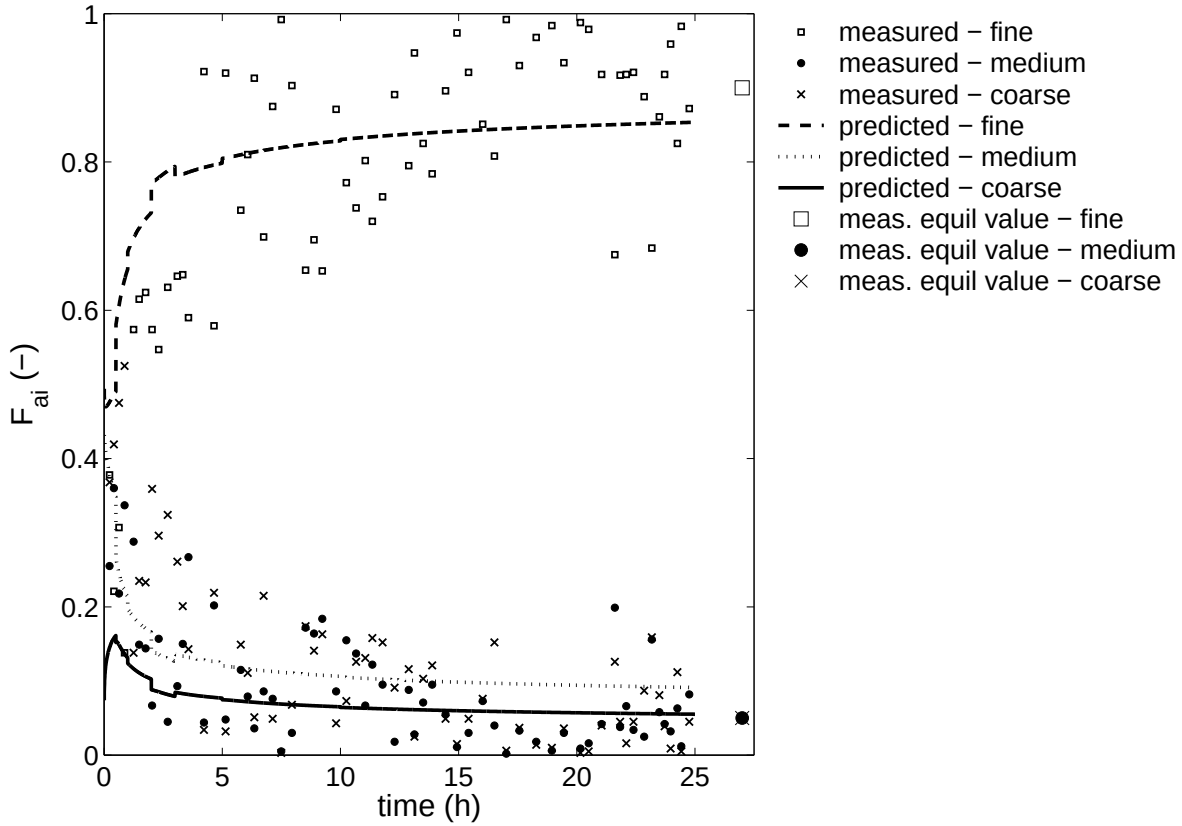

Figure 8.7: Measured and computed time evolution of the volume fraction content of size fractions in the bed load transport, $\bar{F}_{ai}$, for experiment B2.

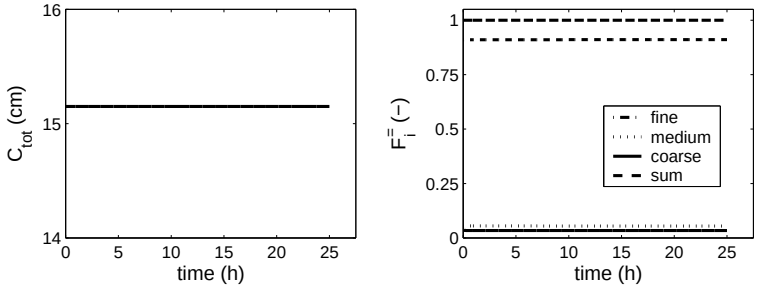

Figure 8.8: Computed time evolution of the total amount of sediment above a fixed datum not reached by the flow, and the computed time evolution of the volume fraction content of size fractions averaged over all elevations above this fixed datum, $\bar{\bar{F}}_i$, for experiment B2.

The disagreement between the computed and measured sorting profiles is larger for A2 than for B2, which appears to be due to the model's inadequate description of the formation of a coarse bed layer. In the sorting evolution model, the dominant sorting mechanism is the grain size-selective deposition down a bedform lee face. The present version of the model does not account for the mechanisms of (1) the winnowing of fines from the trough surface and subsurface and (2) the settling of immobile coarse grains, whereas these mechanisms play a significant role in the formation of a coarse bed layer.

Figure 8.11 illustrates that the computed time evolution of the average composition of the sediment transport lies within the scatter of the measured data. The computed values are fairy close to the measured composition of the sediment transport averaged over the equilibrium period.

8.4.4 Towards equilibrium

For both experiments B2 and A2, calculations have been continued until 500 flow hours. Figure 8.12 shows the computed time evolution of the bed load transport composition. The figure illustrates that, at the end of the experiments (B2 at 25 flow hours, A2 at 18 flow hours), the computed bed load transport composition is already close to its equilibrium composition. Note the log-scale on the horizontal axis. This also applies to the sorting profiles (see Figure 8.13). Between the end of the experiment and 500 flow hours, mainly the very low elevations of the active bed continue adapting towards their equilibrium compositions. This adaptation influences the composition of the bed load transport only slightly (Figure 8.12).

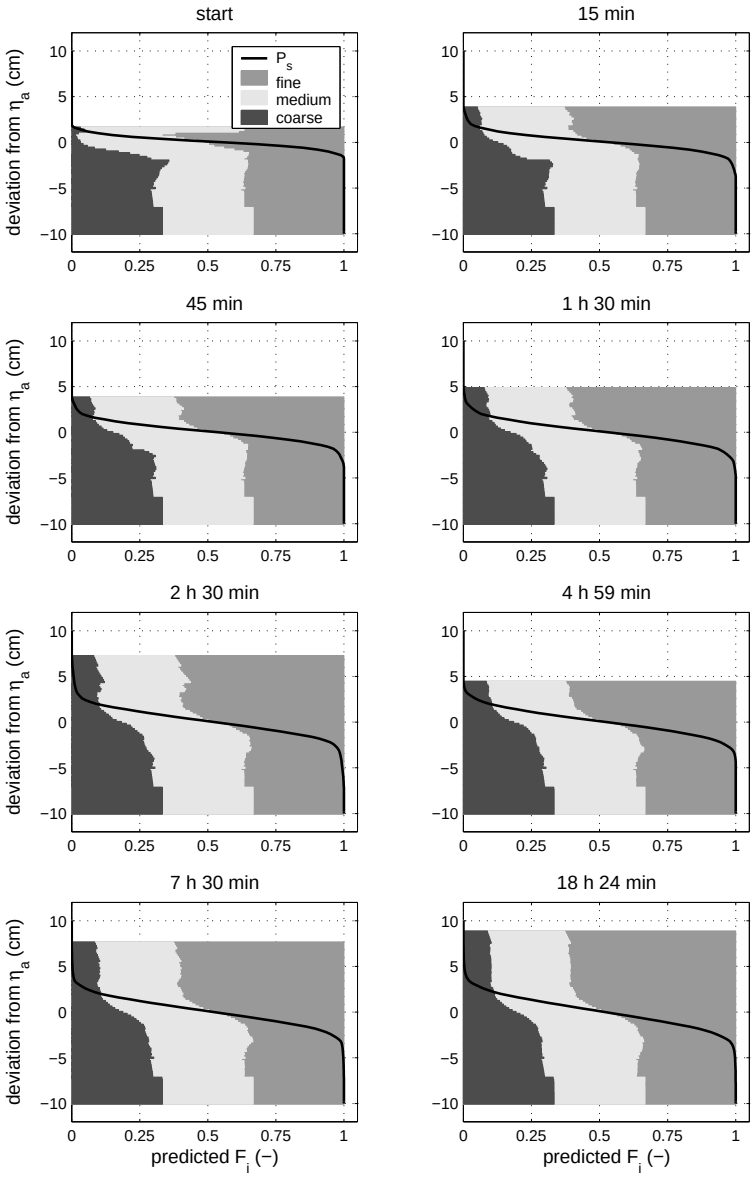

Figure 8.9: The computed time evolution of the sorting profile, $\bar{F}_i$, for experiment A2.

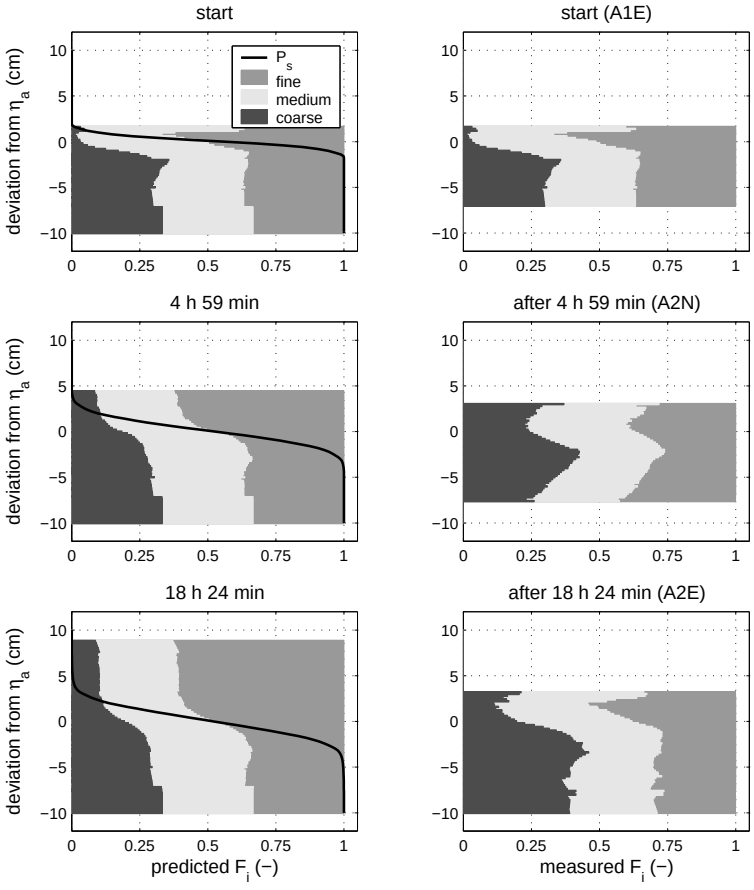

Figure 8.10: Comparison of the measured and computed sorting profiles, $\bar{F}_i$, for the non-equilibrium N-stage and the equilibrium E-stage of experiment A2.

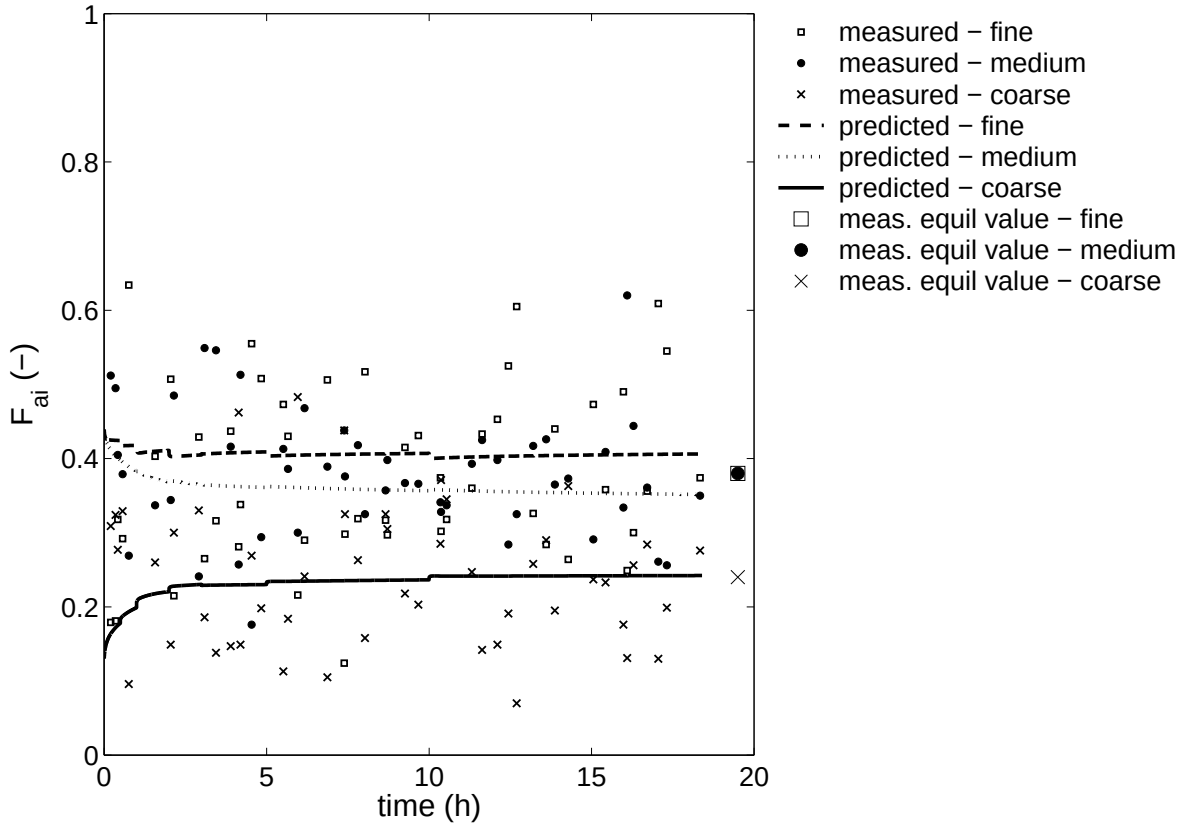

Figure 8.11: Measured and computed time evolution of the volume fraction content of size fractions in the bed load transport, $\bar{F}_{ai}$, for experiment A2.

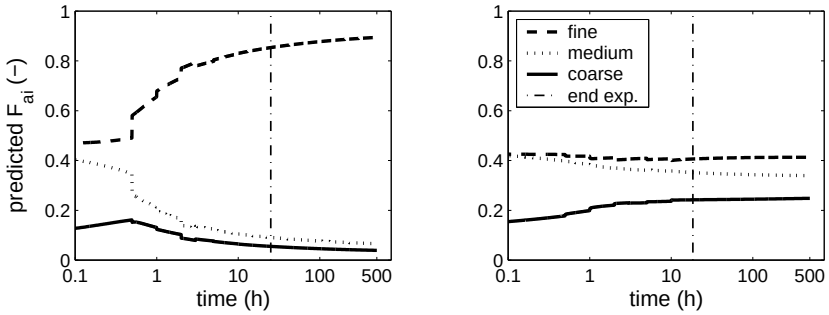

Figure 8.12: The computed composition of the bed load transport until 500 flow hours, for experiments B2 and A2. Note the log-scale on the x-axis.

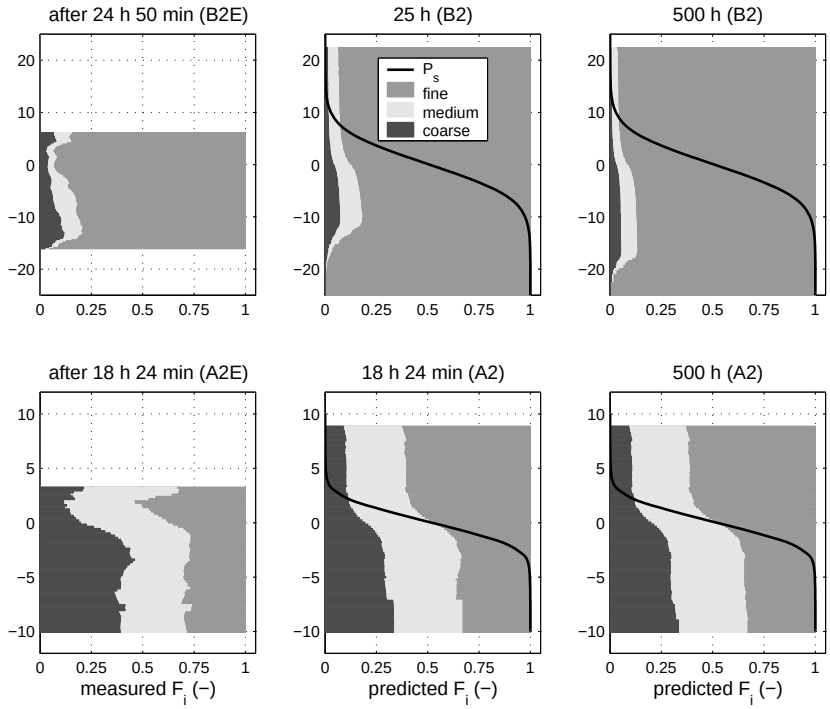

Figure 8.13: The measured sorting profile at the end of the experiment, the computed sorting profile at the end of the experiment, and the computed sorting profile after 500 flow hours, for experiments B2 and A2.

8.5 Discussion

Chapters 6 through 8 have not presented a method for including the effects of net aggradation or degradation upon the vertical sorting profile. A method for incorporating net aggradation or degradation in the continuum sorting model will be proposed in Sections 9.1 and 9.3.

In this chapter, a sorting evolution model has been derived. It predicts the time evolution of both the vertical sorting profile and the average composition of the bed load transport. The following data is required as input to the model:

- the initial sorting profile
- the time evolution of the PDF of relative trough elevations
- the time evolution of the bed load transport rate (not its composition)
- the time evolution of the ratio of the average bedform length to the average bedform height

The sorting evolution model is a simplified version of the continuum sorting model described in Chapter 5. Like the reduction of the continuum sorting model to the equilibrium sorting model (Chapter 6), the reduction to the sorting evolution model is based on the assumption that the composition of the net entrainment at a certain bed elevation is equal to the bed composition at this elevation. The sorting evolution model is a relaxation-type model and a time scale of sorting has been defined.

The sorting evolution model has been verified by comparing the computed time evolution of both the sorting profile and the bed load transport composition with measured data from experiments B2 and A2. It is important to note that, except for the two constants in the lee sorting function that were verified for equilibrium conditions, no parameters in the sorting evolution model have been calibrated against measurements. The computational results agree reasonably well with the data. Nevertheless, the formation of a coarse bed layer in the lower parts of migrating bedforms is not adequately described by the model. It is emphasised that the sorting evolution model's main sorting mechanism is the grain size-selective deposition over the lee face. The model does not allow for grain size-selective entrainment over the stoss face, as all particles present at a certain elevation of the active bed are assumed to be transported over the bedform crest. Particles present on the stoss face, but too coarse to be transported, are therefore not allowed to settle down as the bedform migrates. Instead, these coarse particles are assumed to be transported over the bedform crest and are then deposited onto the lower elevations of the active bed through

the mechanism of grain size-selective deposition down the lee face. Moreover, also the winnowing of fines from the trough surface and subsurface plays a role in the formation of a coarse bed layer and is not included in the model. The mechanisms of winnowing of fines and the settling of immobile coarse particles need to be incorporated in a later version of the model, so as to improve the description of the formation of a coarse bed layer.

The method to account for the effects of a change in time of the PDF of relative trough elevations in the sorting evolution model is a rather artificial one. In the present method, grain size-selective processes are not accounted for, while these processes surely play a role. Further research on this topic is recommended.

In Section 3.2.2, it was explained that the set of equations of the Hirano active layer model may become elliptic in parts of the space-time domain in situations wherein degradation occurs while the substrate is finer than the active layer (*Ribberink*, 1987). A set of equations being elliptic means that, at each point in space and time, the state is determined by the state in all other points. This means that boundary conditions are required at all boundaries of the space-time domain covered by the model. Since imposing conditions in the future is physically unrealistic, the active layer model is obviously not able to model the natural processes in those circumstances. It is, however, not straightforward to analyse the set of equations of the new continuum sorting model for possible ellipticity, since its set of equations is much more extensive than the set of equations of the Hirano active layer model. This analysis has therefore not been performed in the present study. Yet, since the ellipticity of the set of equations of the active layer model appears to be related to the instantaneous mixing of sediment within the discrete bed layers (*Ribberink*, 1987), it is believed that the new continuum sorting model will not become elliptic. There has been no evidence that the Armanini diffusion model, which is another depth-continuous model, may become elliptic under certain conditions, which may confirm the idea that a depth-continuous approach at least partly solves the ellipticity problem.

For the cases considered in the present chapter, the *measured* time evolution of the PDF of relative trough elevations was used as input to the sorting evolution model. However, for cases for which no data on the PDF of relative trough elevations is available, a model is required. Such a model was not developed in the present study. The relation between the PDF of relative trough elevations (or bed surface elevations) and the vertical sorting profile is still an unexplored area of research. This subject matter will be considered in more detail in Section 9.4.1.

Chapter 9

Considerations on application in a morphological model system

In the previous chapters we have focussed on conditions without net aggradation or degradation. For *steady situations*, the continuum sorting model has been reduced to the equilibrium sorting model, whereas, for *non-steady situations*, the continuum sorting model has been reduced to the sorting evolution model. The present chapter will explain how the continuum sorting model can be applied to cases with net aggradation or degradation. Yet, the model has only been tested against experiments in which there was none. The previous chapters have shown that the equilibrium sorting model and the sorting evolution model yield satisfactory results under those conditions.

This notwithstanding, the real value of a sediment continuity model is the description of the interaction among grain size-selective transport, the vertical sorting, *and* net aggradation or degradation. Thus, the next step is to apply the continuum sorting model to situations with net aggradation or degradation. For this purpose, the continuum sorting model model needs to be implemented in a morphological model system for non-uniform sediment. In the present chapter, the author provides methods for doing so, but testing the resulting morphological model system is beyond the scope of this thesis. First, it is discussed how the continuum sorting model can be incorporated in a morphological model system (Section 9.1). Section 9.2 will provide suggestions for applying either the equilibrium sorting model or the sorting evolution model. In Section 9.3, the author proposes a method for including the effects of net aggradation or degradation upon the vertical sorting profile.

Section 9.4 addresses the various components of the morphological model system: the probability density function (PDF) of trough elevations, the average bed surface composition, the bed roughness, the total bed load transport rate, and suspended load transport. Subsequently, we address the matters of plane-bed conditions (Section 9.5) and the spatial discretisation of the model area and the vertical discretisation of the river bed (Section 9.6).

The present chapter will go into characteristics of the new continuum sorting model, i.e. the sorting mechanisms incorporated and the implications of the main assumptions made (Section 9.7). Next, it is discussed how the present study reflects upon existing bed layer models (Section 9.8). The performance of the Hirano active layer model, the Ribberink two-layer model, and the sorting evolution model are compared to measured data from two flume experiments, with respect to the time evolution of the vertical sorting. Finally, a number of case-studies are suggested (Section 9.9).

9.1 Scheme of the morphological model system

Figure 9.1 shows how the continuum sorting model (i.e. the equilibrium sorting model or the sorting evolution model) can be incorporated into a morphological model system for non-uniform sediment. Section 9.2 will explain when to use either the equilibrium sorting model (i.e. initial sorting profile method) or the sorting evolution model. The gray boxes in Figure 9.1 represent the sub-models that are part of the continuum sorting model. The morphological model system requires the initial sorting profile and other initial conditions to be known, and consists of a number of sub-models, which will be discussed in Section 9.4.

Figure 9.1 illustrates that changes in the vertical sorting profile occur through vertical sediment fluxes accompanying

I. a change in time of the PDF of relative trough elevations (see Section 8.2);

II. bedform migration, i.e. grain size-selective deposition down a bedform lee face and the variability in trough elevations (see Chapter 6 if applying the equilibrium sorting model or Chapter 8 if applying the sorting evolution model);

III. net aggradation or degradation (see next section).

Note that it is assumed that these three types of vertical sediment fluxes do not interact with one another. Further research is required to assess whether this assumption is fully justified.

It is important to note that the composition of the bed load transport, $\bar{F}_{ai}$, is not required as input to the morphological model system. As will be explained in Section 9.2, the equilibrium sorting model (i.e. initial sorting profile method) or the sorting evolution model solve for both the vertical sorting profile, $\bar{F}_i$, and the bed load transport composition, $\bar{F}_{ai}$. That the bed load transport composition is described by the continuum sorting model itself is not surprising, considering the strong interaction among the vertical sorting profile (over elevations of the active bed), $\bar{F}_i$, the

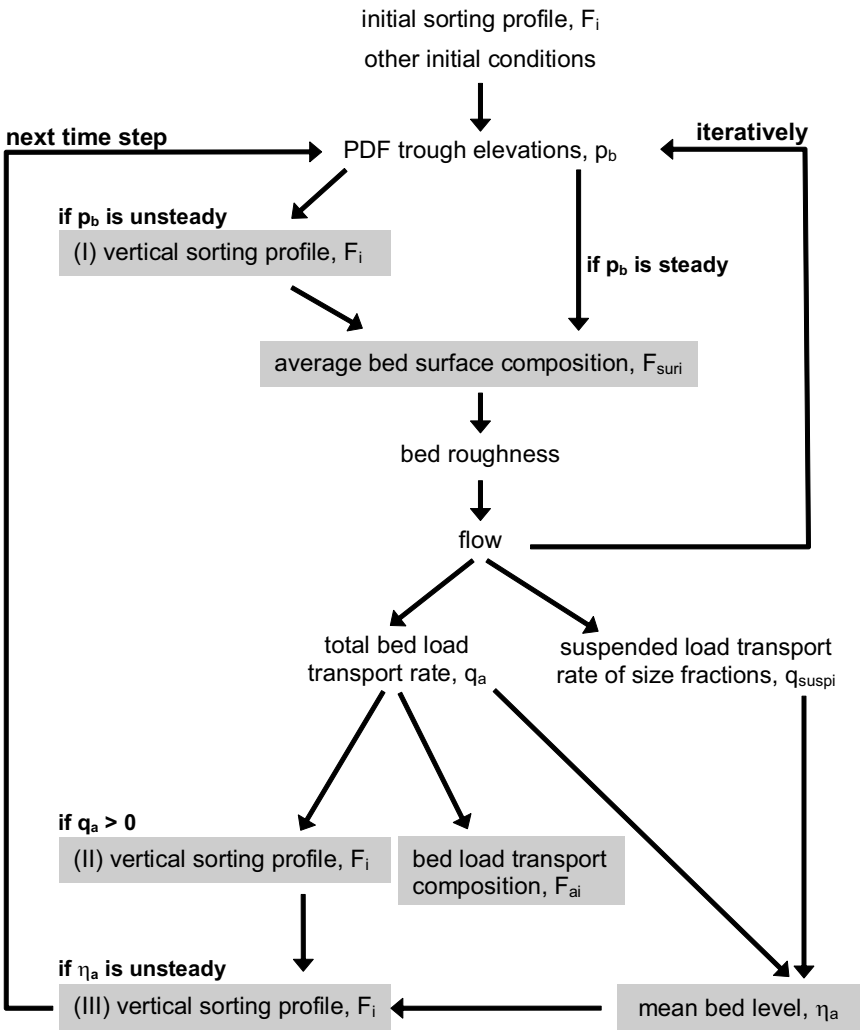

Figure 9.1: Scheme of a morphological model system for non-uniform sediment using the continuum sorting model. Gray boxes represent sub-models that are part of the continuum sorting model. Changes in the vertical sorting profile occur through vertical sediment fluxes accompanying (I) a change in time of the PDF of relative trough elevations; (II) bedform migration, i.e. grain size-selective deposition down a bedform lee face and the variability in trough elevations; (III) net aggradation or degradation.

PDF of relative trough elevations, $\tilde{p}_b$, and the bed load transport composition, $\bar{F}_{ai}$. This strong interaction disallows these components to be modelled independently from one another. This means that we avoid using a sub-model for the composition of the bed load transport, $\bar{F}_{ai}$, which generally is one of the sources of uncertainty in morphological model systems for non-uniform sediment (also see Section 9.4.4). Calibration and verification of such sub-models under flood conditions is rarely possible, since it is hard or even impossible to take samples of the transported sediment during a flood event.

In the previous chapters, *measured* parameters for the PDF of relative trough elevations, the bed shear stress, and the bed load transport rate were used as input to the continuum sorting model. Sub-models for the PDF of relative trough elevations, the bed roughness, the flow, and the bed load transport rate were therefore not required in the present study. Section 9.4 will address the various sub-models in a morphological model system including the continuum sorting model: the PDF of trough elevations (Section 9.4.1), the average bed surface composition (Section 9.4.2), the bed roughness (Section 9.4.3), the total bed load transport rate (Section 9.4.4), and suspended load transport (Section 9.4.5).

First, we will discuss when we should apply either the equilibrium sorting model or the sorting evolution model (Section 9.2) and how vertical sediment fluxes through net aggradation or degradation are included (Section 9.3).

9.2 Equilibrium sorting model or sorting evolution model

Under the constraint of only steady quantities, the continuum sorting model has been reduced to an equilibrium sorting model (Chapter 6). This simplification is also based on the assumption that the composition of the net entrainment at a certain elevation of the stoss face is equal to the bed composition at that elevation. The implications of this assumption will be discussed in Section 9.7.2. The equilibrium sorting model comprises two methods for solving the equilibrium sorting profile. The first method, the *bed load transport composition method*, requires the following input parameters:

- the PDF of relative trough elevations
- the volume fraction contents of size fractions in the bed load transport
- the ratio of the average bedform length to the average bedform height

Note that here all parameters concern *the equilibrium stage*. The second method, which is called the *initial sorting profile method*, solves for both the equilibrium sorting profile and the equilibrium volume fraction contents of size fractions in the bed load transport. It requires the following input parameters:

- at the equilibrium stage, the PDF of relative trough elevations
- at the equilibrium stage, the ratio of the average bedform length to the average bedform height
- at time t_0, the vertical sorting profile
- at time t_0, the PDF of relative trough elevations
- at time t_0, the ratio of the average bedform length to the average bedform height

where t_0 denotes the point in time at which the sorting profile is specified. Both methods show that the computed equilibrium sorting profile is affected neither by the total bed load transport rate, nor by the dimensionless step length.

Based on the assumption that the composition of the net entrainment at a certain elevation of the stoss is equal to the bed composition at that elevation, the continuum sorting model has been reduced to a sorting evolution model (Chapter 8). The sorting evolution model computes the time evolution of both *the vertical sorting profile* and the *volume fraction contents of size fractions in the bed load transport* from the following input parameters:

- the initial sorting profile
- the time evolution of the PDF of relative trough elevations
- the time evolution of the total bed load transport rate
- the time evolution of the ratio of the average bedform length to the average bedform height

It is important to note that, provided that the computation is continued for a very long time, the sorting evolution model yields the same results from the same data as the equilibrium sorting model (i.e. the initial sorting profile method). There seems to be a difference in input data though, as the sorting evolution model requires input on the total bed load transport rate. Yet, this quantity only affects the time scale of the process and not the final equilibrium sorting profile and bed load transport composition.

As addressed in the discussion on time scales in Section 5.5, the equilibrium approach may be applied in morphological models instantaneously, provided that the time scale of large-scale morphological changes , T_m, is much larger than both the time scale of vertical sorting, T_f, and the one of vertical dune dimensions, T_p. For a visual representation of the different time scales, reference is made to Figure 5.14. The time scales of sorting, T_f, and dune dimensions, T_p, by themselves, should be larger than the time scale of dune migration, T_c. This is expressed by (5.101):

$$T_m \gg \max\{T_p, T_f\} \qquad \min\{T_p, T_f\} \gg T_c$$

These constraints may be satisfied in situations with large-scale aggradation or degradation, such as long-term bed degradation after a river bend cut-off or long-term aggradation or degradation due to river training works. For instance, the equilibrium approach may be applied if the time scales are of the following orders of magnitudes:

$$\begin{aligned} T_c &\simeq 5 \text{ days} \\ T_p, T_f &\simeq 50 \text{ days} \simeq 2 \text{ months} \\ T_m &\simeq 500 \text{ days} \simeq 2 \text{ years} \end{aligned}$$

which may be realistic for situations with large-scale aggradation or degradation. For situations with local small-scale aggradation or degradation, e.g., in river bends, it will probably be required to account for the time evolution of both the bed surface elevations and the vertical sorting profile when computing changes in morphology. In that case, the sorting evolution model must be applied.

When considering situations *without* net aggradation or degradation, the equilibrium sorting model may be applied if the time scale of sorting, T_f, is much larger than the one of dune dimensions, T_p. It remains to be studied whether the equilibrium sorting model may be applied to situations for which the sorting time scale is of the same order of magnitude as the one of relative bed surface elevations. It is suggested that this question is studied with respect to the case of a slowly rising flood event (without net aggradation or degradation), for which two case-studies will be proposed in Section 9.9.

A study on the applicability ranges of the equilibrium sorting model and the sorting evolution model is strongly recommended. These ranges will be closely related to the ratios of the various time scales involved, in addition to the specific matter of interest.

9.3 Net aggradation or degradation

Divergences in bed load and/or suspended load transport result in net aggradation or degradation of the river bed. In this section, it will be explained how we calculate the net aggradation or degradation of the river bed and the change in the vertical sorting profile through this net aggradation or degradation. The present section addresses item *'(III) vertical sorting profile'* in Figure 9.1.

In order to include net aggradation or degradation in the continuum sorting model, the following assumptions are made:

1. We neglect the interaction among vertical sediment fluxes through (I) a change in time of the PDF of relative trough elevations, (II) bedform migration (i.e. grain size-selective deposition down a bedform lee face and the variability in trough elevations), and (III) net aggradation or degradation (see Figure 9.1). In order words, while net aggradation or degradation occurs, we assume the PDF of bedform trough elevations, $\tilde{p}_b$, to be steady and vertical sorting fluxes through bedform migration negligible.

2. We neglect the interaction between vertical sediment fluxes through divergences in bed load transport and those through suspended load transport.

3. We assume vertical sediment fluxes through net aggradation or degradation to be distributed over bed elevations according to their exposure to the flow.

4. We assume the composition of the vertical sediment fluxes through net aggradation or degradation to be independent of bed surface elevation.

In reality, assumption 4, viz. that the composition of the vertical sediment fluxes through net aggradation or degradation is assumed to be independent of bed surface elevation, is not necessarily true. Further research is required in order to investigate whether this assumption is justified. It is recommended to conduct flume experiments in which net aggradation or degradation occurs in order to obtain data for calibration and verification of the below formulations for sediment fluxes through net aggradation or degradation.

The equations of the Parker-Paola-Leclair framework for sediment continuity, repre-

sented by (5.11), (5.12), and (5.16), now yield

$$c_b \bar{P}_s \frac{\partial \bar{F}_i}{\partial t} + c_b \bar{F}_i \bar{p}_e \frac{\partial \bar{\eta}_a}{\partial t} = \bar{D}_{ei,mor} - \bar{E}_{ei,mor} \tag{9.1}$$

$$c_b \bar{p}_e \frac{\partial \bar{\eta}_a}{\partial t} = \bar{D}_{e,mor} - \bar{E}_{e,mor} \tag{9.2}$$

$$c_b \frac{\partial \bar{\eta}_a}{\partial t} = \bar{D}_{mor} - \bar{E}_{mor} = -\left(\frac{\partial \bar{q}_a}{\partial x} + \frac{\partial \bar{q}_{susp}}{\partial x} \right) \tag{9.3}$$

where

$$\bar{E}_{e,mor} = \sum_i^N \bar{E}_{ei,mor} \qquad \bar{D}_{e,mor} = \sum_i^N \bar{D}_{ei,mor} \tag{9.4}$$

$$\bar{E}_{mor} = \int_{\eta_{mn}}^{\eta_{mx}} \bar{E}_{e,mor}\, dz \qquad \bar{D}_{mor} = \int_{\eta_{mn}}^{\eta_{mx}} \bar{D}_{e,mor}\, dz \tag{9.5}$$

and where $\bar{q}_{susp}$ denotes the volume of suspended load transport per unit width and time excluding pores and averaged over a series of bedforms (also see Section 9.4.5):

$$\bar{q}_{susp} = \sum_i^N \bar{q}_{suspi} \qquad \bar{F}_{suspi} = \frac{\bar{q}_{suspi}}{\bar{q}_{susp}} \tag{9.6}$$

where $\bar{q}_{suspi}$ denotes the volume of suspended load transport of size fraction i per unit width and time, and $\bar{F}_{suspi}$ the volume fraction content of size fraction i in the suspended load transport. Note that (9.3) yields the change in mean bed level. We now assume the vertical sediment fluxes through net aggradation or degradation to be distributed over bed elevations according to their exposure to the flow, whence the bed elevation-specific entrainment and deposition fluxes are given by

$$\bar{D}_{e,mor} - \bar{E}_{e,mor} = -\bar{p}_e \left(\frac{\partial \bar{q}_a}{\partial x} + \frac{\partial \bar{q}_{susp}}{\partial x} \right) \tag{9.7}$$

and the grain size-specific and bed elevation-specific entrainment and deposition fluxes by

$$\bar{D}_{ei,mor} - \bar{E}_{ei,mor} = -\bar{p}_e \left(\frac{\partial \bar{q}_{ai}}{\partial x} + \frac{\partial \bar{q}_{suspi}}{\partial x} \right) \tag{9.8}$$

Combination of (9.1) and (9.8) yields

$$\frac{\partial \bar{F}_i}{\partial t} = -\frac{\bar{p}_e}{\bar{P}_s} \left\{ \frac{1}{c_b} \left(\frac{\partial \bar{q}_{ai}}{\partial x} + \frac{\partial \bar{q}_{suspi}}{\partial x} \right) - \bar{F}_i \frac{\partial \bar{\eta}_a}{\partial t} \right\} \tag{9.9}$$

where the change in mean bed level, $\partial \bar{\eta}_a / \partial t$, can be calculated from (9.3).

Thus, (9.9) allows us to calculate the effect of net aggradation or degradation upon the vertical sorting profile, representing item '*(III) vertical sorting profile*' in Figure 9.1.

9.4 Sub-models in the morphological model system

9.4.1 PDF of trough elevations

For predictive applications of a morphological model system including the continuum sorting model, a sub-model for the PDF of relative trough elevations, $\tilde{p}_b$, is required. So far, such a model remains to be developed.

At first sight, a straightforward way of developing such a model would be to couple it to a model of the average bedform height. Yet, this approach is not that promising, since well-calibrated models for the average bedform height in situations with non-uniform sediment are presently not available.

The PDF of relative trough elevations appears to depend mainly on the vertical sorting profile, $\bar{F}_i$, and a number of flow parameters. In Chapter 4, it was shown that, over a series of bedforms, the variability in trough elevations can be large, even though the bedform shape may seem rather regular. The relation between the PDF of trough elevations and the vertical sorting profile seems a strong one. This is corroborated by one of the conclusions in Chapter 4, viz. that the variability in trough elevations is strongly limited in cases where a distinct coarse bed layer is present below the migrating bedforms. The relation between the PDF of trough elevations and flow parameters is illustrated by the fact that bedform troughs often become deeper with increasing flow rate. Another effect of an increasing flow rate is that the bedform trough elevations become more irregular, whence the range of relative trough elevations increases. This continues until conditions are reached in which the bedforms are washed out by the flow (upper-regime plane-bed conditions). A first and qualitative analysis of these phenomena was made by *Leclair and Blom* (2003).

In this respect, the recent study on bedform dimensions for uniform sediment by *Niño et al.* (2002) may be well worth looking at. Their model of (the time-evolution of) bedform height, steepness, and migration speeds is based on a number of simple rules. Upon collision with the bed, saltating grains set bed particles into creeping motion. The transport of the creeping particles is related to the local entrainment rate and a creeping length, the latter of which is comparable to the Einstein step length. The basic instability mechanism in the model is the shielding effect of a locally high bed surface elevation. In the lee of a such a high bed surface elevation, the probability of entrainment is set to zero. This instability mechanism generates zones of net entrainment and deposition, resulting in spatially periodic features (bedforms) that migrate downstream. These ideas might be useful in setting up a model of the PDF of relative trough elevations.

Future research on the controls of the PDF of relative trough elevations is strongly recommended. A number of data sets are suitable for studying this: *Ribberink* (1987), *Wilcock and Southard* (1989), *Klaassen* (1992), *Leclair and Bridge* (2001), and the two sets of experiments discussed in Chapter 4. A small advantage is that in the field it is easier and cheaper to determine trough elevations (from measured bed surface elevation profiles) than the composition of the sediment transport, also during flood events.

9.4.2 Average bed surface composition

Being part of a morphological model system, one of the main quantities a continuum sorting model needs to solve for is (the time evolution of) the average composition of the bed surface, $\bar{F}_{suri}$. Since a model of this quantity was not required in the previous part of this study, it has not been mentioned before. It will be required in a morphological model system, however, since it is used in calculating

- the bed roughness,
- the total rate (and composition) of the bed load transport, $\bar{q}_a$ (and $\bar{F}_{ai}$)
- the grain size-specific suspended load transport rate, $\bar{q}_{suspi}$.

In a morphological model system that includes the Hirano active layer model, these quantities will be predicted using external sub-models. This also holds for a morphological model system that includes the continuum sorting model, with the exception of (the time evolution of) the bed load transport composition, $\bar{F}_{ai}$, which is computed by the continuum sorting model, itself (Section 9.1).

In a morphological model system that includes the Hirano active layer model, the composition of the bed surface, $\bar{F}_{suri}$, is equal to the composition of the active layer, whereas, using the continuum sorting model, the average bed surface composition, $\bar{F}_{suri}$, is calculated from

$$\bar{F}_{suri} = \int_{\eta_{mn}}^{\eta_{mx}} \bar{F}_i \, \bar{p}_e \, dz \tag{9.10}$$

where $\bar{F}_{suri}$ denotes the average volume fraction content of size fraction i at the bed surface, weighed over all bed elevations exposed to the flow.

9.4.3 Bed roughness

The present results indicate that the bed roughness is intimately connected to the average bed surface composition and the PDF of relative trough elevations. The part of the bed roughness that is attributed to the grains, i.e. the skin friction, is obviously

closely related to some measure(s) of the composition of the bed surface, e.g., the average bed surface composition, $\bar{F}_{suri}$. The part of the bed roughness that is attributed to the bedforms, i.e. the form drag, seems to be closely related to the PDF of relative trough elevations, which characterises the shape and irregularity of the bedforms.

When using a morphological model system that includes the continuum sorting model, it is advised to use a formulation for the bed roughness that indeed depends on the composition of the bed surface and the PDF of trough elevations. Future research on these relations is strongly recommended.

9.4.4 Total bed load transport rate

An advantage of applying the continuum sorting model is that the composition of the bed load transport is computed by the continuum sorting model itself (also see Section 9.1). Therefore, we need not predict the composition of the bed load transport using a sediment transport model for non-uniform sediment. This notwithstanding, a sub-model for the *total* bed load transport rate is required in case the sorting evolution model is used. Calculating the bed load transport rate usually requires information on the skin friction, some flow parameter, e.g., the Shields parameter, and the average bed surface composition.

Van der Scheer et al. (2002) have evaluated the performance of a number of sediment transport models for non-uniform sediment, by comparing the computed rate and composition of the sediment transport to measured data from flume experiments. The study demonstrates that predictions differ greatly between the various sediment transport models, which indicates the large uncertainties accompanying predictions of sediment transport. The sediment transport models by *Wu et al.* (2000) and *Wilcock and Crowe* (2003) showed the best results in reproducing the rate and composition of the transported sediment. It was demonstrated that computations based on the average composition of the bed surface show much better results than ones based on the composition of the substrate. This is not surprising, considering that the sediment at the bed surface is exposed to the flow, interacts with the flow, and is subject to entrainment. Nearly all sediment transport models appeared to suffer from bad predictions close to conditions of incipient motion. The *Wilcock and Crowe* model showed reasonable results within this range.

It needs to be remarked that *Van der Scheer et al.* (2002) did not test stochastic sediment transport models for non-uniform sediment (e.g., *Bridge and Bennett*, 1992; *Kleinhans and Van Rijn*, 2002), which may well be able to reduce uncertainties in predictions close to conditions of incipient motion. A comparative study is recom-

mended. Another point of interest is that in validating the models *Van der Scheer et al.* only used data from flume experiments. Including data from field experiments would probably influence the results of the study.

For bedform-dominated conditions, the author suggests that the following method might reduce uncertainties accompanying predictions of the *total* bed load transport rate. It seems to be possible to found such predictions on a probability distribution of migration speeds of individual bedforms. This PDF of bedform migration speeds then needs to be coupled to the geometrical properties of those bedforms, which are represented by the previously described PDF of trough elevations and the relation between the relative trough elevation and the bedform height. Using the simple wave approach described in Section 2.1, the method would result in a new type of stochastic model for predicting the total bed load transport rate. The model would be probabilistic in terms of the bedform migration speed, whereas more common stochastic sediment transport models are probabilistic in terms of the Shields stress. In order to use this method in predictive applications, a model for the PDF of bedform migration speeds needs to be derived. In experiments, distributions of migration speeds can be determined from time series of measured bed surface elevation profiles. Further research on this subject matter may be worthwhile.

9.4.5 Suspended load transport

The present version of the continuum sorting model is aimed at bed load transport processes. Yet, a relatively simple way to incorporate suspended load transport in the continuum sorting model is to

1. calculate the composition of the bed surface averaged over a large number of bedforms, $\bar{F}_{suri}$, using (9.10);

2. neglect the interaction between vertical sediment fluxes through bed load transport and suspended load transport;

3. use a model for predicting the grain size-specific suspended load transport, $\bar{q}_{suspi}$, from the average bed surface composition, $\bar{F}_{suri}$, and flow parameters:

$$\bar{q}_{suspi} = f_{\bar{q}_{susp}}(\bar{F}_{suri}, \text{flow parameters}) \tag{9.11}$$

   where $f_{\bar{q}_{susp}}$ represents the model for suspended load transport of non-uniform sediment.

4. assume net aggradation or degradation through divergences in the suspended load transport to be distributed over bed elevations according to their exposure

to the flow and the composition of the sediment fluxes to be independent of bed surface elevation (see Section 9.3).

Since the present study is restricted to conditions dominated by bed load transport, the method proposed here has not been tested. Further research on the incorporation of suspended load transport in the continuum sorting model is required.

9.5 Plane-bed conditions

The present formulations for the grain size-specific and elevation-specific entrainment and deposition rates have been derived for rivers wherein the bedforms are characterised by a lee face (ripples or dunes). *Hassan and Church* (1994) remark how in such rivers the reworking or redistribution of sediment is dominated by the migrating bedforms, whereas in gravel bed rivers with an armour layer under lower-regime plane-bed conditions, the reworking is more sporadic and primarily results from local scour and fill.

Formulations for the grain size-specific and elevation-specific entrainment and deposition rates under plane-bed conditions can be derived by following the procedure suggested by *Parker et al.* (2000). This procedure differs from the method in the present study in that it does not consider particle step lengths. Present research by *Parker et al.* (personal communication, 2002), among which are flume experiments, aims at modelling the PDF of bed surface elevations under plane-bed conditions.

9.6 Spatial and vertical discretisation

The present study is aimed at uniform conditions, whence a discussion on the spatial discretisation of the model area has not been required earlier. In this thesis, the horizontal co-ordinate x, varying only over the scale of large numbers of bedforms, has often been left out of the equations.

The spatial discretisation of the model area must be aimed at distinguishing between statistically homogeneous series of bedforms. In reality, however, homogeneity exists only over short distances and time spans. This means that no matter the outcome, the choice for a certain spatial discretisation will probably always be ambiguous. Herein, an appropriate and practicable choice must be made. The choice obviously also depends on the data available.

Although the approach taken on in the present study is a depth-continuous one, its application in a numerical model will require a vertical discretisation over the river

bed. General guidelines for the choice of the vertical grid size cannot be handed, since it depends on the conditions of the specific case-study. Obviously, the vertical grid size must be small relative to the range of bed elevations that are exposed to the flow.

9.7 Reflection upon the continuum sorting model

9.7.1 Sorting mechanisms

The literature survey on vertical sorting fluxes (Chapter 2) and the two sets of experiments (Chapter 4) have indicated that the following mechanisms may produce significant vertical sorting fluxes under conditions in which bedforms (dunes) and bed load transport dominate:

1. grain size-selective deposition down a bedform lee face,
2. variability in bedform trough elevations,
3. partial transport causing relatively immobile coarse sediment to gather below migrating bedforms,
4. winnowing of fines from the bedform trough surface and subsurface,
5. net aggradation or degradation.

In the new continuum sorting model, mechanisms 1, 2, and 5 are included. Mechanism 1 is accounted for through the newly-developed lee sorting function. Although this function yields good results for the experiments considered, further study is required, so as to increase its range of application. Mechanism 2 is included through the newly-developed method to account for the variability in trough elevations, which yields satisfactory results. Still, in order to use the continuum sorting model in predictive applications, a sub-model for the PDF of relative trough elevations needs to be developed. This has been addressed in Section 9.4.1.

Mechanism 3, partial transport, is not adequately incorporated. The reduction of the full continuum sorting model in Chapter 5 to both the equilibrium sorting model and the sorting evolution model is based on the assumption that the composition of the net entrainment at a certain elevation of the stoss face is equal to the bed composition at that elevation. This implies that size-selective entrainment over the stoss face does not occur. In the model, particles that are present on the stoss face but too coarse to be transported are not allowed to settle down as the bedform migrates. Instead, these particles are transported over the bedform crest and are deposited at the lower

elevations of the active bed through the mechanism of size-selective deposition over the lee face.

Mechanism 4, the winnowing of fines from the trough surface and subsurface, is not included in the model. Comparison of the model computations with the measurements (Chapters 7 and 8) has shown that the continuum sorting model does not adequately describe the formation of a coarse bed layer underneath migrating bedforms. The author attributes this to the mechanisms of winnowing of fines and the settlement of immobile coarse particles being neglected in the model. It is recommended to include these mechanisms in a later version of the model.

9.7.2 Implications of main assumptions

The derivation of the continuum sorting model and its reduced versions, i.e. the equilibrium sorting model and the sorting evolution model, is based on a large number of assumptions. The present section lists the most important ones:

1. Changes in the vertical sorting profile occur through vertical sediment fluxes accompanying (I) a change in time of the PDF of relative trough elevations; (II) bedform migration, i.e. grain size-selective deposition down a bedform lee face and the variability in trough elevations; (III) net aggradation or degradation (see Section 9.1). It is assumed that these three types of vertical sediment fluxes do not interact with one another.

2. A series of irregular bedforms is considered as a series of triangular bedforms with varying trough elevations.

3. The sorting profiles within individual bedforms are assumed to be identical to the sorting profile averaged over the series of bedforms.

4. Sediment fluxes through the winnowing of fines and the settlement of immobile coarse particles are neglected.

5. The composition of the net entrainment through bedform migration at a certain elevation of the stoss face is assumed to be equal to the bed composition at that elevation. (This assumption only applies to both reduced models.)

6. The composition of the net entrainment through a change in time of the PDF of relative trough elevations at a certain elevation is assumed to be equal to the bed composition at that elevation, while the composition of the net deposition fluxes are assumed to be equal to the average composition of the total net entrainment flux.

7. It is assumed that there is no interaction between sediment fluxes accompanying net aggradation or degradation through either a divergence in bed load transport or a divergence in suspended load transport.

8. The composition of vertical sediment fluxes through net aggradation or degradation is assumed to be independent of bed surface elevation.

9. The sediment deposited at a specific elevation of the active bed is assumed to be immediately mixed with all sediment in the series of bedforms at that elevation.

10. The bed porosity is assumed to be steady and uniform over all bed elevations.

The implications of these assumptions are discussed below.

Ad 1 Different types of vertical sediment fluxes
The possible interaction between these three types of sediment fluxes is not well understood. Further research is required to assess whether this assumption is fully justified.

Ad 2 Triangular bedforms with varying trough elevations
Representing a series of irregular bedforms as a series of triangular bedforms with varying trough elevation is not expected to have a significant negative effect upon the results, provided that the imposed PDF of relative trough elevations is accurately described. It is believed that the assumption of each lee face having the same uniform slope is not far from reality, although in reality the slope reduces somewhat towards the lower boundary of the lee face. This is due to the return flow that accompanies the wake overlying the trough area, which makes sediment move towards the upstream lee face. The assumption of each stoss face having a uniform slope may be more crude. Still, large negative effects are not expected, even though the uppermost elevations of the active bed do not seem to be described very adequately. This shortcoming arises from the simple relation between the bedform height and the relative trough elevation for individual bedforms, which is expressed by (5.84). Yet, the uppermost elevations do not influence the model results very much, since these elevations are barely exposed to the flow.

Ad 3 Sorting within individual bedforms
The sorting profiles within individual bedforms are assumed to be identical to the sorting profile averaged over the series of bedforms (also see Section 5.3.2). In other words, we do not distinguish sorting profiles within individual bedforms. This assumption would not be justified in case dimensions of individual bedforms remain steady. Namely, in that case all sediment within an individual migrating bedform

would be taken along with it. The assumption appears to be justified by Figure 2.6, which illustrates the longevity of the deepest troughs. The figure shows that their depths rapidly change, i.e. a deep trough remains deep only over a short distance.

Ad 4 Winnowing of fines and partial transport
In the continuum sorting model, the grain size-selective sorting down the avalanche lee face is the dominant sorting mechanism. Sorting processes through the winnowing of fines and the settlement of immobile coarse particles are not included in the model. Section 9.7.1 has addressed this topic.

Ad 5 Composition of net entrainment flux
In both the equilibrium sorting model and the sorting evolution model, the composition of the net entrainment flux at a certain elevation of the stoss face is assumed to be equal to the bed composition at that elevation. Under this assumption, it has been possible to solve for the equilibrium sorting profile or the time evolution of the vertical sorting profile. Clearly, this assumption prevents armouring over the stoss face from happening completely, whereas measured sorting profiles do show a coarse top layer. This coarse top layer appears to originate from (1) the presence of a thin mobile armour layer on the stoss face and (2) the deposition of sediment that was being transported over the bedform until the flow was turned off. It seems that, in reality, the net entrainment flux at some elevation of the stoss face may be somewhat finer than the average bed composition at that elevation. It has to be studied whether it is desirable and possible to loosen this assumption.

However, if the net entrainment flux at some elevation of the stoss face will be (imposed to be) somewhat finer than the average bed composition at that elevation, one has to be aware of the following. The net entrainment over the stoss face makes the bedforms migrate, and, if the net entrainment flux at a certain bed elevation is imposed to be finer than the bed composition at that elevation, coarse material will be left behind at that elevation. Physically, this is not realistic. In reality, these coarse particles will settle when the dunes migrate as their surrounding finer grains are entrained. Thus, if the above assumption is loosened, the settling of immobile coarse particles must be included in the continuum sorting model.

The new continuum sorting model does not describe the formation of the thin armour layer over a stoss face, so that the computed average composition of the bed surface (Section 9.4.2) may be slightly finer than the measured one. This may affect the computed bed roughness, bed load transport rate, and suspended load transport.

Ad 6 Sediment fluxes through varying PDF trough elevations
A change in time of the PDF of relative trough elevations arises from entrainment or deposition fluxes over the elevations of the bed surface (see Section 8.2). For instance, at the moment that bedform troughs become deeper and crests higher, net entrainment occurs at the elevations of the active bed below the mean bed level, and net deposition occurs at elevations above the mean bed level. At an elevation where net entrainment occurs, the composition of the entrained material is assumed to be equal to the composition at that elevation. At an elevation where net deposition occurs, the composition of the deposited material is assumed to be equal to the average composition of the total net entrainment flux. These assumptions are very practical in the application of the continuum sorting model. In reality, grain size-selective processes play a role in these processes. Further research is required in order to increase our understanding of the effects of these assumptions on the model computations.

Ad 7 and 8 Net aggradation or degradation
In Section 9.3 a method has been proposed in order to include vertical sediment fluxes through net aggradation or degradation in the continuum sorting model. In the present study, the proposed method has not been tested. Further research is required in order to investigate whether it is justified to assume that the composition of the sediment fluxes through net aggradation or degradation is independent of bed surface elevation. In reality, grain size-selective processes surely play a role. It is recommended to conduct flume experiments wherein net aggradation or degradation occurs in order to obtain data for calibration, verification, and possible adaptation of the present formulations.

Ad 9 Deposited material immediately mixed
As mentioned above, it is assumed that all individual bedforms in one series of bedforms are characterised by the same representative vertical sorting profile relative to some arbitrary level. Sediment fluxes onto or from a specific elevation of a certain individual bedform thus directly affect this representative sorting profile. This implies that sediment deposited at some elevation of the active bed is immediately mixed with all sediment in the series of bedforms at that elevation. This causes the computed time scale of vertical sorting to be somewhat smaller than in reality. Further study is required to increase our understanding of the effect of this assumption on the sorting time scale.

Ad 10 Porosity steady and uniform
In the present study the porosity is assumed to be steady and uniform over all bed elevations. Note that this is contradictory to what is stated in Section 4.3.4 on the difference in the bed composition at the average trough elevation between samples

taken at bedform crests and in troughs (Figure 4.16). The turbulent fluctuations in the trough areas cause the fines to be winnowed from the coarse bed layer located below migrating bedforms. This mechanism results in an increase of the porosity of the coarse layer in the trough areas. This notwithstanding, the author believes that including variations in porosity over bed elevations may not be necessary for ultimately incorporating the mechanism of the winnowing of fines in the continuum sorting model.

9.8 Reflection upon the Hirano and Ribberink bed layer models

Chapter 3 has presented an overview of existing sediment continuity models. It was explained that the Hirano active layer model suffers from a number of shortcomings. The most important one is the neglect of vertical sediment fluxes other than through net aggradation or degradation. The assumption that the bed material interacting with the flow can be represented by a distinct surface layer, as proposed by *Hirano* (1971), is too limited to adequately account for sorting processes acting in the river bed. *Ribberink* (1987) recognised the influence of relatively deep bed elevations interacting with the flow and being subject to entrainment and deposition less frequently than higher ones. In order to account for the exchange of sediment through occasional deep bedform troughs, *Ribberink* introduced an additional bed layer, i.e. the exchange layer, below the active layer together with a term describing the sediment exchange between the active layer and the exchange layer (Section 3.2.3). The exchange layer represents the elevations exposed to the flow only occasionally, whence the adaptation time scale of its composition is much longer than the one of the active layer. Still, the introduction of the exchange layer does not completely solve another shortcoming of existing bed layer models, viz. that in certain situations the set of equations becomes elliptic in parts of the space-time domain. This means that solving the set of equations would require future time-boundaries, which is physically unrealistic. A limitation of the present version of the Ribberink two-layer model is that the formulation for the sediment exchange between the active layer and the exchange layer is only applicable to mixtures composed of two grain size fractions.

After the qualitative comparison in Chapter 3, the present section presents a quantitative comparison of the predictive abilities of the Hirano active layer model, the Ribberink two-layer model, and the new continuum sorting model. The models are applied to experiments B2 and A2, which have also been used for the analysis of the sorting evolution model in Chapter 8. The experiments have been described extensively in Chapter 4. For a short description of the experiments, reference is made to Section 8.4.1.

Since the experiments are characterised by conditions without net aggradation or degradation, we can reduce the equations of the Hirano active layer model and the Ribberink two-layer model. Eq. (3.2) of the Hirano model now yields

$$c_b \frac{\partial F_{mi}\,\delta}{\partial t} + c_b\, F_{Ii}\, \frac{\partial \eta_I}{\partial t} = 0 \tag{9.12}$$

where the volume fraction content of size fraction i at the interface between the active layer and the exchange layer, F_{Ii} is given by

$$F_{Ii} = \begin{cases} F_{mi} & \text{rising interface} \\ F_{oi} & \text{lowering interface} \end{cases}$$

The second term in (9.12) cannot be neglected, since we include the effects of changes in time of the average bedform height and thus of the active layer thickness. This implies that also the level of the interface, η_I, varies in time:

$$\eta_I(t) = \bar{\eta}_a - \delta(t) \tag{9.13}$$

For this reason, the terms 'aggradation' and 'degradation' in the expression for F_{Ii} have been rephrased to 'rising interface' and 'lowering interface'.

In the computations presented in this section, we divide the substrate into multiple layers, as was proposed by *Duizendstra and Flokstra* (1998a,b) and *Sloff et al.* (2001) (also see Section 3.2.2). In this way, the model system registers and remembers the composition of previously deposited sediment, which is important in situations when degradation follows aggradation. In the present case, in which no net aggradation or degradation occurs, dividing the bed into multiple layers is important for another reason. The initial average bedform height, and thus the thickness of the active layer, is very small. This is due to the small dunes present at the initial stage of the experiment. Would we not impose the (large) variation of the initial sorting profile over depth, computations would yield worse results.

Using (9.12), we can solve for the time evolution of the composition of the active layer, F_{mi}, from the given time evolution of the active layer thickness, δ. Because of the registration over a large number of bed elevations, we not only solve for the time evolution of the composition of the active layer, but for the time evolution of the complete sorting profile, $\bar{F}_i$.

Section 3.2.3 explained the basic equations of the Ribberink two-layer model. For

cases without net aggradation or degradation, these equations can be reduced to

$$\frac{\partial F_{mi}\delta}{\partial t} + F_{Ii}\frac{\partial \eta_I}{\partial t} = \psi_i \tag{9.14}$$

$$\frac{\partial F_{ei}\delta_e}{\partial t} + F_{IIi}\frac{\partial \eta_{II}}{\partial t} - F_{Ii}\frac{\partial \eta_I}{\partial t} = -\psi_i \tag{9.15}$$

where

$$F_{Ii} = \begin{cases} F_{mi} & \text{rising interface I} \\ F_{ei} & \text{lowering interface I} \end{cases}$$

$$F_{IIi} = \begin{cases} F_{ei} & \text{rising interface II} \\ F_{oi} & \text{lowering interface II} \end{cases}$$

and where the sediment exchange term, ψ_i, is given by

$$\psi_i = E_{ti} - D_{ti} = \gamma_t \frac{q_a}{\lambda_a}\left(F_{ei} - F_{miD}\right)$$

Using these equations, we can solve for the time evolution of both the composition of the active layer, F_{mi}, and the composition of the exchange layer, F_{ei}, from the given time evolution of both the active layer thickness, δ, and the exchange layer thickness, δ_e. Again, because of the registration of the bed composition for multiple bed elevations, we can compute the time evolution of the complete sorting profile, $\bar{F}_i$.

Following the definitions in Section 3.2.4, the active layer thickness and the exchange layer thickness are computed from the average dune height:

$$\delta(t) = 0.5\,\Delta_a(t)$$
$$\delta_e(t) = 1.22\,\delta(t)$$

Herein, the time evolution of the average dune height is accounted for. Transitions in the average dune height occur at the same points in time as the PDF of trough elevations was assumed to change in time (see Figures 8.3 and 8.4).

Since the sediment mixtures used in experiments B2 and A2 were not bi-modal but tri-modal, the description of sediment exchange between the active layer and the exchange layer in the Ribberink two-layer model first needs to be adapted. *Ribberink* (1987) supposed the sediment deposited from the active layer into the exchange layer to be somewhat coarser than the average composition of the active layer, because of the downward coarsening trend within the bedforms. For a well-sorted bi-modal

mixture, *Ribberink* found that the volume fraction content of the *finest* fraction deposited from the active layer into the exchange layer is about 70% of that in the active layer:

$$F_{m1D} = 0.7\, F_{m1}$$
$$F_{m2D} = 1 - F_{m1D}$$

which is given by (3.8) and (3.9). The subscripts 1 and 2 indicate the fine and coarse size fractions, respectively. Now, following (3.8) for the finest size fraction, for a trimodal mixture the formulation for the sediment exchange is adapted to

$$F_{m1D} = 0.7\, F_{m1} \tag{9.16}$$
$$F_{m2D} = F_{m2} \tag{9.17}$$
$$F_{m3D} = 1 - F_{m1D} - F_{m2D} \tag{9.18}$$

Note that these equations comprise only an ad-hoc formulation for the sediment deposited from the active layer into the exchange layer. The formulation has not been calibrated.

The initial sorting profile needs to be imposed to the model computations. For experiments B2 and A2, the initial sorting profile is identical to the final sorting profile of experiments A1 and B1, respectively (also see Chapter 8).

The time evolution of the sorting profile as computed by the Hirano active layer model, the Ribberink two-layer model, and the sorting evolution model is now compared to measured data from the experiments. The results of these computations are presented in Figures 9.2 and 9.3. Appendix G shows the time evolution of the sorting profile as computed using the Hirano active layer model and the Ribberink two-layer model in more detail (see Figures G.1 through G.4).

The left column of plots in Figure 9.2 shows the measured vertical sorting profiles in experiment B2: (a) its initial stage (phase B1E), (b) the non-equilibrium stage (phase B2N), and (c) the equilibrium stage (phase B2E). These measured sorting profiles have been determined by averaging over about 15 core samples taken in the specific phase of the experiment. The solid line represents the probability distribution of bed surface elevations in the corresponding phase of the experiment. We can see how the medium and the coarse size fraction, initially located in the upper parts of the bed, become redistributed over a large range of bed elevations.

The second column of plots in Figure 9.2 shows the time evolution of sorting in experiment B2 as computed by the Hirano active layer model. In the initial phase,

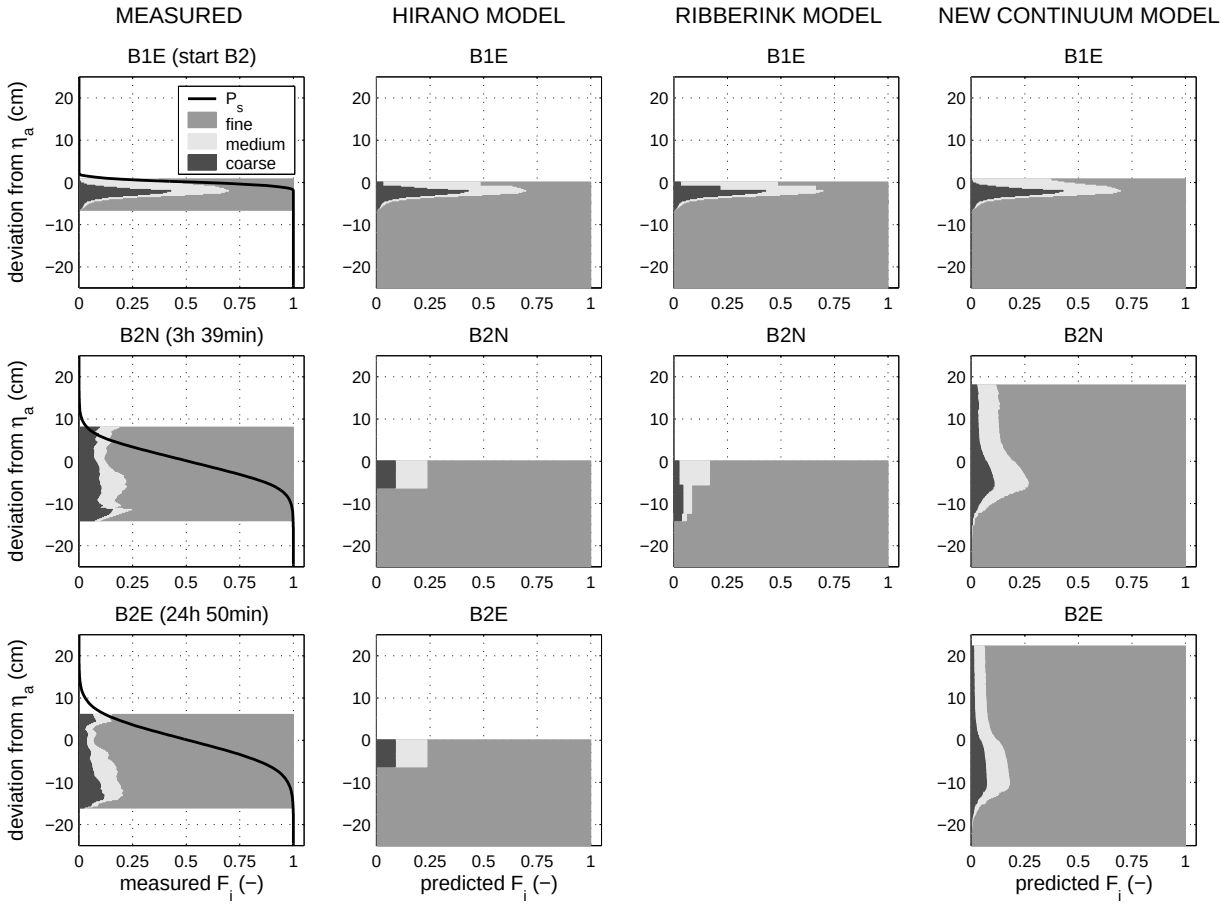

Figure 9.2: The measured time evolution of vertical sorting in experiment B2, and the vertical sorting as computed by the Hirano active layer model, the Ribberink two-layer model, and the sorting evolution model.

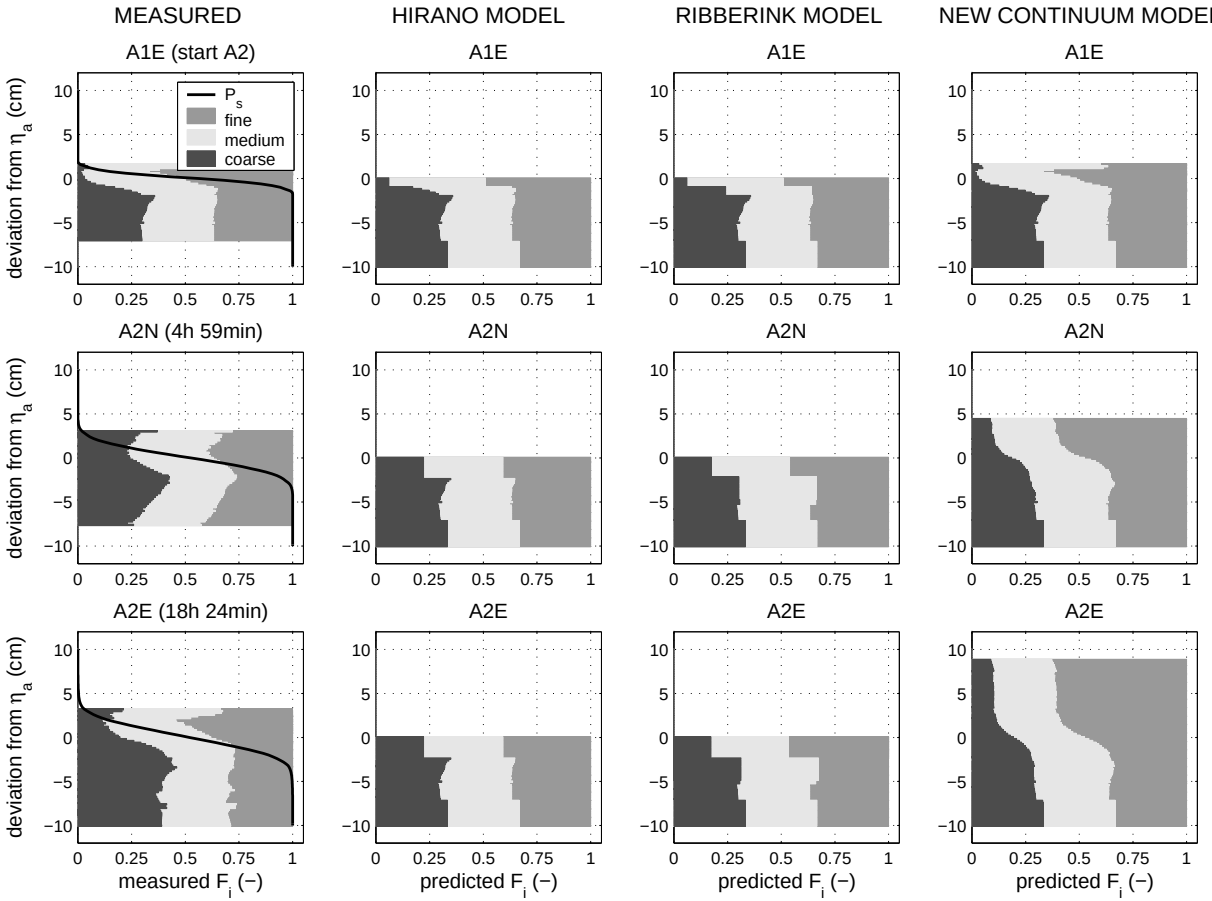

Figure 9.3: The measured time evolution of vertical sorting in experiment A2, and the vertical sorting as computed by the Hirano active layer model, the Ribberink two-layer model, and the sorting evolution model.

the active layer thickness is very small (look closely to see the very thin homogeneous active layer in the upper plot of the second column), which is due to the small dunes present in the initial stage of the experiment. After the start of experiment B2, the imposed average bedform height increases quickly, whence the active layer thickness increases quickly. This increase in active layer thickness can be observed in Figure G.1 in more detail, as well as the time evolution of the composition of the active layer. It is clearly shown that the Hirano active layer model is not able to reproduce the time evolution of the sorting profile in experiment B2. This is not surprising considering the neglect of vertical sorting fluxes in the model.

The third column of plots in Figure 9.2 shows the time evolution of sorting in experiment B2 as computed by the Ribberink two-layer model. In the initial phase, the active layer thickness and exchange layer thickness are very small (look closely at the upper plot of the third column), due to the small dunes present in the initial stage of the experiment. With respect to the range of elevations of the active bed, the model shows better results than the Hirano model. However, for the conditions of experiment B2 the two-layer model appears to behave problematically: it does not guarantee continuity of grain size fractions. This can be understood from the following. The present formulation for the composition of the deposition flux from the active layer to the exchange layer, F_{miD}, given by (9.16) through (9.18), causes the small amount of the coarse size fraction in the active layer to be deposited to the exchange layer. This is due to the fact that the proportion of the fine size fraction in the deposition flux from the active layer to the exchange layer is imposed to be equal to 70% of the proportion of this size fraction in the active layer, which implies that the remaining 30% in this deposition flux is composed of the medium and coarse size fractions. Since experiment B2 is characterised by a large amount of the finest size fraction, this procedure causes the coarse fraction in the active layer to become exhausted. Even when the active layer no longer consists of coarse sediment, (9.18) still imposes that some percentage of the deposition flux from the active layer to the exchange layer is composed of the coarse fraction. This is impossible and 'creates' sediment of the coarse fraction. Although the formulation for the sediment exchange of a mixture of three grain size fractions is only an ad-hoc formulation, the problem can occur for a mixture of two grain size fractions, as well.

The fourth column of plots in Figure 9.2 shows the time evolution of sorting in experiment B2 as computed by the sorting evolution model. Since these results have been extensively discussed in Chapter 8, this will not be done again. Reference is made to Figures 8.5 and 8.6 and the accompanying text.

Figure 9.3 shows the results of the computations for experiment A2. Like for B2, the range of elevations covered by the Hirano active layer is much smaller than the measured range of elevations exposed to the flow. Again, the Ribberink model shows much better results in predicting the range of elevations of the active bed. The Ribberink two-layer model performs in a better way than for B2, since the coarse size fraction in the active layer does not become exhausted.

It can be concluded that the sorting evolution model shows better results with respect to the computed time evolution of the vertical sorting profile than the active layer model and the two-layer model. Based on the present study, it seems to be possible to improve the formulation for the sediment exchange between the active layer and the exchange layer in the Ribberink two-layer model. The author would suggest relating the volume fraction contents of size fractions deposited from the active layer into the exchange layer to both the geometric mean grain size and the arithmetic standard deviation of the active layer material. This would correspond with the formulation for the grain size-selective deposition down the bedform lee face in Section 5.2.5. An improved formulation could be derived by integrating the formulations for the vertical sorting fluxes as derived in the present study over certain ranges of bed elevations.

Yet, an important problem of this procedure is that the determination of the elevations of the interfaces (1) between the active layer and the exchange layer, and (2) between the exchange layer and the substrate are arbitrary. In other words, no matter how the active layer thickness and the exchange layer thickness are defined, these definitions will always be ambiguous. From a physical point of view, there is no support for the definition of discrete bed layers, as can be seen from the measured sorting profiles in Figures 9.2 and 9.3. For instance, the variation of the bed composition over bed elevations is continuous and does not show sudden transitions. It is therefore recommended to eventually leave the concept of discrete bed layers and step over to depth-continuous models. However, from an engineering point of view, it may be useful to improve the formulation for the sediment exchange between the active layer and the exchange layer in the Ribberink two-layer model.

9.9 Suggested case-studies

In the present section, a number of interesting case-studies are proposed. These case-studies have not been carried out within the present study, since testing the new continuum sorting model as part of a morphological model system was beyond the scope of this thesis.

Case-study 1 - Flume experiments with tracer particles
It would be very useful to study the horizontal and vertical dispersion of tracer particles from presently available and new flume experiments. Since grain size-selective processes do not play a role, experiments with tracer particles offer excellent possibilities for an elementary study of vertical sediment fluxes, further validation of the continuum sorting model, and improvements to the description of the vertical sediment fluxes.

Case-study 2 - Field experiments with tracer particles
In addition, application of the sorting evolution model to field experiments with tracers such as those conducted by *Ferguson et al.* (2002) would be interesting. This would enable a comparison of the computed horizontal dispersion of tracers and the computed time-evolution of the sorting profile towards a uniform profile to measured data.

Case-study 3 - Sorting during a flood event in the Waal river, applying the equilibrium sorting model
The equilibrium sorting model consists of two methods to solve for the equilibrium sorting profile. One is based on a given vertical sorting profile at a previous time, with its accompanying PDF of relative trough elevations. It would very interesting to asses whether it is allowed to apply this method to a slowly rising flood event. Divergences in grain size-selective transport during the flood event are simply assumed to be negligible, so that net aggradation or degradation does not occur. The order of magnitude of the various time scales involved need to be compared. The time evolution of the PDF of relative trough elevations needs to be known and it is supposed to show a slowly increasing range of active bed elevations, which later slowly decreases. Applying the equilibrium sorting model implies that the vertical sorting profile adapts to its equilibrium profile as soon as the imposed PDF of relative trough elevations changes in time. The time evolution of both the vertical sorting profile and composition of the bed load transport are computed and compared with measured data. The time evolution of the computed vertical sorting profile will show the formation of a coarse bed layer over the lowest elevations reached by the flow. When in the lowering stage of the flood event the dunes become smaller, the coarse layer remains at its deep elevation. This process is known to occur in the river Waal (*Kleinhans*, 2002) and is also described in Sections 4.1 and 4.5.

Case-study 4 - Sorting during a flood event in the Waal river, applying the sorting evolution model
This case-study concerns the same case as Case-study 3, but now the adaptation time scale of sorting is taken into account. Consequently, the vertical sorting profile does

not immediately adapt to its equilibrium profile. A comparison between the present case-study and Case-study 3 will yield valuable results on whether the equilibrium sorting model may be applied to calculating the time evolution of sorting for the case of a slowly rising flood event.

Case-study 5 - Net aggradation in a flume experiment
The transition between the experiments E8 and E9 from (*Ribberink*, 1987) offers an interesting possibility for comparing the results of morphological model systems including (1) the Hirano one layer model, (2) the Ribberink two-layer model, or (3) the continuum sorting model to measured data from flume experiments. In this experiment the sediment fed to the flume was coarsened, resulting in a coarsening of the bed surface and slow aggradation. The case-study would yield valuable results on

- whether vertical sediment fluxes through bedform migration, changing PDF of relative trough elevations, and net aggradation or degradation may be decoupled;
- whether the method for including vertical sediment fluxes through net aggradation (Section 9.3) is adequate;
- whether formulations for the sorting time scale in the continuum sorting model and the time scale of the exchange layer composition in the Ribberink two-layer model are satisfactory.

Case-study 6 - Theoretical case of downstream fining
Downstream fining through selective transport is related to a (gradual or sudden) decrease in bed slope in downstream direction of the river (e.g., *Deigaard*, 1983; *Ferguson et al.*, 1996). The average flow velocity and bed shear stress then decrease in downstream direction, as well. The sediment characterised by the highest critical bed shear stress (usually the coarsest sediment) is the first to fail being transported down the river. Next, sediment somewhat less coarse, and so on. This results in the well-known pattern of downstream fining that is characteristic for many rivers. The mechanism of downstream fining is accompanied by a slow aggradation of the river bed. Nonetheless, for a specific concave bed level profile, we may say that the longitudinal sorting profile reaches a state of quasi-equilibrium, since the time scale of aggradation is much larger than the time scale of longitudinal sorting. A theoretical case of downstream fining, e.g., by imposing a concave initial bed level profile, may serve as a basis for a comparative study between morphological model systems including the Hirano active layer model, the Ribberink two-layer model, or the new continuum sorting model. It would yield information on the time scale of the adaptation of the longitudinal sorting profile.

Case-study 7 - Downstream fining in the field
A field case of downstream fining, e.g., by imposing the measured concave bed level profile and an initial bed composed of uniform sediment, would enable a comparison of the computed quasi-equilibrium downstream fining profile with measured data.

Case-study 8 - Vertical and lateral sorting near Pannerdensche Kop
The vertical sorting in the Rhine branches near Pannerdensche Kop has been measured, documented, and analysed in great detail (*Gruijters et al.*, 2001a,b; *Kleinhans*, 2002; *Frings and Kleinhans*, 2002). *Frings and Kleinhans* (2002) discuss the vertical and lateral sorting in a number of river bends near Pannerdensche Kop. This river reach was modelled by *Bernabè* (2002) using the two-dimensional morphological model system Delft3D (which includes the Hirano active layer model in addition to a formulation for the grain size-selective lateral transport in river bends). However, a two-dimensional morphological model system including the Hirano active layer model is capable of describing neither the vertical sorting within the migrating dunes, nor the influence of the vertical sorting profile upon the lateral grain size-selective transport in river bends. Application of the continuum sorting model may well lead to better results.

Chapter 10

Conclusions and future research

The main objective of the present study was to modify existing sediment continuity models for rivers with non-uniform sediment, so as to account for vertical sorting fluxes acting in the river bed (Section 1.2). The study was restricted to conditions dominated by bedforms (dunes) and bed load transport. Moreover, the study was limited to investigating vertical sorting processes in situations without net aggradation or degradation. The answers to the following research questions will be summarised in the next sections:

1. Which mechanisms affect the vertical sorting profile under conditions with bedforms and partial transport? Which of these mechanisms need to be incorporated in a new sediment continuity model? (Section 10.1.1)

2. What types of sediment continuity models for non-uniform sediment can we distinguish? What type enables describing the sorting mechanisms in a realistic way? (Section 10.1.2)

3. How can we incorporate the sorting mechanisms in the model? (Section 10.1.3)

4. How well does the new continuum sorting model reproduce the vertical sorting profiles measured in the experiments considered for calibrating and verifying the model? (Section 10.1.4)

5. How can the new continuum sorting model be incorporated in a predictive morphological model system? (Section 10.1.5)

6. How do the present results reflect upon existing bed layer models (e.g., the Hirano active layer model)? (Section 10.1.6)

After that, the author will recommend on topics that require further investigation (Section 10.2).

10.1 Conclusions

10.1.1 Vertical sorting mechanisms

In the present study, two sets of experiments have been conducted in order to investigate grain size-selective transport and vertical sorting under conditions with bedforms and bed load transport. The resulting data will be useful in modelling vertical sorting processes in the river bed and the formation of coarse bed layers.

Three mechanisms dominate the sorting processes within a migrating bedform: the avalanche mechanism at the bedform lee face, partial transport, and the winnowing of fines from the trough surface and subsurface. A migrating bedform is characterised by a downward coarsening trend, which results from the grain size-selective deposition over its lee face. When conditions of partial transport prevail and a significant amount of coarse material does not or barely take part in the transport process, coarse sediment gathers below the migrating bedform, constituting an essentially immobile coarse bed layer that is exposed only in the bedform troughs.

It cannot be concluded from the vertical sorting profile itself whether the lower (coarser) part of a bedform is mobile or essentially immobile. This can only be assessed through analysing (1) the sorting profile in combination with the probability distribution of bed surface elevations, and (2) sorting profiles from core samples taken at the bedform crests, as well as at the troughs.

The winnowing of fines from the trough surface and subsurface is due to the statistics of the turbulent flow in the trough zones of the bedforms. It may cause the trough surface and subsurface to have an increased porosity and to coarsen, more bed material to become available to the transport process, and the coarse layer to subside until a new dynamic equilibrium between entrainment and deposition in the troughs is reached. When a bedform migrates over the trough area, the pores become filled again with finer particles. By taking core samples at bedform crests only, one may overlook the presence of a coarse layer underneath the bedforms.

The experiments point towards a close relation between (the time scale of and the variability in) trough elevations and (the time scale of) the vertical sorting profile. This can easily be understood when considering that, through migration, a bedform redistributes all bed material above its trough elevation. Over a series of bedforms, the variability in trough elevations in space and time can be large. The variability in trough elevations is strongly limited when a distinct coarse layer is present underneath migrating bedforms.

The experiments have shown that vertical sorting fluxes are not bound to situations with net aggradation or degradation. Also the grain size-selective deposition down a bedform lee face and the variability in trough elevations induce vertical sediment sorting. The results indicate that the description of vertical sorting processes in existing sediment continuity models for non-uniform sediment, e.g., the Hirano active layer model, requires modification to account for sorting processes.

10.1.2 Existing sediment continuity models

Four types of sediment continuity models are distinguished. *Burial depth models* describe the time evolution of the movement of (tracer) particles and their burial into the bed. Strictly speaking, they may not be called sediment continuity models, since they do not model the interaction among divergences in sediment transport rate, net aggradation or degradation, and the vertical sorting profile. *Bed layer models* are sediment continuity models in which the bed is divided into a certain number of discrete and homogeneous bed layers. *Grain-scale models* are defined as sediment continuity models that consider sediment entrainment and deposition at the scale of grains, whereas the other types consider processes at a scale of a large number of bedforms. *Depth-continuous models* do not distinguish discrete bed layers. They include a probability density function of bed surface elevations, so as to account for the likelihood of a bed elevation being exposed to the flow. Since the objective of this study is to improve the description of the interaction among divergences in the sediment transport rate, net aggradation or degradation, and the vertical sorting profile, to be applied in large-scale morphological model systems, only the bed layer models and the depth-continuous models are of immediate interest here.

The Hirano active layer model and other bed layer models appear too limited to adequately describe vertical sorting fluxes in the bed. In most bed layer models, vertical sediment fluxes occur through net aggradation or degradation only, whereas flume experiments have shown that this is not true. Another problem of sediment continuity models with discrete bed layers is that in certain situations, the set of equations becomes elliptic in parts of the space-time domain. Solving the set of equations then requires future time-boundaries, which is physically unrealistic. A final problem is that the definition of the thickness of the bed layers remains rather arbitrary. From a physical point of view, it is not straightforward to distinguish between the range of bed elevations interacting with the flow regularly (i.e. the active layer), the range interacting with the flow only occasionally (i.e. the exchange layer in the Ribberink two-layer model), and the range not interacting with the flow, at all (i.e. the substrate). In morphological models, the bed layers' thicknesses are therefore often used as calibration parameters.

In reality, the active part of the bed does not constitute a distinct surface layer as proposed by *Hirano*, but it is rather represented by a probability density function (PDF) of bed surface elevations. This would allow for taking into account that relatively deep bed elevations interact with the flow and are subject to entrainment and deposition less frequently than higher ones. The depth-continuous framework for sediment continuity developed by *Parker et al.* (2000) seems particularly adequate for this purpose. It constitutes a useful basis for the further development of sediment continuity models for non-uniform sediment, since it offers the possibility to relate vertical sorting fluxes to the likelihood of a certain bed elevation being exposed to the flow.

10.1.3 The continuum sorting model

In the present study, a new continuum sorting model has been developed, based on

1. the Parker-Paola-Leclair framework for sediment continuity,
2. the Einstein step length formulation,
3. a newly-developed lee sorting function, and
4. a newly-developed method to account for the variability in bedform trough elevations.

The present study comprehends the derivation of formulations for the grain size-specific and bed elevation-specific entrainment and deposition fluxes as required for the Parker-Paola-Leclair framework. The lee sorting function describes the grain size-specific deposition rate down the avalanche lee face of a bedform. It relates the grain size-specific deposition down the lee face to (1) the difference between the specific grain size and the geometric mean grain size, (2) the arithmetic standard deviation of the mixture, and (3) the bed shear stress.

For equilibrium conditions, the continuum sorting model is reduced to an equilibrium sorting model, which comprises two methods to solve for the equilibrium sorting profile. An important simplifying assumption is that, throughout the active bed, the composition of the net entrainment at a certain elevation of the stoss face is equal to the bed composition at that elevation. For non-equilibrium conditions, the continuum sorting model is reduced to a sorting evolution model. Given the initial sorting profile, the total bed load transport rate, the PDF of relative trough elevations, and the ratio of the average bedform length to the average bedform height, this model numerically solves for the time evolution of both the vertical sorting profile and the bed load transport composition. Both versions of the continuum sorting

model describe sorting through grain size-selective deposition down the bedform lee face and the variability in trough elevations. In addition, methods are proposed in order to account for vertical sediment fluxes through a change in time of the PDF of relative trough elevations and net aggradation or degradation.

The sorting evolution model is a relaxation-type model, which means that a time scale of vertical sorting can be defined. This sorting time scale increases with decreasing bed elevation. Deeper elevations are less frequently exposed to the flow, so that their adaptation of sorting is slower. Moreover, at deeper elevations the amount of sediment to be reworked is larger, which increases the time required for the adaptation of sorting even more.

If one is interested in processes at the time scale of large-scale morphological changes and this morphological time scale is much larger than the time scales of vertical sorting, vertical dune dimensions, and dune migration, one may assume that the vertical sorting profile has reached a state of quasi-equilibrium at each point in time. In these quasi-equilibrium conditions, the equilibrium sorting model may be applied in a morphological model instantaneously. When the time scale of morphological changes is of the same order of magnitude as the time scales of vertical sorting and dune dimensions, we need to take into account the time evolution of the vertical sorting profile when computing changes in morphology. In those circumstances, the morphological model should be based on the sorting evolution model.

The continuum sorting model computes the bed load transport composition by itself, which suggests that there is a strong interaction among the vertical sorting profile, the PDF of relative trough elevations, and the bed load transport composition. It is believed that this strong interaction does not allow for one of the components to be modelled independently from one another. The results indicate that also the bed roughness is intimately connected to the vertical sorting profile and the PDF of trough elevations.

The continuum sorting model is deterministic in the computation of the vertical sorting profile, but probabilistic in terms of the bed surface. This probabilistic element arises from the fluctuations of the bed surface due to the presence of bedforms.

10.1.4 Performance

The equilibrium sorting model was calibrated against the equilibrium phases of experiments B2 and A2 (present study), wherein two constants in the lee sorting function were used as calibration coefficients, and verified against the equilibrium phases

of experiments E3 and E7 by *Ribberink* (1987). Another step in the verification procedure was the comparison of the time evolution of both the sorting profile and the bed load transport composition as computed by the sorting evolution model with the data measured in experiments B2 and A2. The following remarks can be made:

- The agreement between the measured and computed sorting profiles was quite reasonable.
- The computed trend in the sorting profile over the active bed elevations agrees well with the measured one.
- All measured sorting profiles showed a coarse top layer that originated from the presence of a thin mobile armour layer and the deposition of sediment that was being transported over the bedform until the flow was turned off. Due to the assumption that the composition of the net entrainment at a certain elevation of the stoss face is equal to the bed composition at that elevation, this coarse top layer does not show up in the computed sorting profiles.

For the experiments considered in this study, the calibrated lee sorting function served well. Note that the mixtures used in the experiments were artificial. How well the lee sorting function acts for natural sediment mixtures remains to be investigated.

In addition, the lee sorting function was tested against experiments on sorting down a delta face conducted by *Kleinhans* (2002). In about half of the cases, the computed sorting profile covers the measured data reasonably well, but for the other cases the computed sorting is less strong than the measured one. This may be due to the definition of the bed shear stress being inconsistent to the one for dunes. Further research on the avalanche mechanism at the lee face of bedforms is required in order to increase the validity range of the lee sorting function.

Comparison of the model computations with measurements has shown that the continuum sorting model does not adequately describe the formation of a coarse bed layer underneath migrating bedforms. The author contributes this to the mechanisms of winnowing of fines and the settlement of immobile coarse particles being neglected in the model. It is recommended to include these mechanisms in a later version of the model.

10.1.5 Morphological model system

The present study was limited to investigating and modelling the vertical sorting mechanisms for cases without net aggradation or degradation. An important future

step in this research is to analyse the performance of a morphological model system including the new continuum sorting model for cases with net aggradation or degradation. Other topics that require further investigation are:

- PDF of relative trough elevations
- bed roughness
- sorting down an avalanche lee face
- vertical sediment fluxes due to partial transport and the winnowing of fines
- vertical sediment fluxes due to net aggradation or degradation
- vertical sediment fluxes under plane-bed conditions

Future research on these topics will be addressed in the final section of this chapter.

10.1.6 Reflection upon bed layer models

Uncertainties and errors in morphological models of rivers with non-uniform sediment are usually attributed to shortcomings pertaining to the sub-model of sediment transport. This mistakenly neglects shortcomings in the sub-model of sediment continuity, which describes the vertical sorting and the bed surface composition, while the latter is one of the main input parameters for calculating sediment transport and thus morphological changes.

The present study has shown that the Hirano active-layer model and the Ribberink two-layer model lack an adequate description of the vertical sorting mechanisms acting in the river bed. The predictive abilities of the new continuum sorting model and these two bed layer models were quantitatively studied through comparing the computed time evolution of the vertical sorting profile to measured data from two flume experiments. The new continuum sorting model showed a great improvement to the computed vertical sorting profiles.

Since existing bed layer models do not or barely account for vertical sorting mechanisms, it is questionable whether they accurately predict (the time evolution of) the average composition of the bed surface. Since the latter is one of the main parameters determining the bed roughness, sediment transport, and thus morphological changes, the application of bed layer models may induce large uncertainties in the predicted morphological changes and water levels during floods.

10.2 Future research

Note that Section 9.9 has listed some interesting case-studies. Future research on the following subject matter is recommended.

Time scales A study on the applicability ranges of the equilibrium sorting model and the sorting evolution model is strongly recommended. These ranges will be closely related to the ratios of the various time scales involved (i.e. the time scales of large-scale morphological changes, vertical sorting, vertical dune dimensions, and dune migration), in addition to the specific case-study and matters of interest.

Net aggradation or degradation The present study has been focussed on an improved description of vertical sorting processes other than through net aggradation or degradation. Yet, the author does propose a straightforward method for including sediment fluxes through net aggradation or degradation (i.e. through divergences in bed load and suspended load transport). However, testing the new continuum sorting model was limited to situations without net aggradation or degradation. Further research is required in order to investigate whether it is indeed justified to assume that the composition of sediment fluxes through net aggradation or degradation is independent of bed surface elevation. In reality, grain size-selective processes surely play a role. It is recommended to conduct flume experiments wherein net aggradation or degradation occurs in order to obtain data for calibration, verification, and possible adaptation of the present formulations. In order to assess the performance of the new continuum sorting model for cases with net aggradation or degradation, the continuum sorting model needs to be incorporated in a morphological model system.

PDF of trough elevations A sub-model for the PDF of relative trough elevations needs to be developed in order to use the new continuum sorting model in predictive applications. There exists a complex interaction between the PDF of relative trough elevations, the vertical sorting profile, the bed load transport composition, and a number of flow parameters. Also the time evolution of the PDF of relative trough elevations is of interest. A slow or quick increase in dune height and trough depth may have a different effect on the sorting time scale, as well as on the final equilibrium sorting profile.

Bed roughness The present results indicate that the bed roughness is closely related to the average bed surface composition and the PDF of relative trough elevations. The part of the bed roughness that is attributed to the grains, i.e. the skin friction, is related to some measure(s) of the composition of the bed surface. The part of the bed

roughness that is attributed to the bedforms, i.e. the form drag, seems to be closely related to the PDF of relative trough elevations, which characterises the shape and irregularity of the bedforms.

Lee sorting function More experimental work on the avalanche mechanism at the lee face of bedforms is required, so as to increase our understanding of the controls on the grain size-specific deposition down a bedform lee face and to increase the validity ranges of the newly-developed lee sorting function.

Tracer studies Flume experiments wherein the vertical sorting of tracer particles in uniform sediment is measured can be of great help in improving the formulations for the vertical sediment fluxes. The advantage of tracer particles is that grain size-selective processes do not play a role, which enables a fundamental analysis of vertical sediment fluxes.

Partial transport The incorporation of the mechanism of partial transport is open to improvement. Together with the neglect of the winnowing of fines from the trough surface and subsurface, it is held responsible for the inadequate description of the formation of a coarse bed layer underneath bedforms. In the continuum sorting model, immobile coarse particles present on the stoss face are not allowed to settle down as the bedform migrates. Instead, these particles are transported over the bedform crest and are deposited to the lower elevations of the lee face. In reality, through the migration of bedforms, an immobile particle will settle to the elevation of the trough located just upstream without being transported over the bedform crest. This settling of immobile coarse particles needs to be incorporated in a later version of the model.

Winnowing of fines The winnowing of fines from the trough surface and subsurface is not incorporated in the continuum sorting model. Winnowing occurs in case (1) partial transport conditions prevail and a relatively large amount of coarse material does not participate in the transport process, (2) the framework of coarse particles is permeable enough to let finer particles pass, and (3) the statistics of the highly turbulent flow in the trough areas allows fine material to be washed out.

Plane-bed conditions The present formulations for the grain size-specific vertical sediment fluxes in the river bed are limited to bedform-dominated conditions. Formulations remain to be developed for lower-regime and upper-regime plane-bed conditions. Obviously, under plane-bed conditions the variation in bed surface elevations is much less than under bedform-dominated conditions. A different model for the PDF of bed surface elevations will be required.

References

Allan, A. F., and L. E. Frostick, Framework dilation, winnowing, and matrix particle size: the behavior of some sand-gravel mixtures in a laboratory flume, *J. Sedimentary Res.*, *69*, 21–26, 1999.

Allen, J. R. L., Sedimentation to the lee of small underwater sand waves: an experimental study, *J. Geology*, *73*, 95–116, 1965.

Allen, J. R. L., The avalanching of granular solids on dune and similar slopes, *J. Geology*, *78*, 326–351, 1970.

Allen, J. R. L., *Sedimentary structures: their character and physical basis*, Elsevier, Amsterdam, 1984.

Armanini, A., and G. Di Silvio, A one-dimensional model for the transport of a sediment mixture in non-equilibrium conditions, *J. Hydraul. Res., IAHR*, *26*, 275–292, 1988.

Armanini, A., Non-uniform sediment transport: dynamics of the active layer, *J. Hydraul. Res., IAHR*, *33*, 611–622, 1995.

Bagnold, R. A., *The physics of blown sand and desert dunes*, Methuen, New York, 1941.

Bell, R. G., and A. J. Sutherland, Non-equilibrium bedload transport by steady flow, *J. Hydraul. Eng., ASCE*, *109*, 351–367, 1983.

Bencala, K. E., Interactions of solutes and streambed sediment. 2. A dynamic analysis of coupled hydrologic and chemical processes that determine solute transport, *Water Resour. Res.*, *20*, 1804–1814, 1984.

Bennett, J. P., and C. F. Nordin, Simulation of sediment transport and armoring, *Hydrological Science Bull.*, *24*, 555–569, 1977.

Bernabè, M., Bed level and bed material interaction in river morphology. Case study for bifurcation at Pannerdensche Kop with Delft3D, *Preliminary report Q3178*, WL | Delft Hydraulics, 2002.

Blom, A., and M. G. Kleinhans, Non-uniform sediment in morphological equilibrium

situations - Data report Sand Flume experiments 97/98, *Technical Report CiT: 99R-002/MICS-001*, University of Twente, 1999.

Blom, A., J. S. Ribberink, and P. van der Scheer, Bed stratification and sediment transport in flume experiments with a trimodal sediment mixture, in *Gravel-Bed Rivers V CD-ROM*, edited by T. J. Nolan and C. R. Thorne, The New Zealand Hydrological Society, Christchurch, New-Zealand, 2000.

Blom, A., G. Parker, and J. S. Ribberink, Vertical exchange of tracers and non-uniform sediment in dune situations, in *Proc. 2nd IAHR Symposium on River, Coastal and Estuarine Morphodynamics*, edited by S. Ikeda, pp. 207–216, Obihiro, Japan, 2001.

Blom, A., J. S. Ribberink, and H. J. de Vriend, Vertical sorting in bed forms: Flume experiments with a natural and a tri-modal sediment mixture, *Water Resour. Res., 2001WR001088, in press*, 2003.

Blom, A., UT Valbuis. Methode ter bepaling van de samenstelling van sedimentmengsels - Calibratie (in Dutch), *Technical Report CiT: 98W-011/MICS-003*, University of Twente, 1998.

Blom, A., Flume experiments with a trimodal sediment mixture - Data report Sand Flume experiments 1999/2000, *Technical Report CiT: 2000R-004/MICS-013*, University of Twente, 2000.

Borah, D. K., C. V. Alonso, and S. N. Prasad, Routing graded sediments in streams: Formulations, *J. Hydraul. Div., ASCE*, *108*, 1486–1503, 1982a.

Borah, D. K., C. V. Alonso, and S. N. Prasad, Routing graded sediments in streams: Applications, *J. Hydraul. Div., ASCE*, *108*, 1504–1517, 1982b.

Bradshaw, P., and F. Y. F. Wong, The reattachment and relaxation of a turbulent shear layer, *J. Fluid. Mech.*, *52*, 113–135, 1972.

Bridge, J. S., and S. J. Bennett, A model for the entrainment and transport of sediment grains of mixed sizes, shapes, and densities, *Water Resour. Res.*, *28*, 337–363, 1992.

Crickmore, M. J., and G. H. Lean, The measurement of sand transport by means of radioactive tracers, *Proc. Roy. Soc. London A.*, *266*, 402–421, 1962a.

Crickmore, M. J., and G. H. Lean, The measurement of sand transport by the time-integration method with radioactive tracers, *Proc. Roy. Soc. London A.*, *270*, 27–47, 1962b.

Cui, Y., G. Parker, and C. Paola, Numerical simulation of aggradation and downstream fining, *J. Hydraul. Res., IAHR*, *34*, 185–204, 1996.

Deigaard, R., and J. Fredsøe, Longitudinal grain sorting by current in alluvial

streams, *Nordic Hydrology*, *9*, 7–16, 1978.

Deigaard, R., Longitudinal sorting of grain sizes in alluvial rivers, in *Mechanics of sediment transport, Proc. Euromech 156, 12-14 July 1982, Istanbul*, edited by B. M. Sumer and A. Müller, pp. 231–236, A.A. Balkema, Rotterdam, the Netherlands, 1983.

De Vries, M., Applications of luminophores in sandtransport-studies, Ph.D. thesis, Delft University, 1966.

Diplas, P., and G. Parker, Deposition and removal of fines in gravel-bed streams, in *Dynamics of Gravel-bed Rivers*, edited by P. Billi, R. D. Hey, C. R. Thorne, and P. Tacconi, pp. 313–329, J. Wiley & Sons, Chicester, England, 1992.

Di Silvio, G., and A. Marion, Discussion: Transfer function for the deposition of poorly sorted gravel in response to streambed aggradation by Toro-Escobar, C. M., G. Parker, and C. Paola, *J. Hydraul. Res., IAHR*, *35*, 563–566, 1997.

Di Silvio, G., Sediment exchange between stream and bottom: a four layer model, in *Proc. Int. Grain Sorting Seminar, IAHR*, pp. 161–191, Monte Verità, Ascona, Switzerland, 1992a.

Di Silvio, G., Modelling sediment transport under different hydrological and morphological circumstances, in *Dynamics of Gravel-bed Rivers*, edited by P. Billi, R. D. Hey, C. R. Thorne, and P. Tacconi, pp. 363–371, J. Wiley & Sons, Chicester, England, 1992b.

Duizendstra, H. D., and C. Flokstra, Graded sediment in SOBEK - joint research RIZA and WL Delft Hydraulics. Final research 1997-1998, *Technical Report 98.150X Q2347*, RIZA and WL Delft Hydraulics, 1998a.

Duizendstra, H. D., and C. Flokstra, The necessity of modelling non-uniform sediment in a 1-D morphological model for a gravel bed and a sand bed river in the Netherlands, in *Proc.* 1^{st} *Federal Interagency Hydrologic Modelling Conference, Vol. 1 of 2*, pp. 3.63–3.70, Las Vegas, USA, 1998b.

Duizendstra, H. D., Determination of the sediment transport in an armoured gravel-bed river, *Earth Surface Processes and Landforms*, *26*, 1381–1393, 2001.

Einstein, H. A., Der Geschiebetrieb als Wahrscheinlichkeitsproblem (in German), *Mitt. Versuchsanst. für Wasserbau an der Eidg. Techn. Hochschule Zurich*, Verlag Rascher & Co., Zurich, 1937.

Einstein, H. A., The bed-load function for sediment transportation in open channel flows, *Technical Report 1026*, US Dept. Agric., Soil Conserv. Serv., T.B., 1950.

Elliott, A. H., and N. H. Brooks, Transfer of nonsorbing solutes to a streambed with bed forms: Theory, *Water Resour. Res.*, *33*, 123–136, 1997a.

Elliott, A. H., and N. H. Brooks, Transfer of nonsorbing solutes to a streambed with bed forms: Laboratory experiments, *Water Resour. Res.*, *33*, 137–151, 1997b.

Ferguson, R. I., T. B. Hoey, S. Wathen, and A. Werritty, Field evidence for rapid downstream fining of river gravels through selective transport, *J. Geology*, *24*, 179–182, 1996.

Ferguson, R. I., D. J. Bloomer, T. B. Hoey, and A. Werritty, Mobility of river tracer pebbles over different time scales, *Water Resour. Res.*, *35*, 3.1–3.8, 2002.

Fernandez-Luque, R., and R. Van Beek, Erosion and transport of bed-load sediment, *J. Hydraul. Res., IAHR*, *14*, 127–144, 1976.

Fernandez-Luque, R., Erosion and transport of bed-load sediment, Ph.D. thesis, Delft University, 1974.

Fredsøe, J., Shape and dimensions of stationary dunes in rivers, *J. Hydraul. Div., ASCE*, *108*, 932–947, 1982.

Frings, R. M., and M. G. Kleinhans, Sedimentsortering en transportlaagdynamiek. Geologische, antropogene en alluviale invloeden op de beddingsamenstelling van de Rijn rond de Pannerdensche Kop (in Dutch), *Technical Report ICG 02/7*, Netherlands Centre for Geo-ecological Research, 2002.

Frostick, L. E., P. M. Lucas, and I. Reid, The infiltration of fine matrices into coarse-grained alluvial sediments and its implications for stratigraphical interpretation, *J. Geol. Soc. London*, *141*, 955–965, 1984.

Galvin Jr, C. J., Discussion: Sand transport studies with radioactive tracers by Hubbell, D. W. and W. W. Sayre, *J. Hydraul. Div., ASCE*, *91*, 173–178, 1965.

Garcia, M., and G. Parker, Entrainment of bed sediment into suspension, *J. Hydraul. Eng., ASCE*, *117*, 414–435, 1991.

Gruijters, S. H. L. L., J. G. Veldkamp, J. Gunnink, and J. H. A. Bosch, De lithologische en sedimentologische opbouw van de ondergrond van de Pannerdensche Kop. Interpretatie van de meetresultaten. Eindrapport (in Dutch), *TNO report NITG 01-166-B*, Nederlands Instituut voor Toegepaste Geowetenschappen TNO, Zwolle, 2001a.

Gruijters, S. H. L. L., J. G. Veldkamp, J. Gunnink, and J. H. A. Bosch, De lithologische en sedimentologische opbouw van de ondergrond van de Bovenrijn/Niederrhein. Interpretatie van de meetresultaten. Eindrapport (in Dutch), *TNO report NITG 01-*

167-B, Nederlands Instituut voor Toegepaste Geowetenschappen TNO, Zwolle, 2001b.

Hassan, M. A., and M. Church, Vertical mixing of coarse particles in gravel bed rivers: a kinematic model, *Water Resour. Res.*, *30*, 1173–1185, 1994.

Hirano, M., On phenomena of river-bed lowering and armouring below reservoirs, in *Proc. 14th. Hydraul. Lecture Meeting*, 13-14 Feb., Civ. Eng. Ass. Hydr. Committee, Hatsumei Kaikan, 1970.

Hirano, M., River bed degradation with armouring, *Transactions Jap. Soc. Civ. Eng.*, *3*, 194–195, 1971.

Hirano, M., Studies on variation and equilibrium state of a river bed composed of nonuniform material, *Transactions Jap. Soc. Civ. Eng.*, *4*, 128–129, 1972.

Hoey, T. B., and R. I. Ferguson, Numerical simulation of downstream fining by selective transport in gravel bed rivers: model development and illustration, *Water Resour. Res.*, *30*, 2251–2260, 1994.

Holly Jr, F. M., and J. L. Rahuel, New numerical/physical framework for mobile-bed modelling. Part I - Numerical and physical principles, *J. Hydraul. Res., IAHR*, *28*, 401–416, 1990.

Hubbell, D. W., and W. W. Sayre, Sand transport studies with radioactive tracers, *J. Hydraul. Div., ASCE*, *90*, 39–68, 1964.

Hubbell, D. W., and W. W. Sayre, Closure: Sand transport studies with radioactive tracers, *J. Hydraul. Div., ASCE*, *91*, 139–148, 1965.

Jopling, A. V., Origin of laminae deposited by the movement of ripples along a streambed: a laboratory study, *J. Geology*, *75*, 287–305, 1967.

Julien, P. Y., G. J. Klaassen, W. B. M. ten Brinke, and A. W. E. Wilbers, Case study: bed resistance of Rhine river during 1998 flood, *J. Hydraul. Eng., ASCE*, *128*, 1042–1050, 2002.

Karim, M. F., and F. M. Holly, Armoring and sorting simulation in alluvial rivers, *J. Hydraul. Eng., ASCE*, *112*, 705–715, 1986.

Kelsey, A., Modelling the sediment transport process, in *Advances in Fluvial Dynamics and Stratigraphy*, edited by P. A. Carling and M. R. Dawson, pp. 229–261, J. Wiley & Sons, Chicester, England, 1996.

Klaassen, G. J., Morfologie afgepleisterde beddingen - proeven met hoogwatergolven (in Dutch), *Technical Report M2061/Q212*, Delft Hydraulics, 1986.

Klaassen, G. J., Sediment transport in armoured rivers during floods - literature survey, *Technical Report Q790*, Delft Hydraulics, 1990a.

Klaassen, G. J., Experiments with graded sediments in a straight flume. Vol. A (Text) and Vol. B (Tables and Figures), *Technical Report Q788*, Delft Hydraulics, 1990b.

Klaassen, G. J., Experiments on the effect of gradation and vertical sorting on sediment transport phenomena in the dune phase, in *Proc. Int. Grain Sorting Seminar, IAHR*, pp. 127–145, Monte Verità, Ascona, Switzerland, 1992.

Kleinhans, M. G., and L. C. Van Rijn, Stochastic prediction of sediment transport in sand-gravel bed rivers, *J. Hydraul. Eng., ASCE*, *128*, 412–425, 2002.

Kleinhans, M. G., Sorting out sand and gravel: sediment transport and deposition in sand-gravel bed rivers, Ph.D. thesis, Utrecht University, 2002.

Koeppe, J. P., M. Enz, and J. Kakalios, Phase diagram for avalanche stratification of granular media, *Phys. Rev. E*, *58*, R4104–R4107, 1997.

Leclair, S. F., and A. Blom, Relation between the probability distribution of bed elevation and the vertical sorting in subaqueous dunes, in *Program and Abstracts of the 7th Int. Conf. on Fluvial Sedimentology*, edited by J. A. Mason, R. F. Diffendal Jr, and R. M. Joeckel, Open-File Report 60, University of Nebraska, Lincoln, USA, 2001.

Leclair, S. F., and A. Blom, A qualitative analysis of the distribution of bed elevation and the characteristics of associated deposit for subaqueous dunes, in *Proc. 7th Int. Conf. on Fluvial Sedimentology*, University of Nebraska, Lincoln, USA, in press, 2003.

Leclair, S. F., and J. S. Bridge, Quantitative interpretation of sedimentary structures formed by river dunes, *J. Sedimentary Res.*, *71*, 2001.

Leclair, S. F., Preservation of cross-strata due to migration of subaqueous dunes, Unpublished Ph.D. thesis, Binghampton University, New York, 2000.

Leclair, S. F., Preservation of cross-strata due to the migration of subaqueous dunes: an experimental investigation, *Sedimentology*, *49*, 1157–1180, 2002.

Li, Q., The numerical simulation of non-equilibrium graded sediment transport, Ph.D. thesis, Glasgow University, 1995.

Makse, H. A., P. Cizeau, and H. E. Stanley, Possible stratification mechanism in granular mixtures, *Phys. Rev. Lett.*, *78*, 3298–3301, 1997.

Makse, H. A., Stratification instability in granular flows, *Phys. Rev. E*, *56*, 7008–7016, 1997.

Marion, A., and L. Fraccarollo, Experimental investigation of mobile armoring development, *Water Resour. Res.*, *33*, 1447–1453, 1997.

McEwan, I. K., H. M. Habersack, and J. G. C. Heald, Discrete particle modelling and active tracers: new techniques for studying sediment transport as a lagrangian phenomenon, in *Gravel Bed Rivers V*, edited by M. P. Mosley, pp. 339–367, New Zealand Hydrological Society, Christchurch, New Zealand, 2001.

McLean, S. R., J. M. Nelson, and S. R. Wolfe, Turbulence structure over two-dimensional bed forms: Implications for sediment transport, *J. Geophys. Res.*, *99*, 12,729–12,747, 1994.

McLean, S. R., J. M. Nelson, and R. L. Shreve, Flow-sediment interactions in separating flows over bedforms, in *Coherent flow structures in open channels*, edited by P. J. Ashworth, S. J. Bennett, J. L. Best, and S. J. McLelland, pp. 203–226, John Wiley & Sons, 1996.

McLean, S. R., S. R. Wolfe, and J. M. Nelson, Predicting boundary shear stress and sediment transport over bed forms, *J. Hydraul. Eng., ASCE*, *125*, 725–736, 1999.

Mohrig, D., and J. D. Smith, Predicting the migration rates of subaqueous dunes, *Water Resour. Res.*, *32*, 3207–3217, 1996.

Mosselman, E., J. Sieben, C. J. Sloff, and A. Wolters, Effect of spatial grain size variations on two-dimensional river bed morphology, in *Proc. IAHR Symposium on River, Coastal and Estuarine Morphodynamics*, edited by G. Seminara, pp. 499–507, Genova, Italy, 1999.

Nakagawa, H., and T. Tsujimoto, Sand bed instability due to bed load motion, *J. Hydraul. Div., ASCE*, *106*, 2029–2051, 1980.

Nelson, J. M., S. R. McLean, and S. R. Wolfe, Mean flow and turbulence fields over two-dimensional bed forms, *Water Resour. Res.*, *29*, 3935–3953, 1993.

Nelson, J. M., R. L. Shreve, S. R. McLean, and T. G. Drake, Role of near-bed turbulence structure in bed load transport and bed form mechanics, *Water Resour. Res.*, *31*, 2071–2086, 1995.

Niño, Y., A. Atala, M. Barahona, and D. Aracena, Discrete particle model for analyzing bedform development, *J. Hydraul. Eng., ASCE*, *128*, 381–389, 2002.

Packman, A. I., N. H. Brooks, and J. J. Morgan, A physicochemical model for colloid exchange between a stream and a sand streambed with bed forms, *Water Resour. Res.*, *36*, 2351–2361, 2000.

Parker, G., C. Paola, and S. Leclair, Probabilistic Exner sediment continuity equation

for mixtures with no active layer, *J. Hydraul. Eng., ASCE*, *126*, 818–826, 2000.

Parker, G., Selective sorting and abrasion of river gravel. I. Theory, *J. Hydraul. Eng., ASCE*, *117*, 113–149, 1991a.

Parker, G., Selective sorting and abrasion of river gravel. II. Applications, *J. Hydraul. Eng., ASCE*, *117*, 150–171, 1991b.

Park, I., and S. C. Jain, Numerical simulation of degradation of alluvial channels, *J. Hydraul. Eng., ASCE*, *113*, 845–859, 1987.

Pender, G., and Q. Li, Numerical prediction of graded sediment transport, *Proc. Instn. Civ. Engrs, Wat., Marit. & Energy*, *118*, 237–245, 1996.

Philips, B. C., and A. J. Sutherland, Spatial lag effects in bed load sediment transport, *J. Hydraul. Res., IAHR*, *27*, 115–133, 1989.

Philips, B. C., and A. J. Sutherland, Temporal lag effect in bed load sediment transport, *J. Hydraul. Res., IAHR*, *28*, 5–23, 1990.

Powell, D. M., Patterns and processes of sediment sorting in gravel-bed rivers, *Progress in Phys. Geography*, *22*, 1–32, 1998.

Rahuel, J. L., F. M. Holly, J. P. Chollet, P. J. Belleudy, and G. Yang, Modelling of riverbed evolution for bedload sediment mixtures, *J. Hydraul. Eng., ASCE*, *115*, 1521–1542, 1989.

Ribberink, J. S., Experiments with non-uniform sediment in case of bed-load transport, *Communications on Hydraul. and Geotechn. Eng. 83-2*, Delft University, 1983.

Ribberink, J. S., Mathematical modelling of one-dimensional morphological changes in rivers with non-uniform sediment, Ph.D. thesis, Delft University, 1987.

Schick, A. P., M. A. Hassan, and J. Lekach, A vertical exchange model for coarse bedload movement: numerical considerations, in *Geomorhological models - theoretical and empirical aspects*, edited by F. Ahnert, pp. 73–83, Catena Verlag, Germany, 1987a.

Schick, A. P., J. Lekach, and M. A. Hassan, Vertical exchange of coarse bedload in desert streams, in *Desert sediments: ancient and modern*, edited by L. Frostick and I. Reid, pp. 7–16, Geol. Soc. London, 1987b.

Schmidt, K. H., and P. Ergenzinger, Bedload entrainment, travel lengths, step lengths, rest periods - studied with passive (iron, magnetic) and active (radio) tracer techniques, *Earth Surface Processes and Landforms*, *17*, 147–165, 1992.

Seal, R., C. Paola, G. Parker, J. B. Southard, and P. R. Wilcock, Experiments on down-

stream fining of gravel: 1 Narrow channel runs, *J. Hydraul. Eng., ASCE*, *123*, 874–884, 1997.

Sekine, M., and H. Kikkawa, Mechanics of saltating grains. II, *J. Hydraul. Eng., ASCE*, *118*, 536–558, 1992.

Sieben, J., Modelling of hydraulics and morphology in mountain rivers, Ph.D. thesis, Delft University, 1997.

Sloff, C. J., H. R. A. Jagers, Y. Kitamura, and P. Kitamura, 2D Morphodynamic modelling with graded sediment, in *Proc. 2nd IAHR Symposium on River, Coastal and Estuarine Morphodynamics*, edited by S. Ikeda, pp. 535–544, Obihiro, Japan, 2001.

Smith, J. D., Stability of a sand bed subjected to a shear flow of low Froude number, *J. Geophys. Res.*, *75*, 5928–5940, 1970.

Sumer, B. M., S. Cokgor, and J. Fredsøe, Suction removal of sediment from between armor blocks, *J. Hydraul. Eng., ASCE*, *127*, 293–306, 2001.

Tait, S. T., B. B. Willetts, and J. K. Maizels, Laboratory observations of bed armouring and changes in bed load composition, in *Dynamics of Gravel-bed Rivers*, edited by P. Billi, R. D. Hey, C. R. Thorne, and P. Tacconi, pp. 205–225, J. Wiley & Sons, Chicester, England, 1992.

Thomas, W. A., and A. Prasuhn, Mathematical modeling of scour and deposition, *J. Hydraul. Div., ASCE*, *103*, 851–864, 1977.

Toro-Escobar, C. M., G. Parker, and C. Paola, Transfer function for the deposition of poorly sorted gravel in response to streambed aggradation, *J. Hydraul. Res., IAHR*, *34*, 35–53, 1996.

Tsujimoto, T., and K. Motohashi, Static armoring and dynamic pavement, *J. Hydroscience and Hydraul. Eng.*, *8*, 55–67, 1990.

Tsujimoto, T., Instability of longitudinal distribution of fluvial bed-surface composition, *J. Hydroscience and Hydraul. Eng.*, *7*, 69–80, 1990.

Tsujimoto, T., Sediment transport processes and channel incision: mixed size sediment transport, degradation and armouring, in *Incised River Channels: Processes, Forms, Engineering and Management*, edited by S. E. Darby and A. Simon, pp. 37–66, J. Wiley & Sons, Chicester, England, 1999.

Vanoni, V. A., and N. H. Brooks, Laboratory studies of the roughness and suspended load of alluvial streams, *Technical Report E-68*, Sedimentation Laboratory, California Institute of Technology, Pasadena, USA, 1957.

Van der Scheer, P., J. S. Ribberink, and A. Blom, Transport formulas for graded sedi-

ment: behaviour of transport formulas and verification with data, *Technical Report CiT: 2002R-002, ISSN 1568-4652*, University of Twente, 2002.

Van Ledden, M., and Z. B. Wang, Sand-mud morphodynamics in an estuary, in *Proc. 2nd IAHR Symposium on River, Coastal and Estuarine Morphodynamics*, edited by S. Ikeda, pp. 505–514, Obihiro, Japan, 2001.

Wilcock, P. R., and J. C. Crowe, Surface-based transport model for mixed-size sediment, *J. Hydraul. Eng., ASCE*, *129*, 120–128, 2003.

Wilcock, P. R., and B. W. McArdell, Surface-based fractional transport rates: mobilisation thresholds and partial transport of a sand-gravel sediment, *Water Resour. Res.*, *29*, 1297–1312, 1993.

Wilcock, P. R., and J. B. Southard, Bed load transport of mixed size sediment: fractional transport rates, bed forms, and the development of a coarse bed surface layer, *Water Resour. Res.*, *25*, 1629–1641, 1989.

Willis, J. C., Partial armoring of sand beds by gravel, in *Mechanics of alluvial channels*, edited by K. Mahmood, M. I. Haque, and A. M. Choudri, pp. 356–368, Water Resources Publications, Littleton, Colorado, 1988.

Wu, W., S. S. Y. Wang, and Y. Jia, Nonuniform sediment transport in alluvial rivers, *J. Hydraul. Res., IAHR*, *38*, 427–434, 2000.

Yalin, M. S., *Mechanics of sediment transport*, Pergamon Press, Oxford, 1977.

Zanke, U., Über den Einfluss von Kornmaterial, Strömungen und Wasserstanden auf die Korngrossen von Transportkörpern in offenen Gerinnen (in German), *Tech. Rep. 44*, Mitt. Franzius Inst. Hannover, Germany, 1976.

Nomenclature

*	meaning parameter is dimensionless	
$\bar{}$	meaning parameter is horizontally averaged over a series of bedforms	
$\bar{\bar{}}$	meaning parameter is horizontally averaged over a series of bedforms and over a specific range of bed elevations	
$\tilde{}$	meaning parameter is relative to the mean bed level	
a_{iE}	grain size-specific constant in the weighed entrainment rate Θ_{iE}	$[-]$
b_{iE}	grain size-specific constant in the weighed entrainment rate Θ_{iE}	$[-]$
c	bedform migration speed	$[ms^{-1}]$
c_b	sediment concentration within the bed ($c_b = 1 - \lambda_b$)	$[-]$
c_{iE}	grain size-specific constant in the weighed entrainment rate Θ_{iE}	$[-]$
C	Chézy roughness coefficient	$[m^{\frac{1}{2}}s^{-1}]$
$\bar{C}_i$	concentration of size fraction i at elevation z, averaged over a series of bedforms ($\bar{C}_i = c_b\bar{P}_s\bar{F}_i$)	$[-]$
d_i	grain size of size fraction i	$[m]$
d_{mlee}	geometric mean grain size of the lee deposit ($d_{mlee} = \frac{1}{1000}2^{-\phi_{mlee}}$)	$[m]$
d_{xx}	grain size for which xx percent of the sediment mixture is finer	$[m]$
$\bar{D}$	volume of deposited sediment per unit area and time, summed over all size fractions and averaged over a series of bedforms	$[ms^{-1}]$
$\bar{D}_e$	deposition density defined such that $\bar{D}_e dxdz$ is the volume of all size fractions deposited in a bed element with sides dx and dz at elevation z, per unit width and time, averaged over a series of bedforms	$[s^{-1}]$
$\bar{D}_{ei}$	deposition density of size fraction i defined such that $\bar{D}_{ei}dxdz$ is the volume of size fraction i deposited in a bed element with sides dx and dz at elevation z, per unit width and time, averaged over a series of bedforms	$[s^{-1}]$
D_l	deposition rate at the lee face	$[ms^{-1}]$
D_{si}	volume of size fraction i locally deposited onto the stoss face, per unit area and time ($D_{si}(x) = E_{si}(x - \Lambda_i)$)	$[ms^{-1}]$
D_{ti}	volume of sediment of size fraction i deposited from the active layer to the exchange layer in the Ribberink two-layer model, per unit area and time	$[ms^{-1}]$
E	subscript indicating equilibrium conditions	
$\bar{E}$	volume of entrained sediment per unit area and time, summed over all size fractions and averaged over a series of bedforms	$[ms^{-1}]$

$\bar{E}_e$	entrainment density defined such that $\bar{E}_e dxdz$ is the volume of all size fractions entrained from a bed element with sides dx and dz at elevation z, per unit width and time, averaged over a series of bedforms	$[s^{-1}]$
$\bar{E}_{ei}$	entrainment density of size fraction i, defined such that $\bar{E}_{ei} dxdz$ is the volume of size fraction i entrained from a bed element with sides dx and dz at elevation z, per unit width and time, averaged over a series of bedforms	$[s^{-1}]$
E_{snet}	net entrained volume of all size fractions on the stoss face, per unit area and time	$[ms^{-1}]$
E_{si}	volume of size fraction i locally entrained from the stoss face, per unit area and time ($E_{si} = E_{siu} F_i$)	$[ms^{-1}]$
E_{siu}	volume of size fraction i locally entrained from the stoss face, per unit area and time, if only sediment of size fraction i would be present	$[ms^{-1}]$
E_{ti}	volume of sediment of size fraction i entrained from the exchange layer into the active layer in the Ribberink two-layer model, per unit area and time	$[ms^{-1}]$
f	volume fraction content of tracers (equivalent to F for non-uniform sediment)	$[-]$
f_{ds}	dimensionless elevation of the stoss face as a function of its dimensionless horizontal co-ordinate	$[-]$
$f_p(\xi)$	probability density that the step length equals ξ	$[-]$
$\bar{F}_{ai}$	volume fraction content of size fraction i in the bed load transport, averaged over a series of bedforms	$[-]$
F_{ei}	volume fraction content of size fraction i in the exchange layer in the Ribberink two-layer model	$[-]$
$\bar{F}_i$	volume fraction content of size fraction i in the bed at elevation z, averaged over a series of bedforms	$[-]$
$\bar{F}_{leei}$	volume fraction content of size fraction i in the lee deposit, averaged over a series of bedforms	$[-]$
$F_{leeloci}$	volume fraction content of size fraction i in the sediment deposited at elevation z at the bedform lee	$[-]$
F_{mi}	volume fraction content of size fraction i in the active layer	$[-]$
F_{miD}	volume fraction content of size fraction i in the sediment deposited from the active layer into the exchange layer in the Ribberink two-layer model	$[-]$
F_{oi}	volume fraction content of size fraction i in the substrate	$[-]$
F_{Ii}	volume fraction content of size fraction i at the interface between the active layer and the substrate (if the Hirano active layer model is used), or the elevation of the interface between the active layer and the exchange layer (if the Ribberink two-layer model is used)	$[-]$
F_{IIi}	volume fraction content of size fraction i at the interface between the exchange layer and the substrate in the Ribberink two-layer model	$[-]$
$F_p(\xi)$	probability that the step length is larger than ξ	$[-]$
Fr	Froude number	$[-]$

$\bar{F}_{suri}$	volume fraction content of size fraction i at the bed surface, weighed over all bed elevations exposed to the flow over a series of bedforms	$[-]$
$\bar{F}_{suspi}$	volume fraction content of size fraction i in the suspended load transport, averaged over a series of bedforms	$[-]$
$\bar{F}_{topi}$	volume fraction content of size fraction i in the sediment transported as bed load over the bedform crest, averaged over a series of bedforms	$[-]$
$F_{tot,i}$	volume fraction content of size fraction i in the total load transport	$[-]$
g	gravitational acceleration	$[ms^{-2}]$
g_{ds}	dimensionless horizontal co-ordinate of the stoss face as a function of its dimensionless elevation	$[-]$
h	water depth	$[m]$
i	subscript indicating the number of the size fraction	
i_E	energy slope	$[-]$
l	subscript indicating the lee face	
mor	subscript indicating parameter is related to net aggradation or degradation	
N	total number of size fractions	$[-]$
$\tilde{p}_{\eta_b}$	probability density function of trough elevations relative to the mean bed level for a series of bedforms, indicating the probability density that the trough elevation equals z	$[m^{-1}]$
$\tilde{p}_b$	adapted probability density function of trough elevations relative to the mean bed level for a series of bedforms, indicating the probability density that the trough elevation equals z, weighed by the horizontal distance involved	$[m^{-1}]$
$\bar{p}_e$	probability density function of bed surface elevations for a series of bedforms, indicating the probability density that the bed surface elevation equals z	$[m^{-1}]$
$\bar{p}_e^*$	dimensionless probability density function of bed surface elevations for a series of bedforms, indicating the dimensionless probability density that the bed surface elevation equals z	$[-]$
p_e	probability density function of bed surface elevations for an individual bedform, indicating the probability density that the bed surface elevation equals z	$[m^{-1}]$
$\bar{P}_s$	probability distribution of bed surface elevations for a series of bedforms, indicating the probability that the bed surface elevation is higher than z	$[-]$
q	volume of bed load transport per unit width and time (excluding pores)	$[m^2s^{-1}]$
$\bar{q}_a$	volume of bed load transport per unit width and time (excluding pores), averaged over a series of bedforms (excluding pores)	$[m^2s^{-1}]$
$\bar{q}_{susp}$	volume of suspended load transport per unit width and time (excluding pores), averaged over a series of bedforms	$[m^2s^{-1}]$
$\bar{q}_{suspi}$	volume of suspended load transport of size fraction i per unit width and time (excluding pores)	$[m^2s^{-1}]$

$\bar{q}_{top}$	volume of bed load transport at the bedform crest per unit width and time (excluding pores), averaged over a series of bedforms (excluding pores)	$[m^2 s^{-1}]$
q_{tot}	volume of total load transport per unit width and time (excluding pores)	$[m^2 s^{-1}]$
Q_{tot}	volume of total load transport per unit time (excluding pores)	$[m^3 s^{-1}]$
Q_w	flow discharge	$[m^3 s^{-1}]$
R	hydraulic radius	$[m]$
s	subscript indicating the stoss face	
t	time co-ordinate	$[s]$
T_c	time scale of dune migration, i.e. the time required for a bedform to cover its average bedform length $\bar{\lambda}$ ($T_c = \frac{\bar{\lambda}}{c}$)	$[s]$
T_p	time scale of dune dimensions	$[s]$
T_f	time scale of vertical sorting	$[s]$
T_m	time scale of morphological changes	$[s]$
u	average flow velocity	$[ms^{-1}]$
u	subscript indicating the case of sediment of only size fraction i, although hiding-exposure effects may be included	
W	flume width	$[m]$
W_o	width of the flume over which bedforms migrate	$[m]$
x	horizontal co-ordinate	$[m]$
x^*	dimensionless horizontal co-ordinate on the scale of an individual bedform	$[-]$
z	vertical co-ordinate	$[m]$
$\tilde{z}$	vertical co-ordinate relative to the mean bed level $\bar{\eta}_a$	$[m]$
z^*	dimensionless vertical co-ordinate relative to the mean bed level $\bar{\eta}_a$	$[-]$
z_t	bedform crest elevation ($z_t = \eta_t$)	$[m]$
α	dimensionless step length	$[-]$
β	bedform shape factor, defined such that the average trough elevation is located at $\beta\Delta$ below the mean bed level	$[-]$
γ	constant in lee sorting function	$[-]$
γ_t	proportionality factor depending on the subdivision between the active layer and the exchange layer in the Ribberink two-layer model	$[-]$
δ	the active layer thickness	$[m]$
δ_e	the exchange layer thickness	$[m]$
δ_i	lee sorting parameter	$[-]$
Δ	bedform height	$[m]$
Δ_b	trough elevation relative to the mean bed level, i.e. the relative trough elevation ($\Delta_b = \bar{\eta}_a - \eta_b$)	$[m]$
η	local bed surface elevation	$[m]$
η_a	bed surface elevation averaged over a single bedform	$[m]$
$\bar{\eta}_a$	bed surface elevation averaged over a series of bedforms (mean bed level)	$[m]$
η_b	bedform trough elevation	$[m]$

η_t	bedform crest elevation	$[m]$
η_I	elevation of interface between the active layer and the substrate (if the Hirano active layer model is used), or the elevation of the interface between the active layer and the exchange layer (if the Ribberink two-layer model is used)	$[m]$
η_{II}	elevation of interface between the exchange layer and the substrate in the Ribberink two-layer model	$[m]$
η_{mn}	lower limit of the active bed	$[m]$
η_{mx}	upper limit of the active bed	$[m]$
η_{stepi}	step length in z-direction for size fraction i	$[m]$
Θ_i	weighed entrainment rate of size fraction i, indicating the entrainment rate of size fraction i weighed by its volume fraction content at elevation z ($\Theta_i = E_{siu}\bar{F}_i$)	$[ms^{-1}]$
κ	constant in the lee sorting function	$[-]$
λ	bedform length	$[m]$
λ_b	porosity	$[-]$
λ_l	horizontal length of the lee face	$[m]$
λ_s	horizontal length of the stoss face	$[m]$
Λ_i	step length of size fraction i	$[m]$
ν	angle of repose	$[^\circ]$
ρ	density of water	$[kgm^{-3}]$
ρ_s	density of sediment	$[kgm^{-3}]$
σ_a	arithmetic standard deviation of the composition of the lee deposit. Since its unit equals ϕ's unit, which is nonsensical (^{2} log mm), it is simply left out.	$[.]$
$\bar{\tau}_b$	bed shear stress averaged over a series of bedforms	$[Nm^{-2}]$
ϕ_i	grain size of size fraction i on ϕ-scale ($\phi_i = -^2\log 1000\, d_i$). Since ϕ's unit is nonsensical, i.e. ^{2} log mm, it is simply left out.	$[.]$
ϕ_{mlee}	geometric mean grain size on ϕ-scale of the lee deposit	$[.]$
ψ_i	volume of exchange of size fraction i between the active layer and the exchange layer in the Ribberink two-layer model, per unit area and time ($\psi_i = E_{ti} - D_{ti}$)	$[ms^{-1}]$
ω_i	lee sorting function, specifying to what extent a specific size fraction that is transported over the bedform crest is deposited at elevation z of the lee face ($\omega_i = F_{leeloci}/F_{leei}$)	$[-]$

Index

Appendix A

Integral of time derivative $\tilde{P}_s$ over z

Near (28a,b) in the paper by *Parker et al.* (2000), it is argued that the integral $\partial\tilde{P}_s/\partial t$ over z in (5.14) should vanish if $\bar{p}_e$ is symmetric in $\tilde{z}$, i.e. around the mean bed level, $\bar{\eta}_a$. However, Parker (2000, personal communication) later found that the integral term in (5.14) should vanish, regardless of whether or not $\bar{p}_e$ is symmetric in $\tilde{z}$.

Let us consider the integral

$$I = \int_{-r}^{r} \frac{\partial \tilde{P}_s}{\partial t}\, d\tilde{z} \tag{A.1}$$

where $r = \infty$ and

$$\tilde{z} = z - \bar{\eta}_a(x,t) \tag{A.2}$$

denotes the bed elevation relative to the mean bed level, $\bar{\eta}_a$. Now Parker (2000, personal communication) substitutes

$$\bar{P}_s = 1 - \int_{-\infty}^{\tilde{z}} \bar{p}_e\, d\tilde{z}' \tag{A.3}$$

into (A.1):

$$I = -\int_{-r}^{r} \frac{\partial}{\partial t}\left(\int_{-\infty}^{\tilde{z}} \bar{p}_e\, d\tilde{z}'\right) d\tilde{z} \tag{A.4}$$

and rephrases (A.4) by integrating in parts, according to

$$\int g'h = gh\Big| - \int gh' \tag{A.5}$$

where

$$g' = 1 \tag{A.6}$$

$$h = -\frac{\partial}{\partial t}\left(\int_{-\infty}^{\tilde{z}} \bar{p}_e\, d\tilde{z}'\right) \tag{A.7}$$

This yields

$$
\begin{aligned}
I = &- \tilde{z}\left[\frac{\partial}{\partial t}\left(\int_{-\infty}^{\tilde{z}} \bar{p}_e\, d\tilde{z}'\right)\right]\Bigg|_{-r}^{r} + \int_{-r}^{r} \tilde{z}\frac{\partial}{\partial \tilde{z}}\left[\frac{\partial}{\partial t}\left(\int_{-\infty}^{\tilde{z}} \bar{p}_e\, d\tilde{z}'\right)\right] d\tilde{z} = \\
&= -\frac{\partial}{\partial t}\left[\tilde{z}\left(1-\bar{P}_s\right)\right]\Bigg|_{-r}^{r} + \int_{-r}^{r} \tilde{z}\frac{\partial}{\partial t}\bar{p}_e\, d\tilde{z} = \\
&= r\left(\left.\frac{\partial \bar{P}_s}{\partial t}\right|_{r} + \left.\frac{\partial \bar{P}_s}{\partial t}\right|_{-r}\right) + \frac{\partial}{\partial t}\int_{-r}^{r} \tilde{z}\bar{p}_e\, d\tilde{z}
\end{aligned}
\tag{A.8}
$$

Since by definition

$$
\int_{-r}^{r} \tilde{z}\bar{p}_e\, d\tilde{z} = 0 \tag{A.9}
$$

the integral term in (A.8) vanishes. In addition, by definition $\bar{P}_s \to 1$ as $r \to -\infty$ and $\bar{P}_s \to 0$ as $r \to \infty$, so that $\partial \bar{P}_s/\partial t \to 0$ as $r \to \pm\infty$. Under the condition that $\partial \bar{P}_s/\partial t$ converges to 0 faster than r converges to $\pm\infty$ (a condition that holds for, e.g., a Gaussian distribution in which the standard variation is allowed to vary in time), it is seen that the integral $I \to 0$ as $r \to \infty$, thus demonstrating that the integral term in (5.14) should vanish, regardless of whether or not $\bar{p}_e$ is symmetric in $\tilde{z}$.

Appendix B

Constraint to lee sorting function

By integrating the composition of the deposited sediment over the lee face, we should find F_{leei}, which is expressed by (5.69):

$$F_{leei} = \frac{1}{\lambda_l} \int_{\lambda_s}^{\lambda} F_{leeloci}\, dx \tag{B.1}$$

For the lee face is valid:

$$x_l^* = \frac{x - \lambda_s}{\lambda_l} \tag{B.2}$$

$$dx_l^* = -\, p_{le}^*\, dz^* = -dz^* \tag{B.3}$$

$$x_l = \lambda_s \rightarrow z^* = \eta_t^* \tag{B.4}$$

$$x_l = \lambda \rightarrow z^* = \eta_b^* \tag{B.5}$$

so that (B.1) reduces to

$$F_{leei} = -\int_{\eta_t^*}^{\eta_b^*} F_{leeloci}\, dz^* \tag{B.6}$$

With (5.68), (5.72), and (5.73), this becomes

$$F_{leei} = \int_{\eta_b^*}^{\eta_t^*} F_{leei} \left[1 + \delta_i \left(z^* - \tfrac{1}{2} - \eta_b^*\right)\right]\, dz^* \tag{B.7}$$

which, after integration over η_b^* to η_t^* and with $\eta_t^* - \eta_b^* = 1$, results in

$$F_{leei} = F_{leei} \tag{B.8}$$

showing that constraint (5.69) is met.

Appendix C

The PDF of bed surface elevations

In Section 5.3.2, it has been explained how the overall PDF of bed surface elevations, $\bar{p}_e$, is related to the characteristic bedform shape, $\bar{p}^*_{se}$, and the PDF of relative trough elevations, $\tilde{p}_b$. The relation is given by (5.92):

$$\bar{p}_e(z) = \int_{\eta_{bmin}}^{\eta_{bmax}} p_e(z)\, \tilde{p}_b\, d\eta_b = \int_{\eta_{bmin}}^{\eta_{bmax}} \frac{J(z)}{\lambda\Delta}\, (\lambda_s \bar{p}^*_{se}(z) + \lambda_l)\ \tilde{p}_b\, d\eta_b$$

The parameters J, Δ, λ, λ_s, and λ_l are all related to the specific relative trough elevation Δ_b, which is expressed by (5.57) and (5.84) through (5.87). The overall probability distribution of bed surface elevations, $\bar{P}_s$, is given by (5.2).

This appendix explains the determination of the overall PDF of bed surface elevations, $\bar{p}_e$, for the simple case of two triangular dunes. For triangular dunes, the characteristic bedform shape represented by $\bar{p}^*_{se}$ equals $J(z)$, where

$$J(z) = \begin{cases} 1 & \text{if } \eta_b \le z \le \eta_t \\ 0 & \text{if } z < \eta_b \text{ or } z > \eta_t \end{cases}$$

so that (5.92) can be reduced to

$$\bar{p}_e(z) = \int_{\eta_{bmin}}^{\eta_{bmax}} \frac{J(z)}{\Delta}\, \tilde{p}_b\, d\eta_b \tag{C.1}$$

Figure C.1 shows the two triangular dunes and their properties. The small dune, bedform type 1, has the following features: bedform length λ_1, bedform height Δ_1. The PDF of bed surface elevations, p_e, of this individual bedform equals

$$p_{e1} = \frac{J(z)}{\Delta_1} \tag{C.2}$$

For the large dune, bedform type 2, these properties have the subscript 2.

The probability that either one of the bedforms occurs equals $\frac{1}{2}$. Considering locations over the total horizontal distance L, the probability that a location is related to

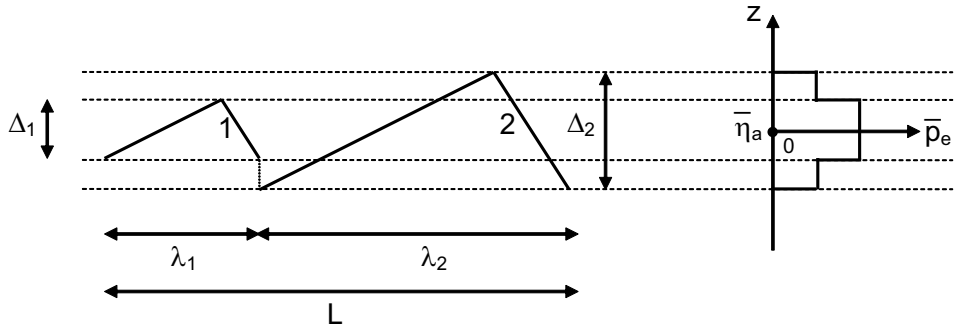

Figure C.1: Two triangular dunes and their overall PDF of bed surface elevations, $\bar{p}_e$.

a dune having either one of the bedforms equals λ_1/L and λ_2/L for the small and the large dune, respectively. The PDF of relative trough elevations, $\tilde{p}_{\eta_b}$, and the PDF of relative trough elevations, $\tilde{p}_b$, then become equal to

$$\tilde{p}_{\eta_b} d\eta_b = \begin{cases} 1/2 & \text{small dune} \\ 1/2 & \text{large dune} \end{cases} \tag{C.3}$$

$$\tilde{p}_b d\eta_b = \begin{cases} \lambda_1/L & \text{small dune} \\ \lambda_2/L & \text{large dune} \end{cases} \tag{C.4}$$

Now, from (C.1) we can determine that, at the mean bed level and at the crest elevation of the large bedform, the overall PDF of bed surface elevations, $\bar{p}_e$, equals

$$\bar{p}_e(\bar{\eta}_a) = \frac{1}{\Delta_1}\left(\tilde{p}_b d\eta_b\right)_1 + \frac{1}{\Delta_2}\left(\tilde{p}_b d\eta_b\right)_2 = \frac{\lambda_1}{\Delta_1 L} + \frac{\lambda_2}{\Delta_2 L} \tag{C.5}$$

$$\bar{p}_e(\eta_{t2}) = \frac{1}{\Delta_2}\left(\tilde{p}_b d\eta_b\right)_2 = \frac{\lambda_2}{\Delta_2 L} \tag{C.6}$$

Note that for a series of triangular bedforms, with the mean bed level of individual bedforms all at the same bed elevation, the overall PDF of bed surface elevations, $\bar{p}_e$, is symmetrical around the mean bed level, $\bar{\eta}_a$.

Appendix D

The PDF of relative trough elevations

For using the continuum sorting model, the probability density function (PDF) of relative trough elevations, $\tilde{p}_b$, is required as input. The equilibrium sorting model was calibrated upon experiments A2 and B2 (present study, Chapter 4), for which the PDF of trough elevations was determined from measurements. The model was verified upon experiments E3 and E7 (*Ribberink*, 1987), for which the PDF of trough elevations was not measured. For these experiments, the PDF of trough elevations was derived from the PDF of bed surface elevations, $\bar{p}_e$, under the assumption of triangular dunes according to (5.84) through (5.87), i.e. with all properties related to the varying relative trough elevations. This appendix explains the procedure of deriving the PDF of trough elevations from the PDF of bed surface elevations.

It is strongly recommended to read Appendix C before one continues.

In Section 5.3.2 and Appendix C, it has been explained how the overall PDF of bed surface elevations, $\bar{p}_e$, is related to the characteristic bedform shape, $\bar{p}^*_{se}$, and the PDF of relative trough elevations, $\tilde{p}_b$. The relation is given by (5.92):

$$\bar{p}_e(z) = \int_{\eta_{bmin}}^{\eta_{bmax}} p_e(z)\, \tilde{p}_b\, d\eta_b = \int_{\eta_{bmin}}^{\eta_{bmax}} \frac{J(z)}{\lambda\Delta}\, (\lambda_s \bar{p}^*_{se}(z) + \lambda_l)\; \tilde{p}_b\, d\eta_b$$

which, for triangular dunes, reduces to

$$\bar{p}_e(z) = \int_{\eta_{bmin}}^{\eta_{bmax}} \frac{J(z)}{\Delta}\, \tilde{p}_b\, d\eta_b \tag{D.1}$$

Transformation of (D.1) now shows how we can determine the PDF of relative trough elevations, $\tilde{p}_b$, from the PDF of bed surface elevations, $\bar{p}_e$:

$$\tilde{p}_b(z) = \begin{cases} 0 & \text{if } z > \bar{\eta}_a \\ \Delta(z) \frac{\partial \bar{p}_e(z)}{\partial z} & \text{if } z \leq \bar{\eta}_a \end{cases} \tag{D.2}$$

Note that in (D.2) the bedform height, Δ, is dependent on the relative trough elevation, Δ_b, whence Δ is dependent on bed elevation z:

$$\Delta(z) = 2\,\Delta_b = 2(\bar{\eta}_a - z) \tag{D.3}$$

which incorporates the relation given in (5.84). Also note that for using (D.2) the overall PDF of trough elevations, $\bar{p}_e$, must be monotonic in z up to the mean bed level, $\bar{\eta}_a$, i.e. $\bar{p}_e$ must increase with z up to the mean bed level. This constraint is satisfied for a series of triangular dunes for which the mean bed level of all individual bedforms is located at the same bed elevation. If $\bar{p}_e$ is not monotonic in z up to the mean bed level and application of (D.2) is desired, one should make a polynomial fit through $\bar{p}_e$ that is monotonic in z up to the mean bed level and apply (D.2) to the fit.

Appendix E

Time evolution of the PDF of bed surface elevations

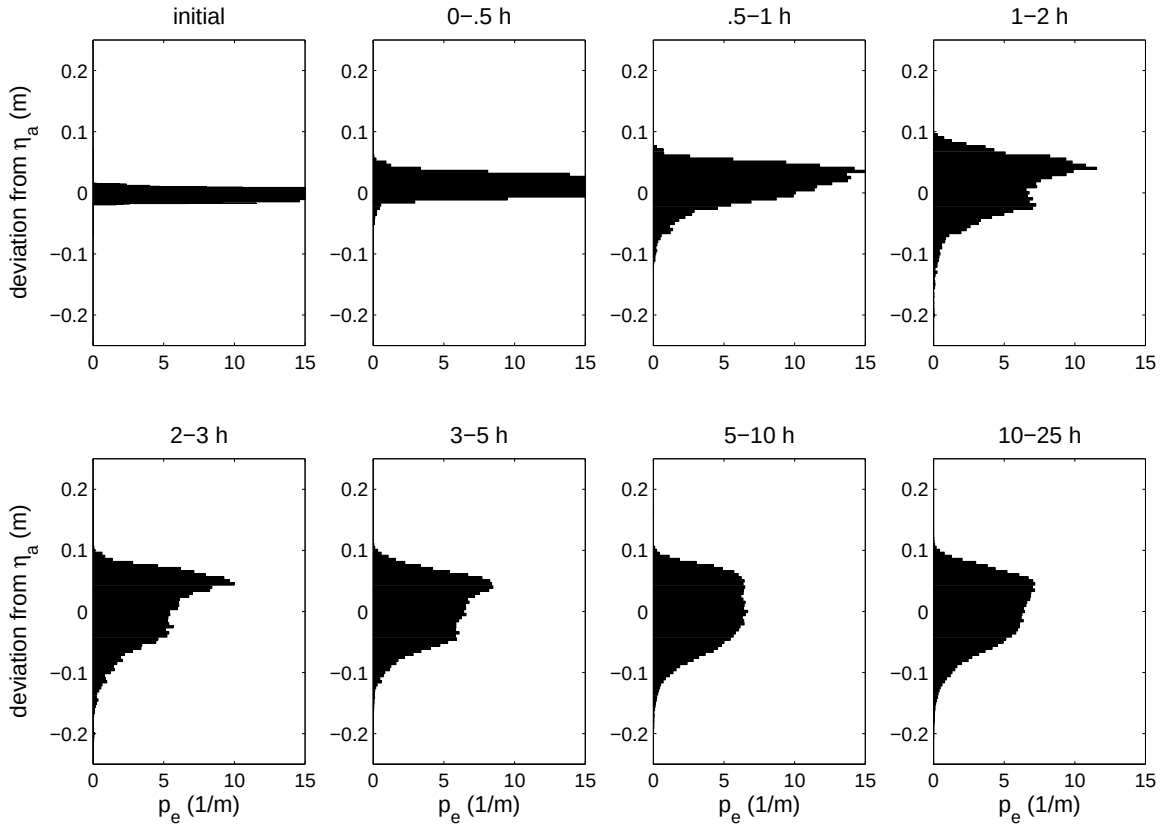

Figure E.1: Measured time evolution of the probability density function of bed surface elevations, $\bar{p}_e$, for experiment B2.

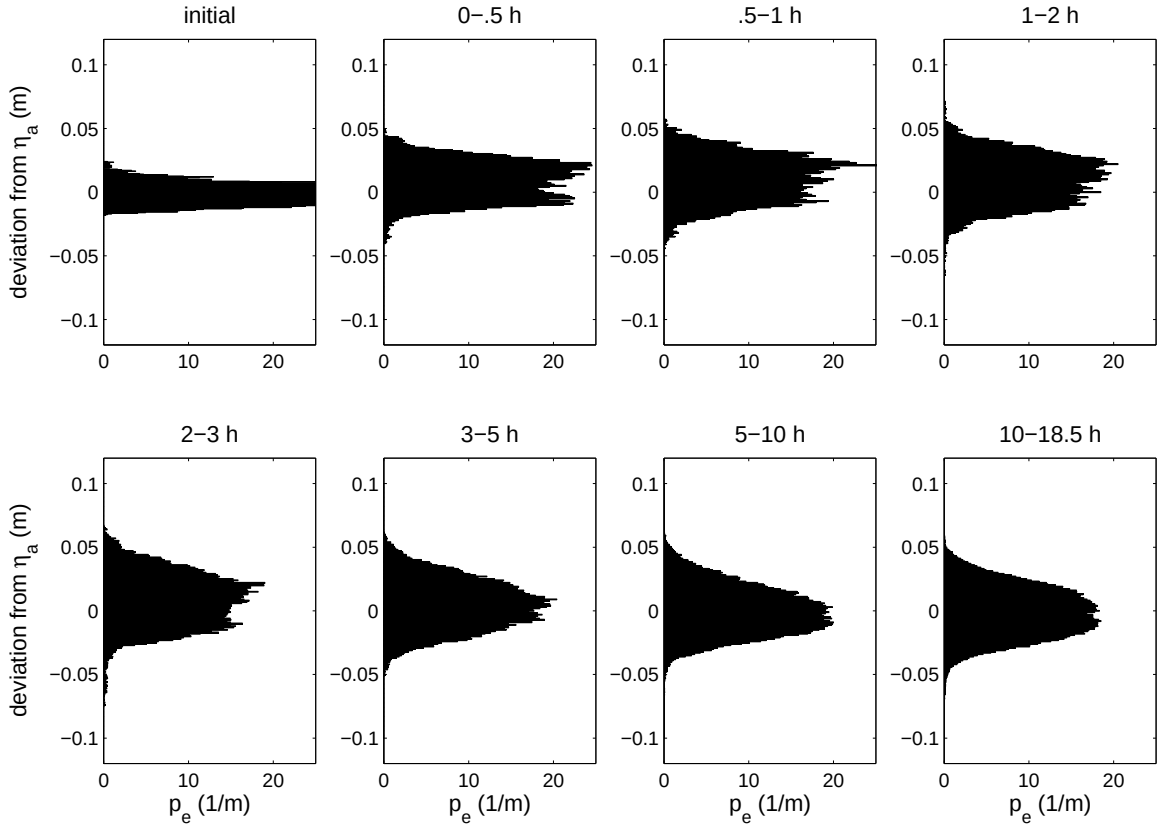

Figure E.2: Measured time evolution of the probability density function of bed surface elevations, $\bar{p}_e$, for experiment A2.

Appendix F

Effects of unsteady PDF of relative trough elevations

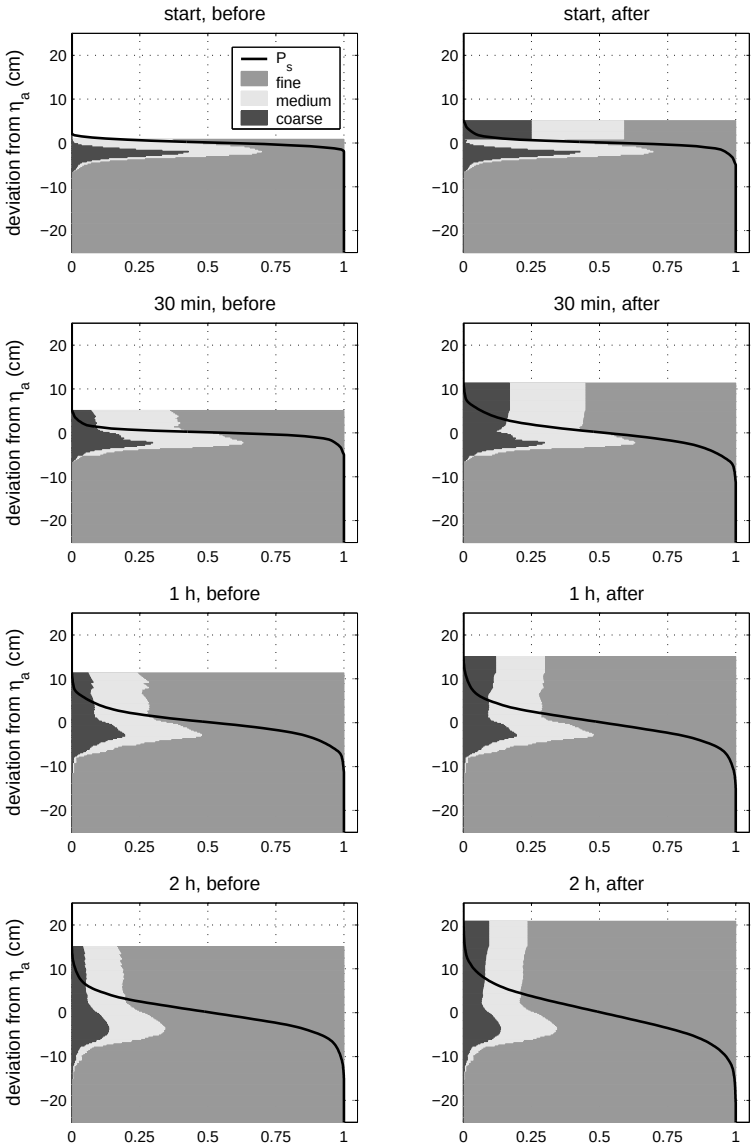

Figure F.1: Sediment rearrangement at times when the PDF of relative trough elevations changes in time, for experiment B2 (1).

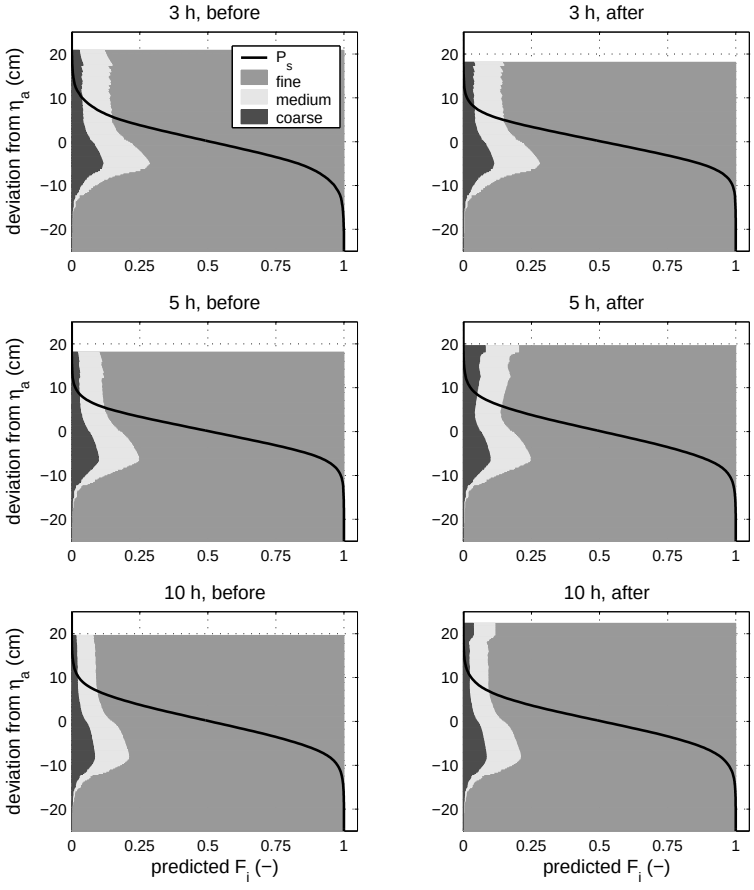

Figure F.2: Sediment rearrangement at times when the PDF of relative trough elevations changes in time, for experiment B2 (2).

Appendix G

Sorting computed by the Hirano and Ribberink models

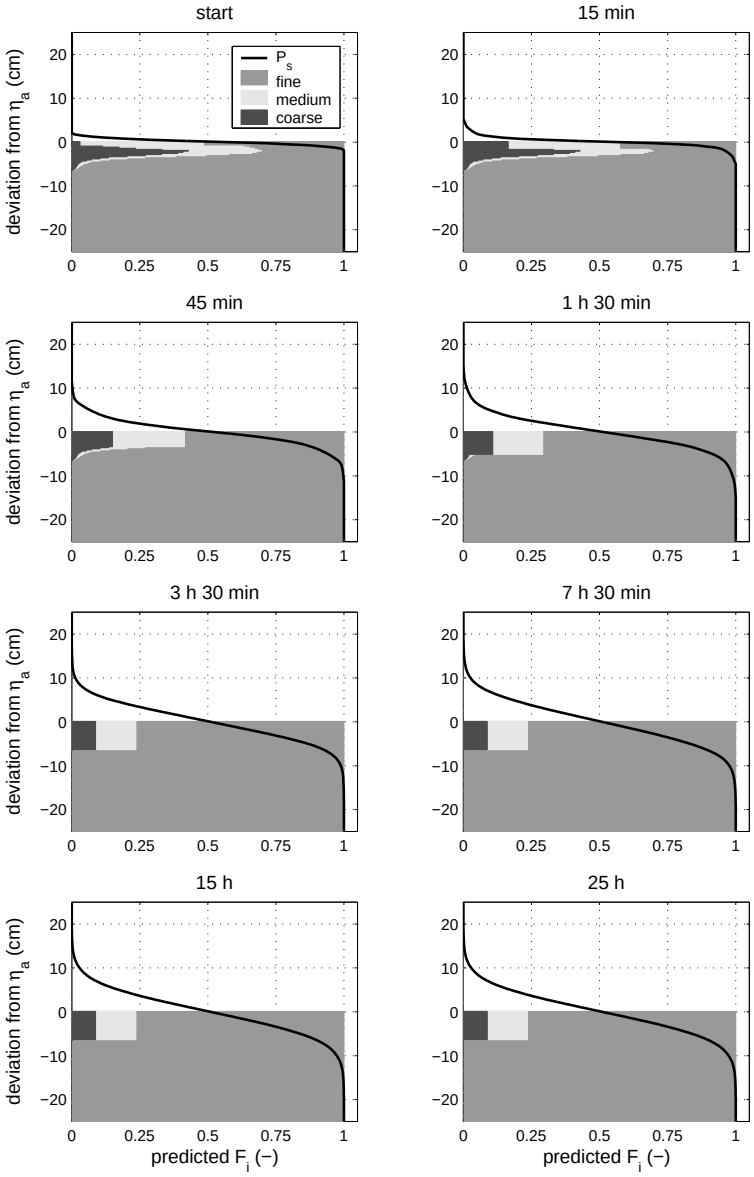

Figure G.1: Computed time evolution of the vertical sorting profile, $\bar{F}_i$, for experiment B2, using the Hirano active layer model.

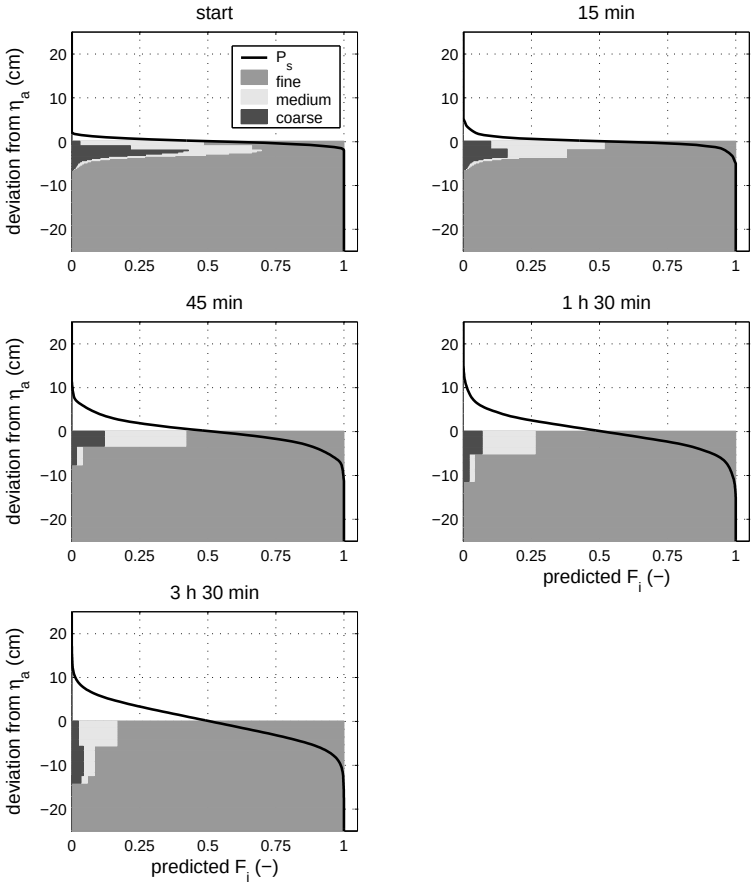

Figure G.2: Computed time evolution of the vertical sorting profile, $\bar{F}_i$, for experiment B2, using the Ribberink two-layer model.

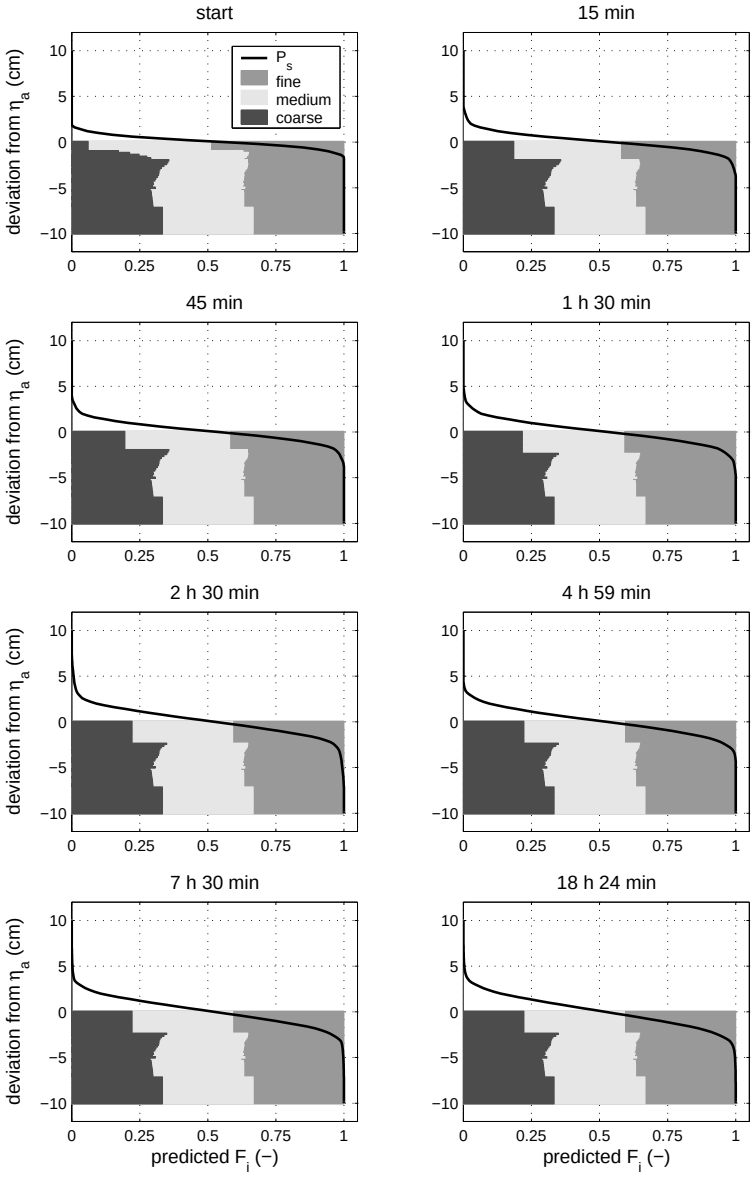

Figure G.3: Computed time evolution of the vertical sorting profile, $\bar{F}_i$, for experiment A2, using the Hirano active layer model.

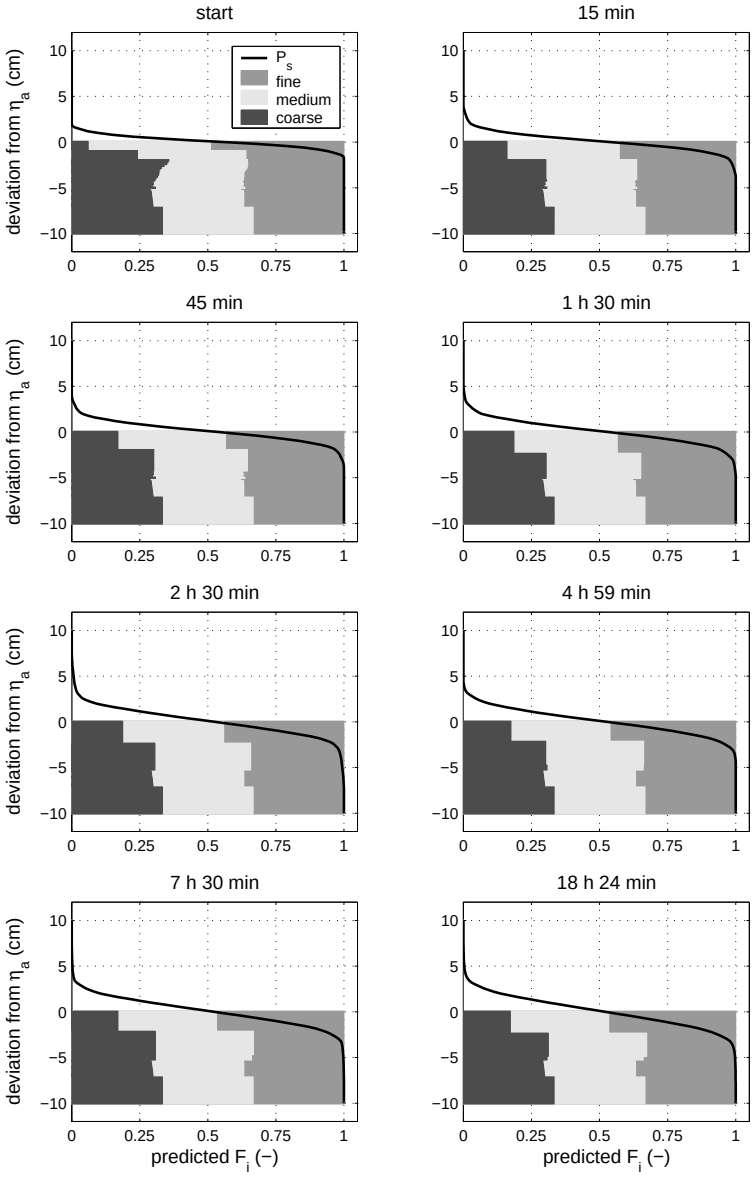

Figure G.4: Computed time evolution of the vertical sorting profile, $\bar{F}_i$, for experiment B2, using the Ribberink two-layer model.

Acknowledgements

The study presented in this dissertation was carried out in the framework of a doctorate studies at the department of Civil Engineering at the University of Twente. The project was supported by the Institute for Inland Water Management and Waste Water Treatment (Rijkswaterstaat RIZA) of the Ministry of Transport, Public Works, and Water Management in the Netherlands, WL | Delft Hydraulics, and the University of Twente. The experiments with the Rhine mixture were funded by the European Union as a Training and Mobility of Researchers (TMR) project and by the combination RIZA-WL-UT (the above three institutes). The experiments with the tri-modal mixture were supported by the combination RIZA-WL-UT. The Netherlands Organisation for Scientific Research (NWO) and the Prince Bernhard Cultural Foundation are acknowledged for their financial support for a three-month stay at the Saint Anthony Falls Laboratory.

I am grateful to my advisors, Huib de Vriend, Gary Parker, and Jan Ribberink, for their continuous scientific support and for reading and commenting on this thesis. Also, the members of an advising committee that watched over the research process are acknowledged: Emiel van Velzen, Arjan Sieben, and David Kroekenstoel (Rijkswaterstaat RIZA), Don Duizendstra (Rijkswaterstaat RIZA, now HKV Consultants), Janrik van den Berg (Utrecht University), and Cor Flokstra and Erik Mosselman (WL | Delft Hydraulics).

During the flume experiments I enjoyed working with Maarten Kleinhans, Klaus Basso, Andreas Dittrich, Peter van der Scheer, Jannet Bredius, Don Duizendstra, Freek de Groot, Joop Ouderling, and Erik Mosselman. A word of thanks goes to all of you.

During the three-month stay at the Saint Anthony Falls Laboratory of the University of Minnesota in Minneapolis, I greatly enjoyed working with Gary Parker. I miss our blackboard sessions with endless series of equations. Michal Tal and Nikki Strong made my stay an even more enjoyable one. This stay also initiated my pleasant contact with Suzanne Leclair.

I thank my former colleagues at the Civil Engineering department, in particular Marjolein Dohmen-Janssen, Henriëtte Otter, Suzanne Hulscher, Mark Zuidgeest, Pieter Roos, Attila Németh, Mascha van der Voort, and Anne-Marie Klijnstra. My Monday-night stay at Marjolein's was an every week joy. I also thank my present colleagues at WL | Delft Hydraulics, in particular Hanneke van der Klis, Bert Jagers, Simone van Schijndel, and Henriëtte Otter. I render thanks to Marjolein Dohmen-Janssen and Lonneke Zuijdwijk for being such devoted 'paranimfen'.

A warm word of thanks goes to Dennis. In the final stage of this project he endured quite a lot. He introduced compulsory Sunday walks and cycling trips in order to get me outdoors. The frequency of our world-travelling cycling trips showed a serious decline. It is too bad that he won our competition in finishing the drafts of our theses by only 3 days.

Astrid Blom
Diemen, January 2003

About the author

Astrid Blom was born in Rijnsburg, the Netherlands, on 4 August 1973. From 1985 to 1991 she attended 'Het Drachtster Lyceum' in Drachten and received her Gymnasium diploma in 1991. In that same year she started her academic studies in Civil Engineering at Delft University of Technology in Delft, where she specialised in river engineering. As a traineeship, she worked for a period of three months at the engineering company CNEC in São Paulo, Brazil. She conducted her final masters project on bank erosion of the river Allier at WL | Delft Hydraulics and received her masters degree, with distinction, in 1997. From 1997 to 2002 she conducted her Ph.D. research at the department of Civil Engineering at the University of Twente in Enschede. In 2000 she spent a period of three months at the Saint Anthony Falls Laboratory of the University of Minnesota in Minneapolis, USA. In 2002 she joined the river engineering department of WL | Delft Hydraulics.